Institut für Chemie – Polymerchemie

Poly(lactide)-Based Amphiphilic Block Copolymers:

Self-Assembly and Stereocomplexation in Aqueous Media

Zur Erlangung des akademischen Grades

„doctor rerum naturalium“

(Dr. rer. nat.)

in der wissenschaftlichen Disziplin „Kolloid-und Polymerchemie“

Eingereicht an der

Mathematische-Naturwissenschaftlichen Fakultät

der Universität Potsdam

Von

Sebastian Noack

Potsdam, April 2019

“The more you know, the more you know you don't know.”

- Aristotle

Published online at the
Institutional Repository of the University of Potsdam:
https://doi.org/10.25932/publishup- 43616
https://nbn-resolving.org/urn:nbn:de:kobv:517-opus4-436168

Declaration

The enclosed research was conducted in the Institute of Chemistry at the University of Potsdam, under the supervision of Prof. Helmut Schlaad between July 2014 and April 2019. This thesis has not been submitted for any other qualifications at this or any other institution. This dissertation is the original work of the author and does not include any research that is the outcome of work done in collaboration with others, except where specifically indicated in the text and acknowledgments.

Eidesstattliche Erklärung

Die vorliegende Arbeit wurde in der Zeit von Juli 2014 bis April 2019 an der Universität Potsdam im Institut für Chemie unter der Leitung von Prof. Helmut Schlaad angefertigt. Die Arbeit ist bisher an keiner anderen Hochschule eingereicht worden und wurde zudem selbständig und ausschließlich mit den angegebenen Mitteln angefertigt. Hiermit erkläre ich an Eides statt, dass ich die vorliegende Arbeit selbstständig verfasst und nur unter Zuhilfenahme der ausgewiesenen Quellen und Hilfsmittel angefertigt habe. Beiträge von Kooperationspartnern wurden explizit gekennzeichnet.

Potsdam, den 12.04.2019 _____

(Sebastian Noack)

Acknowledgments

At this point, I would like to thank many people that gave me the opportunity to work on this thesis and gave me the financial foundation and mental support to bring this thesis to a positive end.

First, I want to thank Professor Dr. Helmut Schlaad for offering me this interesting topic, guiding me through difficult stages during the progress of my work, and supporting me with scientific advice with patience and great dedication to my work. I would like to thank the University of Potsdam for their funding, as well as the "Brückenprogramm Chancengleichheit" that supported me six months financially through a personally and scientifically difficult time, and conclusively gave me the opportunity to end this thesis with high quality. Additionally, I want to thank Dr. André Laschewsky, my mentor, for his supportive scientific thoughts for my topic and his comprehensive knowledge of polymer chemistry. I would like to thank Professor Dr. Joachim Koetz for the enjoyable collaboration to investigate my self-assembled morphologies and discussing my results. Great thanks to Dr. Thomas Wolf from the group of Dr. Frederik Wurm at the Max Planck Institute for Polymer Research in Mainz who offered me one of my phosphonate monomers. I owe great thanks to Professor Dr. Yan Lu at the Institute of Soft Matter and Functional Materials at the Helmholtz-Zentrum in Berlin, as well to Professor Dr. Janne Ruokolainen from the Department of Applied Physics at the Aalto University for having made the cryo-TEM measurements possible.

I would like to thank all the people at the University of Potsdam and Max Planck Institute of Colloids and Interfaces who supported me with different techniques used during the last four years. More precisely, many thanks to Sibylle Rüstig and Dr. Brigitte Tiersch for the variety of TEM and cryo-SEM measurements, to Angela Krititschka, Dr. Matthias Heydenreich, and Olaf Niemeyer for their support with NMR spectroscopy measurements, discussing my results critically and making temperature-sweep experiments possible including a nice excursion to Berlin. Furthermore, I would like to thank Dr. Matthew R. Linford, Dhananjay I. Patel, and Dr. Charlotte Vacogne for the productive collaborations, Dr. Zdravko Kochovski for inviting me to Berlin Adlershof and measure my cryo-TEM samples, Sascha Prentzel and Marlies Gräwert for their help and introductions into SEC, Dr. Dirk Schanzenbach for the support in TGA and DSC measurements, and finally Dr. Anna Bogomolova for helping me with all the light scattering related issues. Special thanks go to Dr. Ines Starke for supporting me with the application for the scholarship, and once again to Sascha Prentzel for his help with all laboratory concerns.

In retrospect, I have to admit that I was lucky to be part of such a nice working group that offered me a friendly atmosphere. You were my inspiration that kept me going in the lab, my improvement through constructive discussions and because of your patience, my rock during this Ph.D.

You gave Shorty a new home, we laughed together, watched more or less good movies in the cinema and thanks to Sarah and Dan Brosnan we had our first Thanksgiving. Thank you Charlotte Vacogne, Felix Behrendt, Afroditi Doriti, Scott Kilbride, Ina Damobowsky, Sascha Prenztel, Boonya Thongrom, Anna Bogomolova, Andreas Hess, Aleksandar Matic, Daniel Rockel, Niels Lüdecke, Tapas Debsharma Shuangyan Hu and Matilde Concilio. I would like to emphasize once more Charlotte, Felix, and Scott who helped me a lot during my Ph.D., especially towards the end.

A person who never was part of the Schlaad group, but deserves special thanks is Dr. Han Miao. Irrespective of whether you worked at the MPIKG or now at the School of Materials Science and Engineering in Georgia, you always had an open ear for my problems that were related to DLS and SLS and figured out how to help me. Thank you! Additionally, I have to thank Peter. Without your focus between the study times, I may never have changed my mind, and this Ph.D. would never have been possible.

Finally, I would like to thank my family. Thank you Mama for supporting me, no matter what I was doing. Thank you Suse for being a fantastic sister. I also want to thank Mathias for giving my mother and her family a new home. Many thanks to “Oma und Opa Lieberose”, ”Oma und Opa Rheinsberg”, “Oma Christa”, my aunt Helga, my uncles Gerald, and Dietmar, and Lutz for being a father when I needed one. Finally, I want to thank my wife Chrissi who gave birth to my two incredible sweet children Elisabeth and Isabella. You three enrich my life when I wake up or come home from a stressful day with your smiles and your wet kisses through your snuffled noses. Chrissi, you supported me through thick and thin during this time as a student, and as a doctoral student with your sacrificing patience. I still can remember the times where you brought me a sandwich for dinner because I stayed for three days and three nights in the office to finish what I started. You are my home. Thank you.

Abstract

Due to its bioavailability and (bio)degradability, poly(lactide) (PLA) is an interesting polymer that is already being used as packaging material, surgical seam, and drug delivery system. Dependent on various parameters such as polymer composition, amphiphilicity, sample preparation, and the enantiomeric purity of lactide, PLA in an amphiphilic block copolymer can affect the self-assembly behavior dramatically. However, sizes and shapes of aggregates have a critical effect on the interactions between biological and drug delivery systems, where the general understanding of these polymers and their ability to influence self-assembly is of significant interest in science.

The first part of this thesis describes the synthesis and study of a series of linear poly(L-lactide) (PLLA) and poly(D-lactide) (PDLA)-based amphiphilic block copolymers with varying PLA (hydrophobic), and poly(ethylene glycol) (PEG) (hydrophilic) chain lengths and different block copolymer sequences (PEG-PLA and PLA-PEG). The PEG-PLA block copolymers were synthesized by ring-opening polymerization of lactide initiated by a PEG-OH macroinitiator. In contrast, the PLA-PEG block copolymers were produced by a Steglich-esterification of modified PLA with PEG-OH.

The aqueous self-assembly at room temperature of the enantiomerically pure PLLA-based block copolymers and their stereocomplexed mixtures was investigated by dynamic light scattering (DLS), transmission electron microscopy (TEM), wide-angle X-ray diffraction (WAXD), and differential scanning calorimetry (DSC). Spherical micelles and worm-like structures were produced, whereby the obtained self-assembled morphologies were affected by the lactide weight fraction in the block copolymer and self-assembly time. The formation of worm-like structures increases with decreasing PLA-chain length and arises from spherical micelles, which become colloidally unstable and undergo an epitaxial fusion with other micelles. As shown by DSC experiments, the crystallinity of the corresponding PLA blocks increases within the self-assembly time. However, the stereocomplexed self-assembled structures behave differently from the parent polymers and result in irregular-shaped clusters of spherical micelles. Additionally, time-dependent self-assembly experiments showed a transformation, from already self-assembled morphologies of different shapes to more compact micelles upon stereocomplexation.

In the second part of this thesis, with the objective to influence the self-assembly of PLA-based block copolymers and its stereocomplexes, poly(methyl phosphonate) (PMeP) and poly(isopropyl phosphonate) ($P^{i}PrP$) were produced by ring-opening polymerization to implement an alternative to the hydrophilic block PEG. Although, the 1,8-diazabicyclo[5.4.0]unde-7-ene (DBU) or 1,5,7-triazabicyclo[4.4.0]dec-5-ene (TBD) mediated synthesis of the corresponding poly(alkyl phosphonate)s was successful, however, not so the polymerization of copolymers with PLA-based

precursors (PLA-homo polymers, and PEG-PLA block copolymers). Transesterification, obtained by ^{1}H-NMR spectroscopy, between the poly(phosphonate)- and PLA block caused a high-field shifted peak split of the methine proton in the PLA polymer chain, with split intensities depending on the used catalyst (DBU for PMeP, and TBD for P^{i}PrP polymerization). An additional prepared block copolymer P^{i}PrP-PLLA that wasn't affected in its polymer sequence was finally used for self-assembly experiments with PLA-PEG and PEG-PLA mixing.

This work provides a comprehensive study of the self-assembly behavior of PLA-based block copolymers influenced by various parameters such as polymer block lengths, self-assembly time, and stereocomplexation of block copolymer mixtures.

Kurzzusammenfassung

Aufgrund seiner Bioverfügbarkeit und (biologischen) Abbaubarkeit stellt Polylactid (PLA) ein interessantes Polymer dar, welches bereits in Verpackungsmaterialien, chirurgische Fäden und in selbst organisierten Wirkstofftransportsystemen eingesetzt wird. Als ein Teil von amphiphilen Blockcopolymeren kann PLA die molekulare Selbstorganisation in wässrigen Lösungen wesentlich beeinflussen. Die gebildeten Strukturen sind dabei essenziell von Faktoren wie der Blockcopolymer Zusammensetzung, Amphiphilie, Proben Vorbereitung und der Enantiomerenreinheit des Monomers abhängig. Die Kenntnis über die beschriebenen Faktoren und das allgemeine Verständnis für die dazugehörigen Polymere sowie die Möglichkeit ihre Selbstorganisation zu beeinflussen, ist von entscheidender Bedeutung in biomedizinischen Anwendungen. Unterschiedliche Größen oder Formen der selbst organisierten Wirkstoffträgern haben einen erheblichen Effekt auf die Wechselwirkung mit dem entsprechenden biologischen System und somit einen essenziellen Einfluss auf den Ausgang der medikamentösen Therapie.

Der erste Teil dieser Doktorarbeit beschreibt die Synthese und Untersuchung einer Serie von Poly(L-Lactid) (PLLA) und Poly(D-Lactid) (PDLA)-basierten amphiphilen Blockcopolymeren mit variierenden PLA (hydrophob) und Polyethylenglycol (PEG) (hydrophil) Kettenlägen, sowie unterschiedlichen Polymersequenzen (PEG-PLA und PLA-PEG). Die genannten PEG-PLA Blockcopolymere wurden mittels organokatalysierter ringöffnender Polymerisation (ROP) hergestellt, wobei das entsprechende PEG-OH als Makroinitiator diente. Im Gegensatz dazu mussten die entsprechenden PLA-PEG Blockcopolymere mittels Steglich Veresterung von modifizierten PLA mit PEG-OH hergestellt werden.

Die Selbstorganisation der PLLA-basierten Blockcopolymeren und deren stereokomplexierten Mischungen in wässriger Lösung erfolgte unter Raumtemperatur und wurde mittels Dynamischer Lichtstreuung (DLS), Transmissionselektronenmikroskopie (TEM), Röntgenstrukturanalyse und Dynamische Differenzkalorimetrie (DSC) untersucht. Dabei wurden kugel- und wurmförmige Strukturen beobachtet, wobei die gebildeten Strukturen vom Lactid Gewichtsanteil im Polymer, sowie der Selbstorganisationszeit abhängig waren. Mit andauernder Selbstorganisation und zunehmender Kristallinität wurden die zuerst gebildeten kugelförmigen Strukturen kolloidal unstabil und es erfolgte ein epitaktisches Wachstum zu wurmförmigen Strukturen in Abhängigkeit der Lactid Kettenlänge. Die stereokomplexierten Blockcopolymer Mischungen hingegen bildeten, unabhängig von der Copolymersequenz der entsprechenden Polymer Partner, hauptsächlich unregelmäßige Ansammlungen kugelförmiger Strukturen welche den Eindruck einer Perlenkette erweckten. Mit dem Einsetzen der Stereokomplexierung zeigten zeitlich aufgelöste Selbstorganisationsexperimente eine

Transformation von bereits gebildeten Strukturen verschiedenster Formen und Größen (Polymer abhängig) zu kompakten Mizellen.

Im zweiten Teil dieser Doktorarbeit wurden, mit dem Ziel die Selbstorganisation von PLA-basierten Blockcopolymeren und deren Stereokomplexmischung vermehrt zu beeinflussen, zwei alternative Polymere zu PEG untersucht. Ähnlich wie PLA, konnten mittels organokatalysierter ROP Polymethylphosphonat (PMeP) und Polyisopropylphosphonat ($P^{i}PrP$) erfolgreich hergestellt werden. Die Blockcopolymer Synthese mit PLA-basierten Polymervorgängern erwies sich jedoch als schwierig. Aufgrund einer Protonenpeakspaltung der Methingruppe in der PLA-Wiederholeinheit konnten mittels ^{1}H-NMR Spektroskopie Umersterungsprozesse zwischen dem Polyalkylphosphonat- und PLA block nachgewiesen werden, welche in Abhängigkeit des verwendeten Katalysators (DBU oder TBD) unterschiedlich stark ausfielen. Das ebenfalls hergestellte $P^{i}PrP$-PLLA Blockcopolymer wies keine Unregelmäßigkeiten in der Polymersequenz auf und wurde anschließend für Selbstorganisationsexperimente mit PLA-PEG und PEG-PLA genutzt.

Diese Arbeit liefert eine umfangreiche Studie zur Selbstorganisation PLA-basierter Blockcopolymere und untersucht verschiedenste Einflussparameter wie Blocklängen, Selbstorganisationszeit und Stereokomplexierung in Polymermischungen.

Table of Contents

Declaration ..... **iv**
Eidesstattliche Erklärung ..... **iv**
Acknowledgments ..... **v**
Abstract ..... **vii**
Kurzzusammenfassung ..... **ix**
Table of Contents ..... **xi**
List of Abbreviations ..... **xv**
1 Introduction and Motivation **1**
2 Theoretical Background **4**
2.1 Self-Assembly 4
2.1.1 Self-Assembly in Bulk 4
2.1.2 Self-Assembly in Solution 6
2.1.3 Crystallization of Polymers 8
2.1.4 Poly(lactide) 10
2.1.5 Poly(phosphoester) 12
2.1.6 Stereocomplexation 16
2.1.7 Self-assembly of-PLA-based Amphiphilic Copolymers 18
3 Analytical Methods **22**
3.1 Differential Scanning Calorimetry (DSC) 22
3.2 Light Scattering 22
3.2.1 Dynamic Light Scattering (DLS) 23
3.2.2 Static Light Scattering (SLS) 25
3.3 Electron Microscopy 28
3.3.1 Transmission Electron Microscopy (TEM) 29
3.3.2 Scanning Electron Microscopy (SEM) 30
4 Synthesis of Poly(lactide)-based Diblock Copolymers **32**
4.1 Choice of the Organic Catalyst 32
4.1.1 DBU and its Limitations towards a Controlled Polymerization 32
4.1.2 An Acid/Base Bifunctional Catalyst 36
4.1.3 Conclusion on Initiator Choice 40

4.2 Synthesis of PEG-PLA Block Copolymers and Characterization 41

5 Poly(lactide)-Based Amphiphilic Block Copolymers: Crystallization Induced Self-Assembly and Stereocomplexation 45

5.1 Experimental 45

5.1.1 Preparation of the Aggregates 45

5.1.2 Sample Preparation for Crystallinity and Crystal Structure Characterization 46

5.2 Results and Discussion 47

5.2.1 Aqueous Self-Assembly of PEG-PLA Block Copolymers 47

5.2.2 Aqueous Self-Assembly of PEG-PLLA/PEG-PDLA Stereocomplexes 53

5.2.3 Self-Assembly PLLA-PEG copolymers and their block copolymer mixtures 57

6 Time-Dependent Self-Assembly of Block Copolymers and Their Stereocomplexes 60

6.1 Experimental 61

6.1.1 Materials 61

6.1.2 Preparation of Self-Assembled Aggregates without the use of Common Solvent 61

6.2 Results and Discussion 62

6.2.1 Time-Dependent Self-Assembly of PLA-based Block Copolymers 62

6.2.2 Time-Dependent Self-Assembly of Stereocomplexed Polymer Mixtures 64

6.3 Conclusion of Self-Assembly Behavior 67

7 Poly(lactide) and Poly(alkyl phosphonates)-based Copolymers 69

7.1 Synthesis 70

7.1.1 Monomers 70

7.1.2 Polymerization 71

7.1.3 Synthesis of Poly(lactide) and Poly(phosphonate)-based Block Copolymers 74

7.1.4 The conclusion of Synthetic and Analytical Research Issues 84

7.2 Self-Assembly 85

7.3 Conclusion 88

8 Summary and Outlook 89

9 Experimental Section 93

9.1 Reagents 93

9.2 Analytical Instrumentation and Methods 93

9.2.1 Nuclear magnetic resonance (NMR) spectroscopy 93

9.2.2 Size exclusion chromatography (SEC) 93
9.2.3 Dynamic and Static Light Scattering (DLS, SLS) 94
9.2.4 Thermogravimetric Analysis (TGA) 94
9.2.5 Differential Scanning Calorimetry (DSC) 94
9.2.6 Wide-Angle X-Ray Diffraction (WAXD) 94
9.2.7 Electron Microscopy (TEM, cryo-TEM; cryo-SEM) 95
9.2.8 Fourier Transformation Infrared Spectroscopy (FT-IR) 95
9.2.9 Matrix-assisted laser desorption/ionization-time-of-flight mass spectrometry (MALDI-TOF MS) 95
9.3 Synthetic Procedures 96
9.3.1 Monomer Synthesis of Alkyl Phosphonate 96
9.3.2 Polymer Synthesis 97
9.3.3 General Synthesis of PEG-PLA Block Copolymers 99
9.3.4 General Synthesis of PLA-PEG Block Copolymers 102
9.3.5 General Synthesis of PEG-PLA-PMeP Copolymers 103
9.3.6 General Synthesis of PEG-PLA-P^{i}PrP Copolymers 105
10 References 107
11 Appendix A 115
11.1 NMR Spectra PLA-based Block Copolymers 115
11.2 NMR Spectra of Precursors 124
11.3 NMR Spectra of Poly(alkyl Phosphonate)s and Poly(lactide)-based Copolymers 128
11.4 Synthesis and Analytics of Initiator Dye-NH_2 135
11.5 Time-Dependent Dialysis of Poly(lactide) and Poly(methyl phosphonate)-based Copolymers 137
11.6 Transesterification Influenced Self-Assembly of PEG-PLLA Copolymers 139
11.7 Temperature-Dependent Self-Assembly of PEG-PLA 143
11.8 Time-Dependent Self-Assembly of Block Copolymer Mixtures (SLS Data) 145
11.9 DBU initiated Poly(lactide) Polymerization 147
12 Appendix B 148
12.1 Journal Publications 148
12.2 Conference Contributions 148

List of Abbreviations

A_2	Second virial coefficient
AAP	Activated Alcohol-Pathway
ATP	Adenosine triphosphate
b^2	Squared scattering power
BA	benzoic acid
Bn	Benzyl
CMC	Critical micelle concentration
CPS	Closely packed spheres
D	Diffusion coefficient
$Đ$	Dispersity index
DBU	1,8-Diazabicyclo[5.4.0]unde-7-ene
DLS	Dynamic light scattering
DMF	Dimethylformamide
DNS	Deoxyribonucleic acid
DSC	Differential scanning calorimetry
E_{int}	Interaction energy
EM	Electron microscopy
f	Mole fraction
FDA	US Food and Drug Administration
$g_2(\tau)$	autocorrelation function
h	Hour
^{i}PrP	2-isopropyl-1,3,2-dioxaphospholane
I_s	Scattering intensity
k_B	Boltzmann constant
LA	Lactic acid
MALDI	Matrix Assisted Laser Desorption/Ionization
MeP	2-methyl-1,3,2-dioxaphospholane
M_n	Number average molar mass
M_w	Weight average molar mass
N	Degree of polymerization
NAP	Nucleophilic-Attack Pathway
NMP	N-methyl-2-pyrrolidone

PCL	polycaprolactone
PDLA	Poly(D-lactide)
PEG	Poly(ethylene glycol) monomethyl ether
PGA	Polyglycolide
$P^{i}PrP$	Poly(isopropyl phosphonate)
PL	Perforated lamellae
PLA	Poly(lactide)
PLLA	Poly(L-lactide)
PMeP	Poly(methyl phosphonate)
PMMA	Poly(methyl methacrylate)
PPO	Poly(propylene oxide)
PTA	phosphotungstic acid
r	Radius
RAFT	Reversible Addition-Fragmentation Chain Transfer
R_g	Radius of gyration
R_h	Hydrodynamic radius
ROP	Ring-Opening Polymerization
SEM	Scanning electron microscopy
SLS	Static light scattering
T	Temperature
TBD	1,5,7-Triazabicyclo[4.4.0]dec-5-ene
TEA	triethylamine
TEM	Transmission electron microscopy
T_g	Glass transition temperature
THF	Tetrahydrofuran
T_m	Melting point
TOF	Time of flight
wt%	Weight percentage
XRD	X-ray powder diffraction
δ	Chemical shift
ΔG_{Mix}	Free Gibbs energy of mixing
ΔH_{Mix}	Free enthalpy of a mixture
ΔS_{Mix}	Entropy of mixing
ϵ	Energy of interactions
η	Viscosity

ϑ	Scattering angle
λ	Wavelength
φ	Monomer fraction
χ	Flory Huggins interaction parameter

1 Introduction and Motivation

When people think about chemistry, particularly in pharmacological context, they imagine mainly the synthesis of molecules into active ingredients. Reagents react with each other to form covalent bonds whereby new products are produced. These new products could potentially provide patients new alternatives to pain management, cancer treatments, and anti-depressants. However, while development of new drugs is a critical need, the development of methods, typically through non-covalent interaction, of getting the desired therapeutic agent to the specific target (i.e., brain, tumor, liver, etc.) achieve the desired interaction and reduce unwanted side-effects (e.g., hair loss from chemotherapy).[1] Ideally, such carrier systems should keep the whole system soluble, and protect the in often hydrophobic drug from degradation, an early metabolism, and unspecific interactions. Additionally, it is responsible for releasing the drug within a therapeutic window (over days to months) to achieve an optimal activity of the therapy.[2,3]

In general, the investigation of spontaneous but controlled non-covalent interactions from components into complex chemical systems as colloids,[4] lipids bilayers,[5] phase separated polymers and block copolymers, self-assembled monolayers,[6] proteins (folded polypeptides)[7] and DNA is called supramolecular self-assembly. Understanding of self-assembly is vital, both from a development of new materials perspective but also from a biology mechanism context, such as the crucial biological role self-assembly plays in the case of proteins. Some proteins can form viral capsids or building the outer shell of bacteria and therefore subject to a specific task.[8,9] Unintentional self-assembly occurs when the system becomes modified by possible unintended side-effects or by diseases that can then cause proteins to aggregate. Alzheimer disease, for example, is caused by conformational changes of the amyloid β-protein, which end up in fibrils, which is a commonly observed feature for this malady.[10]

Self-assembly has found applications in material design or medical applications as drug carrier systems through amphiphilic molecules. The thermodynamic incapability of different segments that interact leads to a phase separation, which produces in various ordered morphologies depending on various parameters. Humans have been using this type of technology for the betterment of humankind for thousand years. One of the most relevant examples is soap. Soaps contain fatty acids that are surfactants with a nonpolar tail and a polar head, which self-assemble into spherical micelles whereby the polar head point toward the water, while the core encapsulates any fat or dirty and thereby providing a cleaning function. Dispersed in water the polar head projects into the water and stabilizing the cased fat in the core. These micelles help to dissolve dirt and grime by encapsulating hydrophobic moieties and washing them away, now dispersed in water.

Like for small molecular aggregates, self-assembly occurs in amphiphilic block copolymers[11–14] or double hydrophilic block copolymers[15–17]. While small molecular aggregates and double hydrophilic

block copolymers have lower stability and higher critical micelle concentration (CMC) then amphiphilic block copolymers, all observed self-assembled morphologies are similar to each other and include spherical micelles, lamellae, and vesicles or other morphologies.[12,16,18,19] Self-assembly of macromolecules has attracted extraordinary attention in the last decades. Indeed, with the progress made in the fields of controlled polymerization techniques, such as ionic living polymerization or controlled radical polymerization (Reversible Addition-Fragmentation Chain Transfer (RAFT)), complex and precise amphiphilic architectures have been made possible. These highly developed architectures vary from block copolymers with two or more different polymer segments to graft, dendritic, cyclic polymers or multiarm structures, which can self-assemble into versatile aggregates by adjusting the conditions.[20–24]

In this thesis, utilizing poly(lactide) (PLA)-based linear block copolymers, new understandings of self-assembly mechanisms will be explored. The polymer sequence, the amphiphilicity of the polymer, and the ability to crystallize is essential in controlling the resulting structures. Using the stereocomplexation phenomenon, PLA-based block copolymers were used to achieve complex self-assembled morphologies or gels.[25] In general, stereocomplexation occur between two complementary stereoregular polymers that interact with each other, such as PLLA and PDLA. Thereby a new crystal structure is realized in modified physical properties such as thermal resistance, or enhanced mechanical stability.[26,27,36–38,28–35] The orientation of the enantiomeric segments of the stereocomplexed-PLA can be parallel or antiparallel, although the parallel alignment was reported to be favored (Figure 1).[27,38]

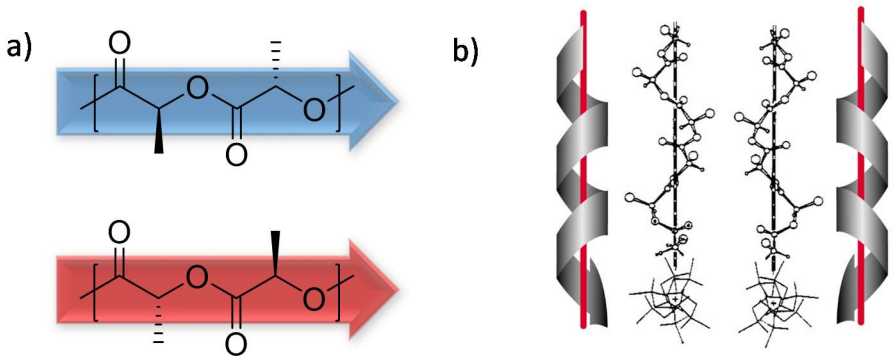

***Figure 1**: a) Poly(L-lactide) (blue) and poly(D-lactide) (red) with a simplified representation of the direction of the polymer b) a pictorial representation of two enantiomeric PLA polymers in a stereocomplex in a parallel orientation. Figure b is adapted from Ikada, Y.; Jamshidi, K.; Tsuji, H.; Hyon, S. H. Macromolecules 1987, 20 (4), 904–906. with permission from American Chemical Society.*[28]

Given the general efficiently self-assembly behavior in aqueous solution of PLA-based block copolymers, the orientation of the stereocomplexed segments may play a crucial role. However, this connection was never considered in the literature before, to the author's knowledge. Most reported PLA-based block copolymers are produced by ring-opening polymerization (ROP) of lactide with a

hydrophilic block as poly(ethylene glycol) methyl ether (PEG-OH) used as the initiator. If used for stereocomplexation, the opposite enantiomeric partner block copolymer was synthesized with the same synthetic route in which the orientations of the two polymers are the same. However, realizing a PLA-based block copolymer with the hydrophilic block attached to the alcohol side of PLA, the mixture of two block copolymers with different polymer sequences could influence the self-assembly in aqueous solution (Figure 2 b). Consequently, this would require a modified synthesis of the corresponding block copolymers, to guarantee that the hydrophilic block is linked to the oxygen terminus of the PLA.

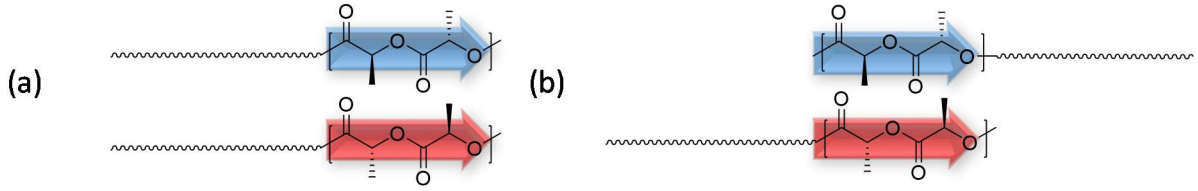

***Figure 2**: Schematic illustration of stereocomplexable mixing partners of PLA-based amphiphilic block copolymers in consideration of their polymer-sequence. (a) a mixture of PLA-based amphiphilic block copolymers with the same polymer-sequence. (b) Hypothesized self-assembly of a mixture of PLA-based block copolymers with different polymer-sequence.*

This doctoral work focused on the synthesis, characterization, and self-assembly of PLA-based block copolymers. More precisely, each chapter focuses on the following topics:

- The synthesis of PLA-based block copolymers by ROP with organic catalysts with its challenges is reported in chapter 4.
- The self-assembly of a series of synthesized PEG-PLA and PLA-PEG block copolymers with different PLA, and PEG chain length and their stereocomplexed mixtures are reported in chapter 5.
- Long-term experiments of the self-assembly of PLA-based block copolymers and their mixtures are presented in chapter 6.
- The synthesis and comprehensive characterization of PLA-based copolymers with additional bonded poly(alkyl-phosphonate)s and the self-assembly behavior of selected polymers are reported in chapter 7

2 Theoretical Background

2.1 Self-Assembly

Even though self-assembly in bulk does not play any role in this doctoral thesis, the theoretical background has to be included to understand the fundamental principles of this phenomenon. Furthermore, this knowledge is necessary to describe the more complex system in solution.

2.1.1 Self-Assembly in Bulk

When two immiscible polymer blocks are linked together that would generally undergo macrophase separation, thermodynamic incompatibility leads to three-dimensional separation, and a complex bulk-or solution-phase behavior can be observed.[39,40] Intending to prevent unfavorable hydrophobic-hydrophilic interactions that would lower the free energy of the system, micro-phase separation occurs, although this results in a loss of entropy. This means that in order for the separation to occur, the free Gibbs energy of mixing ΔG_{mix} is negative, and this must be an enthalpetically driven phenomena (Equation 1).

$$\Delta G_{mix} = \Delta H_{mix} - T\Delta S_{mix}$$

Equation 1

In Equation 1 the free enthalpy of a mixture ΔH_{mix} is the critical parameter that can additionally be described by Equation 2 that includes all essential parameters for the mixing or separation of the system. It is essentially describing the interactions of different blocks depending on the composition of the block copolymer.

$$\Delta H_{mix} \approx k_B T \chi \phi (1 - \phi)$$

Equation 2

Initially developed to describe the interactions between polymer and solvent molecules by a model from Flory and Huggins in 1942,[41,42] this theory can be used to describe the formation of microdomains of block copolymers. Therefore, k_B is the Boltzmann constant, T the temperature, ϕ monomer fraction and χ the Flory Huggins parameter.

To achieve a better understanding of micro-phase separation, three parameters need to be known.[43] The first one is the overall degree of polymerization per macromolecule N consisting of repeating units in segment A and repeating units in segment B (Equation 3).

$$N = N_A + N_B$$

Equation 3

The second parameter is the mole fraction f of monomer A or B (Equation 4)

$$f_A = \frac{N_A}{N}\,;\, f_A + f_B = 1$$

Equation 4

and, the third is the Flory-Huggins interaction parameter χ which is essentially is the sum of the free energy per repeating unit A and B and the degree of polymerization (Equation 5).

$$\chi = \left(\frac{z}{k_b T}\right)[\epsilon_{AB} - \frac{1}{2}\,(\epsilon_{AA} + \epsilon_{BB})$$

Equation 5

The interaction parameter χ_N is described with $k_B T$ (Boltzmann-constant), the immediate neighbors of the monomers in the block-copolymer z, and ϵ, which describes the energy of interactions between AA, BB and AB blocks.[39,43] When χ_N is positive, monomer A and monomer B repel each other and try to minimize the contact between themselves. By trying to minimize the mixing energy ΔG_{mix} through separation, the entropy ΔS_{mix} decreases by forcing the system to a more ordered alignment. In 1994, Matsen and Schick presented a calculated phase diagram for AB diblock copolymers, which later was confirmed by Bates *et al.* with practical results and a reported phase diagram for poly(isoprene)-b-poly(styrene) (Figure 3).[44,45] In this diagram f_A is plotted against χN. However, χ varies inversely with increasing temperature.[39] By increasing the temperature of the system, χN decreases (the temperature dependency is shown in Equation 5). Consequently, an increase of the compatibility and mixing entropy of the two blocks occur and ordered segments become disordered with temperature (i.e., a homogeneous mixture).

By increasing the number of blocks in the block copolymer, the complexity of self-assembly in bulk is, of course greatly expanding. A linear triblock copolymer with three different polymer blocks (ABC) comprises three different Flory-Huggins parameters ($\chi_{AB}, \chi_{BC}, \chi_{CB}$), the volume fraction of three blocks ($f_A + f_B + f_C = 1$), the degree of polymerization N and the variations of the different segments (ABC, BCA, CAB). Based on these parameters various theoretical morphologies exist and, over the past decades, been experimentally.[39,46]

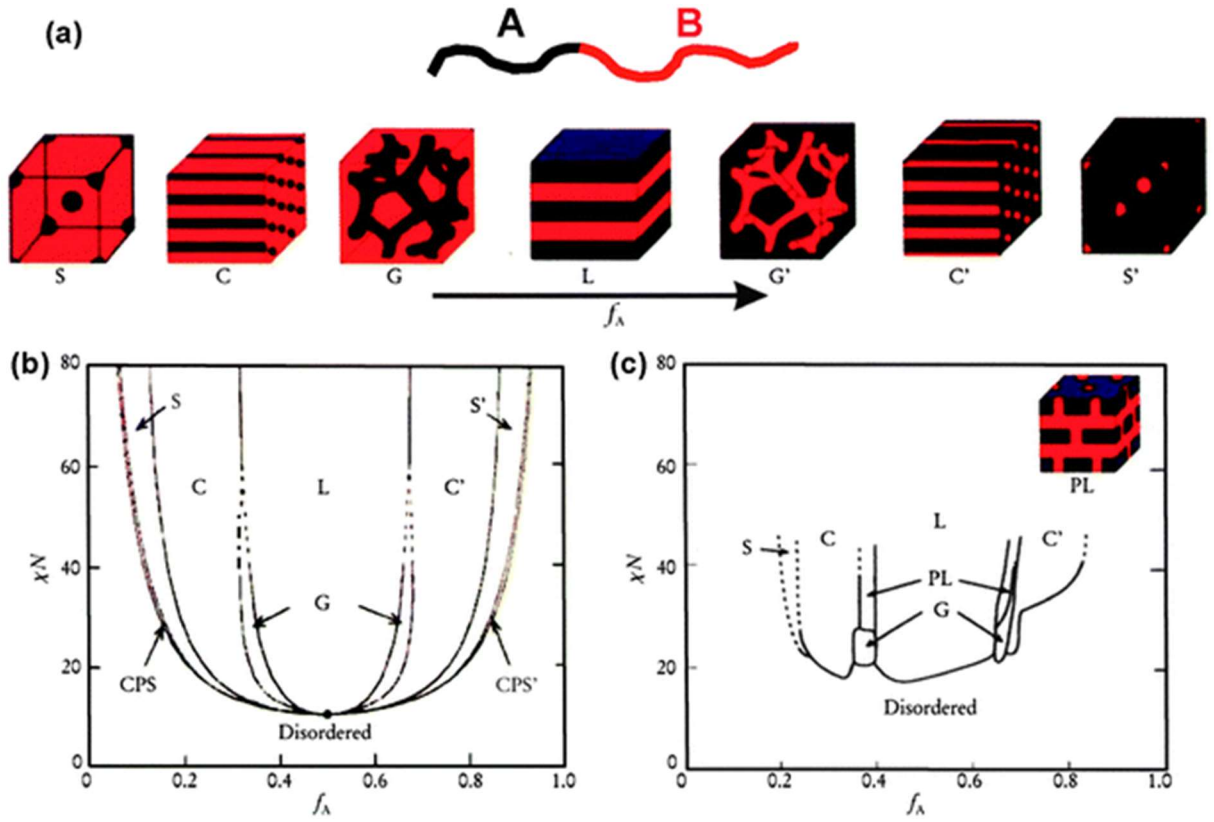

Figure 3: *(a) schematic illustration of idealized morphologies of AB-type block copolymers; S = spherical, C = cylindrical, G = gyroid, L = lamellae (b) theoretical phase diagram Matsen and Schicks reported based on the self-consistent mean-field theory, the segregation parameter χN is plotted against the volume fraction f_A whereas χ is the Flory-Huggins interaction parameter, and N is the degree of polymerization*[44]*, CPS/CPS´ = closely packed spheres (c) experimentally determined phase diagram of poly(isoprene)-b-poly(styrene); f_A represents the volume fraction of poly(isoprene); PL = perforate lamellae. Adapted from Mai, Y.; Eisenberg, A.* Chem. Soc. Rev. ***2012***, 41 *(18), 5969. With permission of The Royal Society Chemistry.*[12]

2.1.2 Self-Assembly in Solution

Self-assembly in solution can be found for double hydrophilic[15–17] or amphiphilic block copolymers[11–14]. In an amphiphilic (*greek, amphis* "both" and *philia* "love") polymer, the hydrophilic (*greek*, *hydor* "water" and *philos* "loving") and the hydrophobic (*greek*, *hydor* "water" and *phobos* "fear") block are linked covalently. Depending on the application and used block copolymer composition, self-assembly occurs in organic and aqueous solutions.

In Chapter 2.1.1 the complexity of micro-phase separation of di- and triblocks was explained by the influence of the Flory-Huggins interaction parameter χ, which essentially describes the energy of the interaction between the different blocks. Through the introduction of solvent interaction, the system becomes much more complex compared to self-assembly in bulk. Additionally it has to be included that most of the time for amphiphilic block copolymers, an additional good solvent, where

both blocks are soluble (common solvent), is used next to the non-solvent (selective solvent and most of the time water), and therefore plays an essential role for the aggregation behavior in solution. In having such a complex system (one block copolymer, one non-solvent, and one common solvent), six χ-parameter (χ_{AB}, χ_{AS}, χ_{AN},χ_{BS},χ_{BN} and χ_{SN}) are needed to explain the self-assembly in solution. Whereas A and B are again represent the two polymer blocks, S stands for the common solvent, and N marks the non-solvent (e.g., water).[12] By adding a non-solvent (water) to the solved polymer, the hydrophobic block gets desolvated and forces all hydrophobic parts to the core of the formed morphology. The resulting aggregate is then stabilized by the hydrophilic parts aiming to the outside and forming the shell of the self-assembled structure. Various morphologies are known for self-assembly in a solution, including spherical and rod-like micelles, vesicles, or lamellar structures. In 2002, Discher and Eisenberg proposed a unifying rule for block copolymers (without stiff/crystalline segments) based on the ratio of hydrophilic to hydrophobic blocks.

- $f_{hydophilic} < 0.45$, spherical micelles
- $f_{hydophilic} > 0.50$, rod-like micelles
- $f_{hydophilic} \approx 0.35$, vesicles
- $f_{hydophilic} > 0.25$, inverted microstructures such as large compound micelles[14]

The type of self-assembled structures also differ with copolymer concentration in solution and can cause a transition from spheres to rods to vesicles with increasing concentration.[47] In case of micro-phase separation in bulk, by separating the hydrophobic part through aggregation, the enthalpy ΔG_{mix} is kept to a minimum, an ordered state is formed and thus entropy ΔS_{mix} is decreased.

The self-assembly behavior in solution can be influenced by various parameters as copolymer composition (described in Chapter 1.1.1.1), the common solvent, polymer concentration, temperature and the rate of water addition when the polymer is initially dissolved in a common solvent.[12,47] The self-assembly process is under thermodynamical control when the mobility of the polymer chains is high enough. With the addition of the non-solvent to the complete solved block copolymer, the hydrophobic core gets desolvated, and the mobility of the chains is reduced. Above a specific content of the non-solvent, the mobility of the chains is too slow, and after a long period, the thermodynamic equilibrium cannot be reached without further adding good solvent. The resulting structures can be considered as kinetically frozen structures.

An additional influence on the formation behavior occurs when the block copolymer contains a rigid polymer. Stiffer segments cause an increase of the Flory-Huggins interaction parameter χ as a consequence, and self-assembly can already be observed even for low molar mass polymers (lower degree of polymerization N) compared to block copolymers without stiff or crystalline segments.[48]

2.1.3 Crystallization of Polymers

Polymer crystallization can occur in polymer-rich phases such as bulk, precipitation from solution or self-assembly in solution. In comparison to crystallization small molecules, the crystallinity of polymers is never 100%, which leads to semi-crystalline materials with different degrees of crystallinity. Nevertheless, this crystallinity can have a dramatic influence on the physical properties of the material. Even though Katz *et al.* observed crystalline polymers by X-ray diffraction, the mechanism of crystallization is a complicated topic, which, even today is not entirely understood.

When Storks realized in 1938 that fully extended polymer chains are longer than the measured lamellar thickness of the observed crystals, he suggested a folding of the polymer chains in the crystal (Figure 4 a).[49] Although, this theory was later confirmed experimentally in 1957 through observation of polyethylene single crystals, at this time the concept of "fringed micelles" (Figure 4 b) was more accepted and the theory of Storks has not gained much attention. Today, both phenomena are accepted and demonstrate the two concepts of crystalline polymers. While proteins and cellulose are crystallized in "fringed micelles", poly(amide)s, polyolefins, and polyesters are known to form folded-chain crystals.

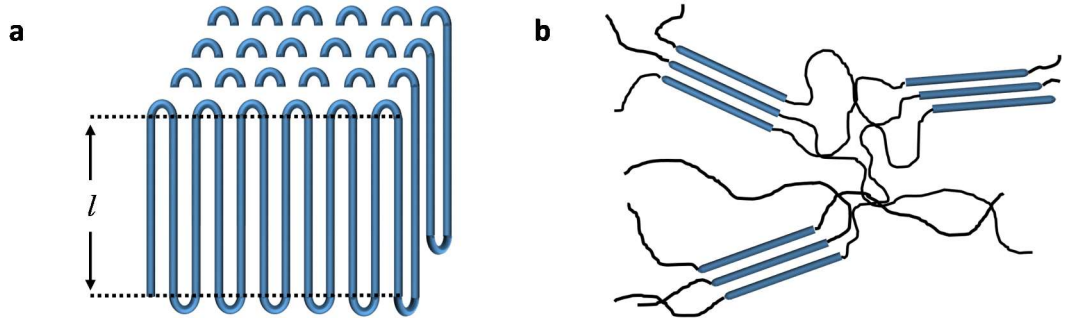

***Figure 4**: Schematic presentation of (a) folded-chain crystal with a lamellar thickness l, (b) "fringed-micelle" with crystalline segments in between amorphous chains.*

The crystallization typically occurs in a two-steps process, with initial nucleation and subsequent growth. The nucleation step itself is separated into two types: homo- and heterogeneous nucleation. In the homogeneous nucleation, small crystals were formed by the parallel alignment of the chains. However, due to thermodynamic reasons, the growth is only possible when the size of the formed crystals are above the critical size. Below the critical size, the crystals disassemble, and no crystal growth occurs. In the heterogeneous or secondary nucleation, additional impurities or already formed crystals were used to increase the nucleation process; therefore, the heterogeneous nucleation is the predominant mechanism in real polymer systems. Various studies on crystallization with added nucleation agents were published; however, the effectiveness of these agents is not fully understood yet.

The crystallization of polymers was described by a model of Hoffmann and Lauritzen, in which the Gibbs-free energy ΔG_E is defined as the determining parameter of crystallization. In a nucleation process, the free energy of the crystallization is given by the difference of the free energy that is needed to form a surface between the crystalline and amorphous part $\Delta G_{surface}$, and the stabilizing free energy of the crystallization $\Delta G_{crystallization}$ (Equation 6).

$$\Delta G_E = \Delta G_{surface} + \Delta G_{crystallizatio}$$

Equation 6

When a small nucleus (embryo) is formed due to fluctuations in density, the surface to volume ratio of this crystalline material is large and therefore $\Delta G_{surface} > \Delta G_{crystallization}$. At this stage ΔG_E is positive, and the embryo tends to disassemble. When the embryo is growing, the volume increases, and which causes a change in surface to volume ratio, which at a certain size leads to a critical maximum of the free energy. Above this critical size, ΔG_E becomes negative ($\Delta G_{surface} < \Delta G_{crystallization}$) and the crystal will grow (Figure 5).

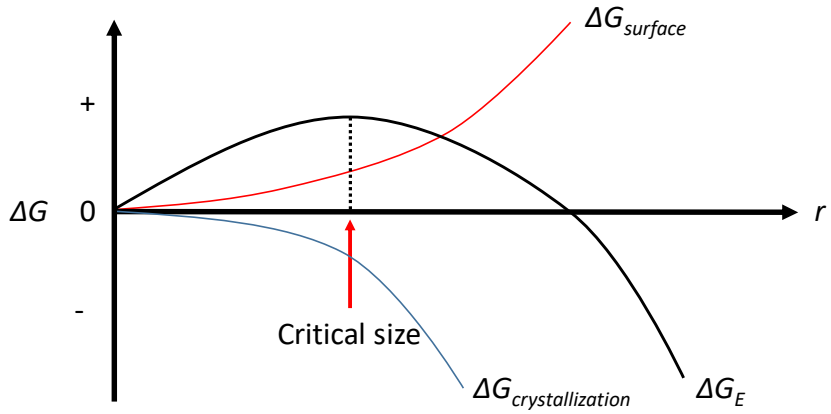

***Figure 5**: Energy evolution of nucleation according to Lauritzen-Hoffman theory.*

Above the critical size, the crystal growth occurs by periodically folded, interconnected chains (Figure 4 a). It is important to note that the theory of Lauritzen and Hoffmann is an oversimplified model, and since their work was published it has been it modified by several people afterward .[50–52] Individual chains need space to assimilate in a crystal, and therefore typically crystallization does not take place for branched or crosslinked polymers. In bulk, the flexibility of polymer chains is given in a range between 30 °C above the glass transition temperature T_g and 10 °C below the melting point T_m.

2.1.4 Poly(lactide)

In this thesis, PLA is used as the hydrophobic component in the amphiphilic block copolymer. Due to the inherent chirality of the monomer, the pure enantiomeric versions PLLA and PDLA are semi-crystalline polymers, and hence other morphologies can be observed as compared to the self-assembled block copolymers with amorphous PLA. For this reason, the next chapter will discuss the reasoning for choosing PLA as the polymer of choice for this work.

2.1.4.1 Lactic Acid

As mentioned in Chapter 1, the building block of PLA is lactic acid, which is the simplest form of hydroxyl acids with an asymmetric carbon (2-hydroxy propionic acid). Lactic acid is the hydroxyl analog of the smallest amino acid alanine and exists in two optical configurations (L(+)- and D(-)-isomers). In nature, the L-form is produced in the human body and some other mammals as well, but both enantiomers are produced in bacterial systems. Lactic acid was isolated for the first time from sour milk by the Swedish chemist Scheele in 1780.[53] Today, it is produced in large scale by bacterial fermentation of carbohydrates such as starch or dextrose (Scheme 1 a-c).[54–56] In industry, 85% of lactic acid is used in food-related fields and acts as an acidic flavoring agent or bacterial inhibitor.

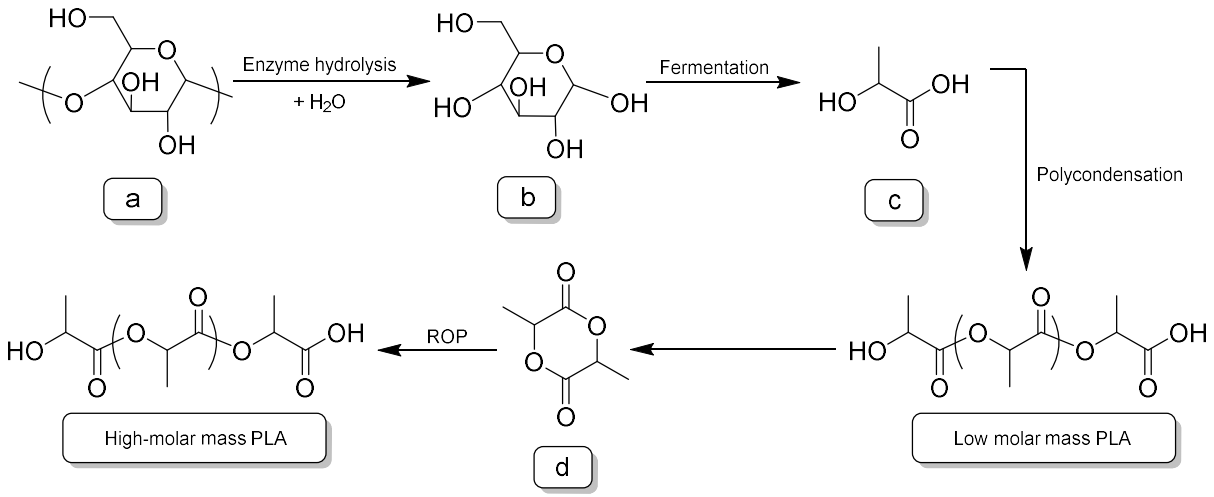

***Scheme 1**: Synthesis of lactic acid and PLA a) from starch by enzymatic hydrolysis to b) Dextrose to the resulting product c) lactic acid by fermentation. Low-molar mass PLA can be synthesized by polycondensation. Depolymerization leads to d) which is the monomer for ROP to high-molar mass PLA.*

2.1.4.2 Synthesis of Poly(lactide)

Since the monomer is produced from renewable resources and the hydrolysis of the polymer leads to harmless products, PLA has found great interest in use for food packaging and medical applications.[57] To obtain a polymer from lactic acid, two synthetic routes are possible. Although polycondensation of lactic acid is the cheapest of both routes, it is not possible to get a high-molar mass polymer in a solvent-free approach or without using specific additives. Competitive reactions occur, such as transesterification, degradation with cleaved water, and "back-biting", which lead to the cyclic diester lactide (Scheme 1 d), resulting in only low-molar mass polymers. To achieve the more useful high-molar mass polymer, PLA needs to be polymerized ROP from the mentioned cyclic lactide (Scheme 1 d).

In 1932, Carothers was able to synthesize polymers from six-membered esters by ROP with $ZnCl_2$ as a catalyst for the first time, although at the time only low-molar mass molecules could be obtained.[58] Since then, many methods have been established to produce PLA from lactide with little or no racemization.[59–66] The ROP with tin(II) bis(2-ethyl hexanoate) (tin or stannous octanoate) as a catalyst is probably the most commonly used because it is approved by the US´s Food and Drug Administration (FDA).[67–69] New organic catalysts, such as 1,8-Diazabicyclo[5.4.0]unde-7-ene (DBU) and 1,5,7-Triazabicyclo[4.4.0]dec-5-ene (TBD), have recently been put forward as good alternatives for ROP of lactide in solution, as they are effective and metal free. In this work, DBU was used as a catalyst, and the mechanism of the polymerization shall be discussed in the next section.

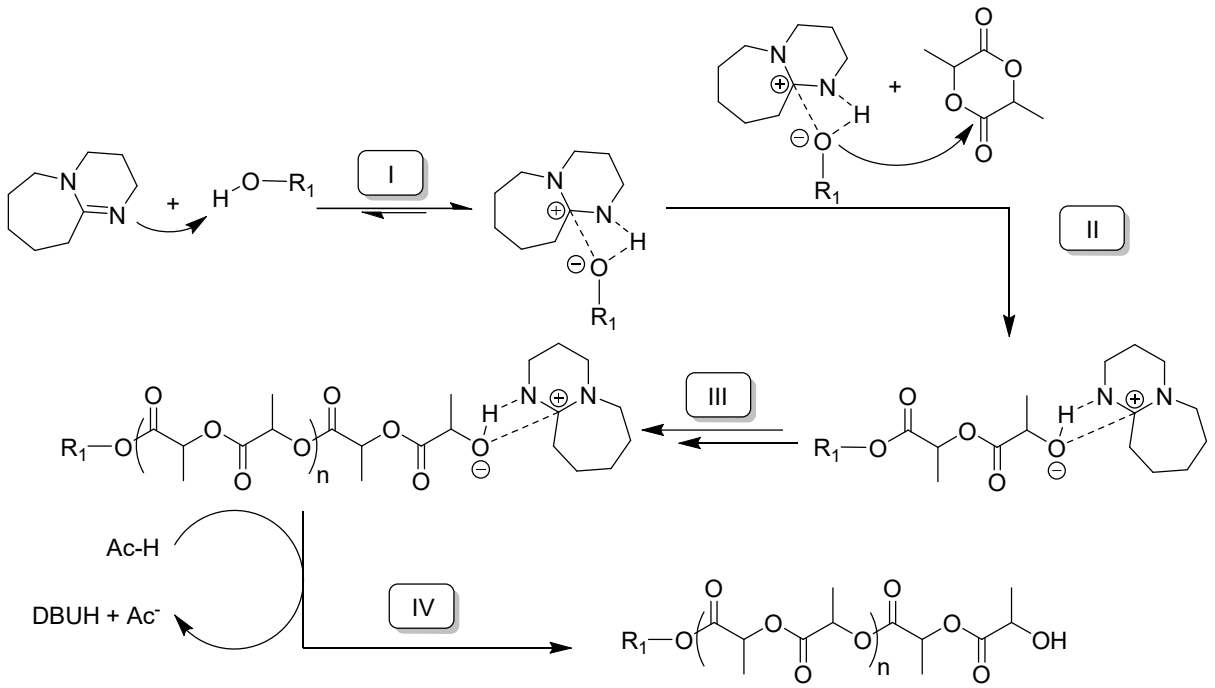

***Scheme 2**: Activated Alcohol Pathway (AAP) of PLA (I) complexation and activation of the initiator (II) the activated alcohol ring-opens the monomer (III) polymerization (IV) Elimination of DBU by adding an excess of an acid to receive PLA with narrow Đ.*

When the mechanism for DBU mediated ROP of lactide is discussed, typically the "Activated Alcohol-Pathway" (AAP), which is presented in Scheme 2, is asserted as the primary mechanism of action.[70] In the first step, the alcohol is activated by DBU through its basic character. The activated species (deprotonated hydroxyl) can open the monomer through nucleophilic attack at the carbonyl, which leads to a propagating species. The propagation occurs until an excess of an acid is used to inactivate the catalyst and therefore terminate the polymerization. As described in the literature, this mechanism is dominant when the initiator (R-OH) to catalyst ratio is [R-OH]:[DBU] ≥ 1. Nevertheless, in addition to the AAP mechanism, a second mechanism can play an essential role within the ROP of lactide. When DBU is in excess ([R-OH]:[DBU] < 1), the "Nucleophilic-Attack Pathway" (NAP) can occur as a competitive reaction. In that case, DBU acts as a nucleophile and initiates the ring-opening polymerization of lactide and generate linear and cyclic polymers.[70,71]

In addition to the aspects of bioavailability and biodegradability, PLA offers an opportunity to modify its physical properties (e.g., melting point, stability, and decomposition) through mixing the enantiomeric partners PLLA and PDLA under certain conditions. These modifications are based on an effect called stereocomplexation, which will be discussed and explained more in detail in the following chapter.

2.1.5 Poly(phosphoester)

In this work, the primary approach was to investigate the aggregation behavior of PLA-based amphiphilic block copolymers and additionally observe the influence of stereocomplexation when two polymers are mixed. As described before in Chapter 1.1.4, PLA-based amphiphilic block copolymers are mainly produced with methoxy polyethylene glycol (PEG-OH) as the initiator to polymerize lactide, whereby a block copolymer with controlled PLA chain length can be obtained. In order to manipulate the aggregation behavior of amphiphilic block copolymers, another hydrophilic polymer was considered. Ideally, this polymer should be usable as an initiating species for lactide polymerization to obtain the same block copolymer-sequence as PEG-PLA. Consequently, when subsequently used for self-assembly, the obtained structures can be compared to the morphologies created by the PEG-PLA block copolymers. At the same time, the polymer should be linkable to the alcohol end of the PLA to produce block copolymers with a different polymer-sequence or triblock copolymers. Therefore, a polymerizable monomer, which can be initiated by a PLA precursor and end up in a hydrophilic block would be the best choice. With this in mind, poly(methyl phosphonate) (PMeP) and poly(isopropyl phosphonate) (P^{i}PrP) (Figure 6), could be found and were selected for this work. The two presented polymers are poly(phosphonate)s and belong as a subclass the poly(phosphoester)s.

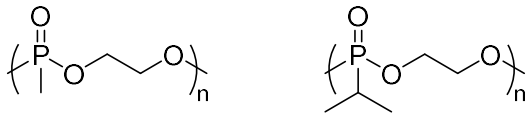

***Figure 6**: (left) poly(methyl phosphonate) and (right) poly(isopropyl phosphonate)*

Poly(phosphoester)s belong to a versatile polymer family that has famous representatives. Adenosine triphosphate (ATP) for example is essential in all living cells in nature and is an energy source for biochemical reactions. Another example, even though with an organic linker between the phosphorus centers, is deoxyribonucleic acid (DNA), which is responsible for the storage of biomedical information and therefore essential for all living species. With the ability to cleave the phosphoester bond enzymatically, poly(phosphoester) can be very interesting for biomedical applications, especially since the possible degradation products as phosphates (PO_4^{3-}) and phosphonates (PRO_3^{2-}) are essential elements in nature and suggests improved biocompatibility and biodegradability. Therefore, poly(phosphonate)s can be seen as a very promising system with low toxicity. By designing the main and side chains, properties like solubility or degradability can be adjusted, meaning that these polymers are of interest in material science. Poly(phosphoester)s can be amorphous, crystalline, hydrophobic or hydrophilic. In industry poly(phosphonate)s have only been utilized as flame-retardant polymer materials. With the ability to vary the side chain, poly(phosphoester) can be achieved in four different subclasses: poly(phosphite)s (or poly(alkylene H-phosphate)s), poly(phosphoamidate)s, poly(phosphate)s, and poly(phosphonate)s (Figure 7).

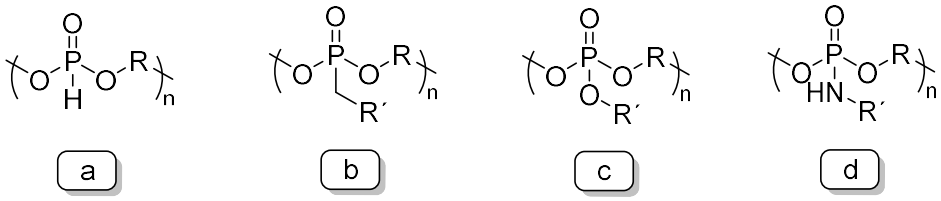

***Figure 7**: Subclasses of poly(phosphoester)s (a) poly(phosphite), (b) poly(phosphonate), (c) poly(phosphate) and (d) poly(phosphoamidate).*

Poly(phosphoester)s can be synthesized by various techniques including polycondensation, polyaddition and Ring-Opening Polymerization (ROP) (Scheme 3).[72–76] However, due to side reactions, classical polycondensation cannot be used to produce high molar mass polymers. [77–82] Additionally, no hydrophilic polymers has been reported so far via this polymerization technique. Similarly, due to the presence of side reactions and the limited amount of required starting materials, polyaddition only plays a subordinate role. Nevertheless, a promising method is the already mentioned ROP of cyclic monomers. Six-membered or five-membered monomers can be polymerized by the cationic or anionic pathways.

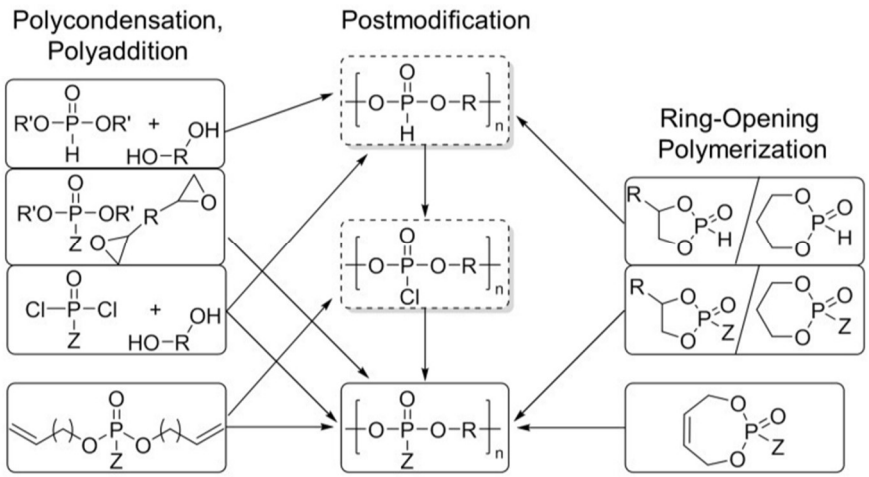

***Scheme 3**: Overview of synthetic pathways to poly(phosphoester)s (Z = O-alkyl, o-aryl, alkyl, Cl, H; R = alkyl, aryl).[76] Reprinted with permission from John Wiley & Sons Inc, Copyright 2015.*

Pencezk *et al.* reported the ROP of cyclic phosphates using an anionic initiator. They utilized six-membered cyclic monomers, which unfortunately have a lower ring strain and resulted in just low molar mass polymers. The five-membered rings were able to ring-open directly with the initiator attack and polymerize via living polymerization. Similar to PLA, $Sn(Oct)_2$, DBU or TBD can be used to produce hydrophilic and hydrophobic poly(phosphoester).[83–85]

Wurm *et al.* adapted this method and reported a living polymerization of cyclic five-membered phosphonates. This was accomplished by synthesizing the monomers in a two-step synthesis (Scheme 4 a). Afterward, they were able to polymerize the cyclic monomer via DBU mediated ROP with primary alcohol and synthesized a water-soluble polymer (Scheme 4 b). Since poly(phosphonate)s have reduced opportunities of transesterification during polymerization, as compared to poly(phosphate)s, a more controlled synthesis is possible.

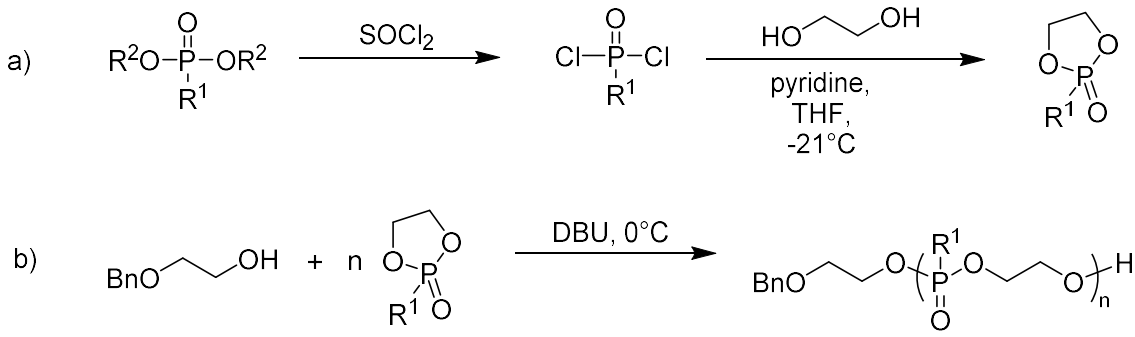

***Scheme 4:** (a) General synthesis of cyclic phosphonate monomers; (b) polymerization of cyclic phosphonates initiated by 2-(benzyloxy)ethanol and catalyzed by DBU at 0°C in dichloromethane.*

Although poly(phosphonate)s have diminished possibility of unwanted transesterifications during the polymerization, two possible side reactions still can occur. This can be rationalized by having a closer look at the structure. A poly(phosphonate) is built from two phosphoester bonds in the main

chain and an alkyl or aryl in the side chain. While for poly(phosphate)s two intra-molecular and two intermolecular transesterifications are possible, there are just two transesterification-pathways (one inter- and one intramolecular) are accessible for poly(phosphonate)s.[86] In Scheme 5 the intramolecular (a) and the intermolecular (b) transesterification of poly(phosphonate)s is presented. The first pathway is describing a cleavage between the phosphorous and the side chain where a polymer species with a cyclic polymer is formed. The second pathway is caused by cleaving the main-chain, which result in polymer cycles and oligomers, which effect molar mass dramatically. An inter-molecular break between the phosphorous atom and the side chain (Scheme 5, pathway 3) causes a hyperbranched architecture with an increase of the molar mass. The last possibility is a rearrangement of the polymer structure (Scheme 5, pathway 4), which looks similar to the non-transesterificated species but will lead to a detectable increase of dispersity (Đ). As mentioned before, only pathways 2 and 4 are available for poly(phosphonate)s and therefore offer a promising alternative to PEG in this thesis.

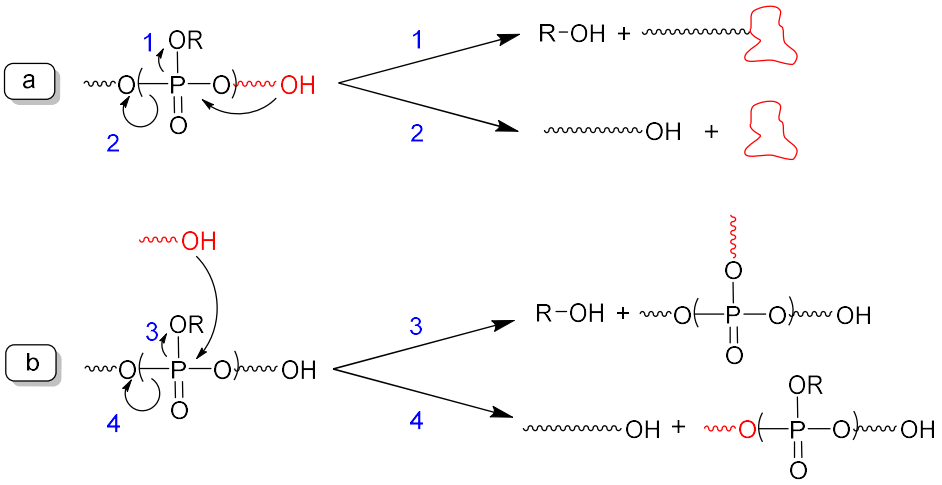

Scheme 5: *Possible pathways for transesterification of PPEs on a (a) intra-molecular and (b) inter-molecular level; (1) cleavage of the side chain of the polymer, causing a formed ring on the polymer chain; (2) break the bond in the main chain which leading to oligomeric ring and smaller polymers than before the transesterification; (3) causing a branched polymer structure by an attack of another polymer at the phosphor; (4) reshuffled polymer structure with broader PDI.*[86]

2.1.6 Stereocomplexation

Stereocomplexation is a rare phenomenon in polymers, only existing in for a few cases. In general, it is an interaction between two polymers, leading to altered physical properties, compared to the parent polymers. A famous example of this behavior is poly(methyl methacrylate) (PMMA), which produce a 1:2 stereocomplex between an isotactic and syndiotactic PMMA conformation.[87] Although until somewhat recently, the general structure was not completely resolved, Elwin Schomaker reported in 1989 a 9_1 double-stranded helix (nine repeating units MMA per turn) of an isotactic chain that is surrounded by a 18_1 helix of the syndiotactic PMMA chain (Figure 8). Thereby, one isotactic unit is enclosed by two syndiotactic units. This lead to a sterically preferred conformation between the two chains, stabilizing the complementary strands by van-der Waals interactions.[88,89]

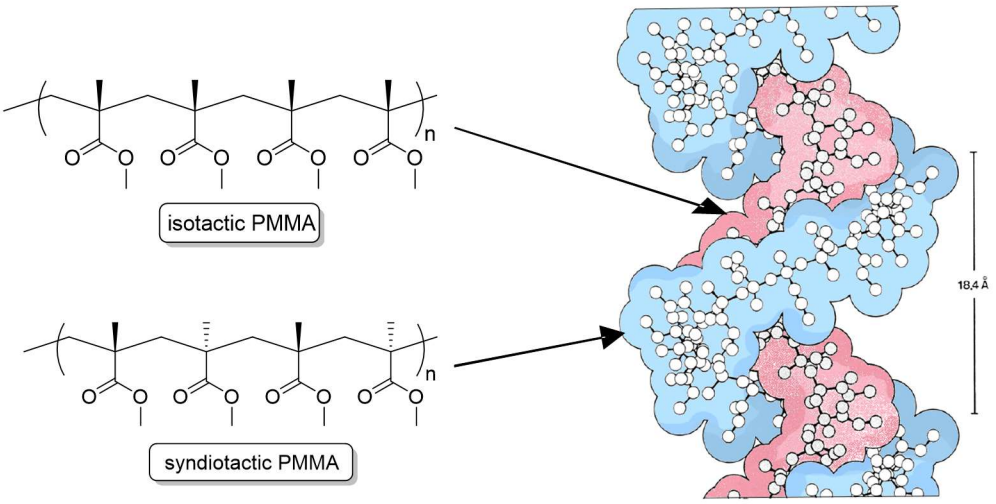

Figure 8: *Schematic presentation of the PMMA-SC consisting out of syndiotactic and atactic polymer chains. The atactic polymer (9_1 helices) is surrounded by the syndiotactic PMMA formed as a 18_1 helix. Figure adapted with permission from Schomaker, E.; Challa, G.* Macromolecules ***1989***, 22 *(8), 3337–3341. Copyright 2018 American Chemical Society.*

A stereocomplex can also be formed between two enantiomeric, optically active polymers with the same chemical composition, which is the case for PLA. The stereocomplex consists of PLLA and PDLa which is most effective in an equimolar ratio (1:1) and is stabilized by van-der-Waals interactions between oxygen and hydrogen atoms. In contrast to the parent polymers, the stereocomplex shows a characteristic increase of the melting temperature of approximately 50 °C. Additionally, in highly concentrated solutions the stereocomplex is not soluble in common solvents for the parent polymers.[90] Instead, slow gelation or precipitation can be observed.[29] The stereocomplex-formation for homopolymers can occur under certain conditions. When dissolving the enantiomeric parent polymers of low concentrations, no crystallization occurs upon mixing. Through precipitation in a non-solvent like methanol, the PLA-stereocomplex will be formed, dependent on the molar mass of the parent polymers and stirring rate.[31] It is worth noting that molar mass is a crucial factor for the

stereocomplexation of PLA. Typically, low molar mass PLA form stereocomplexes are formed without any constraints, while for PLAs above 50 kDa the stereocomplex formation is incomplete and additional homopolymer crystallization occurs. Stereocomplexation can also be observed in the melt, whereas the critical molar mass (the molar mass where stereocomplexation and homo-crystallization occur at the same time) is lower compared to mixtures in solution. With the aim to suppress homo-crystallization, different nucleators can be added to promote the stereocomplexation.[91,92]

In comparison to the single enantiomeric homopolymer of PLA, which crystallizes in a pseudo-orthorhombic or hexagonal cell, the crystalline mixture of PLLA and PDLA is packed generally side by side in a triclinic cell with a 3_1 helix conformation (three lactic acid units per turn / Figure 9).[93] Force Field Simulations from Brizzolara *et al.* have revealed an interaction energy (E_{int}) for antiparallel-orientated PLA-stereocomplex of 111 kcal/mol and 119 kcal/mol for parallel-orientated stereocomplex, which seems to be the preferred conformation.[38]

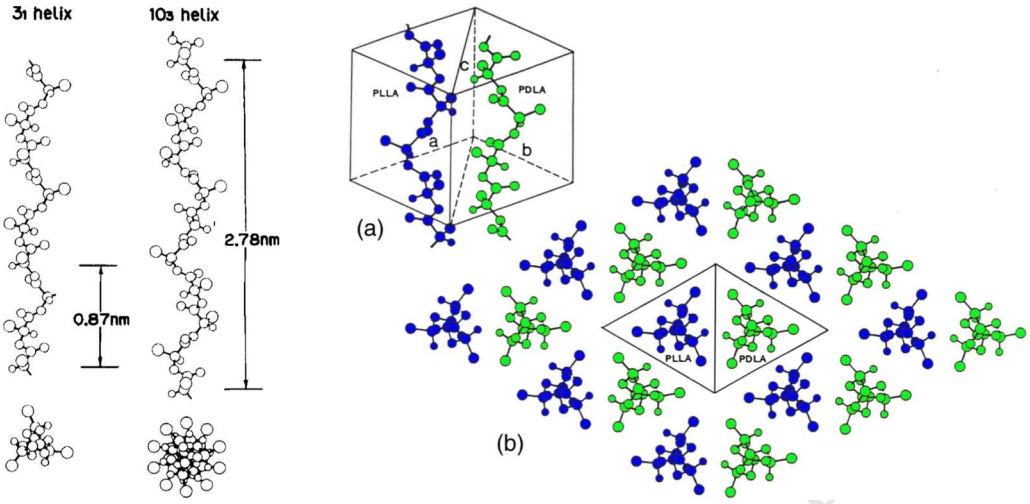

Figure 9: *(left) Models of a 3_1 and 10_3 helix of PLA (right) packaging model of PLA-SC in a triclinic cell based on a 3_1 helix whereas the PLLA having a left-handed and the PDLA a right-handed orientation. Adapted from Okihara, T.; Tsuji, M.; Kawaguchi, A.; Katayama, I.; Tsuji, H.; Hyon, S.; Ikada, Y.* J. Macromol. Sci. Part B Phys. ***1991***, 30:1-2 *(June 2012), 119–140. with permission from Journal of Macromolecular Science, Part B.*

Finally, it has to be noted, that different polymer types can also form stereocomplexes, which are called a hetero-stereocomplexes. One of the most common of these combinations is PLA as a complex-partner to modify and improve the properties of the opposite enantiomeric partner such as poly(2-hydroxybutyrate) or leuprolide.[94–97]

Up to this point, the described stereocomplexation behavior has only been described for homopolymers; it can also be observed and used in amphiphilic systems like copolymers, which self-assemble in solutions or in the melt. The influence of this effect will be described more in detail in Chapter 2.1.7.

2.1.7 Self-assembly of-PLA-based Amphiphilic Copolymers

To underline the idea behind this doctoral thesis, a brief summary shall give an insight into the field of PLA-based amphiphilic block copolymers. The following chapter will guide through the important scientific steps and will present the state-of-the-art of this topic. Additionally, this chapter will point out interesting supplements that should be investigated more in detail within this doctoral work to achieve a better understanding in the field of PLA related self-assembly.

The possibility of combining two polymers with different properties in one chain offers excellent opportunities in applications, and therefore it is not surprising that amphiphilic block copolymers have gained significant interest in science that remains today. The first time an application of an amphiphilic block copolymer was reported in 1955, when Emil A. Vitalis presented a patent, in which polyester-block-methoxy polyethylene glycol was used to impregnate textiles to make them resistant to water and improve the strength of the material.[98] However, in the following years, the interest in degradable materials that can be used for nanoparticles or as micellar drug carriers increased, leading to several studies dealt that with polyester-block-methoxy poly(ethylene glycol) polymers, including polyglycolide (PGA), polycaprolactone (PCL) and poly(lactide) (PLA) as the hydrophobic part. Especially for drug carrier systems self-assembly plays an important role and a general understanding of this mechanism is essential. In drug delivery systems the active substance is loaded in the inner hydrophobic core, and hydrophilic blocks (such as PEG) form the outer shell of the micelle to guarantee the transport of the active substance in the human body. At the same time, absorption and extraction by the reticuloendothelial system are prevented by the hydrophilic block, enabling long circulation times. Currently, PLA-based amphiphilic block copolymers play a unique role in the study of self-assembly systems because the racemic nature of the monomer affects the obtained morphologies such that different results can be achieved according to the starting material. Nevertheless, the general understanding of the self-assembly behavior of PLA-based block copolymers still seems to be incomplete since various investigations have examined different aspects under varying conditions.

An amphiphilic block copolymer can consist of amorphous poly(lactide) (PDLLA) and the corresponding hydrophilic segment. Therefore, poly(lactide) and poly(ethylene glycol) (PLDLA-PEG) were investigated to replace poly(ethylene oxide)-poly(propylene oxide) triblock copolymer (PEO-PPO-PEO) as a drug delivery system. In several publications, it was shown that different sizes of spherical micelles could be obtained by varying the chain length of the amorphous PDLLA block (Figure 10).[99–101]

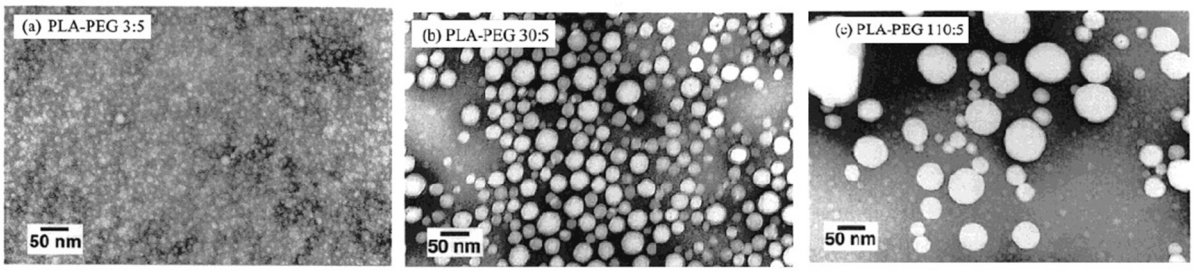

Figure 10*: spherical micelles with different sizes based on the hydrophobic PLA segment. Increasing micelle sizes were observed with increasing amorphous PLA chain length. Adapted with permission from Riley, T.; Stolnik, S.; Heald, C. R.; Xiong, C. D.; Garnett, M. C.; Illum, L.; Davis, S. S.; Purkiss, S. C.; Barlow, R. J.; Gellert, P. R.* Langmuir ***2001****,* 17 *(11), 3168–3174. Copyright 2018 American Chemical Society).*[100]

A more complicated situation arises when the enantiomerically pure PLLA or PDLA are used in an amphiphilic system. As mentioned previously, the enantiomerically pure PLA can crystallize and therefore affect the self-assembly behavior significantly. Fujiwara *et al.* presented a PEG-PLLA block copolymer with molar mass ~ 10 kDa and a weight fraction of PLA of ~ 50%. After self-assembly in water from THF and further sonication, spherical micelles with an amorphous PLA core were obtained. However, after annealing the sample an increase of the crystallinity and a transformation from spheres to helical rods was observed, which was indicated by IR spectroscopy.[102] Similar results were also found by Petzetakis *et al.* and Sun *et al.* who presented poly(L-lactide)-b-poly(acrylic acid) (PLLA-PAA) block copolymers with a crystallizable PLA content of < 50%. They postulated crystallization-driven self-assembly triggered by temperature and an additional common solvent, similar to the mechanism presented previously by Fujimara.[103–105] Nevertheless, a different picture was created by Wang *et al.* in 2016, who showed differently shaped morphologies including rods, micelles, vesicles, and lozenges depending on the additionally used common solvent (tetrahydrofuran, 1,4-dioxane or N,N-dimethylformamide) and amphiphilicity of the PLLA-PEG block copolymer (Figure 11).[106] However, in contrast to Fujimara, Wang *et al.* worked at room temperature and mainly with block copolymers that have PLA weight fractions > 50%. Consequently, all observed morphologies were formed without the influence of higher temperatures, indicating the existence of additional parameters that affect self-assembly.

When stereocomplexation is also considered, the complexity of self-assembly increases. Although there are various reports of multiple PLA-arm block copolymers,[107–111] non-sterocomplexed[112,113] and stereocomplexed triblock[114,115] copolymers including two PLA segments in one polymer, these complex polymers will not be highlighted in this summary. With the intention of understanding the possibilities offered by stereocomplexed PLA-based block copolymer mixtures, this doctoral thesis will focus on linear block copolymers including one PLA block in the main chain.

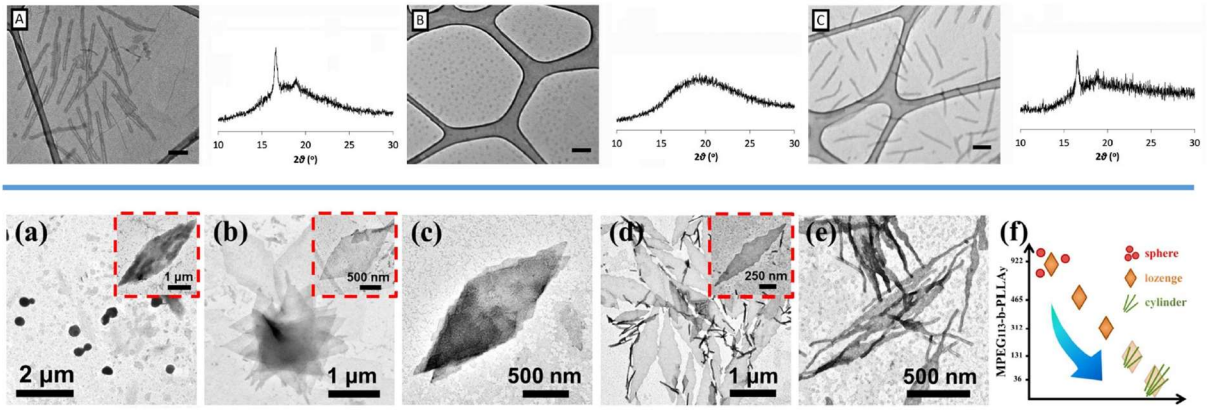

Figure 11*: first raw) Representative EM images of PLA-PAA BCPs with its corresponding WAXD patterns. A) a crystallized sample which followed by B) erasing crystallinity C) recrystallization through an increased temperature. (Adapted from Petzetakis, N.; Dove, A. P.; O'Reilly, R. K.* Chem. Sci. ***2011****,* 2 *(5), 955–960. With permission of The Royal Society Chemistry.)*[104] *Second raw) self-assembled PEG-PLA BCPs with decreasing PLA chain length from left to right. (Adapted with permission from Wang, Z.; Cao, Y.; Song, J.; Xie, Z.; Wang, Y.* Langmuir ***2016****,* 32 *(37), 9633–9639. Copyright 2018 American Chemical Society).*[106]

The first self-assembled structures of stereocomplexed PLA-based block copolymers were reported by Kang *et al.* who described micelles in the range 30-60 nm, depending on the lactide content in the block copolymer (Figure 12). Surprisingly, no significant difference in size was found compared to the parent polymers, which, however, were only studied by DLS experiments. Information on the shape of the morphologies were not provided.[116] Similar results of stereocomplexed polymer mixtures were found by different groups, in which spherical micellar morphologies were produced. However, the sample preparation differed within various reports, which had an impact on the self-assembly mechanisms. On the one hand, the corresponding block copolymer mixtures were simultaneously and directly dissolved in Millipore water, and the obtained morphologies were investigated independent of time.[117]On the other hand, an additional common solvent is used to dissolve the block copolymer mixture first, before adding water to the system.[118] Finally, as a combination of both, block copolymers were also dissolved in the common solvent, mixed in water, and self-assembled individually before mixing. Here, the influence of temperature was studied.[105] It has to be noted that all block copolymers in the described publications had different molar masses and/or block copolymer compositions.

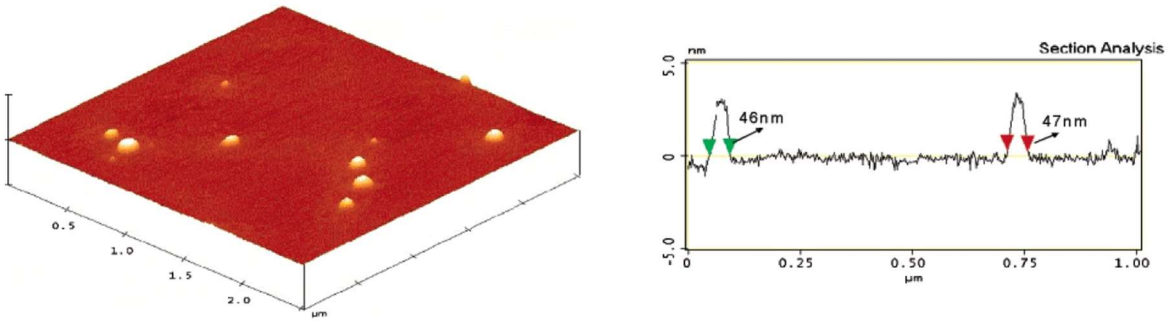

***Figure 12**: AFM image of a stereocomplexed polymeric micelle of PEG-PLLA and PEG PDLA. Adapted with permission from Kang, N.; Perron, M.-È.; Prud'homme, R. E.; Zhang, Y.; Gaucher, G.; Leroux, J.-C.* Nano Lett. ***2005**,* 5 *(2), 315–319. Copyright 2018 American Chemical Society.*[116]

In summary, all discussed approaches reported by these versatile working groups were entirely different and focused on one specific aspect of the self-assembly process. For this reason, this doctoral thesis will address the following questions.

1) Do the previously described rod-like aggregates only occur under the influence of temperature and the addition of a common solvent?
2) How do PLA chain length and the PLA weight fraction affect the self-assembly behavior?
3) How does the stereocomplexation affect the self-assembled morphologies?
4) Can a polymer mixture of PLA-based block copolymers with different polymer sequence influence the obtained morphologies?
5) Can the latter described effect be additionally enforced by polymer mixtures of block copolymers with a different hydrophilic segment on each individual block copolymer?

3 Analytical Methods

3.1 Differential Scanning Calorimetry (DSC)

Differential scanning calorimetry is a comparative method that is used to measure heat differences of a sample that are caused by a physical transition (e.g., melting, evaporation), or chemical reactions (e.g., degradation). In general, two crucibles are subjected to a linear temperature increase, whereby the relative heat flow is measured. While one crucible contains the analyst, the other crucible is empty, and the reference. When the sample undergoes a phase transition during the heating or cooling process, a temperature differences between the sample and the reference occurs through the thermal response of the sample. For instance, at endothermic transitions (e.g., melting, T_m) additional heat is required, which can be observed as a positive peak. In contrast to that, in exothermic transitions (e.g., crystallization, T_c) the produced heat will be rendered to the calorimeter, resulting as a negative peak. The glass transition T_g of an amorphous polymer, which is a second-order transition, can be observed by an endothermic shift of the DSC curve.

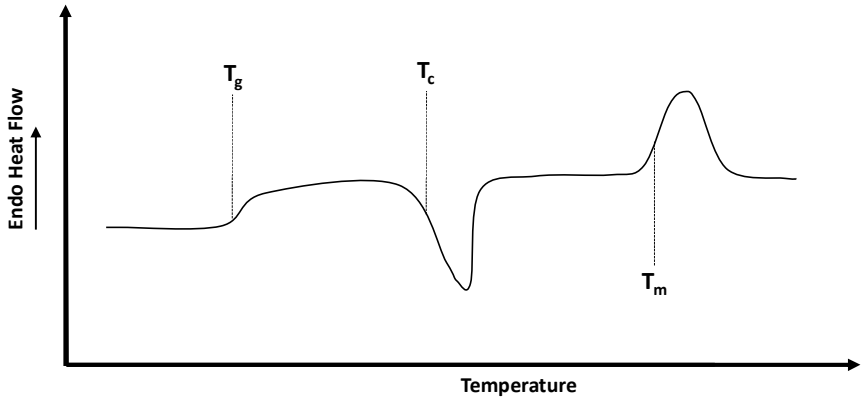

Figure 13: *Schematic illustration of a DSC thermogram.*

3.2 Light Scattering

Interaction of radiation with material can be described by absorption or scattering, where the latter is defined by a change of the direction of propagation of the photons. In daily life, this phenomenon can be observed as well. When a laser is used in a dark room, the laser is still remotely visible caused by scattering of the laser beam by dust particles in the air along the laser path, whereby larger particles cause an increased scattering effect than smaller ones. Additionally, large particles cause scattering in the forward direction, while small particles tend to scatter in all directions regularly. Thus, for intensity

descriptions, the angle needs to be involved to obtain information about the size of the particle that causes beam scattering.

In polymer and colloidal chemistry, light scattering as an analytical is used through two different methods: dynamic light scattering (DLS) and static light scattering (SLS). In both methods, a monochromatic light source is used which, as described before, is essential to obtain valuable information. In Figure 14 a typical setup for light scattering is presented. The aperture consists of a laser (e.g., helium-neon laser; λ = 633 nm), an attenuator, a sample holder in a toluene bath and the angle-dependent detector. The attenuator is needed to reduce the intensity of the laser to avoid damage to the detector. After the attenuator, the beam is split to receive a reference of the incident intensity of the beam, with the second part of that split is incident upon the sample, which is placed in a cuvette. The cuvette itself is placed in a toluene bath. In the end, the scattered light can be detected at specific angles Θ whereby the signal gets autocorrelated for data analysis.

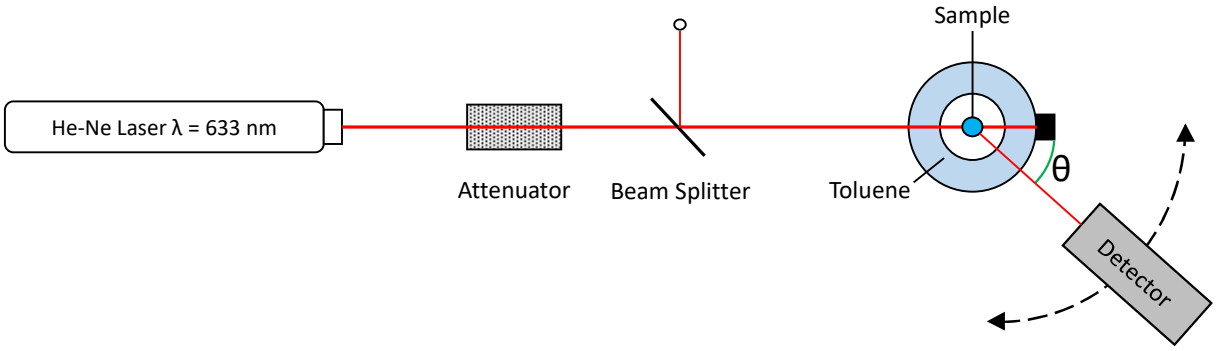

Figure 14: *Schematic construction a light scattering aperture.*

3.2.1 Dynamic Light Scattering (DLS)

DLS utilized monochromatic light to detect the scattering of the incident light on the scattering source (e.g., polymer or particle in solution). Thereby, the so-called Doppler Effect will result either in destructive phases that neutralize each other or in mutually constructive phases that will produce a detectable signal, which further gets autocorrelated.

Because DLS is measured at a specific angle, the area of the detector is minimal in comparison to measurements with SLS, which measured the signal at multiple angles θ resulting in the mean intensity. In consequence, the measured intensity fluctuates, caused by the diffusion of the particles or molecules that move randomly with respect to each other. Therefore, large particles move slowly and small particles move faster, which in combination leads to the mentioned fluctuation (Brownian motion; Figure 15). DLS typically measures the diffusion coefficient D of the particles, which is determined through measurements of the speed of particles in solution.

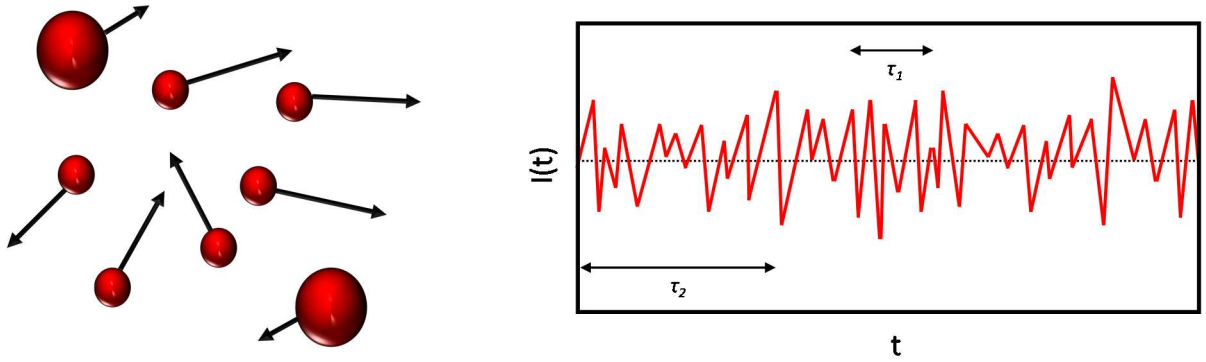

***Figure 15**: (left) Schematic presentation of the Brownian motion, depending on the size of the particle and friction between particle and solvent; (right) schematic presentation of the scattering intensity fluctuation with different correlation times τ.*

The diffusion is correlated to the friction f, which essentially describes the retarding force of particles with the surrounding solvent (Equation 7).

$$f = 6\pi\eta_s r$$

Equation 7

Even though Equation 7 is valid for spherical particles, it additionally can be used for non-spherical particles when constants become modified. The viscosity is described by η_s and the radius of the particle by r. As a result, the friction is higher with bigger radius r or increased viscosity η_s. The diffusion coefficient D can be described as follows:

$$D = \frac{B}{\left(\frac{4\pi n}{\lambda} \cdot sin\left(\frac{\theta}{2}\right)\right)^2}$$

Equation 8

Where the wavelength λ, the scattering angle θ and the refractive index of the solvent n are included in the equation. At the same time, a constant B is embedded, determined through measurements of the solution and the treatment of the data through a so-called autocorrelation function $g_2(\tau)$, which is a sum of the measured intensities (Equation 9). When a solution, with included particles of the same shape and sizes, is measured, $g_2(\tau)$ can be described as:

$$g_{2,theor}\ (\tau) = (A \cdot e^{-B\tau})^2 + 1$$

Equation 9

Thereby, τ is a time variable and representing the so-called correlation time that describes the time separation between light scattering events in the sample (Figure 15 right). A and B are constants and are mathematically translated through fitting between a theoretical and measured autocorrelation

function $g_2(\tau)$. If the solution contains more than one kind of particles, Equation 9 has to be extended to Equation 10.

$$g_{2,theor}\ (\tau) = (A_1 \cdot e^{-B_1\tau} + A_2 \cdot e^{-B_2\tau} + \ldots)^2 + 1$$

Equation 10

As mentioned before, in practice, DLS gives not direct sizes of particles immediately, but rather the diffusion coefficient D of the particles. With the knowledge, that the diffusion depends on friction and the size of the particles (Equation 7), the diffusion coefficient D is additionally thermal energy dependent and can be described as:

$$D = \frac{k_B T}{f}$$

Equation 11

Including Equation 7 into Equation 11, the diffusion coefficient can be described by the resulting Einstein-Stokes equation.

$$D = \frac{k_B T}{6\pi\eta R_h}$$

Equation 12

As a result, Equation 12 can determine the hydrodynamic radius of polymers or aggregated samples. If the solution contains monodisperse particles, the radius measured will be very close to the real radius of the particles in solution. However, if the solution contains more polydispersity particles, the calculated radius needs to be taken with caution. Based on the fact, that the scattering intensity is proportional to the radius of the particle to the power of six (Rayleigh scattering; $I \sim \frac{r^6}{\lambda^4}$), bigger particles having greater influence and will cause to higher values shifted r or R_h. Therefore, it is important to work under dust-free conditions and in diluted systems to exclude artifacts by large dirt particles or overlapping polymers chains.

3.2.2 Static Light Scattering (SLS)[119]

In comparison to DLS, SLS does not depend on the fluctuation of the particle, but rather time averaged scattering intensity I_s is measured in static light scattering (SLS) to determine the weight average of the molar mass M_W, the radius of gyration R_g and the second viral coefficient A_2. In the following chapter, the basic concept of SLS is explained.

The polarizability of the molecule is defining the ability to shift charges within a molecule. When an electromagnetic wave (light) interact with the molecule, an oscillating dipole is created and causes emitting of an electromagnetic wave with the same wavelength as the incident light beam (elastic scattering) at a specific angle (scattering angle). For molecules larger than 20 nm, multiple dipoles can be created within one particle, and the emitted light will cause interferences. The scattering intensity I_s is angle dependent and non-isotropic (Figure 16). For diluted solutions with particles or polymers smaller than $\lambda/20$, the scattering intensity I_s is independent of the scattering angle because of the insignificant phase difference of the emitted light.

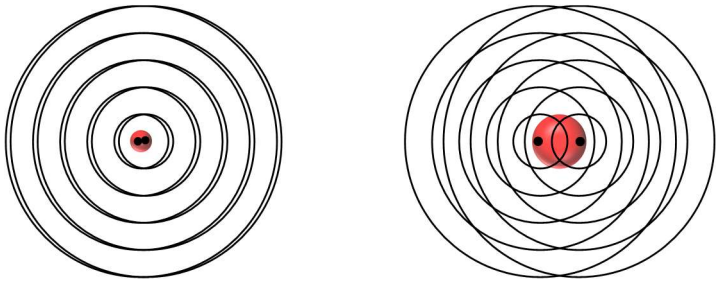

Figure 16: *(left) Schematic interference patterns of scattered light from small particles, (right) interference of scattered light from larger particles with more than one scattering centers, leading to an angular dependence scattering intensity (out of simplification only two centers are shown in both illustrations).*

In SLS experiments, the scattering intensity I_s is detected at a specific angle θ with additional variations of θ. Multiple angles result in multiple scattering intensities and scattering volumes. These values need to be normalized to receive a scattering angle and scattering volume independent value. As a result of this procedure, the absolute scattering intensity can be described by the Rayleigh ratio R (or absolute scattered intensity). The Rayleigh ratio R encapsulates the experimental setup (wavelength λ, sample detector distance r_D and scattering volume V) and experimental conditions like concentration c, molar mass M, scattering intensities of the solvent $I_{solvent}$ and its refractive index $n_{D,0}$ and the scattering intensity of the solution $I_{solution}$ with its refractive index increment $\left(\frac{\partial n_D}{\partial c}\right)$ (Equation 13). The latterly mentioned parameter is a concentration-dependent refractive index of the polymer solution and has to be measured individually or recalculated by known theoretical values.

$$R = b^2 \cdot \frac{cM}{N_L} = \frac{4\pi^2}{{\lambda_0}^4} {n_{D,0}}^2 \left(\frac{\partial n_D}{\partial c}\right)^2 \cdot \frac{cM}{N_L} = (I_{solution} - I_{solvent}) \frac{{r_D}^2}{V}$$

Equation 13

In practice, the total scattered intensity R of the particles in solution is experimentally determined scattered intensities of the solution $I_{solution}$, of the solvent $I_{solvent}$, and the scattering standard $I_{standard}$

(e.g., toluene, described in chapter 3.2) and renormalized through the absolute scattering intensity of the standard $I_{std,abs}$ (literature known).[119]

$$R = (I_{solution} - I_{solvent}) \cdot \frac{I_{std,abs}}{I_{standard}}$$

Equation 14

Including the van´t Hoff equation for real solutions (Equation 15), Equation 16 result from Equation 13 and describes solutions with small-sized particles (d < 10 nm) included, where the contrast factor K is defined through the squared scattering power b^2. The second virial coefficient A_2 describes the interactions between the solvent and the dissolved particles, whereby no interaction occurs when the value is zero.

$$\frac{\partial \pi}{\partial c} = kT \left(\frac{1}{M} + 2A_2 c + \dots\right)$$

Equation 15

$$\frac{Kc}{R} = \frac{1}{M} + 2A_2 c + \cdots$$

Equation 16

In practice, typical particle (especially polymeric particle) solutions containing larger particles than 10 nm which need to be examined. As described before, in that case, the scattering angle θ is no longer independent, and now the so-called scattering vector $\vec{q}$ has to be included. This value can experimentally be determined by the scattering angle θ and the wavelength of the laser λ. The scattering vector $\vec{q}$ can be described as the difference between the wave vector of the incident light $\overrightarrow{k_0}$ and the wave vector of the scattered beam $\vec{k}$ ($\vec{q} = \vec{k} - \overrightarrow{k_0}$). By including the reflective index of the solvent *n*, for elastic scattering processes, the scattering vector can be described as in Equation 17.

$$|\vec{q}| = q = \frac{4\pi \cdot sin\left(\frac{\theta}{2}\right)}{\lambda}$$

Equation 17

Angle-Dependent scattering intensity is the consequence and represents a summation of all scattering centers Z of the single particle. A form factor $P(q)$ has to be introduced to describe the relative distances between all scattering centers $\overrightarrow{r_{i,j}}$ (Equation 18).

$$P(q) = \frac{1}{Z^2} \sum_{i=1}^{Z} \sum_{j=1}^{Z} exp\left(-i\vec{q}\overrightarrow{r_{ij}}\right)$$

Equation 18

When assuming an isotropic, homogeneous particle, the so-called center mass coordinate system can be introduced, and the Cartesian coordinate $\vec{r_i}$ with can be replaced by a center of mass based position vectors $\vec{s_i}$. Conclusively, the particle form factor can be described can be described as

$$P(q) = \left(1 - \frac{1}{3}q^2 s^2 + \cdots\right)$$

Equation 19

where s^2 is the squared radius of gyration R_g. Since in reality not only isotropic particles exist, various form factors $P(q)$ are described, including monodisperse small particles, homogeneous spherical particles, hollow sphere with a thin shell, disks and thin cylindrical particles. However, it has to be mentioned that no matter which form factor is used, it only gives an average combination of all the particles present in the solution. In general, with the use of the form factor $P(q)$ into the Zimm equation (Equation 20) M_W, A_2, and R_g can be determined.

$$\frac{Kc}{R} = \frac{1}{M_w P(q)} + 2A_2 c + \cdots$$

Equation 20

3.3 Electron Microscopy[120]

The human eye is limited in its ability to perceive radiation from the electromagnetic spectrum within a range of 300 – 700 nm. Furthermore, the visible light has to interact with objects by scattering (reflection or refraction) to make them visible for the eye. In the early 20th century it was discovered that electrons have a wavelike character, which as a result leads to better resolution when compared to optical methods and specimen of less than 1 nm are detectable. However, also in electron microscopy (EM), the specimen has to interact with the irradiated electrons and scatter them somehow to make specimen things visible. Figure 17 presents the emission of electrons and electromagnetic waves, which interact with the specimen. Therefore, it has to be mentioned that the amount of scattering depends on the atomic composition of the sample. More atomically heavy atoms scatter more intense than lighter ones. The incident electron beam can be either passed through the sample (transmitted) or scattered back. At the same time, it can interact with the sample whereby electrons in the form of secondary electrons or Auger electrons are released. Additionally, X-rays of specific energy, depending on the sample composition, are scattered back. In the following chapters two EM techniques (TEM and SEM), which use different types of electrons to render images, are presented.

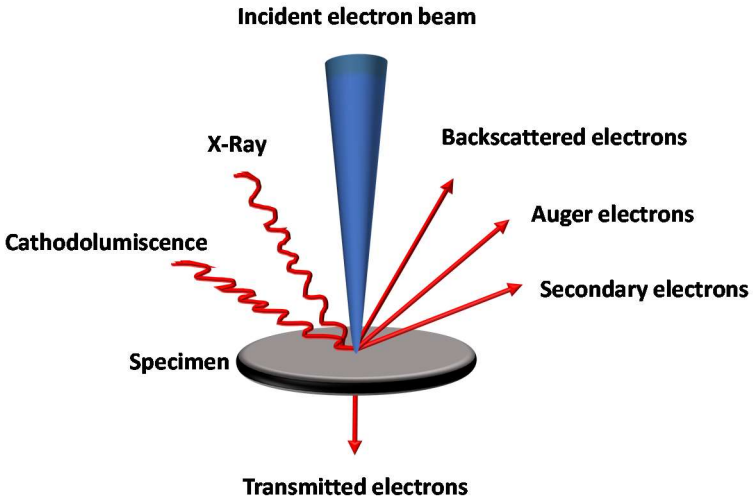

***Figure 17**: Schematic presentation of the interactions of an electron beam with the specimen.*

3.3.1 Transmission Electron Microscopy (TEM)[120]

As the name implies, for TEM the through the electrons transmitted through the sample are detected. Therefore, the sample has to be very thin to permit the transmission. Unlike the transmission of light through glass the detected electrons in TEM are mainly scattered in the same direction as the laser path of the beam. Hence these electrons are detectable as described in chapter 3.2. Therefore, the wavelength of the electron beam is defined by the acceleration voltage (de Broglie; Equation 21), such that different TEM apertures can be used to investigate different types of samples with corresponding resolutions. Typical acceleration voltage for TEM is in a range from 80 kV to 400 kV, and a vacuum is applied to avoid interaction of the incident laser electron beam with air. Usually, the sample is placed on a copper grid, which afterward is covered by a conductive layer, such as carbon, to provide an electronic charge of the specimen.

$$\lambda = \frac{h}{m_e \cdot V_e} = \frac{h}{\sqrt{2m_e \cdot e \cdot U_e}}$$

Equation 21

In principle, the TEM unit is built similar to a light microscope. The electrons exiting from the cathode are accelerated to the anode and bundled through a Wehnelt cylinder. Subsequently, condenser lenses focus the electron beam before passing the sample depending on the thickness and electron transparency of the sample. As previously described, the electrons are then scattered more

or less through the specimen. The objective lens renders the first image of the sample that in further beam path will later be enlarged through the projector lenses.

More complicated than in standard light microscopy is the way to achieve contrast in TEM, especially for polymer materials. When the incident beam is transmitted through the specimen, scattering occurs due to the atoms of the sample. Consequently, a change of the direction in the electron beam occurs. The dependency of the angle of the scattering is related to the thickness of the sample itself and the atomic number of the atoms in the sample. The bigger the atomic number and the larger the thickness of the sample, the higher is the number of electrons in the beam scattered at a high angle. Through a contrasting blend that permanently excludes all high-angle scattered electrons, only electrons without a too large change in direction can pass this stage. Areas with a high number of excluded electrons result in darker areas and produce the contrast in TEM. However, in samples with no significant difference in density additional contrast agents are used to observe the described phenomenon.

To investigate samples in solution, cryogenic transmission microscopy (cryo-TEM) can be used. Therefore, the solution becomes frozen with liquid ethane to guarantee a rapid freezing process to avoid crystallization of water. Therefore, to avoid the destruction of the sample, cryo-TEM operates at a low electron emission voltage.

3.3.2 Scanning Electron Microscopy (SEM)[121,122]

In SEM secondary and backscattered electrons are detected to visualize the topology of the sample. In this case, the electron beam scans the surface of the sample whereby the detector processes the amount of energy of the detected electrons to generate an image of the topography of the specimen. Secondary electrons are produced from the emission of the valence electrons within the sample material when the electron beam enters the specimen. The energy of secondary electrons can only reach a maximum of 50 eV (Figure 18), wherefore they are easily absorbed by the specimen when created at a deep region of the sample. Consequently, the secondary electrons that can be detected are more likely to have been generated from the surface of the specimen. Additionally, it has to be mentioned that the number of secondary electrons is greater when the incident electron beam enters a tilted surface, which leads to different brightness areas in the SEM image.

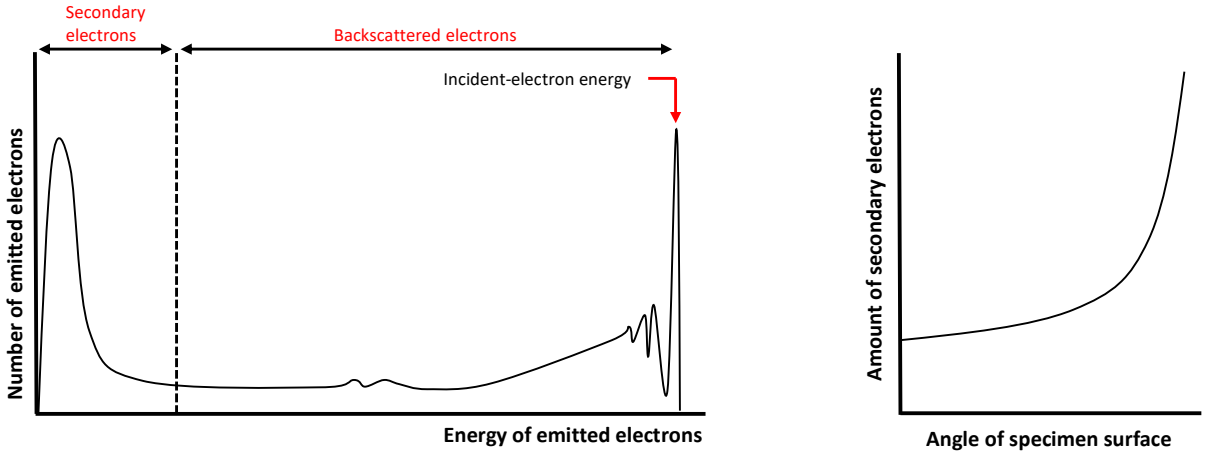

Figure 18: *(left) Energy distribution of electrons emitted from the specimen (right) Relation between the incidence angle of the electron probe and the secondary electron yield.*

As seen in Figure 18, the backscattered electrons have much higher energy compared to the secondary electrons. These electrons are scattered through the sample and are emitted out of the specimen, and thus they offer information from deeper regions from the sample than secondary electrons. The amount of backscattered electrons is related to the atomic number of the atoms in the specimen and is larger with a larger atomic number, which leads to a brighter region in the SEM image.

Similar to TEM, cryogenic scanning electron microscopy (cryo-SEM) is a promising technique to investigate samples in solution. Sample preparation typically involves first, placing the sample in a preparation chamber and gets frozen with liquid nitrogen, fractured, thus and reveals the inner of the solution and the structure of the sample.

4 Synthesis of Poly(lactide)-based Diblock Copolymers

4.1 Choice of the Organic Catalyst

In the last decade, the interest in metal-free, organo-catalyzed ring opening polymerization (ROP) has increased. In literature, DBU is known as a non-nucleophilic base and has been reported for ROP of cyclic esters such as ε-caprolactone, δ-valerolactone, and lactide with good control over molar mass and dispersity. Nevertheless, the mechanism of DBU mediated ROP is not completely understood yet, and recent results postulate a variety of reaction pathways including the nucleophilic attack of DBU on the monomer. The bifunctional organocatalysis was found to be an excellent alternative to tertiary amines, phosphines, or *N*-heterocyclic carbenes.[123] Bifunctional catalysts like DBU/benzoic acid (BA) is proposed to promote the activation of the monomer toward an electrophilic attack and a nucleophilic activation of the initiator.[124] In the intention to choose the right catalyst for the ROP of lactide for the synthesis of block copolymers, DBU, and DBU/BA were investigated more in detail in this work. Within this chapter, the mechanism of DBU mediated polymerization is discussed, including side-reactions and limitations for the polymerization lactide. Since in literature DBU/BA was proposed to yield in a controlled polymerization of lactide, this catalyst was supposed to be a promising alternative. However, it turned out that it was more challenging than expected.

4.1.1 DBU and its Limitations towards a Controlled Polymerization

DBU is a well-known catalyst and belongs to the class of amidines, which in polymerizations activates the initiating/propagating hydroxyl group by hydrogen bonding.[125] At the same time, under certain conditions, DBU itself can initiate the polymerization, and the lactide polymerization follows the "Nucleophilic-Attack Pathway" (NAP) as shown in Scheme 6, species a. It is proposed that DBU acts as the nucleophilic initiator whereby a zwitterion is generated. The zwitterion can further react by several pathways including a pathway that results in cyclic PLAs (Scheme 6 pathway a to c).[71] However, the zwitterion is also able to deprotonate the DBU whereby a terminating ketene aminal group results (Scheme 6 b). With an excess of DBU, the neutral PLA can furthermore go into chain growth.[70,71] It has been shown that it can react terminally with nucleophiles, such as alcohols and moisture, thereby regenerating DBU (Scheme 6 pathway b to c and d).[126]

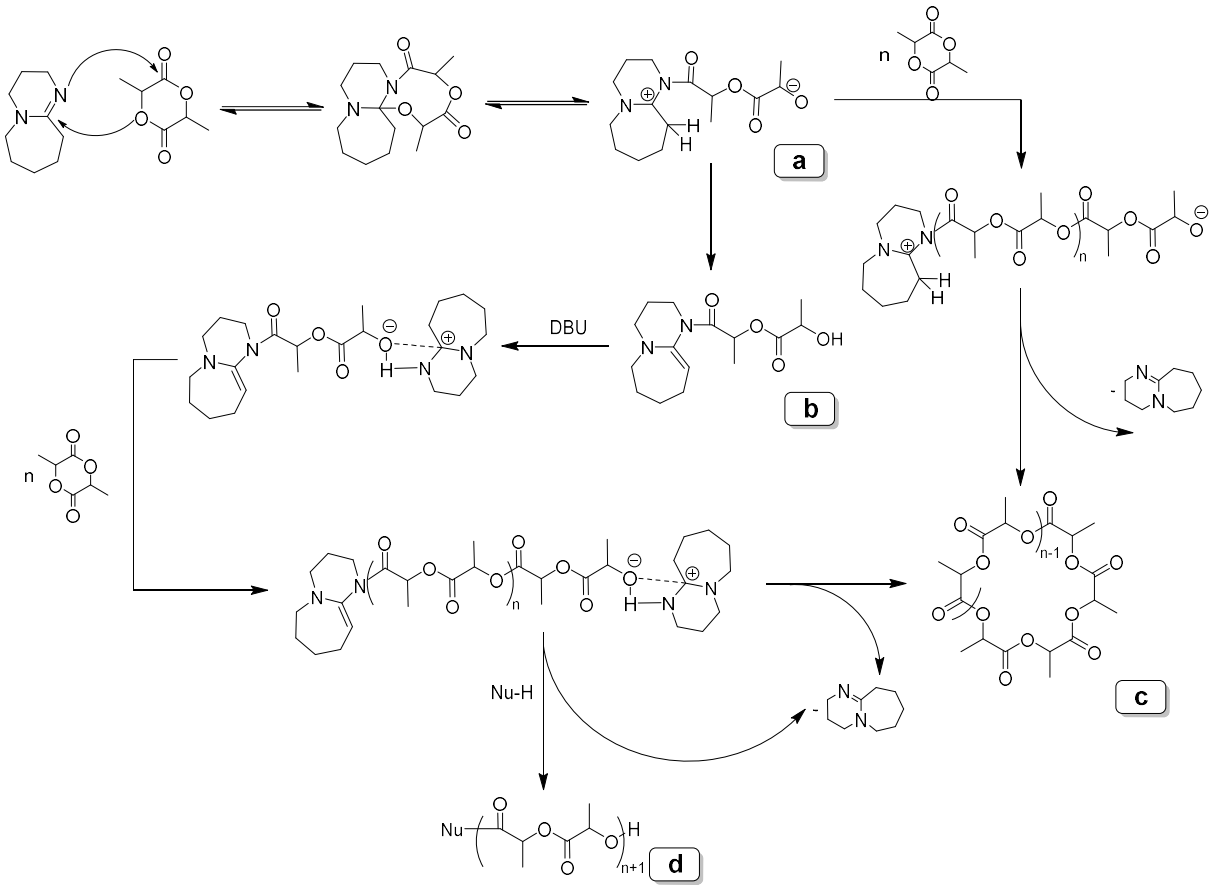

Scheme 6: *Proposed mechanism for the DBU-mediated polymerization of lactide.*

In order to support the nucleophilic character of DBU, a time-dependent polymerization of lactide with DBU (ratio of 100:1) and no additional nucleophilic initiator was performed for 120 min. The polymers were precipitated and further investigated by SEC and MALDI-TOF MS analyses to observe the time-dependent chain growth and its polymer composition (to determine the end group). Within one minute, the polymerization was already advanced, and the MALDI-TOF MS spectrum revealed polymers with a molar mass of $M_n \sim 2500$ g/mol (Figure 19 b). The monomer conversion (x_P) was not determined. However, assuming $X_P = M_n \frac{[I]_0}{[M]_0}$, the monomer conversion can be expected to be ~ 17% after one minute. As described in prior literature, linear PLA chains with -COOH and -OH as terminal groups were identified, whereby the molar mass of the corresponding polymers can be calculated as $M_n/Da = n \times 144.04 + 18 + 39$. Even if one aspect that was not taken into account in the mechanism presented in scheme 6, it has to be noted that also an uneven amount of lactyl repeating units was observed in the MALDI-TOF mass spectra, which is a result of transesterification during the polymerization (Figure 19 c). A second polymer species with an unknown terminal group that has a molecular weight of 56 g/mol was observed in the spectrum, which was not detected for higher molar mass polymers. Although, the latter described m/z peaks would fit to cyclic PLA chains doped with Na^+, this explanation is unlikely since the matrix was potassium trifluoroacetate. Finally ,it

has to be noted that the obtained molar mass obtained by MALDI-TOF MS after 120 min was lower than the theoretical one. Assuming a complete initiation through DBU, this result indicates relevant proportions of side-reactions such as cyclization or transesterifications.

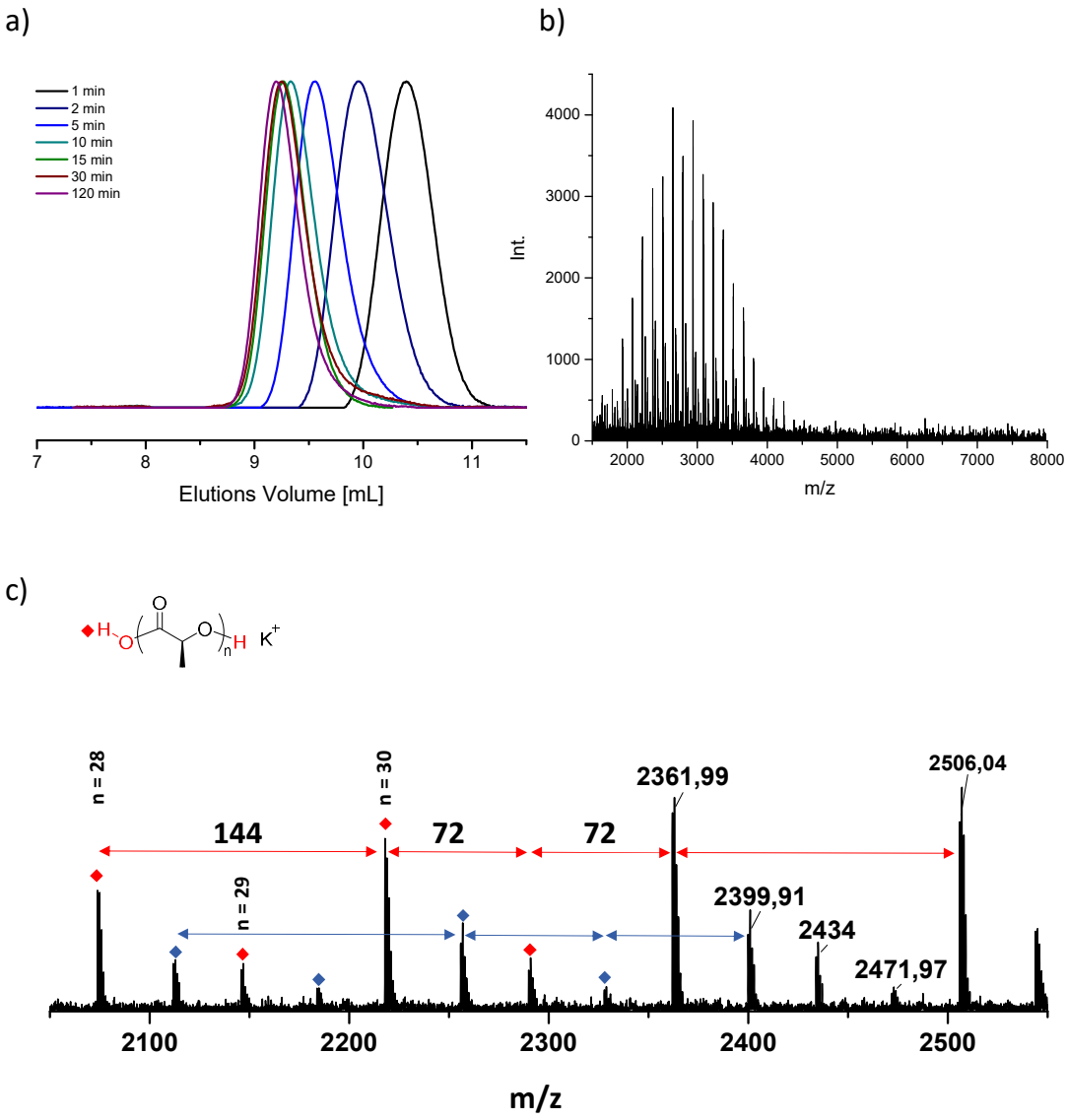

Figure 19: *a) SEC traces of time-dependent PLA polymerization with DBU in the absence of an additional initiator. All polymerizations were terminated with a three-fold excess of benzoic acid and precipitated in Et_2O. b) MALDI-TOF mass spectrum (reflector mode) of quenched polymerization after one minute. c) Extract from spectrum b) (red series corresponds to linear PLA chains terminated with COOH and OH; blue series corresponds to a PLA with unknown end groups with a molecular weight of 56 g/mol).*

The NAP is also reported as a competitive reaction when the alcoholic initiator (such as PEG-OH) is in low quantities compared to DBU.[70] The usual molar ratio of DBU to lactide is 1:100. Consequently, that the maximum chain length, where a controlled polymerization would take place, is 200 lactyl units(lactide is the cyclic dimer of lactic acid, and therefore two repeating units per ring opening occur, $M_n \sim 14{,}400$ g/mol). It is proposed that due to the competitive reaction of individual

growing homo-PLA shifting chains, bimodal distributions can be obtained during the PEG-PLA block copolymer synthesis, an effect that was also observed in this work. Investigated by SEC experiments, increasing intensities of an additional species can be observed with increasing reaction times. Interestingly, the intensities are also depended on the chain length of the initiator, whereby the shorter PEG-OH precursor (2000 Da, Figure 20 a) causes a stronger bimodal distribution than the reaction with the longer PEG-OH (5000 Da, Figure 20 b). As mentioned before, this effect can only be determined by SEC experiments since the analysis with ^{1}H-NMR spectroscopy only presents the number average molar mass of PLA in the system Figure 20 d).

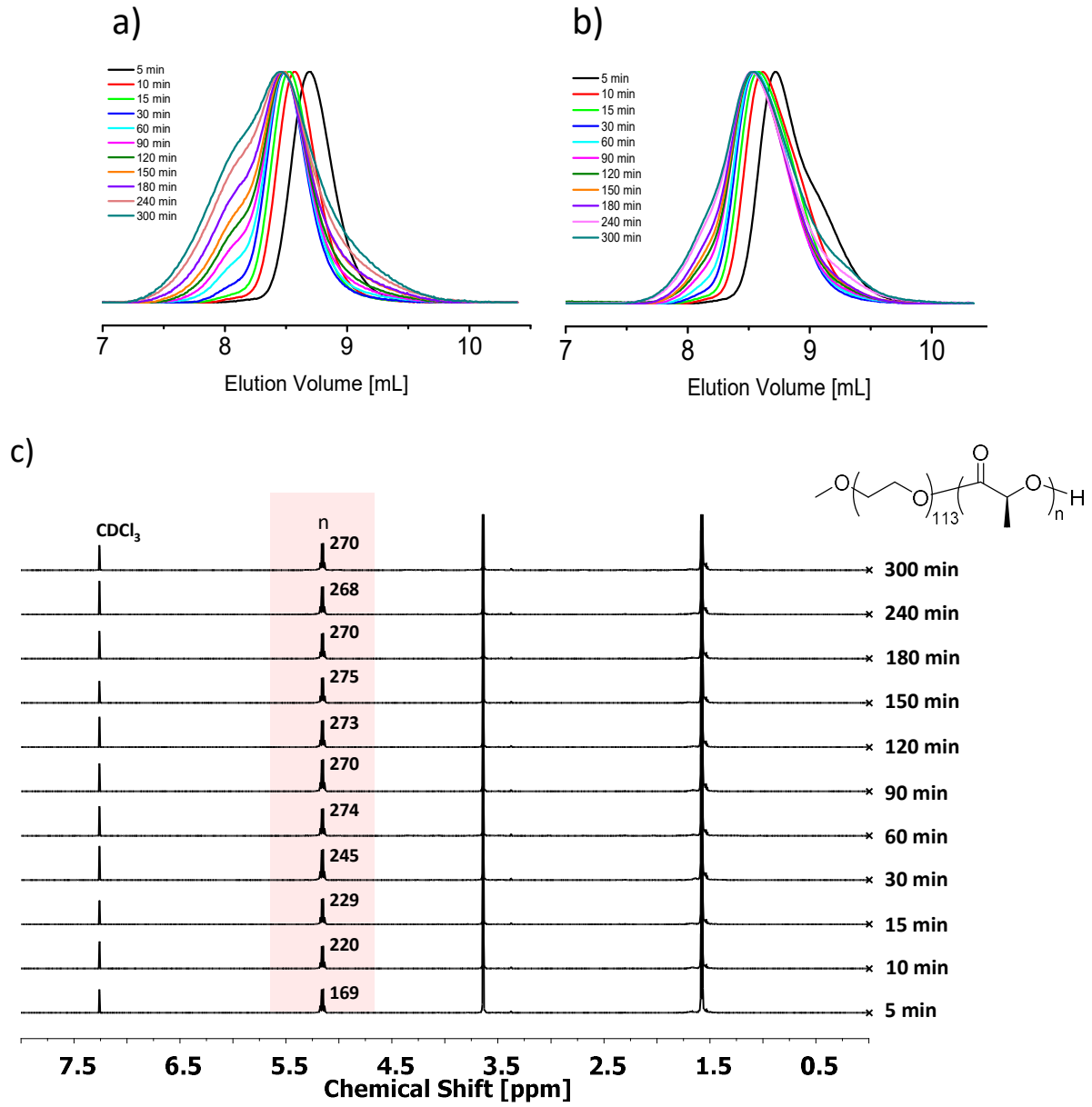

Figure 20: *SEC traces (eluent THF) of time-dependent PEG-PLA block copolymers synthesis. a) Reaction initiated with PEG_{45}; aimed PLA chain length of 277 repeating units (Initiator: DBU = 0.8:1). b) Reaction initiated with PEG_{113} and an aimed PLA chain length of 277 (Initiator: DBU = 0.8:1). d) stacked ^{1}H-NMR spectra ($CDCl_3$, 500 MHz) of time-dependent PEG-PLA block copolymer synthesis of approach b with PEG_{113} as an initiator (Initiator: DBU ratio = 0.8:1).*

Surprisingly, in this thesis, a similar effect was found although the initiator exists in excess compared to DBU (1.44:1). During the polymerization, an unidentified smaller species can be observed, which growth in molar mass and intensity with increasing reaction time (Figure 21). As mentioned before, this observation is in contrast to the described assumption of Sherck *et al.*[70], who only described the NAP when DBU is in excess to the initiator where further research is recommended to investigate the mechanistic process of DBU mediated PLA polymerization more in detail.

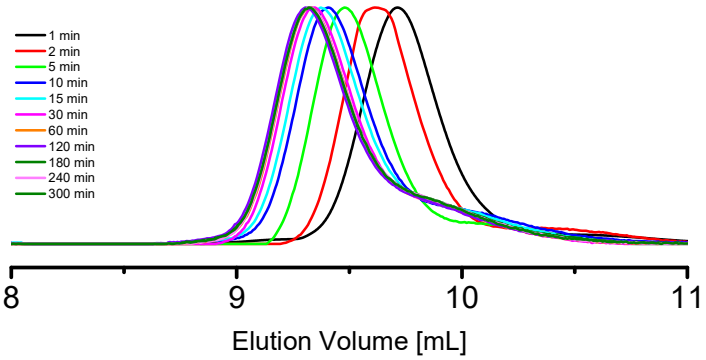

Figure 21: *Reaction initiated with PEG_{113} and an aimed PLA chain length of 139 (Initiator: DBU = 1.44:1).*

With these limiting cases in mind, it was tried to modify the PLA synthesis by the use of another catalytic system to avoid side reactions or transesterifications. Therefore, the reported bifunctional catalyst DBU/BA, which enables an electrophilic and nucleophilic activation, seems to be a good alternative. It would allow to use weaker nucleophiles but still cause the polymerization of PLA.[63]

4.1.2 An Acid/Base Bifunctional Catalyst

As described before, DBU can be quenched by an organic acid, e.g., benzoic acid. Therefore, it was counter-intuitive that the equimolar ratio of DBU and benzoic acid was unable to stop the reaction. However, instead of quenching the reaction, both reagents form an acid/base conjugate, which can polymerize lactide as well. Coady *et al.* [127] reported a controlled lactide polymerization by activation of the monomer by the protonated DBU and a nucleophilic activation of the initiator by the deprotonated benzoic acid. Although the polymerization is dramatically slower than with DBU, this bifunctional catalyst was investigated for the polymerization of PLA-based block copolymers in this doctoral thesis. The DBU/BA salt was synthesized as described in the literature[127], dried under high vacuum and analyzed by ^{1}H- and ^{13}C-NMR spectroscopy (Figure 22).

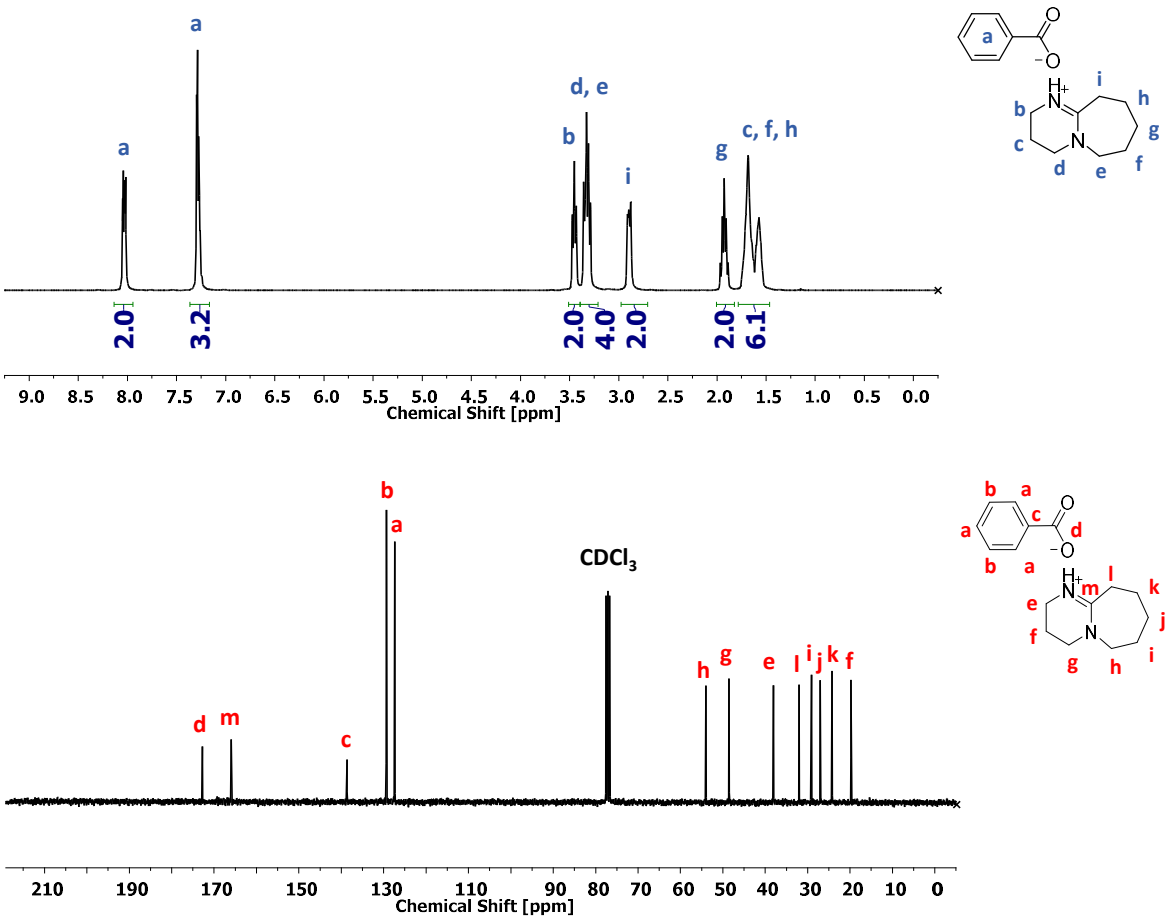

***Figure 22**: [1]H-NMR (300 MHz) and [13]C-NMR (75 MHz) spectra of the synthesized DBU/BA catalyst in $CDCl_3$.*

However, the ROP of PLLA with PEG_{113}-OH as the initiator did not yield in a quantitative conversion, although multiple approaches were made. With the aim to figure out the issue and to optimize the reaction, different monomer concentrations and drying methods for all components were chosen (Table 1). However, no significant differences in the composition of the received block copolymer were found. After precipitation in a non-solvent, lactide conversions between 25-55% were observed by ^{1}H-NMR spectroscopy end group analysis. Additionally, after workup a competitive PLLA homopolymer was observed. The competing homopolymerization of lactide initiated by the catalyst was additionally supported by an individual approach with L-lactide and the bifunctional catalyst salt in solution without an additional initiator. Within 40 hours, unreacted L-lactide and a PLLA-homopolymer with a chain length of 25 lactyl units were observed by ^{1}H-NMR spectroscopy.

Table 1: *Synthesis approaches of different block copolymer synthesis with the bifunctional catalyst DBU/BA*

Sample	Initiator	$[M]_0$	Drying process	Time	Theoretical $DP_{n\ (L\text{-}LA)}$	Measured $DP_{n\ (L\text{-}LA)}$[a]	$DP_{n\ (PLLA)}$[a]
1	PEG-OH	0.1	*D I*[b]	24h	20	5	-
2	PEG-OH	0.15	*D I*[b]	24h	20	11	-
3	PEG-OH	0.3	*D II*[c]	24h	20	7	-
4	PEG-OH	0.45	*D II*[c]	24h	20	5	9
5	PEG-OH	0.15	*D III*[d]	24h	20	12	15
6	-	0.7	*D III*[d]	40h	-	-	25

[a] Measured by ^{1}H-NMR spectroscopy. [b] Recrystallization of L-lactide, dry DCM. [c] Recrystallization of L-lactide, dry DCM, and all dissolved components stored over 3Å molecular sieves. [d] New dry solvents, recrystallization of L-lactide, dry DCM, and all dissolved components stored over 3Å molecular sieves.

Even though no competitive reaction was observed in the literature for the polymerization of PLLA and no explicit reason for the competitive PLLA polymerization within a block copolymer synthesis can be proven so far, two potential side reactions coming into question. First, a linear PLLA chain can be initiated by water. However, all reagents were extensively dried individually with different drying methods before synthesis, but no significant changes were noticed. Therefore, considering the similarities to the presented side reactions with DBU, it seems that the PLLA-homopolymer is a product from the NAP. However, since the NAP would not be possible with the reported mechanism of Coady *et al.,* it can be assumed that the catalytic mechanism of DBU is not changed with the addition of benzoic acid but that the reactivity is reduced. The bifunctional catalyst can be seen as an equilibrium between the dissociated and non-dissociated species, whereby the equilibrium is shifted to the deactivating side with the addition of benzoic acid. Nevertheless, DBU still exists in the equilibrium and can act as a nucleophile as described before. The reduced reactivity of DBU also explains the slow polymerization rate, which additionally will be decreased when one DBU is inserted into a PLA polymer chain and the ratio of DBU to BA as an available catalytic system is reduced. Nevertheless, once the monomer is opened by DBU, the polymerization takes place until a further excess of benzoic acid quenched the reaction. Due to transesterification during the polymerization, the resulting PLA has broad molar mass distributions and a molar mass that is independent of the monomer to catalyst ratio (Figure 23 b).[70,71] This can be supported by a MALDI-TOF MS experiment, which was done within 14 days after the monomer and catalyst solvation without any additional initiator. In the MALDI-TOF mass spectrum, a broad distribution with m/z up to ≈10,000 can be observed. The detected repeating units corresponding to the sodium adducts (M+23 Da) of lactide and its smaller in intensity potassium adducts (M+39 Da). Nevertheless, through end group analysis of the corresponding MALDI-TOF MS spectra, linear PLA chains with -COOH and -OH terminal groups could be identified (Figure 23 a).

Although ROP initiated by moisture cannot be completely excluded with certainty, however, these results are similar to phenomena presented before with DBU. In contrast to the postulated mechanism by Coady *et al.,* these results indicate the catalytic effect of DBU instead of the acid/base conjugate.

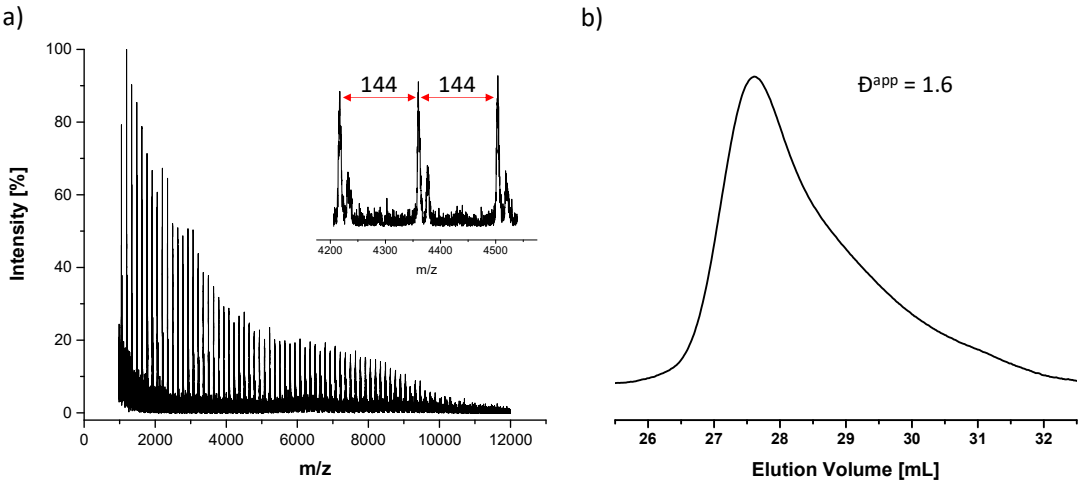

***Figure 23**: a) MALDI-TOF MS spectra of PLLA initiated by bifunctional organic catalyst DBU/BA and b) corresponding SEC trace (eluent THF).*

Consequently, under the described conditions and an equimolar of the initiator to catalyst ratio, the bifunctional catalyst does not work out for the synthesis of PLA-based block copolymers.

4.1.3 Conclusion on Initiator Choice

Due to the occurrence of transesterification, the choice of the right catalyst for the synthesis PLA is crucial. Therefore, in this chapter, two organic catalysts (DBU and DBU/BA) were examined for the synthesis of PLA-based block copolymers. Firstly, the limiting cases of DBU mediated ROP of lactide were shown. On the one hand, DBU can act as an initiator itself, whereby the polymerization of lactide occurs by the "Nucleophilic-Attack Pathway" (NAP). As already described in the literature, this polymerization can be observed when no additional nucleophilic initiator is added to the system, or DBU exists in excess to the initiator. However, a similar phenomenon (bimodal distributions, detected by SEC) was observed even though DBU exist in lower quantities than the initiator. This indicates, on the one hand, the existence of the NAP at although DBU exists in low quantities, or, on the other hand, the presence of still unidentified side reactions during the polymerization. However, to clarify these issues, the system needs to be investigated more closely in the future and will not specifically be explored in this work.

With the intent to avoid these side reactions, a DBU/BA bifunctional catalyst was investigated. This catalyst was reported in the literature, but not used for the synthesis of block copolymers. It was found to be impractical for the PEG-OH initiated block copolymer synthesis, due to competitive homopolymerizations of lactide during block copolymer synthesis. It is assumed that in contrast to the reported mechanism, the unprotonated DBU is responsible for the catalytic effect. Due to the acid-base equilibrium, the unprotonated DBU occurs only in small quantities. Consequently, the catalytic activity is reduced, and the polymerization rate slowed down with an increasing amount of benzoic acid in the system. The assumptions can be supported by similar competitive reactions that were observed for DBU mediated lactide polymerizations, as presented at the beginning of the chapter and in the previously reported literature.

Consequently, in this doctoral work DBU was further used for the synthesis of the PEG-PLA block copolymers, since the aimed lactyl chain length in the block copolymers was set to a maximum of 140 repeating units. The reaction conditions were adjusted to obtain defined PLA chain length and polymers with narrow molar mass distributions.

4.2 Synthesis of PEG-PLA Block Copolymers and Characterization

Two series of PEG_m-PLLA_n (A) and PEG_m-PDLA_n (B) block copolymers (*m*, *n*: average numbers of ethylene oxide and lactide repeating units, respectively) were synthesized by organo-catalyzed ring-opening polymerization of L- or D-lactide using α-methoxy-PEG_m-OH as macroinitiator (Scheme 7). Two different PEG samples with *m* = 45 and 113 were selected, and the chain length of PLA varied between *n* = 18 and 145 (*i.e.*, weight fraction of PLA, w_{PLA} = 0.21 – 0.84). The reaction was quenched with benzoic acid and purified by precipitation and subsequently dialyzed against tetrahydrofuran (THF) and water for a couple of days. Additionally, two amphiphilic PLA -PEG_{113} block copolymers with enantiomeric pure PLLA and PDLA were synthesized. After that, the corresponding PLA homopolymers were synthesized and end groups modified with succinic anhydride in a second step. Finally, PEG_{113} was added to the polymer via a Steglich esterification (Scheme 7 b). The polymers were purified by precipitation and dialysis as described before. After this, all polymers were freeze-dried and stored at -20°C and were stable over months. The products were characterized by ^{1}H-NMR spectroscopy through end-group analysis, infrared spectroscopy, and size-exclusion chromatography to prove the chemical structure and targeted molar mass as well as molar mass distribution.

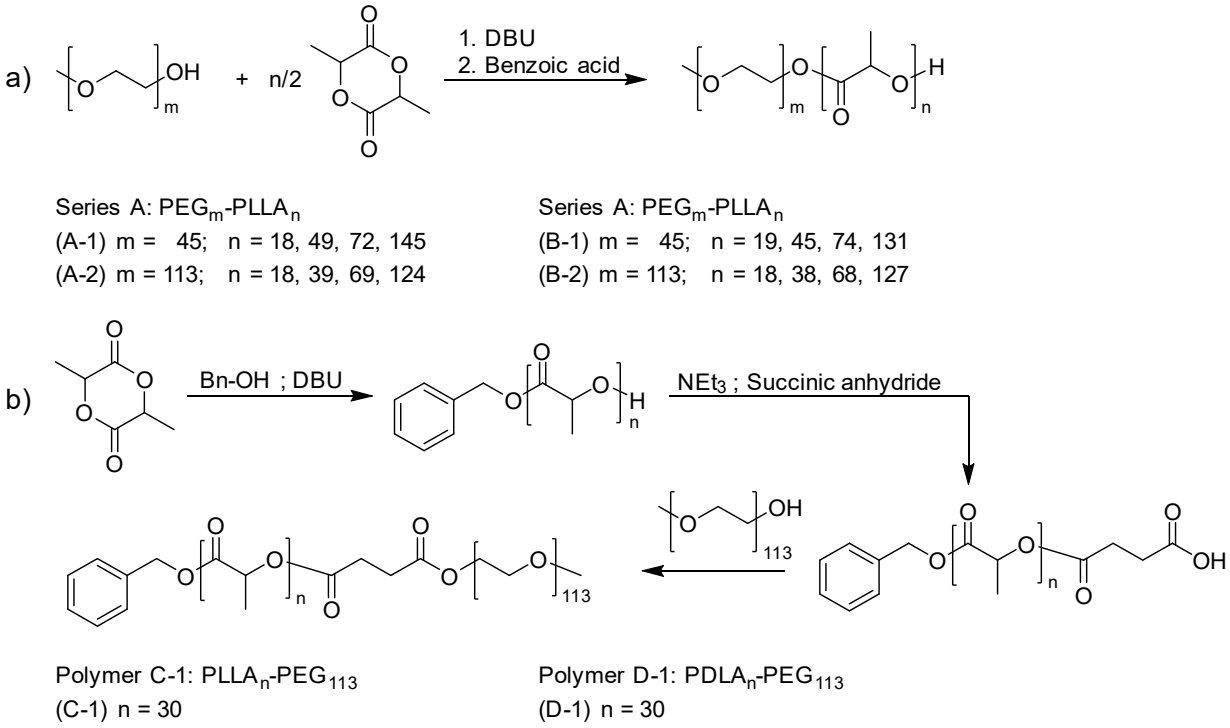

***Scheme 7**: Scheme of polymerization of PLA-based amphiphilic block copolymers (a) ring opening polymerization of lactide, initiated with PEG_{45} or PEG_{113} (b) multiple step synthesis of corresponding PLA-PEG block copolymers.*

A representative ^{1}H-NMR spectrum of a PEG-PLA block copolymer is presented in Figure 24. The repeating units were calculated by end group analysis whereby the singlet of the methoxy-group of PEG (Figure 24; proton *a*) or the multiplett of three corresponding protons *h* and *d* can be used to determine the length (n) of the PLA block. Furthermore, for all polymers narrow size distributions ($Đ^{app}$) were obtained (Figure 24 b-d), and PLA chain length close to the theoretical values.

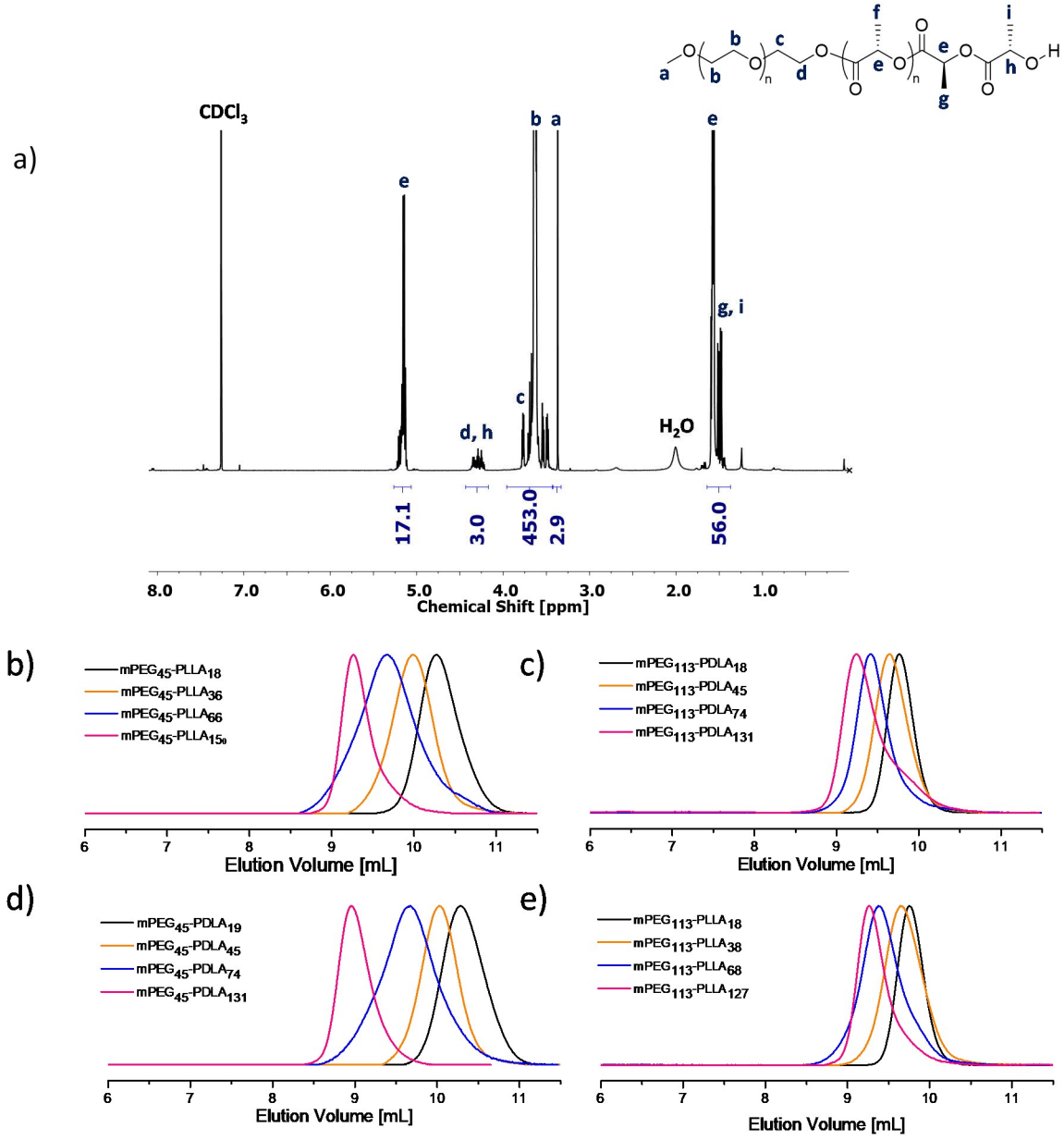

Figure 24:*(a) ^{1}H-NMR spectra ($CDCl_3$, 500 MHz) of synthesized PEG_{113}-$PLLA_{18}$ (b, c, d, e) SEC RI traces (eluent THF) of all synthesized PEG-PLA block copolymers*

In contrast to the PEG-PLA block copolymers, the end group analysis of the PLA-PEG copolymers can proceed by normalizing the two protons *g* as shown in Figure 25 and using this as a reference peak. It must be noted, that the value of the integral at the chemical shift (δ) of 5.24 – 5.03 ppm is not the

actual amount of protons in the repeating unit. The total value of the integral must be subtracted with the number of protons of position *b*, which is superimposed by the protons of *c* (Figure 25 a and b).

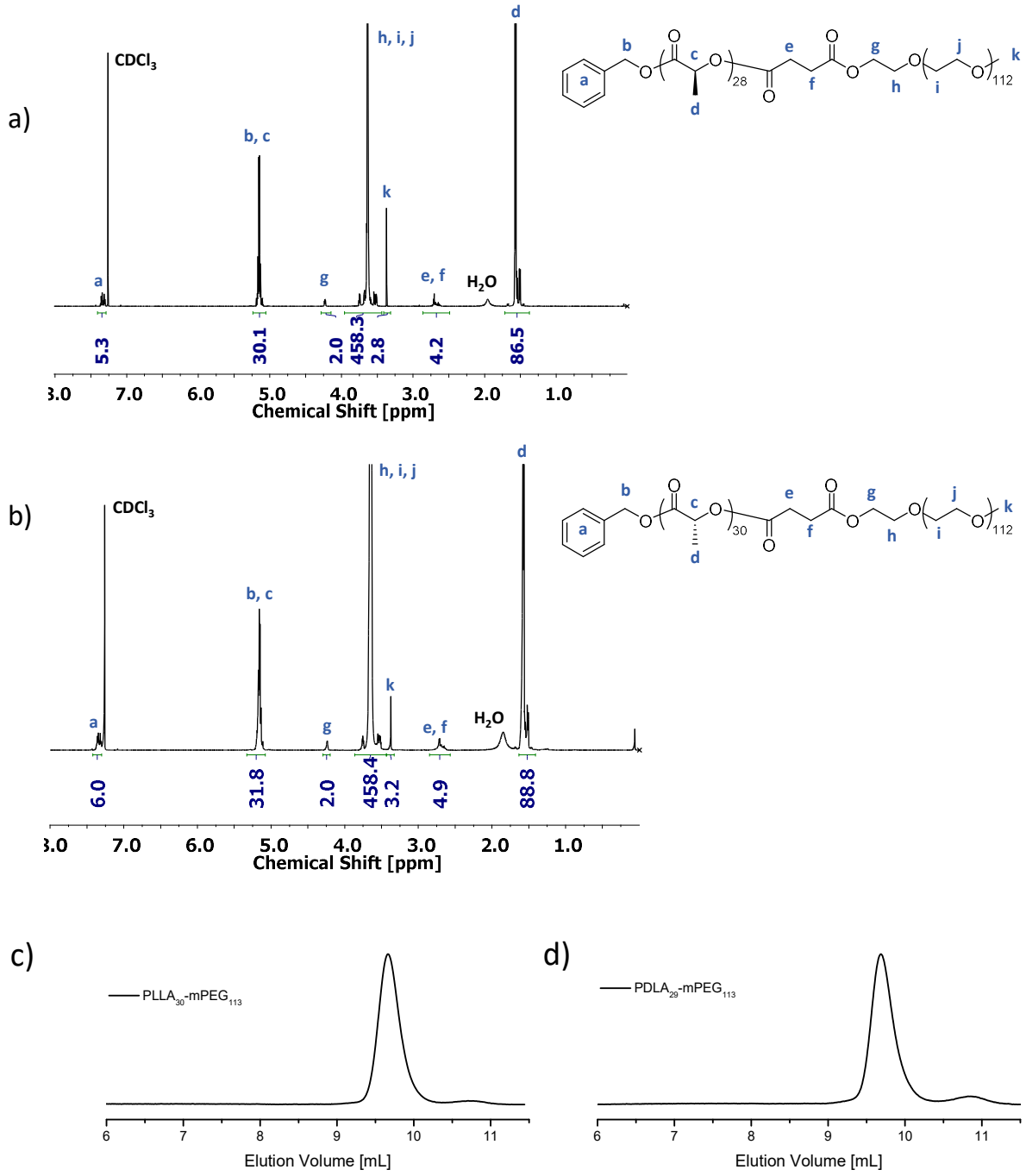

Figure 25: *^{1}H-NMR spectra (500 MHz) of synthesized PLA-PEG block copolymers in $CDCl_3$ and the corresponding SEC RI traces in THF (a, c) $PLLA_{30}$-PEG_{113} (b, d) $PLLA_{30}$-PEG_{113}*

However, in the SEC traces (eluent THF) an additional peak between 10.2 – 11.5 mL with different intensities was detected for both samples (Figure 25 c and d). This peak corresponds to the modified PLA that acted as the precursor, as described before (Scheme 7 b). Even after multiple purification attempts (precipitation, dialyzing against THF and THF/ water mixture) the precursor was

not removed completely. Based on SEC, the PLLA-COOH and PDLA-COOH residue in the presented products constitute approximately 3 wt% for $PLLA_{28}$-$mPEG_{113}$ and 6 wt% for $PDLA_{30}$-$mPEG_{113}$. Consequently, the calculated chain length for both block copolymers is affected to higher values, and the chain should be shorter than evaluated by ^{1}H-NMR spectroscopy. However, the calculated difference is in an error range of 1-2 repeating units.

***Table 2**: Molecular characteristics of PEG-PLA and PLA-PEG block copolymers*

Series	Sample [a]	w_{PLA} [a]	M_n^{app} (g/mol) [b]	$Đ^{app}$ [b]
A-1	PEG_{45}-$PLLA_{18}$	0.39	5.400	1.10
	PEG_{45}-$PLLA_{49}$	0.64	8.200	1.10
	PEG_{45}-$PLLA_{72}$	0.72	11.300	1.21
	PEG_{45}-$PLLA_{145}$	0.84	13.400	1.10
A-2	PEG_{113}-$PLLA_{18}$	0.21	10.800	1.04
	PEG_{113}-$PLLA_{39}$	0.36	11.800	1.07
	PEG_{113}-$PLLA_{69}$	0.50	15.400	1.11
	PEG_{113}-$PLLA_{124}$	0.64	17.100	1.07
B-1	PEG_{45}-$PDLA_{19}$	0.41	5.400	1.10
	PEG_{45}-$PDLA_{45}$	0.62	7.800	1.09
	PEG_{45}-$PDLA_{74}$	0.73	10.900	1.21
	PEG_{45}-$PDLA_{131}$	0.83	13.300	1.10
B-2	PEG_{113}-$PDLA_{19}$	0.21	10.800	1.04
	PEG_{113}-$PDLA_{38}$	0.35	11.900	1.07
	PEG_{113}-$PDLA_{68}$	0.49	15.100	1.08
	PEG_{113}-$PDLA_{127}$	0.65	15.600	1.08
C-1	$PLLA_{28}$-PEG_{113}	0.30	11.900	1.03
D-1	$PDLA_{30}$-PEG_{113}	0.30	11.500	1.03

[a)] Copolymer composition (w_{PLA} = weight fraction of PLA in the block copolymer) and the average number of repeating units were determined by ^{1}H-NMR spectroscopy (500 MHz, $CDCl_3$). [b)] Apparent number-average molar masses (M_n^{app}) and dispersity indexes ($Đ^{app}$) were determined by SEC (eluent: THF, calibration: polystyrene).

Figure 26 shows the block copolymers used in this study and their hydrophilic and hydrophobic in a schematic form.

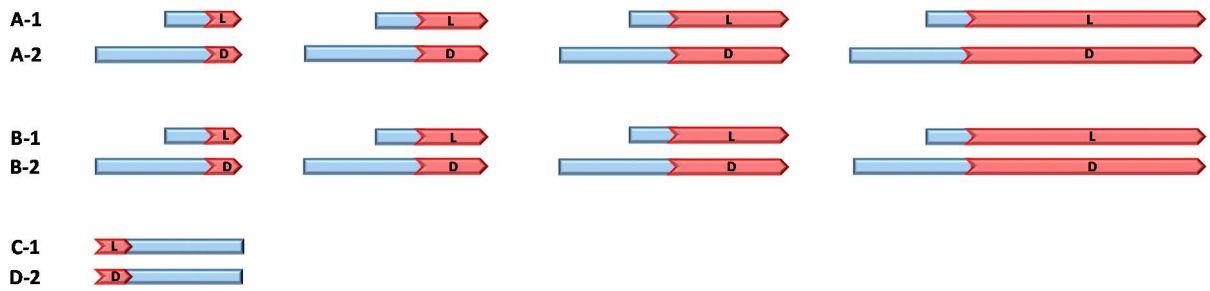

Figure 26: *Illustration of all synthesized PEG-PLA and PLA- PEG block copolymers used for the self-assembly experiments. The blue sections represent the hydrophilic PEG blocks, and the red-striped section represents the PLLA or PDLA blocks (slash stripes represent the L-configuration, and the backslash-like stripes represent the D configuration, respectively).*

5 Poly(lactide)-Based Amphiphilic Block Copolymers: Crystallization Induced Self-Assembly and Stereocomplexation

5.1 Experimental

The PLA-based block copolymers used for this study are described in chapter 4 and presented in Table 2 including PEG-PLA and PLA-PEG copolymers. See Appendix for all synthesis and analytic details.

5.1.1 Preparation of the Aggregates

The self-assembly of the PEG-PDLA and PDLA-PEG block copolymers is not expected to differ from that of the PEG-PLLA and PLLA-PEG block copolymers. Therefore, experiments involving the self-assembly in solution of only one polymer species (as opposed to mixtures) were performed using the series A-1, A-2, and C-1, according to a previously reported protocol.[106] It should be mentioned that all preparations and experiments were performed at room temperature, which is below the glass transition temperature (*i.e.*, T_g > 35°C) of the PLA block. [128]

All PLLA-based amphiphilic block copolymers were dissolved 1,4-dioxane at a concentration of 0.1 wt%. A thrice amount of Millipore water was subsequently added with a flow rate of 0.03 mL/min under constant stirring. The mixtures were then placed in a dialysis bag (molar mass cutoff of 1000 g/mol) and dialyzed against Millipore water for three days to remove the 1,4-dioxane. The resulting aqueous dispersions contained ~ 0.02 wt% polymer and were used for DLS and TEM analysis. The dispersions were used to prepare samples for TEM and DLS characterization. However, for DLS analysis, a second sample was prepared, in which the dispersion was filtered (0.45 µm pores/cut-off).

For the stereocomplexes, a 1:1 mixture of the individual block copolymers individually dissolved in 1,4-dioxane, with matching PLLA/PDLA chain length were prepared, following the same procedure as described before. Additionally, the self-assembly of PEG_{113}-$PDLA_{18}$ (B-2) and $PLLA_{30}$-PEG_{113} (C-2) was examined in order to investigate the influence of the polymer block sequence the stereocomplexed structures.

5.1.2 Sample Preparation for Crystallinity and Crystal Structure Characterization

To determine the crystallinity and the crystal structure of PLA within the self-assembled morphologies, 1wt% solutions of PEG-PLLA, and PLLA-PEG block copolymers and the corresponding mixtures were prepared. In literature, it has been shown that the crystallinity of the PLA block is affected by the common solvent that is used within the self-assembly. Due to different abilities of different common solvents to solvate the PLA and PEG blocks, the resulting self-assembled structures in aqueous solution, and obtained crystallinities of PLA can vary with the choice of the common solvent. Nevertheless, the solubility parameters of 1,4-dioxane and tetrahydrofuran (THF) are quite similar and does not cause a remarkable difference in the observed crystallinity of PLA.[106]

For the individual block copolymers, the corresponding polymers of series A-1 and A-2 were dissolved in THF and subsequently added into water (three times the volume of THF). The organic solvent was removed by evaporation in a laminar flow of air for one day, which led to a polymer concentration of 1 wt%. For the stereocomplexed mixtures, the block copolymers were individually dissolved in THF, mixed with the matching partner, and added to water (three times the volume of THF). As done with the single block copolymers, the organic solvent was also removed by evaporation under laminar flow, and dispersions with a polymer concentration of 1 wt% were obtained. Finally, all dispersions were then either freeze-dried immediately or shaken for three days before lyophilization. The solid samples were used for characterization by differential scanning calorimetry (DSC) and wide-angle X-ray diffraction (WAXD).

5.2 Results and Discussion

5.2.1 Aqueous Self-Assembly of PEG-PLA Block Copolymers

The DSC analyses (Figure 27) of the freeze-dried amphiphilic block copolymers revealed two melting points per sample. The lower one at around 40°C and 55°C, was allocated to the PEG_{45} and PEG_{113} blocks, respectively. Although the hydrophilic block is not crystalline in solution, the melting point is caused by the sample preparation for DSC and WAXD that included lyophilization. The glass transition temperature T_g for PEG is typically below 0°C.[129] Therefore, the polymer can organize during the freeze-drying process and create crystalline domains within the polymer block. The second melting point was ascribed to the PLLA block, and increases with increasing PLLA chain lengths. This melting point and its enthalpy were not affected by the preparation method since every step was performed below the glass transition temperature of PLA and correspond to the crystallinity of the self-assembled structures in aqueous solution. The degree of crystallinity χ_{PLLA} was calculated according to Equation 22

$$\chi_{PLLA} = \frac{\Delta H_{cc} - \Delta H_m}{\Delta H_{100\%} \cdot w_{PLLA}} \cdot 100\%$$

Equation 22

where ΔH_{cc} is the cold crystallization enthalpy, ΔH_m is the melting enthalpy of the PLA block, $\Delta H_{100\%}$ is the melting enthalpy of a virtually 100% crystalline PLA with 93.1 J/g,[130] and w_{PLLA} is the weight fraction of the PLA block in the block copolymer. After one day of self-assembly in solution, the crystallinity of the PLLA block varied between 22 and 46%. Interestingly, the degree of crystallinity increased to as much as 57% with progressive maturity of the block copolymer solution, thereby highlighting the slow crystallization process of PLA-based block copolymers below the PLLA´s T_g. However, the most hydrophilic sample PEG_{113}-$PLLA_{18}$ exhibited a rather low crystallinity around 15% independent of time.

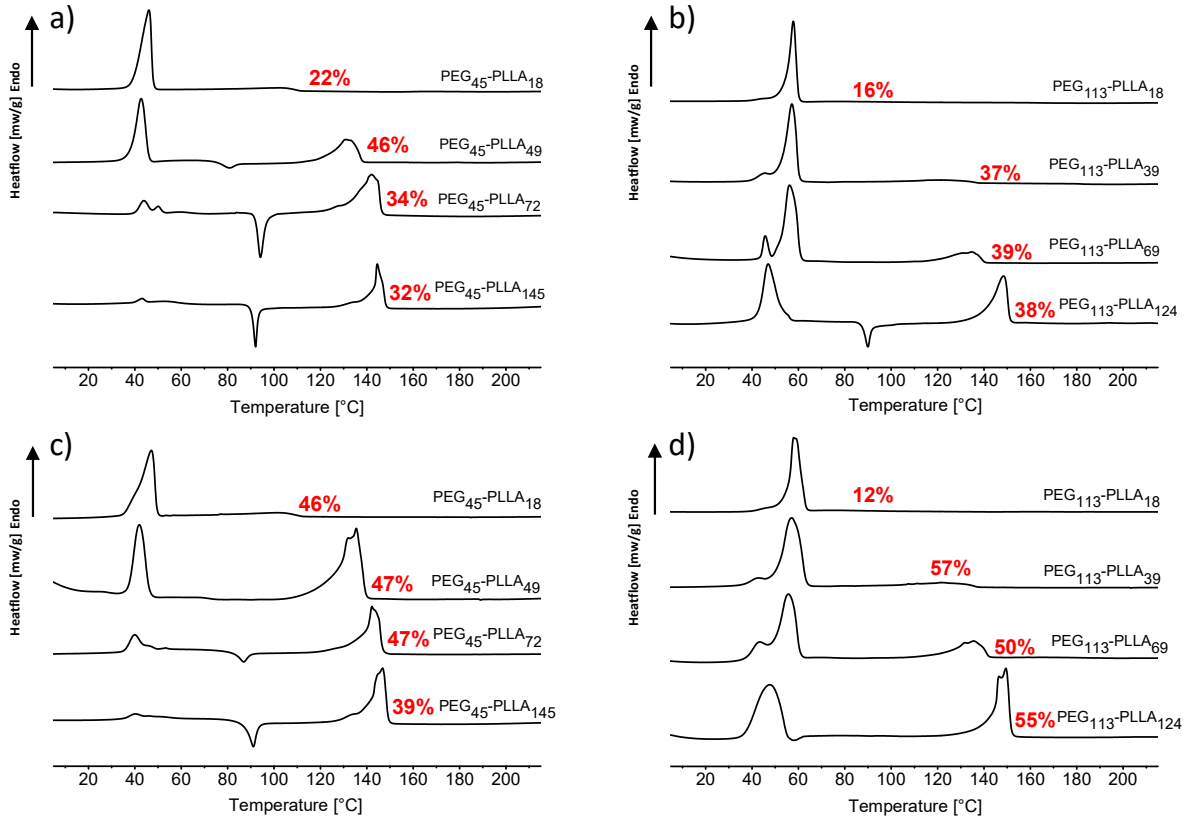

Figure 27: *DSC curves (first heating cycle) of self-assembled and freeze-dried PEG-PLLA block copolymers (a, b) self-assembly for one day before freeze-drying (c, d) self-assembly for four days and freeze-dried. The values in red correspond to the crystallinity of the PLA block.*

Dynamic light scattering (DLS) measurements (Figure 28) were carried out with unfiltered samples, like those used for TEM measurements, as well as with a filtered version of the original sample as a control. The solutions that were filtered with 0.45 µm filters generated DLS results with different size distributions compared to the unfiltered samples. The measured sized were smaller, indicating a loss of material. Big worm-like structures or vesicles, as observed in literature before[106], might be filtered off. However, against the expected trend, large structures with an apparent hydrodynamic radius $R_h > 100\ nm$ can be observed for the most hydrophilic block copolymers (i.e., with the largest PEG/PLA ratios). An increasing amount of small species with $R_h \sim 10 - 20\ nm$ was observed for polymers with longer PLLA blocks, even though the large aforementioned species did not disappear entirely whether the solution was filtered or unfiltered. Nevertheless, as mentioned in chapter 3.2.1, DLS is an intensity-weighted measurement technique. As such, the technique overestimates the larger structures in solutions containing species of different sizes. As a result, species with R_h of $10 - 20\ nm$ are in fact the dominant fraction in the sample.

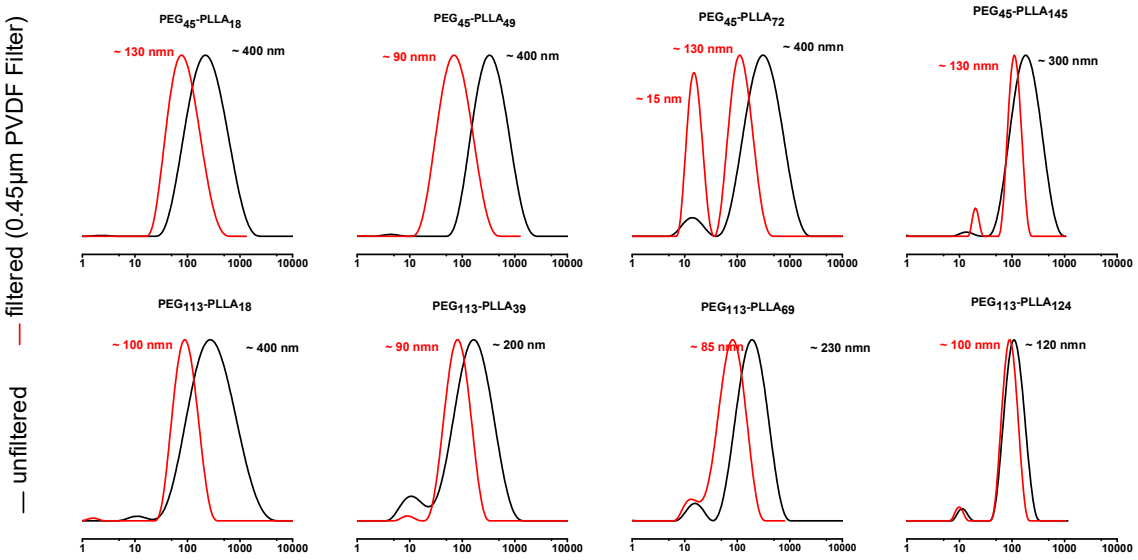

Figure 28: *DLS measurements of self-assembled block copolymers of series A-1 (Top line) and A-2 (Bottom line). The black colored curves correspond to the unfiltered and the red one to the filtered polymer dispersions.*

Due to the small difference in density and the resulting low contrast of polymers in the transmission electron microscopy (TEM),[120] the dried aqueous PEG-PLLA block copolymer dispersions were stained negatively with phosphotungstic acid (PTA). This way, the hydrophilic PEG shell appeared dark, whereas the PLLA core appeared lighter in the micrographs. As presented in Figure 29, the block copolymers formed dominantly either spherical or worm-like core-shell aggregates, depending on the PLLA and PEG block lengths.

By comparing the two series A-1 (Figure 29, left column), and A-2 (Figure 29, left column) a similar trend for the structure transition with increasing PLA block length was identified for both series. However, by taking a closer look into the structures, slight differences between the two series become noticeable. With PEG_{45} as the precursor, the block copolymers PEG_{45}-$PLLA_{18}$, PEG_{45}-$PLLA_{49}$, and PEG_{45}-$PLLA_{72}$ mainly aggregated into the aforementioned microns-long worm-like structures as well as into spherical micelles, but to a lesser extent. It should be noted that with an increasing PLLA chain length the ratio of worm-like to spherical structures decreases and finds its minimum with PEG_{45}-$PLLA_{145}$. For the latter block copolymer, primarily spherical structures were formed. Similarly, with an increasing hydrophobic block length, i.e., PLA chain length, the diameter of the spherical structures increased. For example, spheres generated by PEG_{45}-$PLLA_{18}$, PEG_{45}-$PLLA_{49}$, PEG_{45}-$PLLA_{72}$, and PEG_{45}-$PLLA_{145}$ had diameters of 8.3 ± 1.0, 15.6 ± 1.5, 19.4 ± 1.1 and 25.3 ± 2.2 nm, respectively, whereas the worm-like aggregates had relatively constant diameters of around 11-12 nm, irrespective of the PLLA block length.

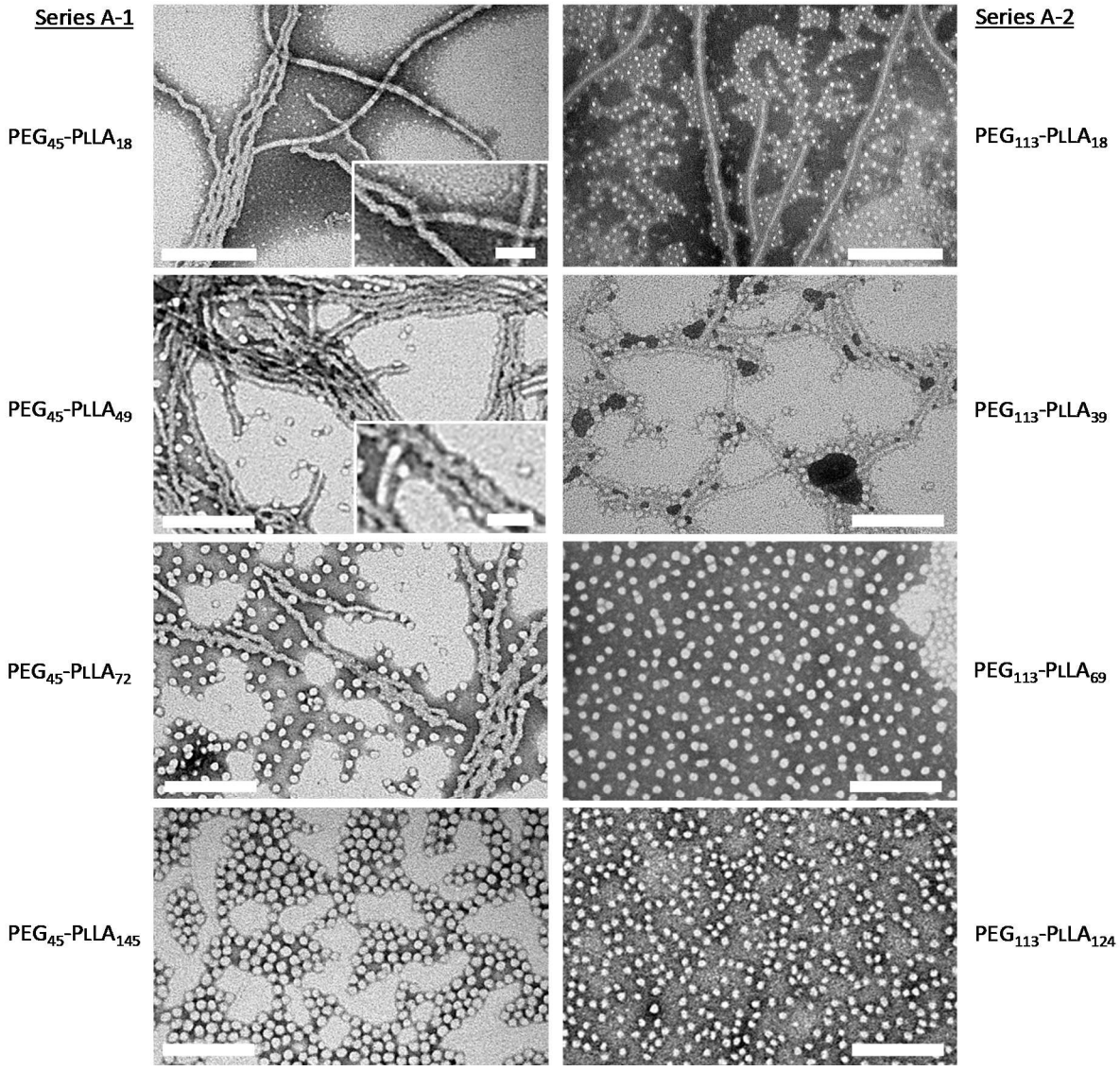

***Figure 29**: TEM images (negative staining) of aggregates resulting from PEG-PLLA block copolymers of series A-1 (left) and A-2 (right); scale bar = 200 nm (insets: 50 nm).*

In the A-2 series (with PEG_{113} as the hydrophilic block) a transition from worm-like to spherical morphologies can be observed as well. However, with an increasing hydrophobic fraction in the block copolymer, the ratio of worm-like to spherical structures varies slightly from that of block copolymers of series A-1 (PEG_{45}). For the polymers with shorter PLLA blocks (PEG_{113}-$PLLA_{18}$ and $mPEG_{113}$-$PLLA_{49}$), spherical morphologies make up the majority of the species. In addition, the wormlike structures disappear completely at shorter PLLA chain length compared to block copolymers initiated with PEG_{45} (Figure 29, 3rd row; PEG_{45}-$PLLA_{72}$ vs. PEG_{113}-$PLLA_{69}$). The mentioned worm-like structures cannot be observed for the samples PEG_{113}-$PLLA_{74}$ and PEG_{113}-$PLLA_{131}$. However, with increasing hydrophobicity (i.e., for higher PLLA to PEG ratios) the diameter of the spheres produced by PEG_{113}-$PLLA_{18}$, PEG_{113}-$PLLA_{45}$, PEG_{113}-$PLLA_{74}$ and PEG_{113}-$PLLA_{138}$ increased from 8.8 ± 1.0 to 13.2 ± 1.3 to 19.1 ± 1.9 and 24.1 ± 2.4, similar to the trend observed for the A-1 series. The diameters of the worm-like

morphologies are with 9.0 ± 1.1 and 11.7 ± 1.3 nm also in the same range as presented for the A-1 series (Figure 30), which indicates a general mechanism for the formation of worm-like structures.

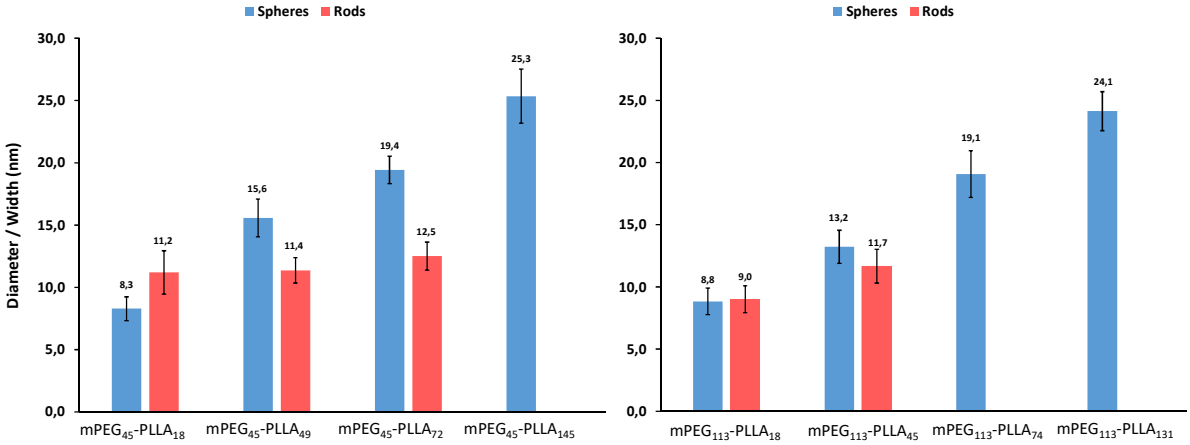

***Figure 30**: Average diameter or width of the spherical or rod-like structures of series A-1 and A-2 whereby the blue blocks correspond to the diameter of the spherical and the red blocks to the width of the rod like structures The average values are determined by statistical measurements of the observed structures. The error bar corresponds to the standard deviation of each morphology.*

In general, the relative amount of worm-like structures was found to decrease with a decreasing PLA chain length, which can also be confirmed by the previously reported DLS results. Additionally, in the TEM micrographs, the worm-like morphologies seemed to consist of small helical subunits. It was proposed that due to higher chain mobility, and an additional increased steric demand, the formation of worm-like structures is partly suppressed the longer is the hydrophilic chain (e.g., PEG_{113}). This is evident within the two investigated polymer series. Nevertheless, due to a relatively constant diameter of approximately 9-12 nm, the worm-like structures can be expected to contain semi-crystalline PLLA chains which are folded orthogonally to the length axis, as described earlier.[106] However, considering that the morphology of the structures should be related to the hydrophilic-hydrophobic ratio, and that an increase of the hydrophobic segments should cause a lower curvature of the formed morphology, [131] the opposite trend (i.e., from micelles to worm-like structures with increasing PLLA block length) should be observed in both series. Although, Wang *et al.* observed a transition from cylinders to small vesicles of about 50 nm,[106] any evidence of vesicles could not be observed in this work. Instead, our spherical structures were found to be compact micelles, with a core diameter that was found to increase with increasing PLLA chain length. The aggregation number can be calculated according to:[132,133]

$$Z = \left(\frac{1}{6} \cdot \pi \cdot {d_{core}}^3\right) / \left(\frac{m_0 \cdot n}{\rho_0 \cdot N_L}\right)$$

Equation 23

where m_0 stands for the molecular weight of the monomer ($72.1\ g \cdot mol^{-1}$), n for the average number of lactyl units (calculated by ^{1}H-NMR spectroscopy), ρ_0 for the bulk density of amorphous PLA ($\sim$ 1.26 cm^{-3}), and N_L for the Avogadro number. The aggregation number Z is increasing with increasing PLLA chain length (Table 3). By calculating the distance b between the neighboring chains at the core-corona interface through Equation 24, the spherical morphologies were found to be densely packed micelles. This is in contrast to the results of Wang *et al.,* who observed small vesicles with an approximate size of 50 nm.[106]

$$b = \sqrt{\frac{\pi\ {d_{core}}^2}{Z}}$$

Equation 24

The increasing amount of chain folds can explain the growing inter-chain distances b from 1.1 to 1.8 nm within the core with increasing PLLA chain length (Figure 31). Nevertheless, the distances b are far smaller than known systems, which could be introduced by crystallization of PLA in the core.[134]

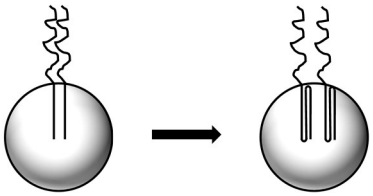

Figure 31: *Illustration of increasing inter-chain distances introduced by chain folding with increasing PLA chain length.*

Table 3. *The crystallinity of PLLA and characteristics of spherical micelles formed by PEG-PLLA block copolymers*

Series	***Sample***	***Crystallinity*** [a] ***(%)***	D_h [b] ***(nm)***	d_{core} [c] ***(nm)***	***Z*** [d]	***b*** [e] ***(nm)***
A-1	PEG_{45}-PLLA$_{18}$	22 → 43	n/a	8.3 ± 1.0	170	1.1
	PEG_{45}-PLLA$_{49}$	46 → 47	n/a	15.6 ± 1.5	430	1.3
	PEG_{45}-PLLA$_{72}$	34 → 47	32	19.4 ± 1.1	560	1.4
	PEG_{45}-PLLA$_{145}$	32 → 39	40	25.2 ± 2.2	620	1.8
A-2	PEG_{113}-PLLA$_{18}$	16 → 12	n/a	8.8 ± 1.1	210	1.1
	PEG_{113}-PLLA$_{39}$	37 → 57	19	13.2 ± 1.3	330	1.3
	PEG_{113}-PLLA$_{69}$	39 → 50	33	19.1 ± 1.9	550	1.4
	PEG_{113}-PLLA$_{124}$	38 → 55	36	24.1 ± 1.6	620	1.7

[a] The crystallinity of PLA in samples containing spherical and worm-like aggregates, determined by DSC. The two values correspond to the crystallinity of samples isolated after one day or 4 days, respectively. [b] Hydrodynamic diameter, $D_h = 2 \cdot R_h$, determined by DLS. [c] Diameter of PLLA core of micelles, determined by quantitative analysis of TEM images (Figure 1) considering at least ~100 particles. [d] Aggregation number. [e] The inter-chain distance at core-corona interface.

Despite the consistent trend of both series, predicting the final morphologies, their relative ratios and sized remains challenging. A general prediction model remains to be elucidated. After following the time-dependence behavior of the polymer solution by DSC (after one day, and after four days), two processes involved in the self-assembly PLLA or PDLA-based amphiphilic block copolymers were identified. The first one is the micro-phase separation, which is responsible for the formation of PEG-PLLA micelles through dispersion in water. This process is faster than the crystallization step, which takes places after and can be observed by DSC experiments, where a noticeable increase in crystallinity can be observed with time. Consequently, the initially formed spherical micelles should consist of the amorphous PLLA core and the PEG corona, as described earlier in the literature with racemic PLDLA or sonicated PLLA block copolymers.[99–101,104] However, unlike other protocols described in the literature,[105,108–110,113] in the present study, all micelles were prepared below the T_g of PLA. As such, the exchange dynamics of chains can be considered as slow. Consequently, the micelles were kept in a "frozen" state. Following the subsequent crystallization step, the micelles become colloidally unstable and it was proposed that an epitaxial growth with other unstable micelles resulted into worm-like structures. The fusion from spherical to worm-like morphologies was facilitated with shorter PLLA and shorter PEG blocks. Longer PEG block partially suppress the formation of worm-like structures. Shorter PLLA chains should produce a folded lamellar crystal with less amorphous defects than longer PLLA chains. As a result, the amount of worm-like morphologies increases with decreasing PLA blocks sizes.

5.2.2 Aqueous Self-Assembly of PEG-PLLA/PEG-PDLA Stereocomplexes

To study the influence of stereocomplexation on the self-assembly behavior of polymer pairs, a 1:1 ratio of PEG-PLLA (series A-1 and series A-2) and PEG-PDLA (series B-1 and B-2) with equivalent PLLA and PDLA chain lengths were prepared and characterized by DSC, TEM, DLS, and WAXD using the same protocols as described above.

The DSC thermograms showed a higher melting point (T_m) for PLLA-PEG/PDLA-PEG mixtures ($\sim$ 200°C) (Figure 32) than for the one-species solutions ($\sim$ 140°C) (Figure 27). This increase in T_m confirms that PLLA/PDLA were produced in the former cases. It should be noted that neither melting transitions of pure PLLA or PDLA segments were observed, nor the appearance of cold crystallization peaks while heating were observed. The degrees of crystallinity (calculated according to Equation 22) were found to be in the range of 36 to 50%, with a $\Delta H_{100\%}$ of 155 J/g for the D/L mixture (i.e., when the stereocomplex is formed).[135] The stereocomplexation behavior was further confirmed by WAXD measurements (Figure 32). Due to the presence of amorphous portions in the polymer, the peaks are quite broad. Nevertheless, for all polymer mixtures, characteristic diffraction peakss of the triclinic cell at 2Θ $\sim$ 12 and 21°, with intensities related to the weight fraction of PLA in the block copolymer

mixtures, were observed. Typically, an additional peak for the stereocomplex should be expected at 2Θ ~ 24°. However, this peak is most likely hidden under an intense peak from the crystalline PEG, which show a set of diffraction peaks at 2Θ = 19, 22, 23, 26 and 30°, as reported in former studies.[111,136,137]

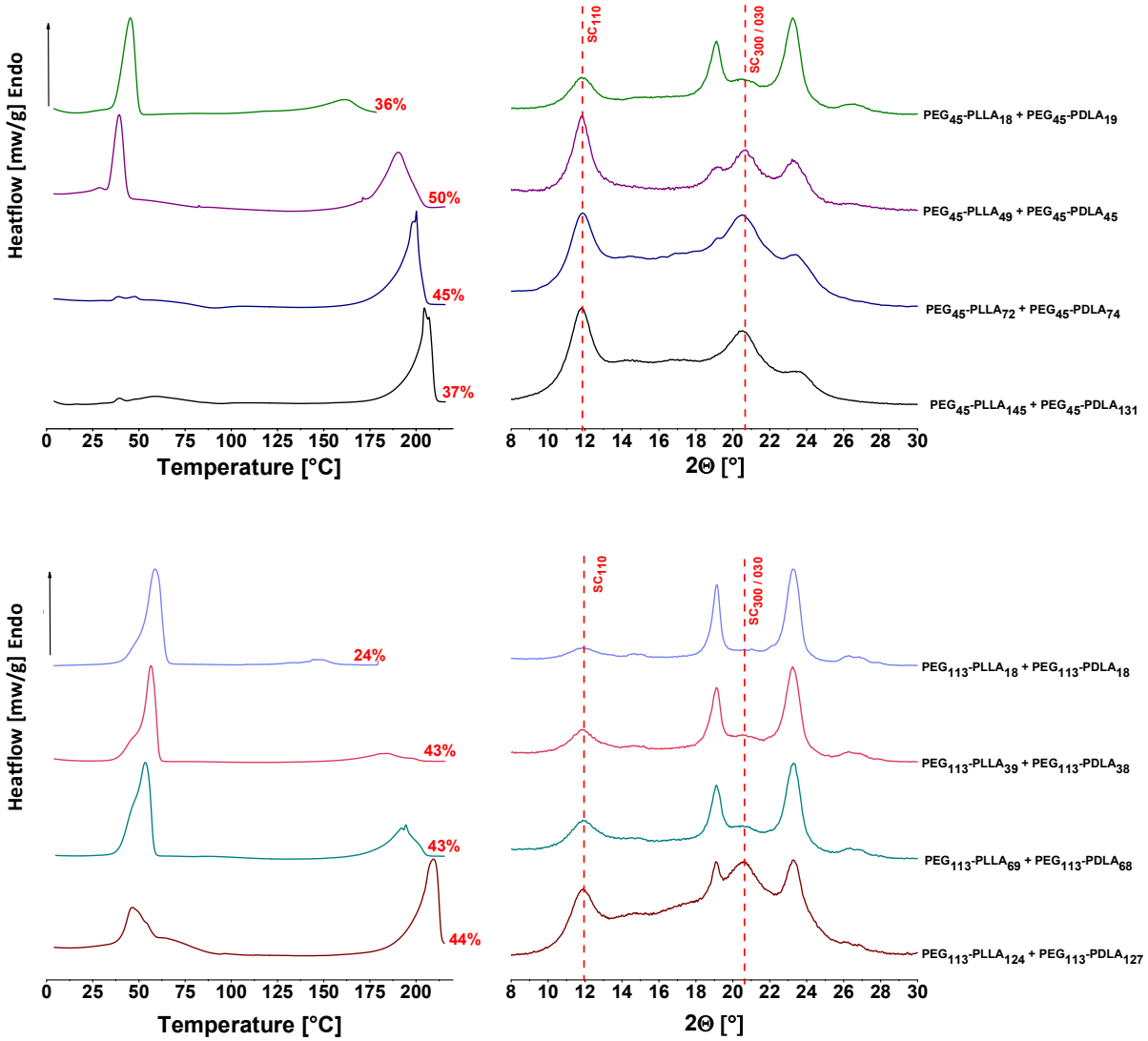

Figure 32: *(Top Line) DSC curves (first heating cycle) and WAXD pattern of stereocomplexed PEG-PLLA / PEG-PDLA block copolymer mixtures from series A-1+B-1. (Bottom Line) DSC curves (first heating cycle) and WAXD diffraction pattern of stereocomplexed PEG-PLLA / PEG-PDLA block copolymer mixtures from series A-2+B-2. The percentages given above the curves, corresponding to the crystallinity of the PLA block*

According to DLS analyses (Figure 33), the unfiltered stereocomplexed samples assemble into large aggregates with hydrodynamic radii of $R_h \sim 90 - 500\ nm$. After filtration structures with $R_h \sim 80 - 100\ nm$ and occasional with $\sim 10 - 50\ nm$ remaining in solution. These results are comparable to those for the PEG-PLLA block copolymers parents reported above (Figure 28). These results are indicative of the presence of large species. However, the shape of these species cannot be determined since this method just reveal the apparent R_h . In contrast to the DLS results, the stereocomplexation

has a significant impact on the self-assembled structures of the block copolymer mixtures, as revealed by TEM analysis. The larger stereocomplexed aggregates were not worm-like, as observed for PEG-PLLA systems, but irregular clusters, which did not allow a precise evaluation of diameters and length of the obtained morphologies. With shorter PLA chains, the formation of spherical aggregated connected in a bundle seemed to be favored, especially when longer hydrophilic blocks were used. Those bundles took on a shape comparable to pearl-necklesses when larger PLA blocks were used.

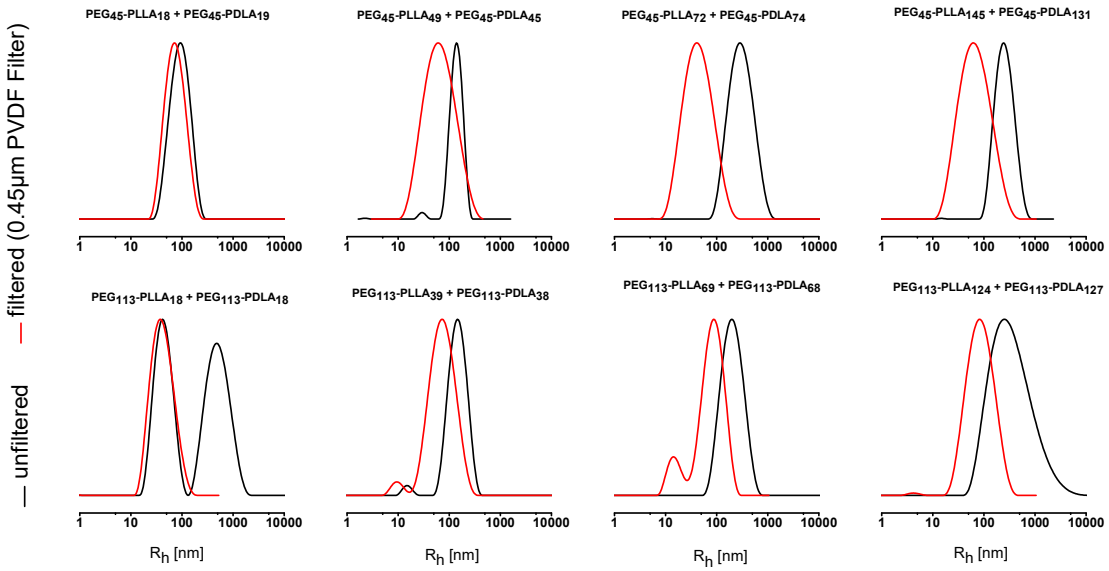

***Figure 33**: DLS measurements of stereocomplexed block copolymers mixtures of series A-1 + B-1 (Top line) and A-2 + B-2 (Bottom line). The black colored curves corresponds to the unfiltered and the red one to the filtered polymer dispersions.*

These morphologies are very similar to those observed by Sun et al., which underwent a stereocomplexation-driven transformation of crystalline cylindrical nanoparticles of PLLA-poly(acrylic acid) and PDLA-poly-(acrylic acid) into spheres.[105] However, such a reorganization relies on a unimer-exchange mechanism, which is induced by the introduction of an additional common solvent (THF), an annealing step, or both. Nevertheless, the self-assembly of stereocomplexed block copolymers is still not completely elucidated yet. The following paragraph will introduce some hypotheses for the mechanism.

The solvation of polymer chains in the present block copolymers is solvent-dependent and therefore a crucial parameter in the early stages of the self-assembly mechanism. In comparison, the known Hildebrandt solubility parameters of dioxane ($\delta_{Dioxane}$ = 20.5 $MPa^{1/2}$), PLLA (δ_{PLLA} = 19.3 $MPa^{1/2}$), and PEG (δ_{PEG} = 19.5 $MPa^{1/2}$) are similar to each other. Hence dioxane can be seen as a good solvent for both blocks.[106] As a result, in the single block copolymers, the PLLA blocks can rearrange and crystallize more easily than in solvents that do not solve the polymer so well. The repulsion between the PEG block is large and aggregates with a curvature were more likely to be produced. In case of the stereocomplexable polymer mixtures, the dissolution of the PEG blocks should not be affected, where

the same stereoscopic space than for the single block copolymers is required and should not influence the obtained morphologies. However, as shown in former studies that reported gelation or precipitation of stereocomplexed PLA in concentrated solutions, the solubility parameter of the stereocomplexed PLA is changed massively.[29] In this regard, it is assumed that in this study (with a low polymer concentration) the mobility of two clashing PLLA and PDLA chains in solution is reduced massively. Due to the mutual affinity to each other, the repulsion is small, and the resulting mixture occupies a smaller stereoscopic space than without stereocomplexed segments. Consequently,

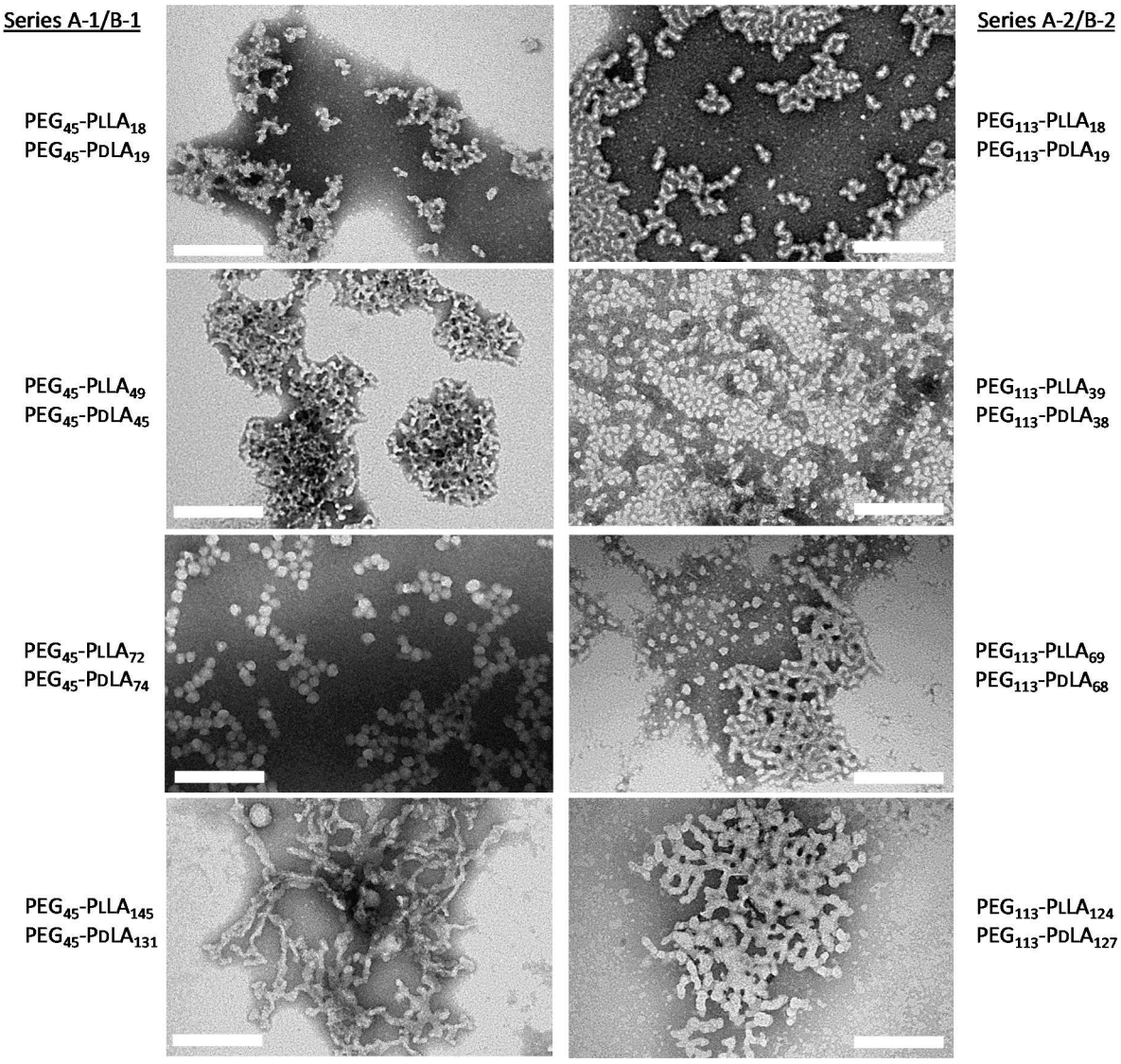

Figure 34: TEM images (negative staining) of aggregates of PEG-PLLA/PDLA-PEG stereocomplexes from the A-1/B-1 (left) and A-2/B-2 (right) series; scale bar = 200 nm.

spherical morphologies should be favored as observed for the polymers with a short PLA chain length. With an increasing PLA block fraction and reduced chain mobility of the individual chains, an incomplete interaction of the PLLA and PDLA chains is expected (as in case of a fringed-micelle) and would result in more complex morphologies as seen in Figure 34.

In addition, thermodynamic of self-assembly may be affected by the stereocomplexation of PLLA and PDLA chains. The self-assembly is under thermodynamical control when the amount of the common solvent and the mobility of the chains is sufficiently high. Conclusively, the change of the aggregation number Z in the morphology, and the morphological transition is fast. However, by adding water to the common solvent, the equilibrium is changed, and the morphologies become kinetically frozen above a specific water content.[12] Since this effect in dependent on the polymer compositions, and polymer chain lengths, and therefore cannot be predicted easily, this equilibrium is expected to be affected by stereocomplexation. The maximal amount of water added to the common solvent, within the self-assembly is still under thermodynamical control, could be reached at a smaller volume of water in the common solvent, whereby this effect should additionally be enhanced with increasing PLA chain length. Consequently, the stereocomplexed structures freeze rapidly and result in less defined morphologies.

Finally, it should be mentioned that in contrast to the parent block copolymers presented above, for stereocomplexes, no time-dependent experiments were performed. However, since Sun *et al.* presented a morphology transition at 65°C within 30 hours, and in this study, the stereocomplexation was also performed at room temperature, the detectable effect may be rather small under the chosen conditions.

5.2.3 Self-Assembly PLLA-PEG copolymers and their block copolymer mixtures

In the course of this thesis, it was decided to create a block copolymer with the hydrophilic segment attached to the alcohol end group of the PLA block (PLA-PEG block copolymer; Table 2). In order to investigate the self-assembly behavior PLA-based polymer mixtures including block copolymers with opposite polymer sequence. Due to a challenging work up step for the PLA-PEG block copolymers with remaining homo-PLA in the system (even after extensive purification steps), only two PLA-PEG block copolymer samples with a rather small PLA block length were synthesized. Nevertheless, considering larger chain mobility for block copolymers with smaller PLA blocks, the corresponding self-assemblies were expected to be more controlled, thereby producing reliable results that give more valuable information about the self-assembly of PEG-PLA + PLA-PEG block copolymer mixtures.

Similarly to the PEG-PLA block copolymers in Series A-2, block copolymer P_LLA_{28}-PEG_{113} produced spherical and worm-like morphologies with a diameter of $\sim$ 12 ± 2 nm and a width of $\sim$ 11 ± 2 nm, respectively. The two species cannot be, however, be quantified so far (Figure 35). As observed earlier in chapter 5.2.1, in DLS the filtered solutions showed a shift to smaller values, which can be again interpreted as a larger species, possibly worm-like aggregates. Since the self-assembled

morphologies should not affect by the block polymer sequence of single block copolymers (PEG-PLA block copolymer vs. PLA-PEG block copolymer), and the polymer composition in similar to PEG_{113}-$PLLA_{18}$ (A-2 series), it was not surprising that spherical and worm-like structures were obtained and where therefore consistent with the results described in chapter 5.2.1.

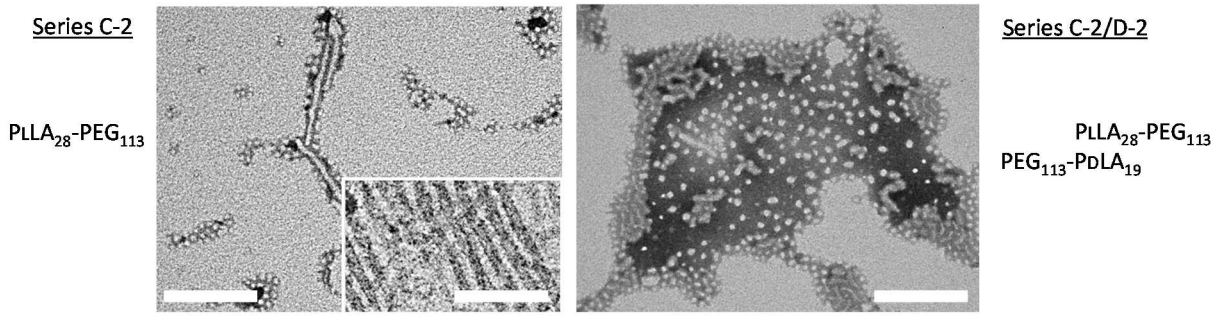

Figure 35: *TEM images (negative staining) of aggregates from $PLLA_{28}$-PEG_{113} block copolymer (left) and corresponding stereocomplexed $PLLA_{28}$-PEG_{113} + PEG_{113}-$PDLA_{18}$ block copolymer mixture (right); scale bar = 200 nm).*

As mentioned before, the PLA-PEG block copolymers were synthesized to influence the self-assembly of PLA-based block copolymers by creating PEG-PLA + PLA-PEG block copolymer mixtures. However, as seen in Figure 35 (right image), the PEG-PLA + PLA-PEG mixture of $PLLA_{28}$-PEG_{113} and PEG_{113}-$PDLA_{18}$ does not influence the obtained structures compared to the stereocomplexed mixtures presented in the chapter above. The stereocomplexation was demonstrated by WAXD pattern and DSC experiments (Figure 36) that were similar to the analogous PEG_{113}-$PLLA_{18}$ and PEG_{113}-$PLLA_{18}$ + PEG_{11}3-$PDLA_{18}$ (Figure 32). However, the morphologies obtained by TEM did not show any evidence of vesicular structures but instead irregular clusters of spherical aggregates with diameters of $\sim$ 12.5 ± 1.5 nm, as observed in chapter 5.2.1.

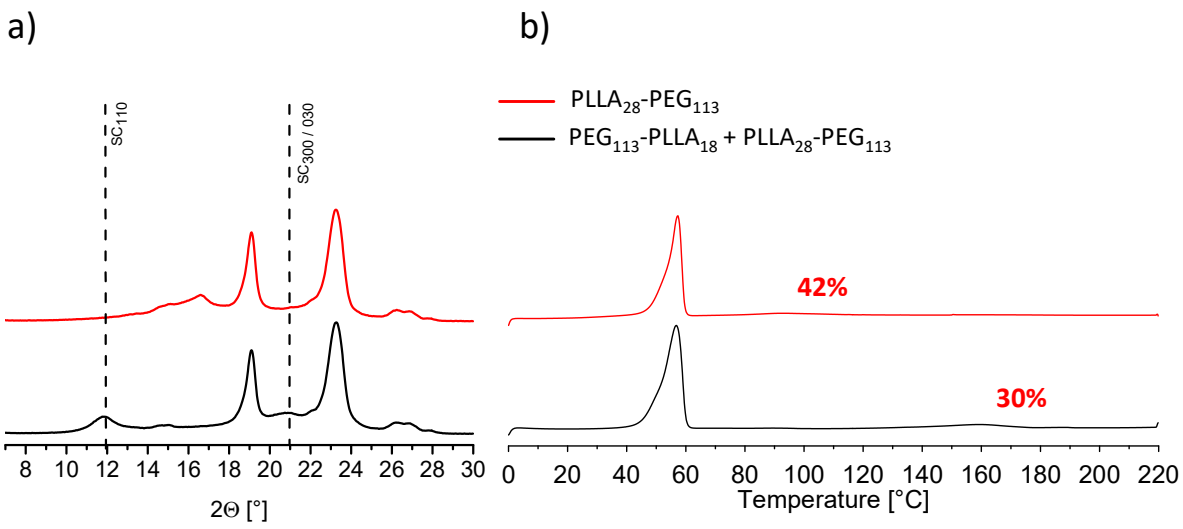

***Figure 36**: a) WAXD pattern of self-assembled and freeze-dried PLLA$_{30}$-PEG$_{113}$ block copolymer (red line) and corresponding stereocomplexed PLLA$_{28}$-PEG$_{113}$ + PEG$_{113}$-PDLA$_{18}$ block copolymer mixture (black line). b) DSC curves (first heating cycle) of self-assembled and freeze dried PLLA$_{28}$-PEG$_{113}$ block copolymer (red line) and corresponding stereocomplexed PLLA$_{28}$-PEG$_{113}$ + PEG$_{113}$-PDLA$_{18}$ block copolymer mixture (black line) with corresponding crystallinity values.*

Therefore, the preferred chain orientation in stereocomplexes seems to be less relevant or more complicated than expected, and the macrophase separation should be the dominant parameter in the self-assembly process. Consequently, the polymer segments in a stereocomplexes can align in an anti-parallel or parallel fashion to achieve the smallest possible surface. Since the PEG-PLA and PLA-PEG block copolymers can be directly dissolved in water without an additional common solvent, and therefore the chain mobility is high, it is assumed that with time a change in morphology and resulting crystallinity occurs. Due to time-managements no time-dependent experiments for the chosen conditions described in this chapter. It is reasonable to expect that over a longer period, well-defined spheres could form, as suggested by earlier studies.[105]

6 Time-Dependent Self-Assembly of Block Copolymers and Their Stereocomplexes

The investigation of crystallization-driven self-assembly of PLA-based block copolymers and their corresponding stereocomplexes, described in Chapter 5 suggested that a time-dependent transformation of the morphologies took place, which is driven by crystallization. However, in the case of block copolymers with short PLA segments, good solubility in water and low crystallinities were observed. These properties are expected to favor a unimer exchange and thus make the block copolymers more susceptible to time-dependent changes. It is still to be assumed that the formation of worm-like morphologies results from the crystallization of PLA (e.g., epitaxial growth for block copolymers with long PLA blocks). However, the evolution of these morphologies could be based on different mechanisms, since the properties of the block copolymers change with increasing PLA block length. In this chapter, the time-dependent study of the self-assembly of single block copolymers with a short PLA block (DP_n = 18- 30 lactyl units) and of the corresponding D/L mixtures is presented. DLS and cryo-SEM were used to determine the diameter of the self-assembled structures, and cryo-TEM was used to investigate the hydrophobic core. The data produced by these techniques were combined to produce an accurate picture of the morphologies that were formed by this time-dependent self-assembly process.

6.1 Experimental

6.1.1 Materials

The synthesis of the used block copolymers PEG_{45}-$PLLA_X$ and PEG_{113}-$PLLA_X$ were described in Chapter 5 and the Appendix. Their properties are listed in Table 4.

***Table 4**: Molecular characteristics of PEG-PLA and PLA-PEG block copolymers*

Series	Sample [a]	w_{PLA} [a]	M_n^{app} (g/mol)[b]	$Đ^{app}$ [b]
A-1	PEG_{45}-$PLLA_{18}$	0.39	5.400	1.10
A-2	PEG_{113}-$PDLA_{18}$	0.21	10.800	1.04
B-1	PEG_{45}-$PDLA_{19}$	0.41	5.400	1.10
B-2	PEG_{113}-$PDLA_{19}$	0.21	10.800	1.04
C-2	$PLLA_{28}$-PEG_{113}	0.30	11.900	1.03
D-2	$PDLA_{30}$-PEG_{113}	0.30	11.500	1.03

[a)] Copolymer composition (w_{PLA} = weight fraction of PLA in the block copolymer) and the average number of repeating units were determined by ^{1}H-NMR spectroscopy (500 MHz, $CDCl_3$). b) Apparent number-average molar masses (M_n^{app}) and dispersity indexes ($Đ^{app}$) were determined by SEC (eluent: THF, calibration: polystyrene).

6.1.2 Preparation of Self-Assembled Aggregates without the use of Common Solvent

All block copolymers were dissolved individually in Millipore water at a concentration of 0.5 wt% and shaken overnight. PEG-PLA + PEG-PLA and PEG-PLA + PLA-PEG 1:1 block copolymer mixtures were prepared, shaken for 5 minutes, and finally filtered with a 0.22 µm PVDF filter (before placed in a DLS cuvette). In contrast to Chapter 4, block copolymer mixtures with different hydrophilic chain length (PEG_{45} and PEG_{113}) were additionally prepared to investigate the influence of different hydrophilicity of each individual block copolymer in the stereocomplexes. Subsequently, all block copolymers and block copolymer mixtures were measured by DLS and cryo-SEM at different times over a course of 14 days. To obtain reliable R_h values, constant fitting parameters were chosen. As described in chapter 4 and in contrast to the literature (i.e., annealed polymer solutions), the dispersions were kept at room temperature without stirring.

6.2 Results and Discussion

6.2.1 Time-Dependent Self-Assembly of PLA-based Block Copolymers

Even though all polymers have a similar PLA chain length, the observed hydrodynamic radii R_h measured by DLS are different depending on hydrophilic PEO chain length and amphiphilicity of the block copolymers. In Figure 37, the aqueous dispersion of particles with two enantiomeric block copolymers PEG_{45}-PLLA and PEG_{45}-PDLA$_{19}$ are presented, which contain $R_h \sim 50 - 60\ nm$. Surprisingly, the size does not change dramatically within the first 14 days, whereas cryo-SEM and cryo-TEM micrographs reveal a different trend, showing the presence of micron long bundles forming over time (Figure 38).

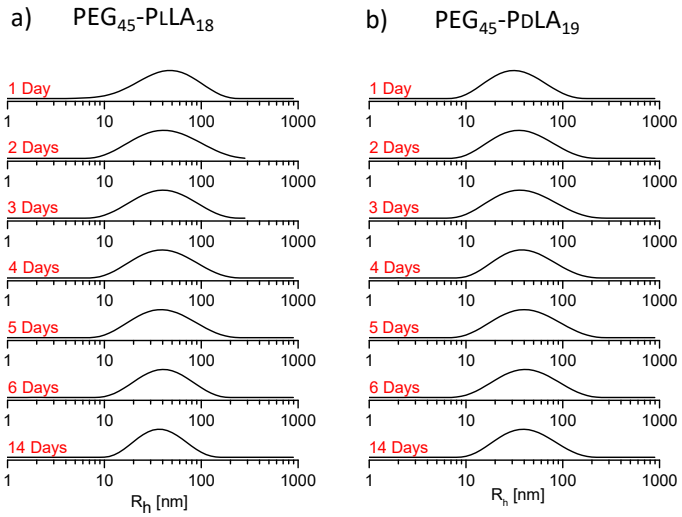

Figure 37: *Time dependent DLS measurements a) PEG_{45}-PLLA$_{18}$ and b) PEG_{45}-PDLA$_{19}$ block copolymers directly dissolved in water, no significant change in the hydrodynamic radius occur within 14 days of self-assembly.*

After one day spherical structures with varying diameters ($d = 30 - 50\ nm$) were observed by cryo-SEM. After 14 days, additional aggregates appeared, which had a worm-like morphology with a width d of approximately $25\ nm$ (Figure 38, 14 days). However, these results are consistent with the data reported in chapter 4, and the spherical structures consist of block copolymers with an amorphous PLA core. As crystallization proceeds (Table 3), the epitaxial growth of the worm-like structure takes place, and worm-like structures, in addition to spherical morphologies are observed. The ratios of the coexisting morphologies are strongly dependent on the self-assembly process and therefore crystallization time; a quantitative analysis of the ratio of spheres to worm-like structures is not possible at this point. However, this trend was supported by cryo-TEM of the aged aqueous dispersion presented in Figure 38. Some of the observed aggregates were spherical micelles with a

core-shell architecture, but mostly worm-like aggregates, were present consisting of a hydrophobic PLA core of approximately $d \sim 10\ nm$.

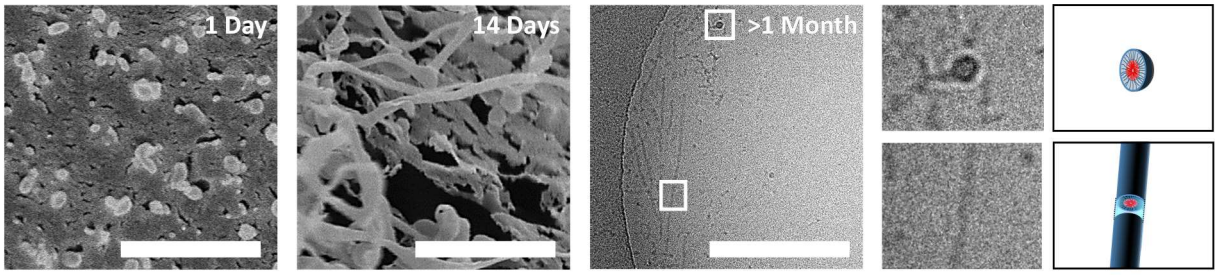

***Figure 38**: Time dependent cryo-SEM (1-14 days) and cryo-TEM micrographs of the aged PEG_{45}-PLLA_{18}, which was directly dissolved in water at a concentration of 0.5 wt%. Through cryo-SEM measurements, the shell-included structure of the assembled morphologies can be observed. In cryo-TEM the hydrophobic core own a higher contrast and lighter regions for the hydrophilic chain as seen in the magnified extracts on the right; scale bar 500 nm. Additionally, schematic illustrations of obtained morphologies are presented in the black framed boxes.*

In contrast to the DLS results described above, PEG_{113}-PLLA_{18} and PEG_{113}-PDLA_{18} (Figure 39 a and b) show bimodal distributions of a fast and a slow diffusing species corresponding to smaller ($\sim 20\ nm$) and larger ($\sim 120\ nm$) aggregates, respectively. Even though DLS overestimates the concentration of the larger aggregates, DLS data showed that larger aggregates, that are worm-like structures, increase with time, thereby indicating a transition of the morphologies. As seen in Figure 36, top row, worm-like morphologies can be found in aqueous solution even though in lower quantity than for PEG_{45}-PLLA and PEG_{45}-PDLA_{19}. As demonstrated by others,[105] the fusion of spheres to worm-like species can be accelerated when the dispersion are annealed at 60°C. Within 2 h, the smaller species completely disappeared and only large aggregates with a R_h between 80 to 120 nm were observed (Appendix).

In contrast to the DLS data of PEG_{113}-PLLA_{18} and PEG_{113}-PDLA_{18}, the PLA-PEG block copolymers PLLA_{30}-PEG_{113}- and PDLA_{30}-PEG_{113} showed a broad distribution, thereby indicating the presence of aggregates of a variety of sizes, including small spheres and large worm-like structures (Figure 39, bottom row). Even though both PLA-PEG block copolymers have a similar polymer composition as PEG_{113}-PLLA_{18} and PEG_{113}-PDLA_{18}, the concentration of worm-like structures appears to be larger within a shorter period of time. However, DLS does not allow to identify the morphological transition since R_h is relatively constant within 14 days. It can be assumed that small species with $R_h \sim 20$ nm represents the major species at the beginning of self-assembly for PEG_{113}-PLLA_{18} and PEG_{113}-PDLA_{18}. The small shift in the R_h to higher radii with time supports a transition from spheres to worm-like structures (Figure 39, bottom row), which is also supported by cryo-TEM.

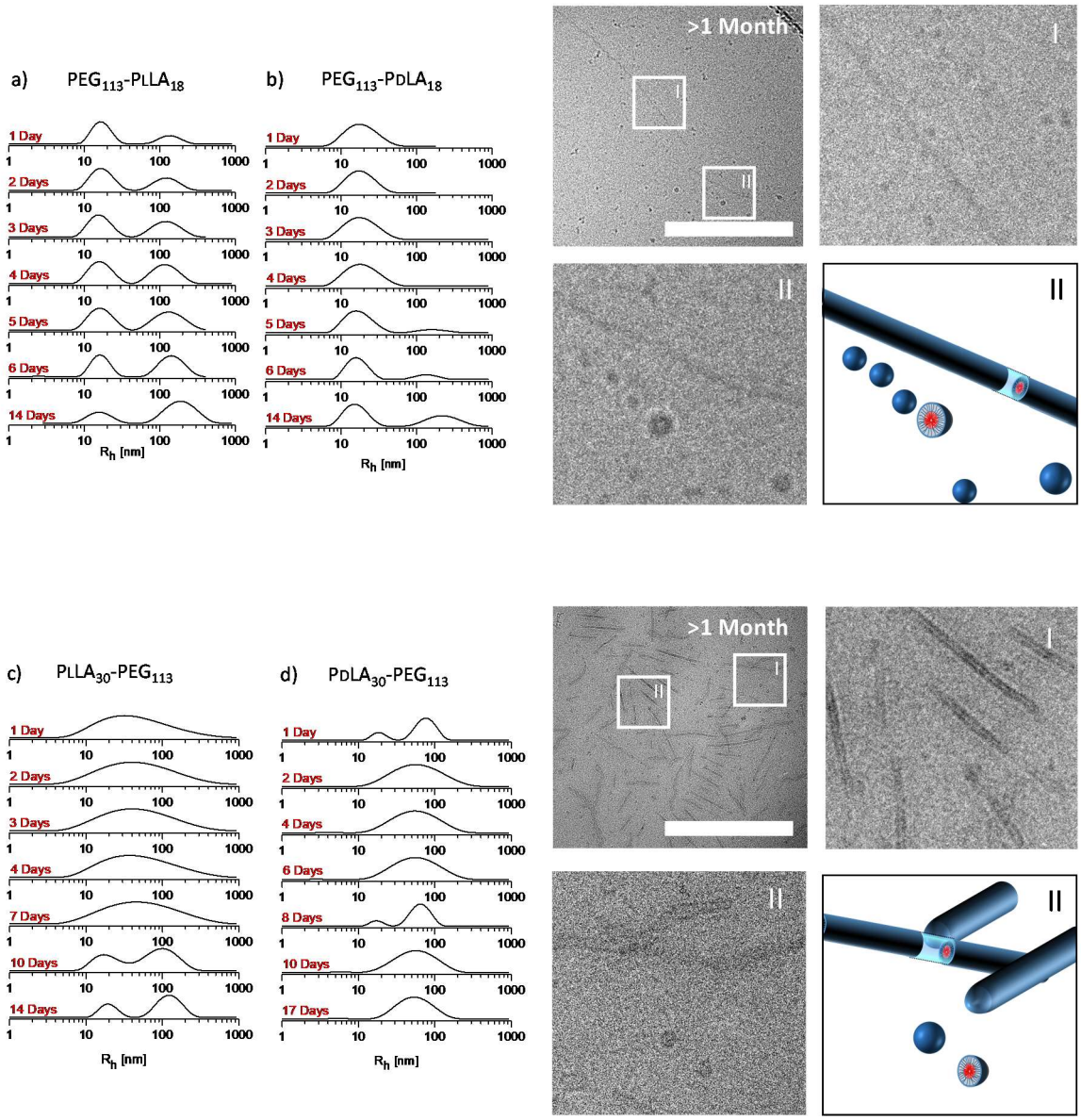

Figure 39: *Time dependent DLS measurements and corresponding cryo-TEM micrographs a) PEG_{113}-PLLA$_{18}$ and b) PEG_{113}-PDLA$_{18}$ c) PLLA$_{28}$-PEG_{113} d) PDLA$_{30}$-PEG_{113} block copolymers directly dissolved in water. Polymer concentration = 0.5 wt%. Additionally, schematic illustrations of obtained morphologies are presented in the black framed boxes, scale bar 500 nm.*

6.2.2 Time-Dependent Self-Assembly of Stereocomplexed Polymer Mixtures

Before presenting the results, it should be highlighted that all parent polymers were already dispersed in aqueous solution and therefore self-assembled for 24h before all mixtures were prepared. Nevertheless, all polymer mixtures, irrespective of symmetric (PEG-PLA + PEG-PLA or PLA-PEG + PLA-PEG block copolymer) or asymmetric polymer-sequence (PEG-PLA + PLA-PEG block copolymer), self-assembled into more compact micelles within 14 and 21 days as observed for the parent polymers. Due to the small amount of PLA in the block copolymers, the melting enthalpy of the PLA block is small (~ 16%). However, within the first 10 minutes the stereocomplex is produced without the presence of

any homo-crystalline segments (Figure 40), indicates a high D/L-lactide affinity and fast unimer exchange that can break up the already produced homo PLLA or PDLA crystals.

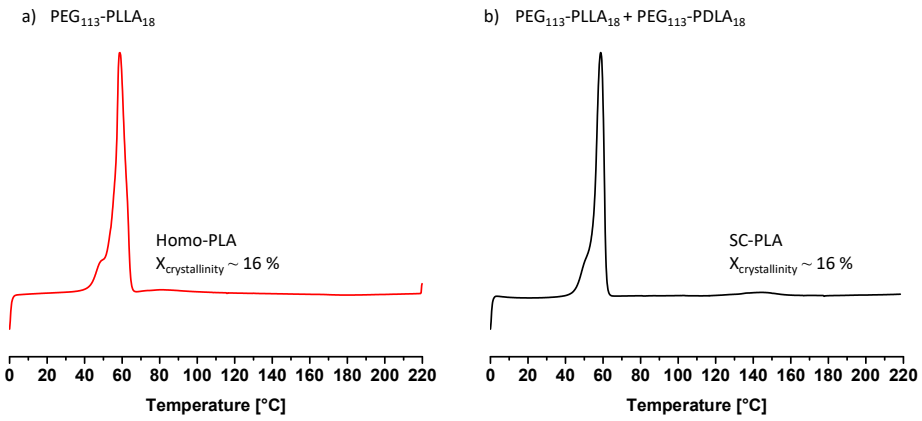

Figure 40: *DSC curves (first heating cycle) of a) self-assembled (24h) and further freeze-dried PEG_{113}-PLLA_{18} block copolymer (red line) and b) corresponding PEG-PLA + PEG-PLA stereocomplexed PEG_{113}-PLLA_{18} + PEG_{113}-PDLA_{18} block copolymer mixture (black line, 10 min) with corresponding crystallinity values.*

The time-dependent hydrodynamic radii and the diameter of the individual morphologies are presented in Table 5.

Table 5*: Summary of dime dependent apparent average hydrodynamic radii and measured diameter of polymer mixtures determined by DLS and cryo-SEM*

Mixture [a]	R_h^{app} ***(nm)***	R_h^{app} ***(nm)***	$d_{Micelle}$[b] **(nm)**	$d_{Micelle}$[b] **(nm)**
	1st Day	***21 Days***	***1st Day***	***14 Days***
PEG_{45}-PLLA_{18} + PEG_{45}-PDLA_{19}	43	25	58 ± 19	26 ± 7
PEG_{113}-PLLA_{18} + PEG_{113}-PDLA_{18}	17	16	16 ± 2	16 ± 2
PEG_{113}-PLLA_{18} + PEG_{45}-PDLA_{19}	27	18	N/A	N/A
PLLA_{28}-PEG_{113} + PDLA_{30}-PEG_{113}	70	27	33 ± 11	20 ± 5
PEG_{45}-PLLA_{18} + PDLA_{30}-PEG_{113}	63	30	N/A	N/A
PLLA_{28}-PEG_{113} + PEG_{113}-PDLA_{18}	70	38	53 ± 24	15 ± 3

[a] Copolymer composition and the average number of repeating units were determined by ^{1}H-NMR spectroscopy (500 MHz, $CDCl_3$). b) Statistical diameter determination of observed spherical morphologies in cryo-SEM

With the exception of PEG_{113}-PLLA_{18} + PEG_{113}-PDLA_{18}, which despite stereocomplexation is relatively stable with time, a dramatic reduction of the apparent hydrodynamic radii for all polymer mixtures compared to the beginning of that experiment was observed. However, the resulting diameters of the morphologies measured by cryo-SEM differ by a factor of two to the hydrodynamic

diameters measured by DLS. This discrepancy can be explained by the fact that the intensity-weighted in DLS spectra can shift to larger hydrodynamic radii, which does not reflect the actual size distribution.

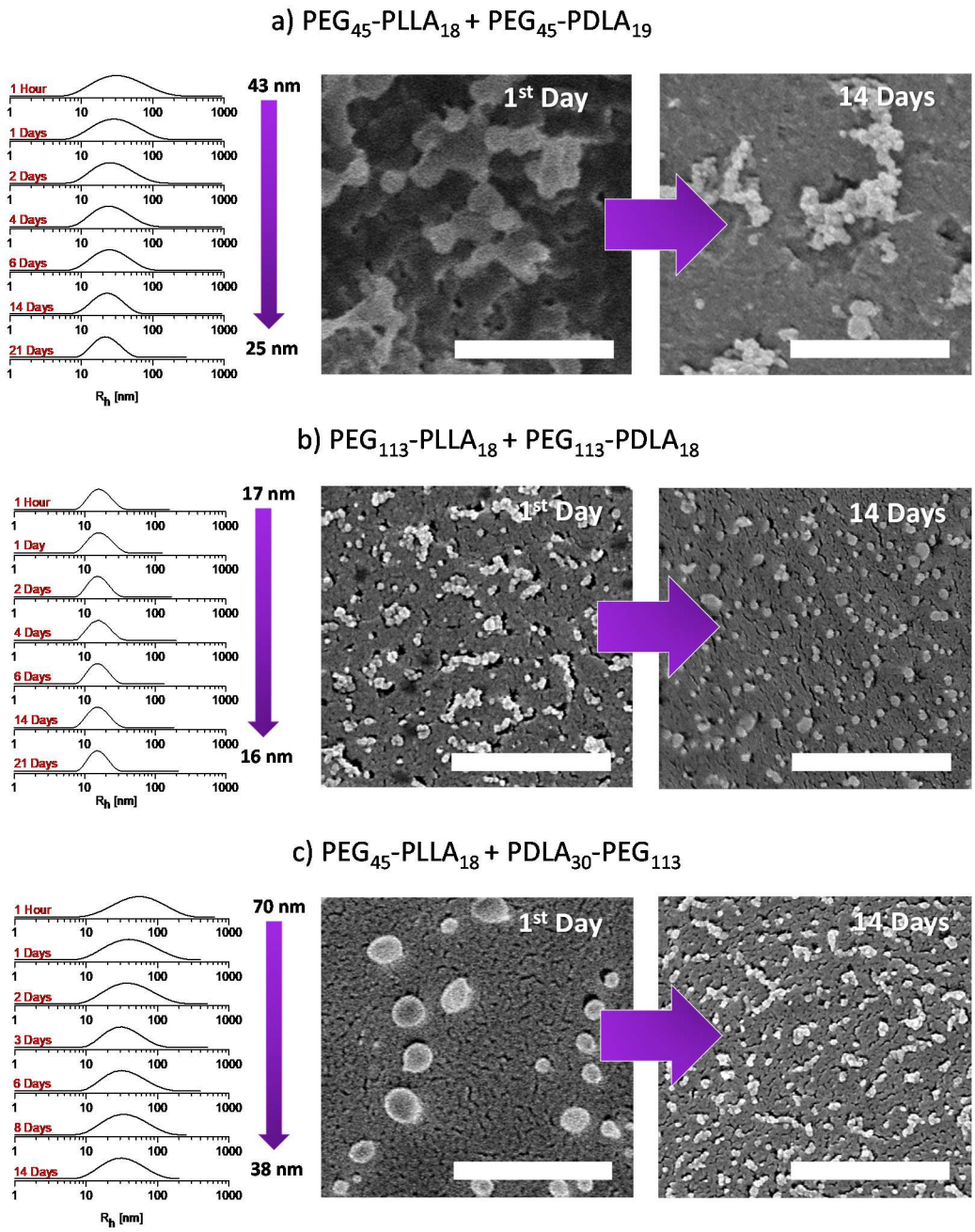

Figure 41: *Time-dependent DLS measurements and corresponding cryo-SEM micrographs of stereocomplexed polymer mixture a) PEG_{45}-$PLLA_{18}$ + PEG_{45}-$PDLA_{19}$ b) PEG_{113}-$PLLA_{18}$ + PEG_{113}-$PDLA_{18}$ and c) PEG_{45}-$PLLA_{18}$ + $PDLA_{19}$-PEG_{113}; Polymer concentration = 0.5 wt%; scale bar 500 nm.*

After six weeks, the hydrodynamic radii of the block copolymer mixtures further decreased, whereby an R_h of approximately ~ 15 nm seems to be the recognizable limit (Figure 42). Nevertheless, all morphologies where found to be spherical and have a smaller R_h than $\lambda/20$ (i.e., ~30 nm), hence the same size is observed independent of angle, as seen in Figure 42. Because the diffusion coefficients

are below the resolution limit for DLS and are all of similar values, clusters of di- or trimers or small elongated structures that are still below 30 nm, as seen in Figure 41, cannot be reliably quantified.

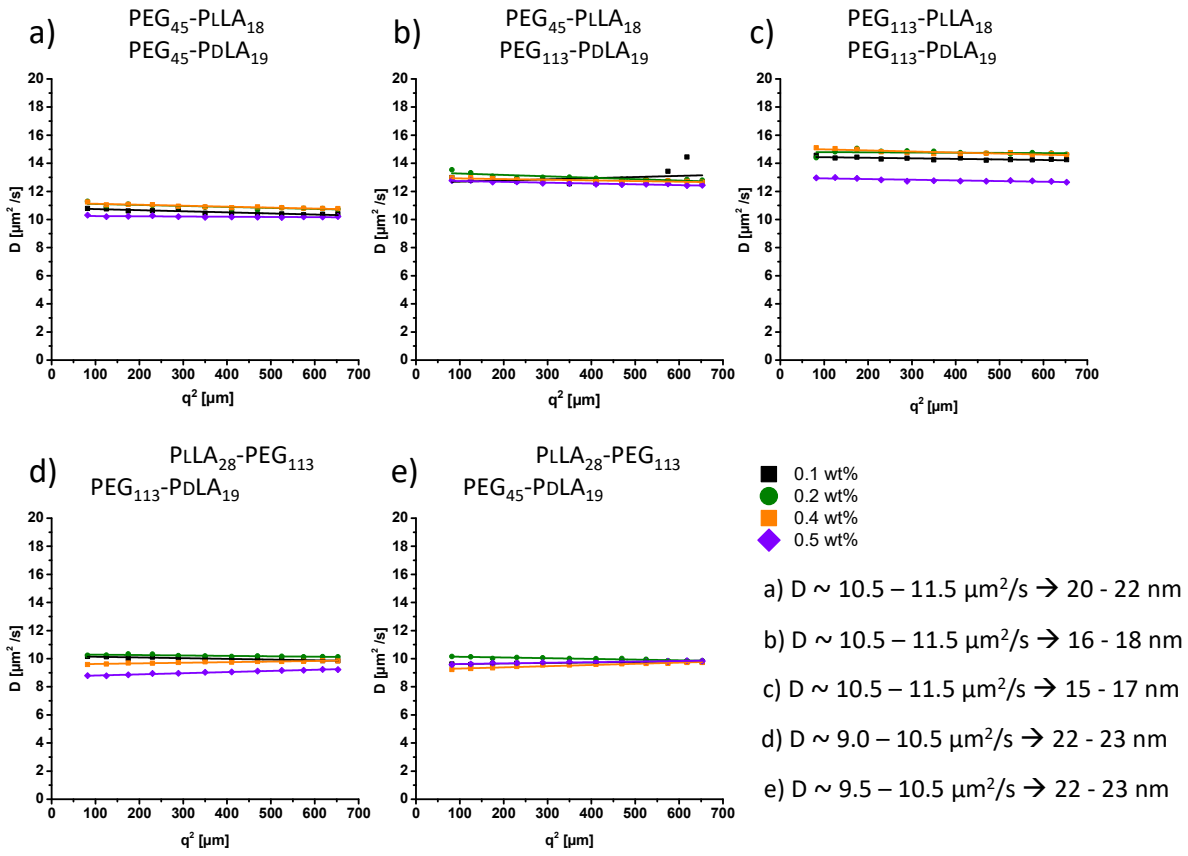

Figure 42: *Concentration and time-dependent DLS measurements. The observed diffusion coefficient D is plotted against the square scattering vector q^2.*

6.3 Conclusion of Self-Assembly Behavior

In Chapter 4 and 5, the self-assembly behavior of individual PEG-PLA and PLA-PEG amphiphilic block copolymers in solution with different PLA and PEG chain lengths was investigated. Additionally, PEG-PLA + PLA-PEG and PEG-PLA + PEG-PLA polymer mixtures with similar PLA chain length were prepared to study the influence of the stereocomplexation in the self-assembly in dilute aqueous solution. Samples were analyzed by DLS, TEM, cryo-SEM, and cryo-TEM. The influence of time on the crystallization mechanism and the resulting morphologies was demonstrated. These time-dependent studies allowed to understand the self-assembly behavior of PLA-based block copolymers better. For PEG-PLA copolymers solutions, irrespective of the PEG-PLA or PLA-PEG nature of the block copolymers, single PEG-PLA block copolymers were found to assemble into spherical micelles and worm-like structures. DLS and TEM measurements showed that the number of worm-like species decreased with

increasing PLA chain length. It was, therefore, proposed that two self-assembly mechanisms occur within the presented series, depending on the PLA chain length. As indicated by time-dependent experiments, block copolymers with short PLA blocks were found to have higher chain mobility in solution. This mobility allows a unimer exchange between the spherical micelles, thereby enabling a morphology transition to worm-like structures upon crystallization of the PLA block. However, above a certain PLA chain length, which is also dependent on the chain length of the hydrophilic block, a different self-assembly mechanism occurs. It was, therefore, proposed that the block copolymers with a long PLA block firstly assemble into colloidally stable spherical micelles, with a mostly amorphous PLA core. As crystallization proceeds, the spheres become unstable, and an inter-micellar fusion takes place, generating worm-like structures. However, due to smaller chain mobility, this effect was found to slow down with increasing PLA block length. Due to the increasing steric shielding effect of PEG with increasing block length the fusion from spherical micelles to worm-like structures were additionally influenced and more worm-like structures were produced by block copolymers with a smaller PEG block. The self-assembly of PEG-PLA block copolymers was found to be affected by the temperature. Self-assembly experiments conducted at a temperature below the T_g of the PLA blocks took place over a longer period of time than for experiments conducted at 60°C.

Interestingly, in crystalline stereocomplexes, worm-like morphologies were not observed, and the epitaxial growth seemed to be prevented. Pearl-neckless morphologies were favored by block copolymers mixtures with small PLA blocks. Irregular-shaped clusters were predominantly found for polymer mixtures with longer PLA blocks. The polymer block sequence of the block copolymer mixtures (PEG-PLA + PEG-PLA, PEG-PLA + PLA-PEG, PLA-PEG + PLA-PEG) did not have a significant influence on the aggregate morphologies.

7 Poly(lactide) and Poly(alkyl phosphonates)-based Copolymers

With the objective to expand the PLA based block copolymer catalog and achieve block copolymer mixtures with different polymer sequence and different hydrophilic segments attached to the PLA, poly(alkyl phosphonates) seems to be a promising alternative to PEG. Due to the similar polymer synthesis to PLA, poly(alkyl phosphonate)s offer an opportunity to synthesize new di- or triblock copolymers by sequential ring-opening polymerization from the corresponding alkyl phosphonate monomers. Thus, intensive purification steps, such as for PLLA-PEG and PDLA-PEG described before can be avoided. Nevertheless, due to the natural ability of PLA to undergo transesterifications during polymerization, the analysis of the mentioned block copolymers proved to be more difficult than expected.

In the following chapter, the synthesis and analysis of PLA-based block copolymers with poly(alkyl phosphonate)s as the hydrophilic block are reported. With the aim to produce different hydrophilic polymers that, due to their different hydrophilicity, influence the self-assembly in aqueous solutions, two different phosphonate monomers were chosen. The polymerization conditions of the individual monomers had to be adjusted since the reactivity was proven to be different from each other. Finally, some selected copolymers were investigated in terms of their self-assembly behavior and compared to the morphologies previously described in Chapter 5.

7.1 Synthesis

7.1.1 Monomers

For this work, the group of Dr. Frederik Wurm provided the 2-isopropyl-1,3,2-dioxaphospholane (^{i}PrP) (Figure 45; Figure 46), and the detailed synthesis of 2-methyl-1,3,2-dioxaphospholane (MeP) and other used chemicals are listed in the Appendix. The purified MeP monomer was obtained as reported[138] and analyzed by ^{13}C, ^{31}P, and ^{1}H-NMR spectroscopy. Due to the diastereotopic protons of the ethylene bridge (proton b), the ^{1}H-NMR spectrum presents two multiplett signals between 4.50 – 4.00 ppm and a doublet corresponding to the methyl group through coupling with the phosphorus at 1.66 ppm (^{2}J of 17.5 Hz) (Figure 43). In the ^{31}P-NMR spectrum a single peak at 49.9 ppm is observed, which proves the successful formation of a strained phosphonate as published before (Figure 44).[139]

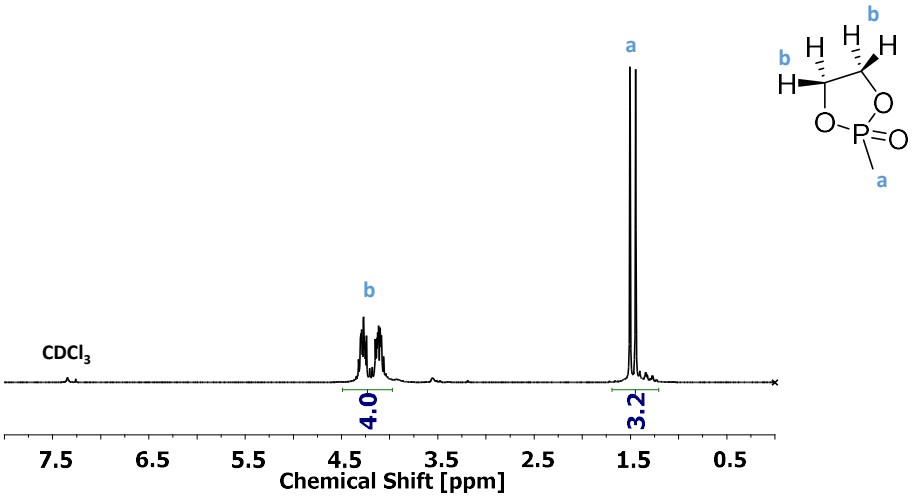

Figure 43: *^{1}H-NMR (300 MHz) spectrum of the 2-methyl-1,3,2-dioxaphospholane (MeP) in $CDCl_3$.*

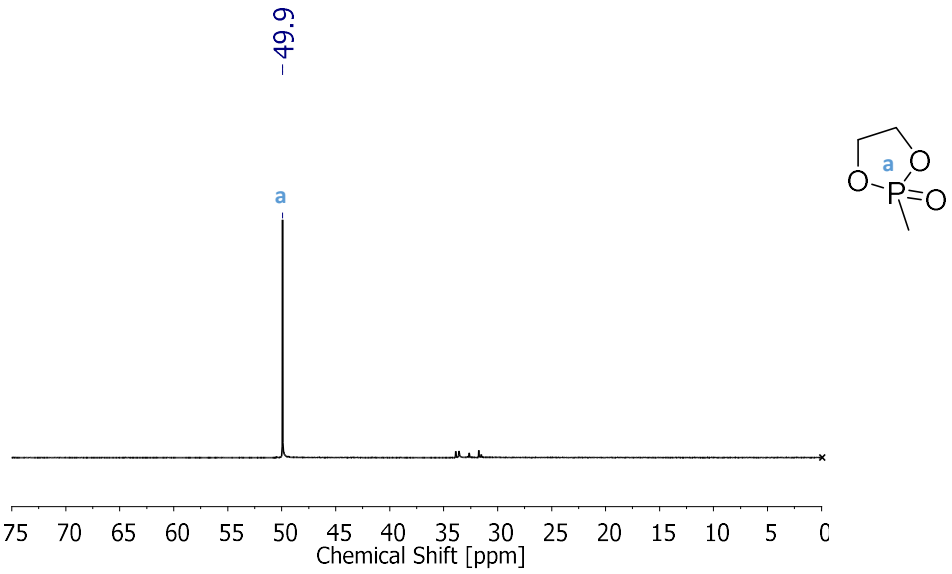

Figure 44*: ^{31}P-NMR (121.44 MHz) spectrum of the 2-methyl-1,3,2-dioxaphospholane (MeP) in $CDCl_3$.*

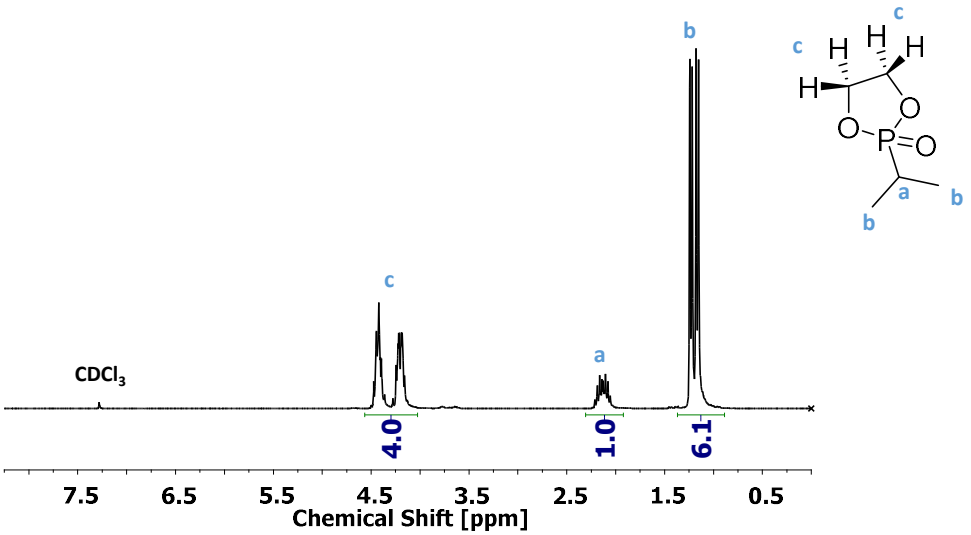

***Figure 45**: [1]H-NMR (300 MHz) spectrum of the 2-isopropyl-1,3,2-dioxaphospholane ([i]PrP) in $CDCl_3$.*

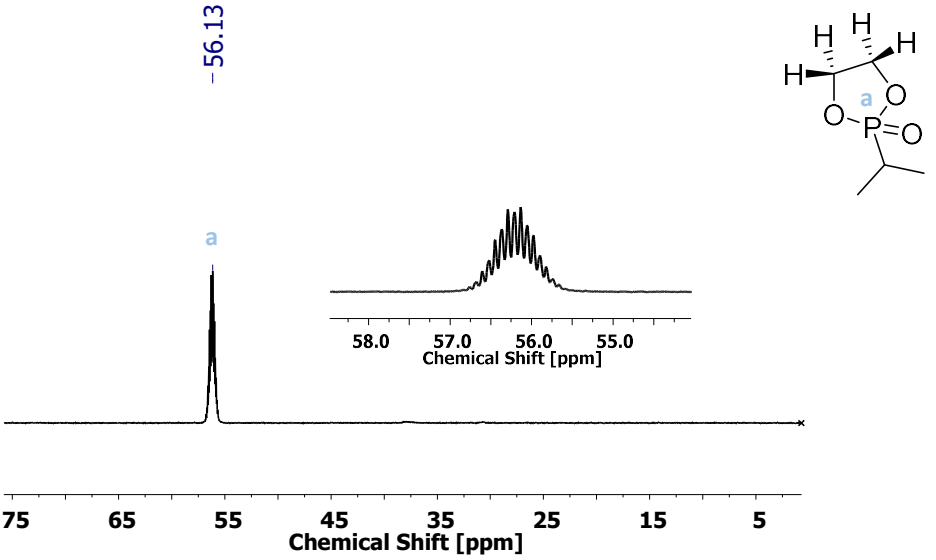

***Figure 46**: [31]P-NMR (121.44 MHz) spectrum of the 2- isopropyl-1,3,2-dioxaphospholane ([i]PrP) in $CDCl_3$.*

7.1.2 Polymerization

With the aim to establish the best polymerization conditions for MeP and [i]PrP, the corresponding homopolymers were synthesized before applying the approaches to the PLA-based precursors (see Chapter 5). In 2014 Wurm et al. reported a living polymerization of 2-methyl-1,3,2-dioxaphospholane (MeP) to generate poly(ethylene methylphosphonate), initiated by a primary alcohol and catalyzed by DBU.[139] Even though the conditions seem to be comparable to the polymerization of lactide, the effect of DBU differs for the ring-opening polymerization of the phosphonate. Considering of the fact that for the alkyl phosphonates the initiator to catalyst ratio $[I]_0$:$[DBU]_0$ was reported with 1:1.5 or higher,[139,140] the relative amount of catalyst in the system can be quite high when targeting short poly(alkyl

phosphonate) chain length. Since PLA-based precursors will be further used in this thesis, transesterification would be more probable with the presence of a larger amount of catalyst. Therefore, the polymerization conditions needed to be modified to reduce the amount of catalyst.

As summarized in Table 6 it is noticeable that the side group, does not only influence the resulting physical properties, such as water solubility, it also changes the reactivity and the ability to open the cyclic monomer. For MeP, it was possible to reduce the amount of the catalyst (DBU) to an equimolar amount compared to the initiator. ^{i}PrP, on the other hand, does not react with different nucleophiles and DBU as the catalyst at all. However, due to the higher activity, 1,5,7-triazabicyclo[4.4.0]dec-5-ene (TBD) was able to induce the ring-opening polymerization. The hindered reactivity from ^{i}PrP toward DBU-catalyzed nucleophiles can be explained by a stronger positive inductive effect (electron donating) of the isopropyl group compared to a methyl group. Furthermore, the sterically more demanding isopropyl side chain attached to the phosphor additionally hindered the polymerization under the described condition, which was also confirmed by the Wurm group.[141]

Table 6: Summary of polymerization approaches of MeP and ^{i}PrP with different catalysts and their corresponding concertation

	Monomer	**Initiator**	**Catalyst**	**$[M]_0$:$[I]_0$:$[Cat]_0$**	**Measured DP_n [a]**
1	MeP	Bn-OH	DBU	100:2.4:1	n.p.
2	***MeP***	***Bn-OH***	***DBU***	***100:2.4:2.4***	***37***
3	^{i}PrP	Bn-OH	DBU	100:3:1	n.p.
4	^{i}PrP	Dye-C2-NH_2	DBU	100:3:1	n.p.
5	^{i}PrP	Bn-OH	DBU	100:3:3	n.p.
6	***^{i}PrP***	***Bn-OH***	***TBD***	***100:3:1***	***31[b]***
7	***^{i}PrP***	***Bn-OH***	***TBD***	***100:3:3***	***102[c]***
8	***^{i}PrP***	***Bn-OH***	***TBD***	***100:5:5***	***36[b]***
9	***^{i}PrP***	***Bn-OH***	***TBD***	***100:3:3***	***58[b]***

All reactions were done under dry conditions and pre-dried reagents within 45-60 min. n.p. is corresponding to no polymerization detected. [a)] The average number of repeating units were determined by ^{1}H-NMR spectroscopy (300 MHz, DMSO-d_6 and $CDCl_3$).

The ring opening can be observed by ^{31}P-NMR and ^{31}P,^{1}H-HMBC-NMR spectroscopy, which is a heteronuclear multiple bond correlation experiment whereby ^{1}H and ^{31}P cores can be correlated to clarify the structure of complex molecules. The chemical shift of ~ 50 and 56 ppm of the corresponding cyclic monomers shift to ~ 36-38 ppm, which thereby identify the ring opened phosphorester (Figure 47 b). The molar mass was determined by end group analysis in ^{1}H-NMR spectroscopy, whereby the

methylene group of the initiating benzyl alcohol group at 5.08 ppm was compared with the backbone signals at 4.38 – 4.00 ppm.

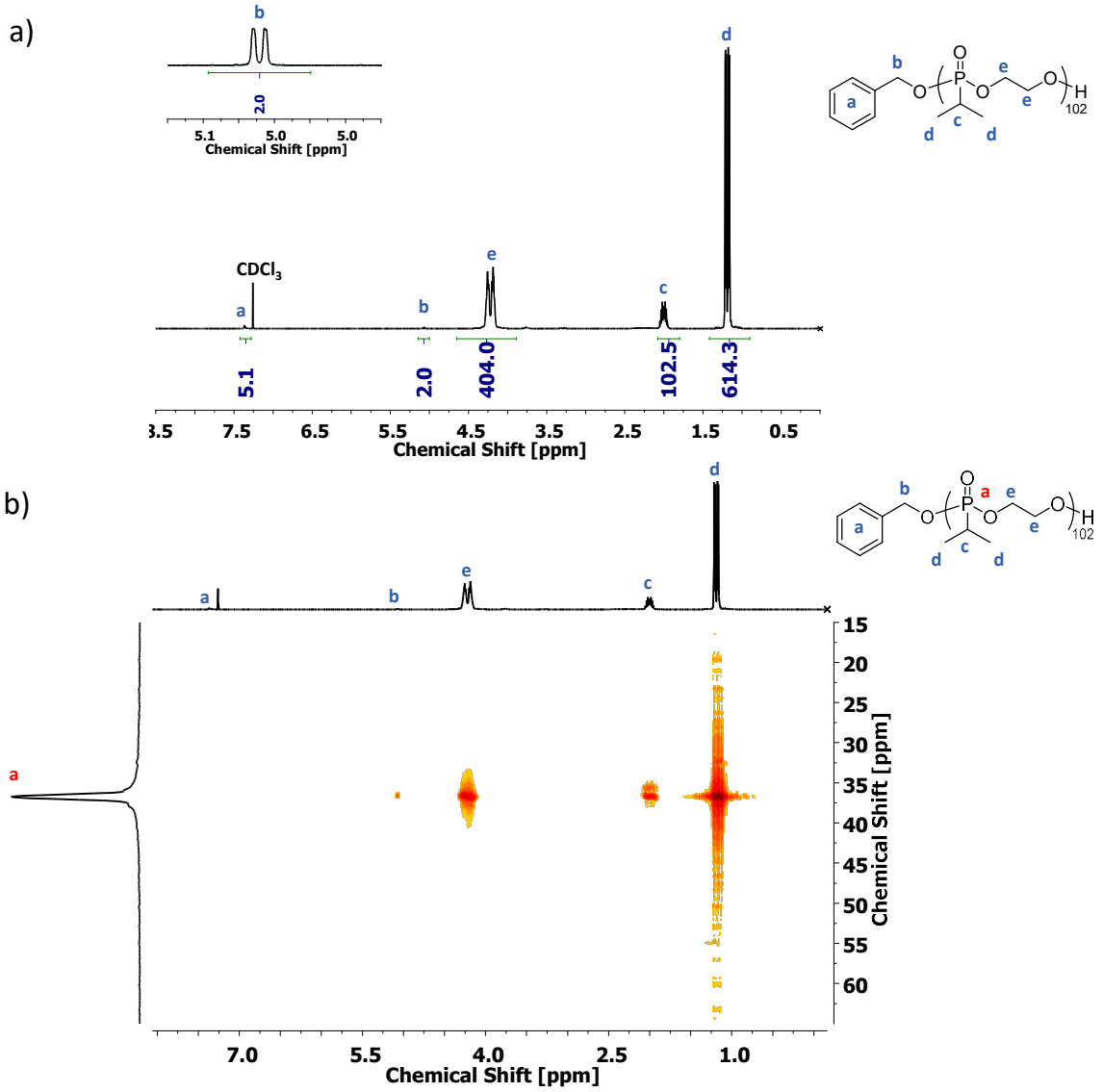

Figure 47: *a) ^{1}NMR (500 MHz) spectrum of the P^{i}PrP$_{102}$ in $CDCl_3$ after precipitation and additional dialysis against water. b) Corresponding ^{31}P,^{1}H-HMBC (300 MHz) spectrum of P^{i}PrP$_{102}$ in $CDCl_3$.*

Surprisingly, however, the synthetic approaches with an equimolar ratio of catalyst to initiator always lead to a higher calculated molar mass than expected. This, on the one hand, could be explained by incomplete initiation of the initiator. Since on prior reactions it was shown that the within the chosen reaction time, a complete monomer consumption was achieved, this possibility can be neglected. On the other hand, longer calculated polymer blocks can be obtained through the removal of shorter polymers within the purification processes such as precipitation or dialysis. Therefore, sample 7 (Table 5) was analyzed by ^{1}H-NMR spectroscopy after precipitation and dialyzing the sample against water. An increase in the number average molar mass was observed, which indicated that the molar mass

distribution might not be as narrow as aimed for and the chain length calculated by ^{1}H-NMR spectroscopy is dramatically affected by the purification method. Consequently, the removal of lower molar mass fractions can be assumed during dialyzing the product. However, SEC analyses failed as either the polymer interacted with the column (THF) and/or the polymer could not be detected by RI/UV. For the sake of completeness, it has to be noted that all precipitated polymers contained a slight amount of the catalyst.

Based on the results shown above it was decided to reduce the catalyst to initiator ratio to 1:1, which represents an improvement for the synthesis of block copolymers as compared to the already described poly (alkyl phosphonate) synthesis in literature.

7.1.3 Synthesis of Poly(lactide) and Poly(phosphonate)-based Block Copolymers

7.1.3.1 Synthesis of the Precursors

With the aim to study the self-assembly of the individual block copolymers and their corresponding mixtures, PLLA- and PDLA-based precursors were prepared. The synthesized precursors (PLA or PEG-PLA) were purified by precipitation and subsequently dialyzed against THF or water. The obtained polymers were analyzed by ^{1}H-NMR spectroscopy and SEC to determine the polymer chain length and the apparent molar mass distribution ($Đ^{app}$) of the individual polymers. As seen in Figure 48, the used PEG_x-PLA_y block copolymers are already known polymers, which were investigated more in detail in chapters 5 and 6. Nevertheless, in consideration that the synthesized poly(alkyl phosphonate)s interact with the SEC column in THF and due to the iso-reflective behavior of the polymers in NMP, all precursors were additionally measured in NMP by the use of a viscometer detector. Even though, all samples were calibrated against polystyrene the observed values differ from obtained data with SEC in THF, which can be explained by the different ability of the polymers to swell in the used eluent or indicating adhesion of the polymers with the SEC column. Since the latter mentioned effect and the influence of poly(alkyl phosphonate) segments that will influence the hydrodynamic volume to an unknown extent, the molar mass will furthermore be determined by ^{1}H-NMR spectroscopy. The corresponding SEC-elugrams will be illustrated to discuss results in the next chapter. The in Table 7 presented polymer P^iPrP_{40} is a hydrophilic polymer, which in the following section will be used to create PLA-P^iPrP block copolymer.

See Appendix for all synthesis details; analytical results summarized in Table 7.

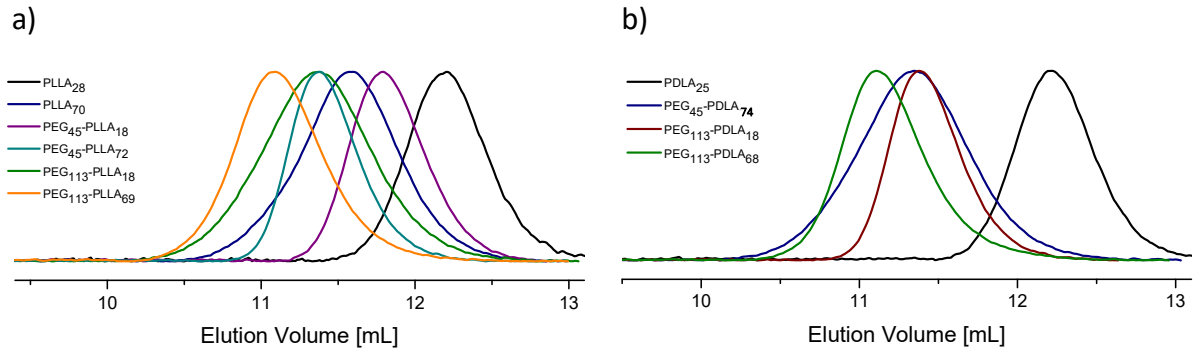

***Figure 48**: SEC-Viscometer traces of synthesized precursors (eluent NMP) a) PLLA-based precursors b) PDLA-based precursors.*

***Table 7**: Molecular characteristics of synthesized precursors for further di-and triblock copolymers with poly(phosphonate)*

Precursor[a]	M_n (g/mol) [a]	M_n^{app} (g/mol)[b]	$Đ^{app}$ [b]	M_n^{app} (g/mol)[c]	$Đ^{app}$ [c]
PLLA$_{28}$	2.100	3.000	1.12	2.000	1.40
PDLA$_{25}$	1.900	3.000	1.11	1.900	1.40
PLLA$_{70}$	5.100	8.300	1.13	6.700	1.35
P^{i}PrP$_{40}$	6.100	-[d]	-[d]	-	-
PEG$_{45}$-PLLA$_{18}$	3.400	5.400	1.10	4.400	1.28
PEG$_{45}$-PLLA$_{72}$	7.200	10.900	1.21	8.900	1.44
PEG$_{45}$-PDLA$_{74}$	7.300	11.300	1.21	9.500	1.41
PEG$_{113}$-PLLA$_{18}$	6.300	10.800	1.04	9.300	1.16
PEG$_{113}$-PDLA$_{18}$	6.300	10.800	1.04	9.100	1.17
PEG$_{113}$-PLLA$_{69}$	10.000	15.400	1.11	13.400	1.27
PEG$_{113}$-PDLA$_{68}$	10.000	15.100	1.08	12.700	1.25

[a)] Copolymer composition and the average number of repeating units were determined by ^{1}H-NMR spectroscopy (300 or 500 MHz, $CDCl_3$). [b)] Apparent number-average molar masses (M_n^{app}) and dispersity indexes ($Đ^{app}$) were determined by SEC (eluent: THF, calibration: polystyrene).[c)] Apparent number-average molar masses (M_n^{app}) and dispersity indexes ($Đ^{app}$) were determined by SEC (eluent: NMP, calibration: polystyrene).[d)] obtained polymer is not soluble in THF and immediately used for further reactions.

7.1.3.2 Synthesis of Poly(lactide)- and Poly(phosphonate)-based Block Copolymers

The 2-alkyl-2-oxo-1,3,2-dioxaphospholanes MeP and ^{i}PrP were polymerized, as described in chapter 7.1.2, with DBU and TBD respectively. Considering the overall aim of investigating the self-assembly behavior of the single block copolymers and their corresponding mixtures, the precursors, presented in chapter 7.1.3.1, were used. For the poly(alkyl phosphonates) an individual chain length between 28 and 41 repeating units was targeted, which correspond to a molar mass between 3.500 and 5.000 g/mol depending on the used monomer. After precipitation and subsequent dialysis of all polymers in

water, the ring opening process was observed by ^{31}P-NMR spectroscopy. The poly(alkyl phosphonate)s chain length was calculated by ^{1}H-NMR spectroscopy by comparing the initiating group of the precursor (methoxy or benzyl group) and the backbone signals of the phosphonates at 4.40 - 4.00 ppm (see in chapter 7.1.2). Interestingly, the observed chain length for all triblock copolymers, except for of PEG_{45}-PDLA_{82}-PMeP$_{33}$ (Table 8, polymer 3), have a smaller value than the theoretical one which was targeted, although, under the applied conditions the quantitative monomer conversion should be reached (Table 8, Polymer 3-5 and 6-10).[139,141] In contrast, the diblock copolymers are longer than aimed for, which has also been observed for the phosphonate homopolymers (such as P^{i}PrP$_{40}$) (chapter 7.1.2 and 7.1.3.1).

***Table 8**: Molecular characteristics of synthesized poly(alkyl phosphonate) and poly(lactide)-based copolymers*

	Precursor		**Polymer**					
	Sample[a]	**V_p (mL)[b]**		**Sample[a]**	**M_n (g/mol)[a]**	**aimed PP DP_n**	**V_p (mL)[b]**	**$Đ^{app}$ [b]**
1	**PLLA_{28}**	12.20	MeP	**PLLA_{33}-PMeP$_{50}$**	8.600	41	11.81	1.70
2	**PLLA_{70}**	11.60		**PLLA_{88}-PMeP$_{49}$**	12.400	41	11.45	2.00
3	**PEG_{45}-PLLA_{18}**	11.79		**PEG_{45}-PLLA_{19}-PMeP$_{20}$**[c]	5.800	41	11.72	1.35
4	**PEG_{45}-PLLA_{18}**	11.79		**PEG_{45}-PLLA_{20}-PMeP$_{36}$**	7.800	41	11.64	1.41
5	**PEG_{45}-PLLA_{72}**	11.37		**PEG_{45}-PLLA_{72}-PMeP$_{18}$**	9.400	28	11.35	1.71
6	**PEG_{45}-PDLA_{74}**	11.34		**PEG_{45}-PDLA_{82}-PMeP$_{33}$**	12.000	28	11.25	1.59
7	**PEG_{113}-PLLA_{18}**	11.38		**PEG_{113}-PLLA_{18}-PMeP$_{20}$**	8.700	41	11.32	1.53
8	**PEG_{113}-PDLA_{18}**	11.44		**PEG_{113}-PDLA_{18}-PMeP$_{25}$**	9.400	41	11.32	1.37
9	**PEG_{113}-PLLA_{69}**	11.10		**PEG_{113}-PLLA_{69}-PMeP$_{24}$**	12.900	41	11.05	1.29
10	**PEG_{113}-PDLA_{68}**	11.10		**PEG_{113}-PDLA_{64}-PMeP$_{29}$**	13.100	41	11.11	1.31
11	**PLLA_{28}**	12.20	^{i}PrP	**PLLA_{22}-P^{i}PrP$_{27}$**[c]	6.100	33	11.60	1.80
12	**PDLA_{25}**	12.21		**PDLA_{22}-P^{i}PrP$_{26}$**[c]	5.500	33	11.62	1.88
13	**PEG_{113}-PLLA_{18}**	11.44		**PEG_{113}-PLLA_{11}-P^{i}PrP$_{18}$**[c]	8.500	33	11.35	1.28

[a)] Copolymer composition, the average number of repeating units and resulting molar mass were determined by ^{1}H-NMR spectroscopy (300 and 500 MHz, $CDCl_3$). [b)] Elution volume (V_p^{app}) and dispersity indexes ($Đ^{app}$) were determined by SEC (eluent: NMP, calibration: polystyrene). If not labeled with c), the polymerizations were done under the same conditions at room temperature for 2h before quenching the reaction. [c)] polymerization time = 1h

Due to the possibility of transesterification, which can take place in both the polyphosphonate and PLA block, the difference in chain length could be explained by this effect. Although the side reaction within the PLA block is faster, with the use of a PLA-based diblock precursor that has a large weight fraction of PEG, which will not undergo any side reaction and additionally shielding the PLA block, the transesterification within the phosphonate chain seems to dominate. This assumption additionally can be supported by the PLA chain length of the triblock copolymers, which are still comparable to the observed values of the used diblock precursors. For the synthesized diblock copolymers (Table 8; entry 1 and 2) the calculated chain length of the PLA part increased compared to the precursors (homo PLA). Since the PLA chain length is not able to grow without any new lactide monomer, the measured increasing chain length may be a result of transesterification from the phosphonates with the lactide block. Therefore, small PLA homopolymers get cleaved off by transesterification and would be removed within the purification process. At the same time, a lower amount of the initiating benzyl alcohol would be noticed in ^{1}H-NMR spectroscopy. Consequently, the chain length seems to increase, since the end group analysis is shifted to a higher terminal group to polymer main chain ratio. At this point, all individual explanation were assumptions and cannot be quantified so far. Therefore, this effect needs to be investigated more in detail in the future.

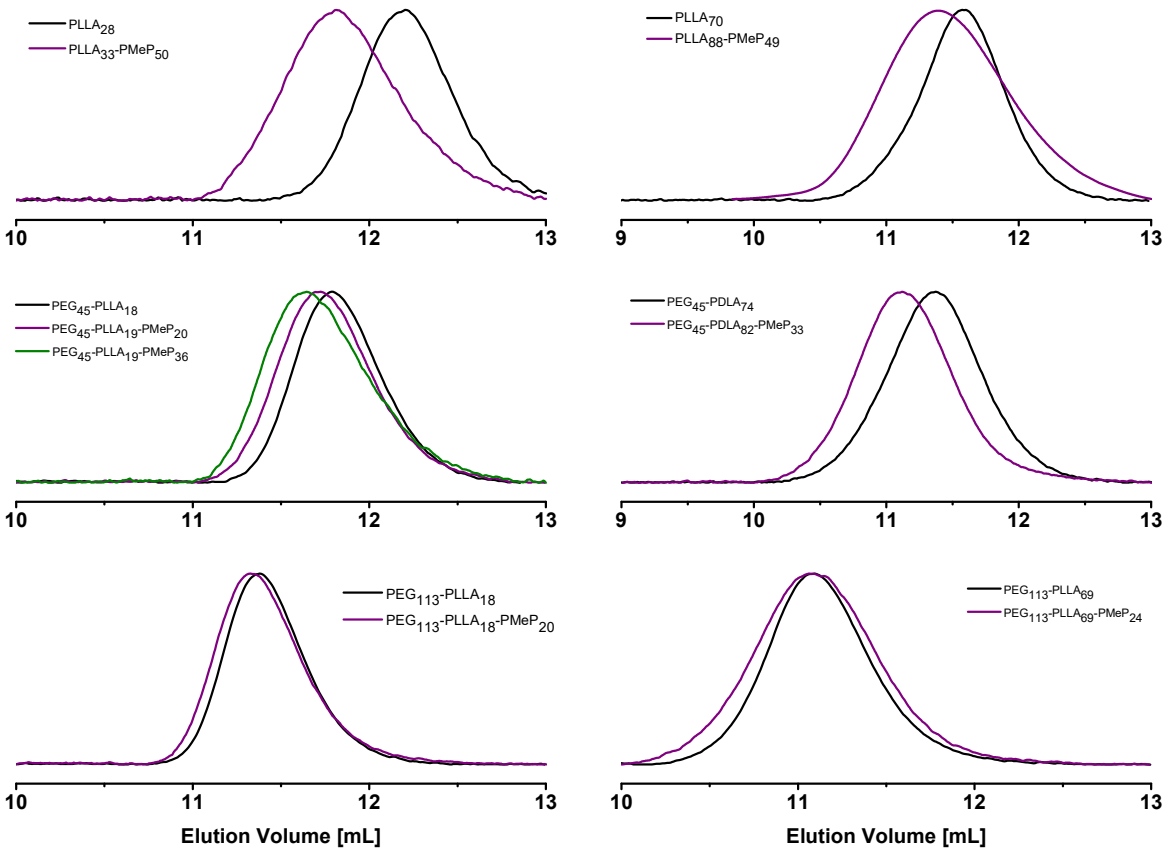

***Figure 49**: SEC-Viscometer traces (eluent NMP) of synthesized PLLA and PMeP-based copolymers (purple and green curves). The black curves correspond to the precursors.*

By comparing the maxima of the elution volume of the synthesized polymers with its precursors, a shift to smaller volumes is generally noticeable, whereby the difference of the individual elution maxima decreases with increasing molar mass of the precursor. At the same time, the molar mass distribution becomes broader, which additionally indicates side reactions such as transesterifications (Table 8 and Figure 49).

Nevertheless, more interesting is the evaluation of the NMR spectra since an interesting phenomenon can be observed. As seen in Figure 50, after PMeP polymerization with the corresponding precursors, in addition to the backbone (~ 4.43 – 4.00 ppm), and methyl peaks (~ 1.70 – 1.30 ppm) an unexpected multiplett peak is detectable at ~ 5.07- 4.96 ppm (Figure 50). However, by HSQC- and $^{13}C,^{1}H$-HMBC-NMR spectroscopy the peak can be identified as a portion of the methine group (Figure 51, Figure 52, proton c), which surprisingly also exhibits multiple cross relaxations with the phosphorus of the PMeP segment.

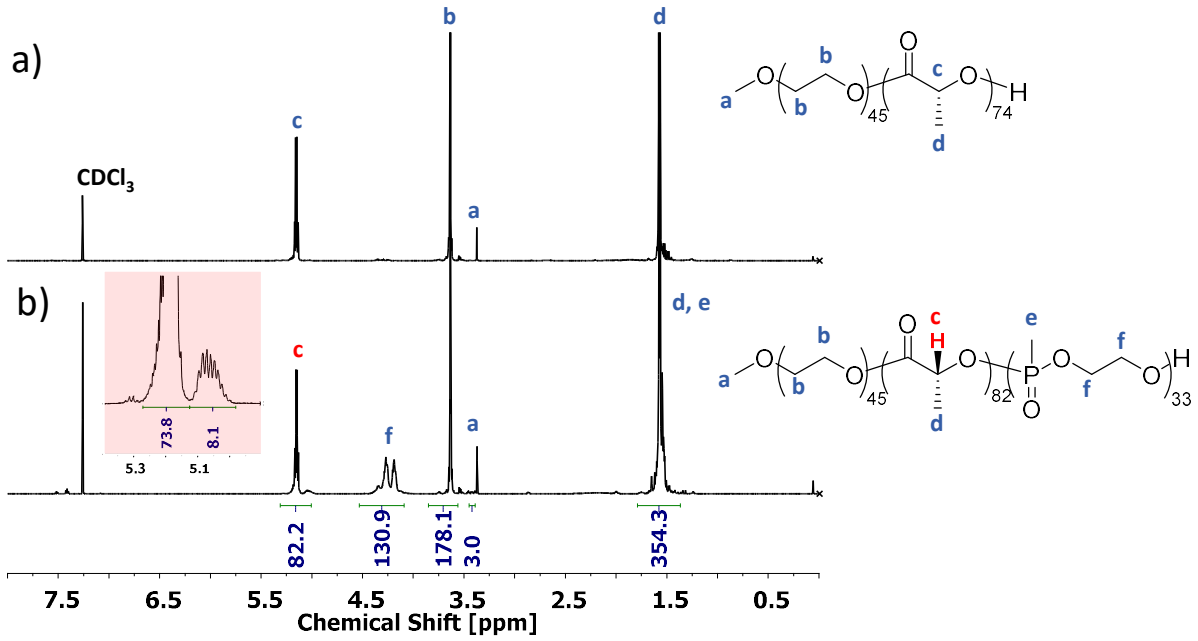

Figure 50: *a) ^{1}H-NMR (500 MHz) spectrum of the precursor PEG_{45}-$PDLA_{74}$ in $CDCl_3$ after precipitation and additional dialysis against water. b) Corresponding ^{1}H-NMR (500 MHz) spectrum of PEG_{45}-$PDLA_{82}$-$PMeP_{33}$ in $CDCl_3$.*

By comparing the ^{1}H-NMR spectrum of the synthesized copolymers with those of the precursors, it should be noted that the number of the corresponding proton c in the lactyl repeating unit match with the evaluated values of the already mentioned precursors. Although the ratio between the main peak at ~5.25- 5.10 ppm and the minor peak at ~ 5.10 - 4.98 ppm of the PMeP-PLA-based copolymers is ~ 0.85:0.15. The obtained integrals of the smaller peak are still too large to be seen as the corresponding interfacial proton of PLA to PMeP. Especially for the polymers with a longer PLA block the integral is related up to 8 protons as seen in Figure 50.

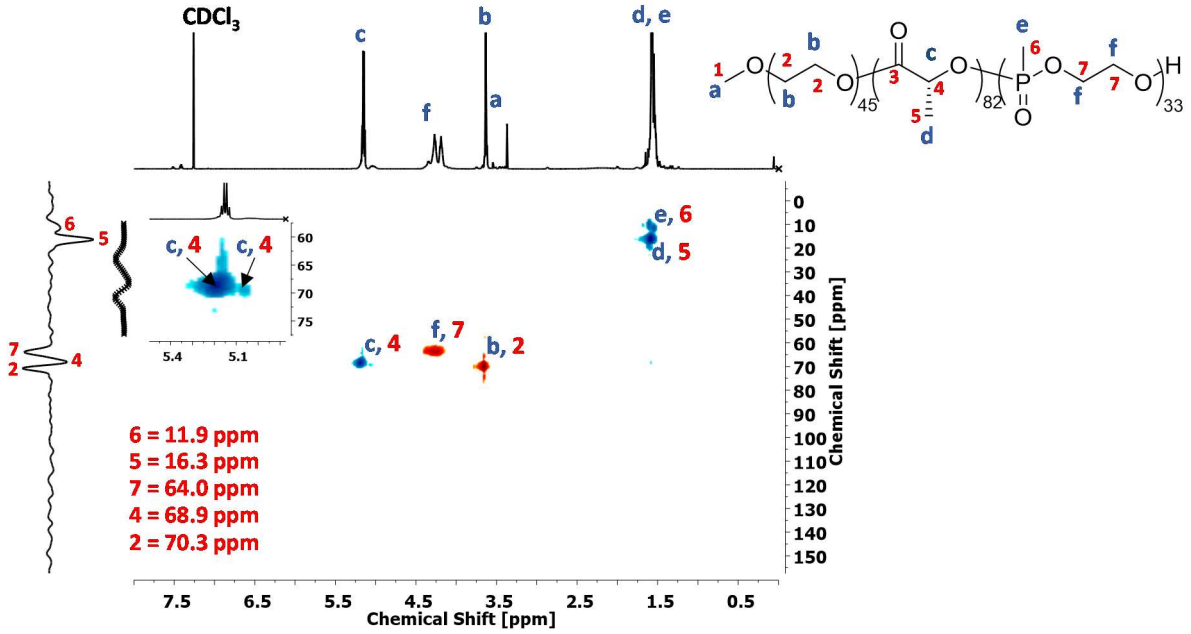

***Figure 51**: Typical HSQC-NMR spectrum (300 MHz, x-axis: ^{1}H chemical shift (ppm), y-axis: ^{13}C chemical shift (ppm)) of PEG_{45}-$PDLA_{82}$-$PMeP_{33}$ in $CDCl_3$*

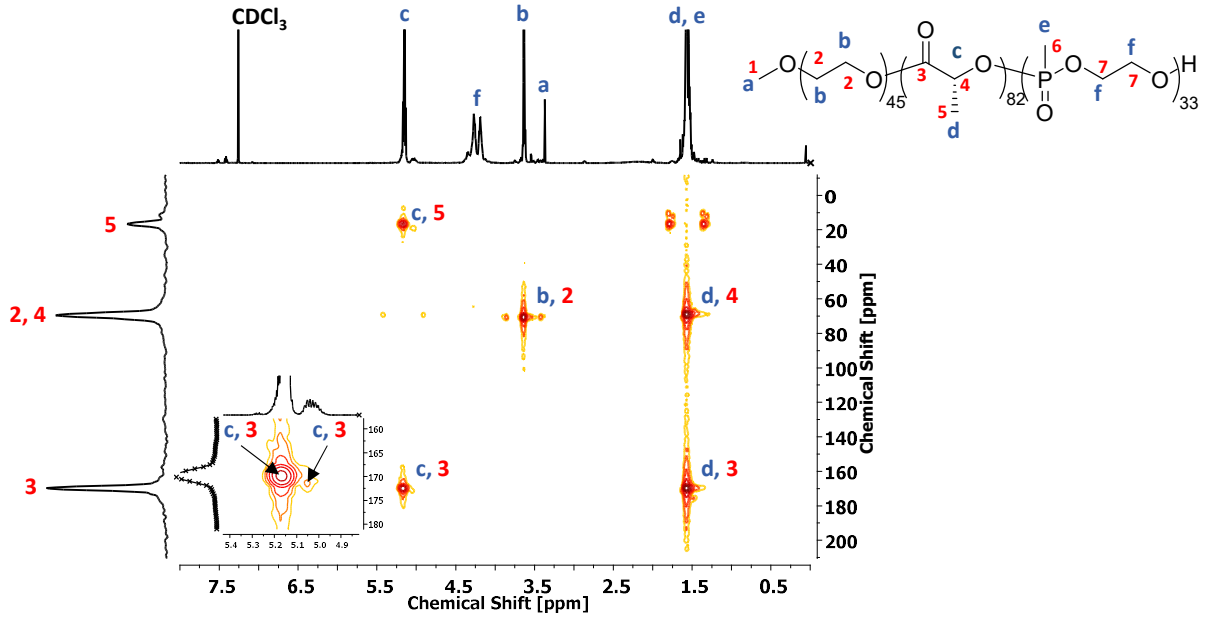

***Figure 52**: ^{13}C, ^{1}H-HMBC spectrum (300 MHz, x-axis: ^{1}H chemical shift (ppm), y-axis: ^{13}C chemical shift (ppm)) of PEG_{45}-$PDLA_{82}$-$PMeP_{33}$ in $CDCl_3$.*

Nevertheless, due to the correlation with carbon 4 and the additional presence of the negative ^{13}C signal (a result of the included Attached Proton Test (ATP) experiment in HSQC, Figure 51), it is particularly evident that the observed peak responds to the proton c. However, a slightly downfield shifted cross-relaxation of proton c with a carbonyl (3) and methyl (5) carbons can be observed, which suggests a slightly changed chemical environment (Figure 52).

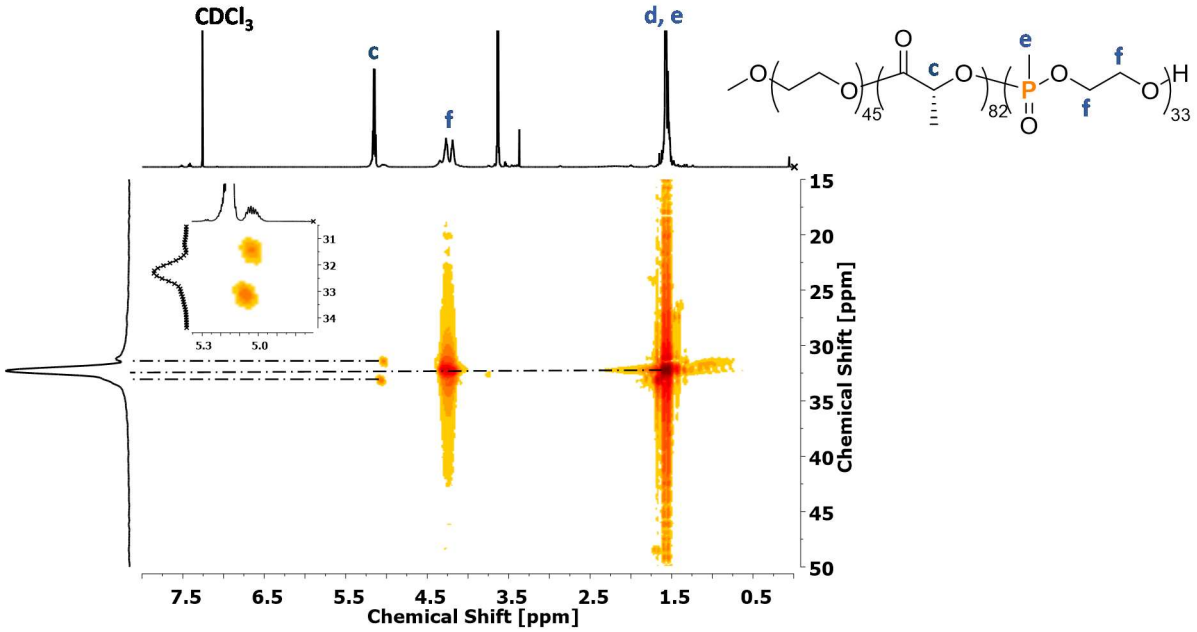

***Figure 53**: Typical $^{31}P,^{1}H$-HMBC spectrum (300 MHz, x-axis: ^{1}H chemical shift (ppm), y-axis: ^{31}P chemical shift (ppm)) of PEG_{45}-$PDLA_{82}$-$PMeP_{33}$ in $CDCl_3$. Out of simplicity only the coupling protons c, e, and f were presented*

The cross relaxation between the ^{31}P signal at 32.29 ppm with the backbone of the ethylene bridge in the MeP (Figure 53, proton f) repeating unit and the methylene side chain (Figure 53, proton e) was expected. Nevertheless, the minor ^{31}P-NMR signals at 33.21 and 31.54 ppm with the already discussed proton c indicates a different chemical environment for some protons in position c that could be caused by transesterification. The presence of two correlating ^{31}P-NMR signals is not completely solved yet. However, including all possibilities of transesterifications, various products exist (Figure 54). The ^{31}P-NMR signal at 33.21 ppm should correspond to the cross-coupling between the phosphorous in the PMeP main chain and the described proton c at the end group of the PLA block. Due to transesterification in “the first generation”, whereby only intramolecular and intermolecular attacks from terminal phosphonate polymer are possible, the ^{31}P-NMR signal is not changed, most likely because the neighboring groups to the corresponding phosphorus are not changed as well (Figure 54 a). Nevertheless, in the “second generation” of transesterification, a PEG-PLA block copolymer (that was produced in the “first generation” of transesterification) could finally attack the phosphorus in the main chain and could create a copolymer with one phosphorus that is included in a PLA chain. This phosphorus can have cross relaxations between two methine groups (Figure 54 b), which however, would have created a different chemical environment and could explain the high field shifted peak at 31.54 ppm.

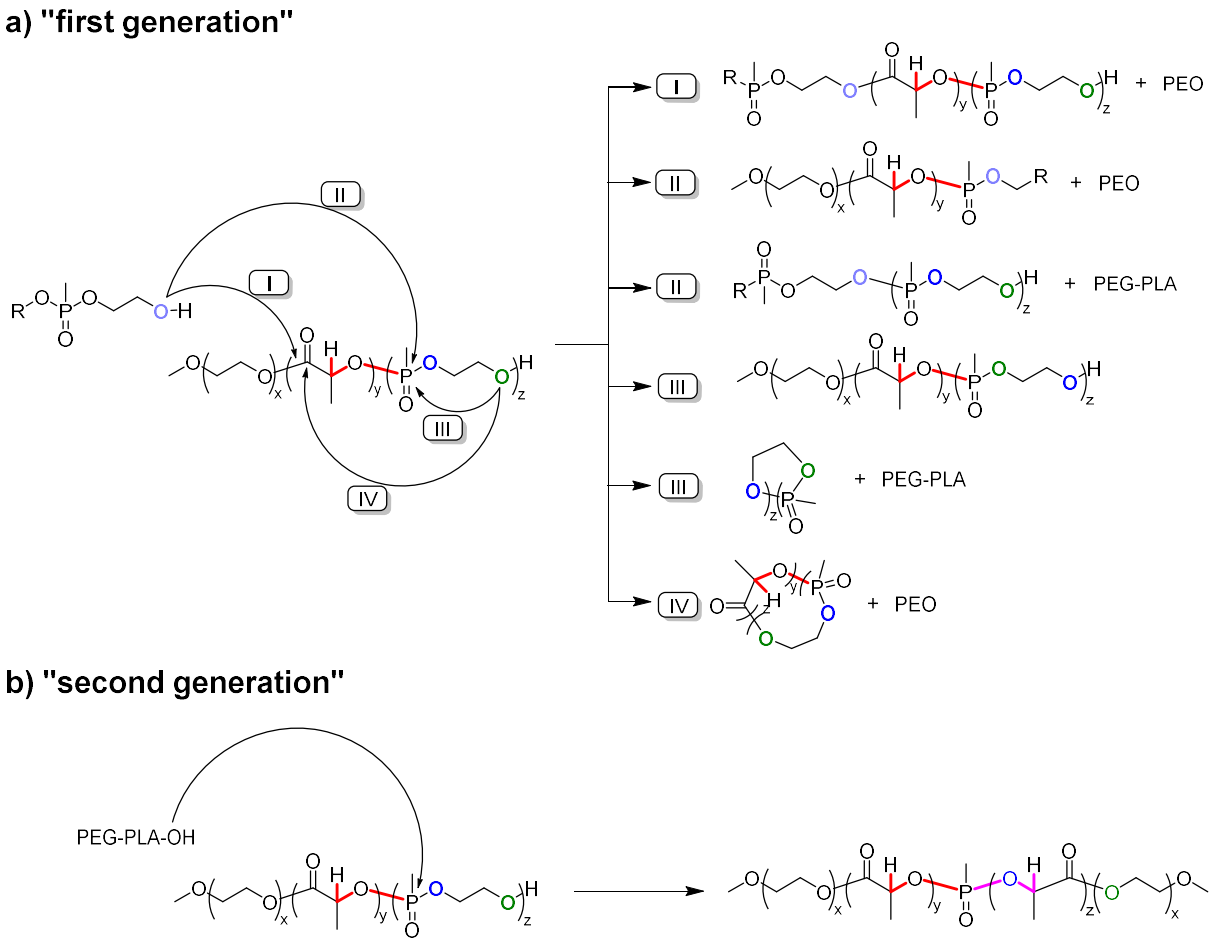

Figure 54: *a) "first generation" intra- and intermolecular transesterification and their resulting products. Cross-relaxation between the methine group and the phosphorous atom in the main chain over three bonds (red). b) Possible transesterification reaction in the "second generation" that result in PEG-PLA-P-PLA-PEG copolymer.*

By the analyses of the P^{i}PrP-based copolymers that were synthesized with TBD, a similar trend was observed. In SEC, the polymers PLLA$_{21}$-P^{i}PrP$_{26}$ and PDLA$_{22}$-P^{i}PrP$_{27}$ require a smaller elution volume than the used precursors but with broader distribution. The aimed triblock copolymer does not elute differently compared to its precursor. However, as described above, the determined PLLA chain length was affected during the polymerization of ^{i}PrP.

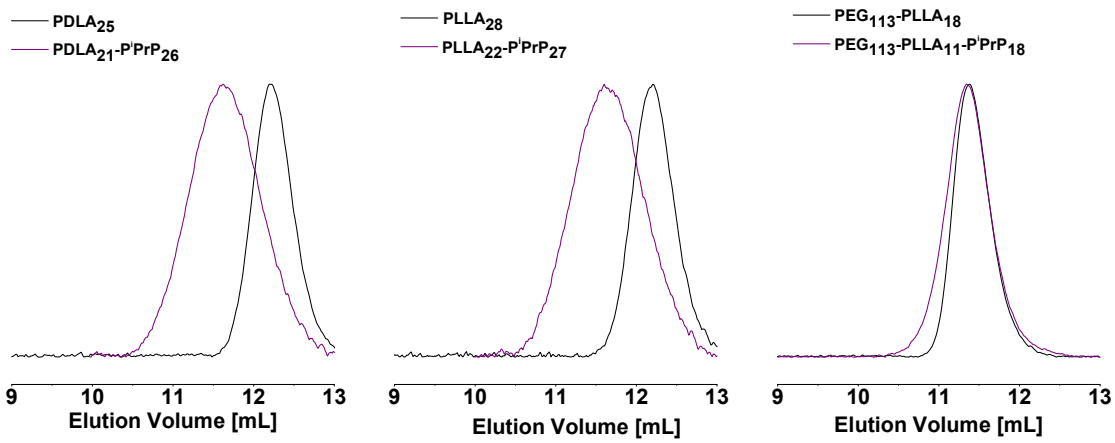

Figure 55: *SEC-Viscometer traces (eluent NMP) of synthesized polymers $PDLA_{21}$-P^iPrP_{26}, $PLLA_{22}$-P^iPrP_{27} and PEG_{113}-$PLLA_{11}$-P^iPrP_{18} copolymers (purple curves) and the corresponding precursors (black curves).*

In ^{1}H-NMR spectroscopy, all P^iPrP-based copolymers present the splitting of the proton peak at position c, whereby here the splitting is more intense (~ 0.45:0.55, Figure 57) and multiple cross-correlations between the phosphorus (~ 36.80 ppm) and these protons can be observed. This phenomenon plus the affected PLA and P^iPrP chain length indicate an intense transesterification process occurring during the polymerization. Additionally, temperature dependent ^{1}H-NMR spectroscopy experiments in DMSO-d_6 does not affect the peak split in any case, meaning aggregation behavior and related conformational induced breakdowns of the peak can be excluded (Figure 58).

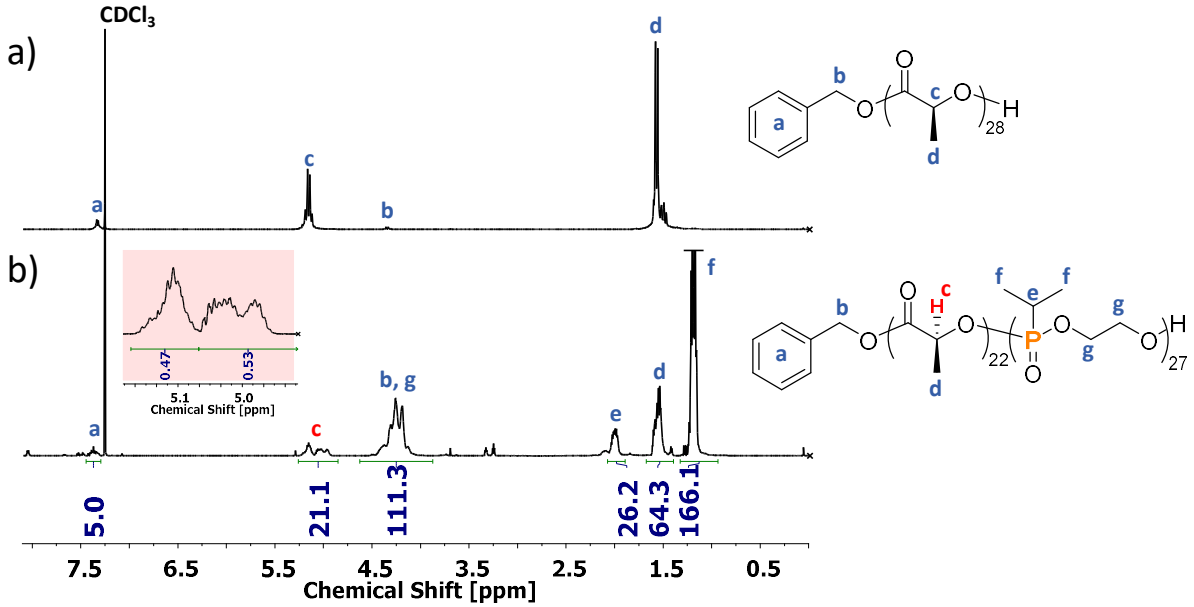

Figure 56: *a) ^{1}H-NMR (500 MHz) spectrum of the precursor $PLLA_{28}$ in $CDCl_3$ after precipitation and additional dialysis against water. b) Corresponding ^{1}H-NMR (500 MHz) spectrum of $PLLA_{22}$-P^iPrP_{27} in $CDCl_3$.*

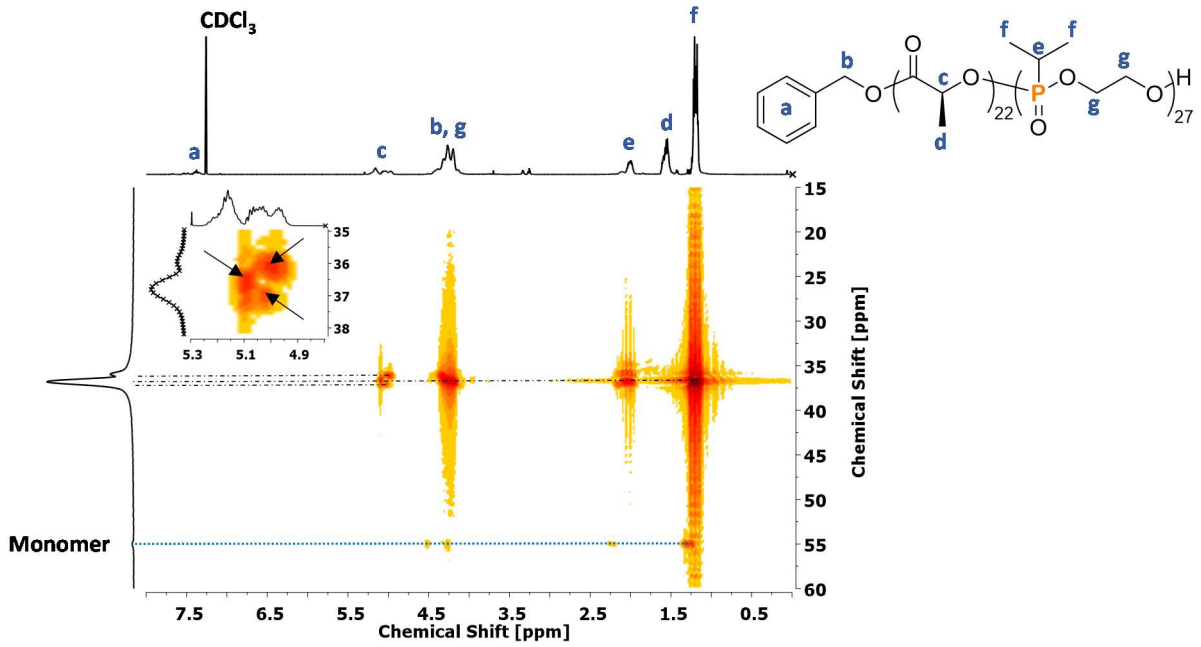

***Figure 57**: Typical $^{31}P,^{1}H$-HMBC spectrum (300 MHz, x-axis: ^{1}H chemical shift (ppm), y-axis: ^{31}P chemical shift (ppm)) of P_LLA_{22}-P^iPrP_{27} in $CDCl_3$.*

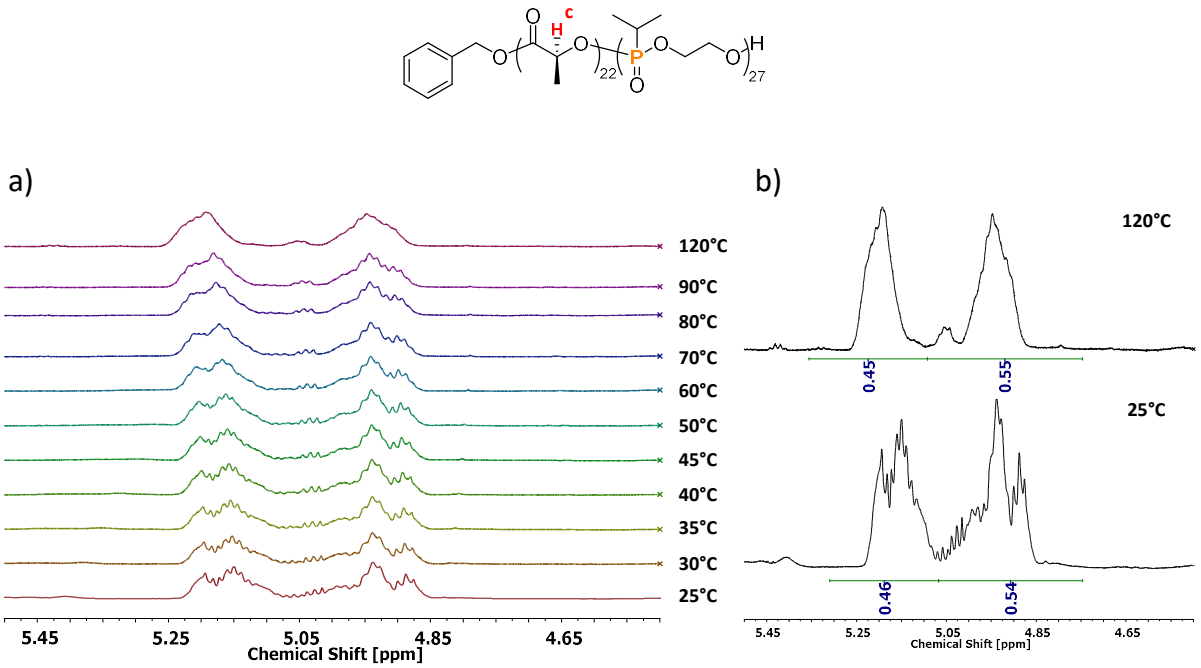

***Figure 58:** Temperature-dependent ^{1}H-NMR spectra (600 MHz) of P_LLA_{22}-P^iPrP_{27} in $CDCl_3$ in DMSO-d_6. a) a stacked presentation of the corresponding region of proton c (5.50 – 4.50 ppm) between 25 to 120 °C. b) peak ratio of the separated peaks at 25 and 120°C.*

To proof the presented conclusions, the PLA-based block copolymer P^iPrP_{40}-P_DLA_{18} was produced as a comparison. Therefore, P^iPrP_{40} was synthesized and further used as a precursor for the polymerization, as described in chapter 7.1.3.1. However, the final block copolymer did not show peak

splitting. Since the amphiphilic character of this polymer is comparable to the latter presented diblock copolymer that had the characteristic peak split, this split is an effect that was caused during the poly(phosphonate) polymerization. Additionally, the PLA chain length was also not affected and obtained as expected (Figure 59).

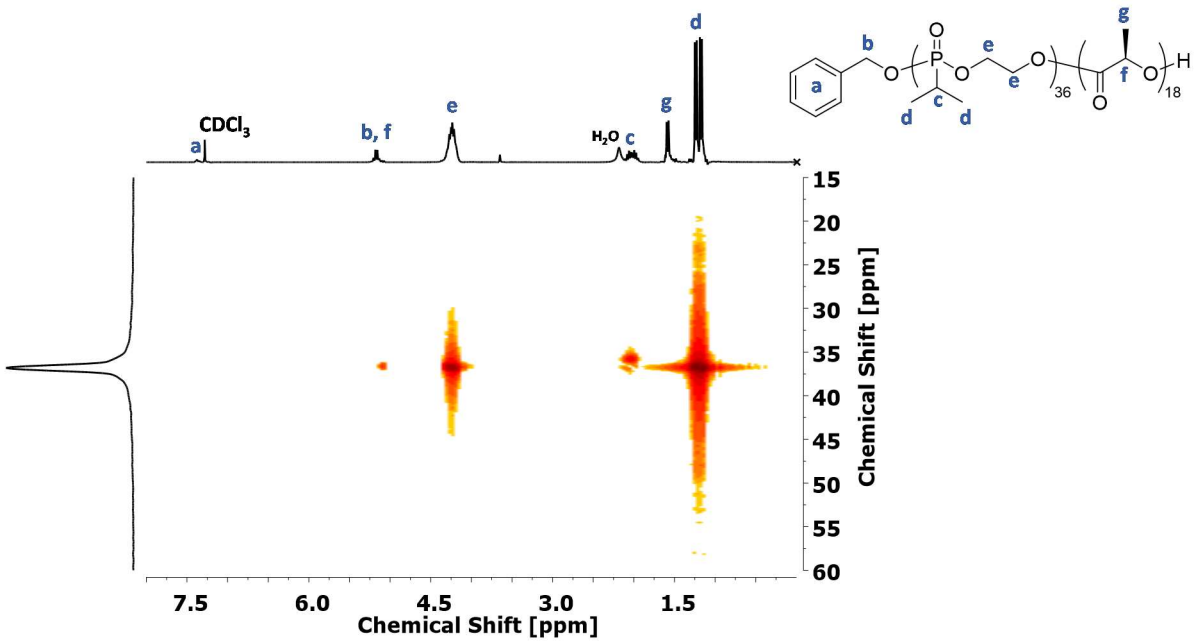

Figure 59: *Typical $^{31}P,^{1}H$-HMBC spectrum (300 MHz, x-axis: ^{1}H chemical shift (ppm), y-axis: ^{31}P chemical shift (ppm)) of $P^{i}PrP_{27}$-$PDLA_{18}$ in $CDCl_3$.*

7.1.4 The conclusion of Synthetic and Analytical Research Issues

In this chapter, the ROP of alkyl phosphonates was studied. To get a better understanding of the further planned synthesis of di- or triblock copolymers, the corresponding homo-PMeP, and $P^{i}PrP$ were produced with DBU or TBD as the catalyst, firstly. Through customized reaction conditions the homopolymers were obtained, which, however, showed a longer polymer chain than expected and evidence for transesterification reactions. Subsequently, a series of poly(lactide) and poly(alkyl-phosphonate)- based copolymers were synthesized and characterized by SEC and NMR spectroscopy. However, the desired di- and triblock copolymers initiated by PLA-based precursors presented a split in the ^{1}H-NMR spectroscopy peak of the corresponding methine group in the lactyl-signal. Additionally, multiple cross-correlations between the phosphorus in the main chain and the shifted proton peaks were detected by 2D-NMR spectroscopy. The intensity of the peak split seems to correlate with the used catalyst, whereby TBD as the stronger base also affects the phenomenon more intense than DBU. A chemical shift introduced by self-assembly can be excluded since the same effect was shown in different deuterated solvents ($CDCl_3$ and DMSO-d_6). Additionally, to exclude conformational induced splitting, temperature dependent ^{1}H-NMR spectroscopy was done. However, no significant change was

observed. Nevertheless, the acquired polymer-sequence cannot be solved so far. In this work, it is suggested that this effect may be caused by transesterification, which could explain multiple cross-correlations investigated in $^{31}P,^{1}H$-HMBC. However, the type and length of the initiator seem to affect the transesterification reaction in general. With low-molecular-weight initiators and homo-PLA initiators the obtained poly(alkyl phosphonate) chain length is longer than expected, and copolymers initiated with diblock precursors have a shorter poly(alkyl phosphonate) chain length than targeted.

As a consequence, the synthesized copolymers (excluding $P^{i}PrP_{27}$-$PDLA_{18}$) may not be considered as real block copolymers since various transesterification reactions between the poly(lactide) and poly(alkyl phosphonate) segments are possible. In the future, time-dependent polymerizations with both catalysts may be an excellent opportunity to understand the peak-split effect better and investigate the appearance of this split with time.

7.2 Self-Assembly

Even though the self-assembly behavior of the PLA and poly(alkyl phosphonates) cannot be discussed is such detail as the self-assembly was discussed in Chapter 4, it is still interesting to study the obtained morphologies of selected samples of PMeP-based copolymers and the block copolymer $P^{i}PrP_{27}$-$PDLA_{18}$. In order to prove that the self-assembly of the PMeP- and PLA-based copolymers are not affected by degradation in aqueous solutions, time-dependent dialysis experiments were done over seven days. Therefore three representatives were chosen that were firstly dissolved in THF and further added to a thrice amount of Millipore water. The polymer solutions were placed in a dialysis bag and further dialyzed for 24h, 72h, and 168h before freeze-drying. Afterward, the obtained polymer was investigated by ^{1}H-NMR spectroscopy and SEC (eluent NMP). With the exception of PEG_{45}-$PLLA_{20}$-$PMeP_{36}$, where small PMeP oligomers that were produced by transesterification were removed within the first 24 hours (and led to a slight shift to a smaller elution volume), no significant change was detected by neither SEC (Figure 60) nor ^{1}H-NMR spectroscopy (Appendix). Consequently, degradation can be excluded, and self-assembly can proceed under the described conditions.

The aggregates of all poly(alkyl phosphonate)s and PLA-based copolymers in water were measured by DLS; results are summarized in Table 9. The hydrodynamic radii vary from 10 to 350 nm, whereby the larger radii can be assumed as worm-like morphologies of different length, like the block copolymers in Chapter 4. The investigation of these samples by TEM confirmed this assumption, whereby both spherical and worm-like structures were detected. The diameters and widths of the observed cores with $\sim$ 10 nm are smaller than the used precursors described in Chapter 4. The presence of the worm-like structures seems to decrease with PLA chain length whereby the core diameter of the spheres with $\sim$ 12 ± 3 nm was relatively constant with independent PLA chain length. Nevertheless, a longer PMeP chain seems to lead to a hindered formation of worm-like morphologies

as it does for PEG_{45}-PLLA_{19}-$PMeP_{36}$ in direct comparison to PEG_{45}-PLLA_{19}-$PMeP_{20}$. However, since transesterification during the synthesis cannot be excluded, no further self-assembly mechanism will be discussed

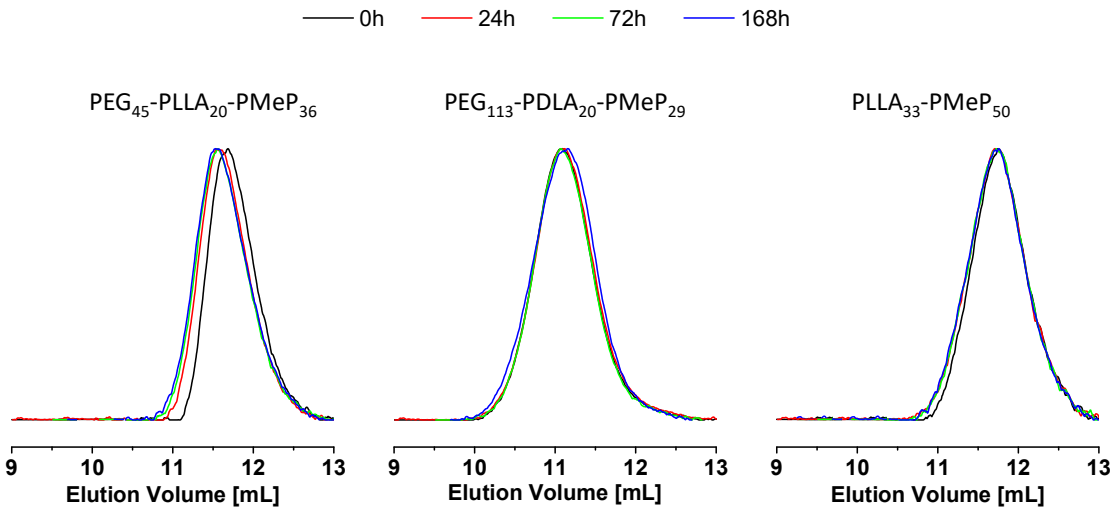

***Figure 60**: SEC traces (eluent NMP) of time-dependent dialyzed PEG_{45}-PLLA_{20}-$PMeP_{36}$, PEG_{113}-PDLA_{20}-$PMeP_{29}$, and PEG_{45}-PLLA_{20}-$PMeP_{36}$, before dialysis, after 24, 72 and 168 hours.*

Table 9: Summarized hydrodynamic radii investigated by DLS and observed morphologies and corresponding diameter investigated by TEM

Sample[a]	DLS[b]	TEM[c]		
	$R_{h,app}$ (nm)[b]	Morphology	$d_{core,worms}$ (nm)	$d_{core,spheres}$ (nm)
PLLA_{33}-$PMeP_{50}$	53	-	-	-
PLLA_{88}-$PMeP_{49}$	150	-	-	-
PEG_{45}-PLLA_{19}-$PMeP_{20}$	10/350	Worms	~ 10	-
PEG_{45}-PLLA_{20}-$PMeP_{36}$	18	Spheres	~ 10	9 ± 1
PEG_{45}-PLLA_{72}-$PMeP_{18}$	23	Spheres, Worms	~ 10	12 ± 1
PEG_{45}-PDLA_{82}-$PMeP_{33}$	-	-	-	-
PEG_{113}-PLLA_{18}-$PMeP_{20}$	25	-	-	-
PEG_{113}-PDLA_{18}-$PMeP_{25}$	30	-	-	-
PEG_{113}-PLLA_{69}-$PMeP_{24}$	12	Spheres, Worms	~ 10	13 ± 1
PEG_{113}-PDLA_{64}-$PMeP_{29}$	12/150	-	-	-
P^{i}PrP_{36}-PDLA_{20}	90	Spheres, Worms	18 ± 1	-

[a] Copolymer composition, the average number of repeating units were determined by ^{1}H-NMR spectroscopy (300 and 500 MHz, $CDCl_3$). [b] DLS measurements were done in aqueous solution at 0.5 wt%. All polymers were initially dissolved in THF before dropping into the aqueous solution and evaporated overnight [c] TEM experiments have proceeded as described in Chapter 4.

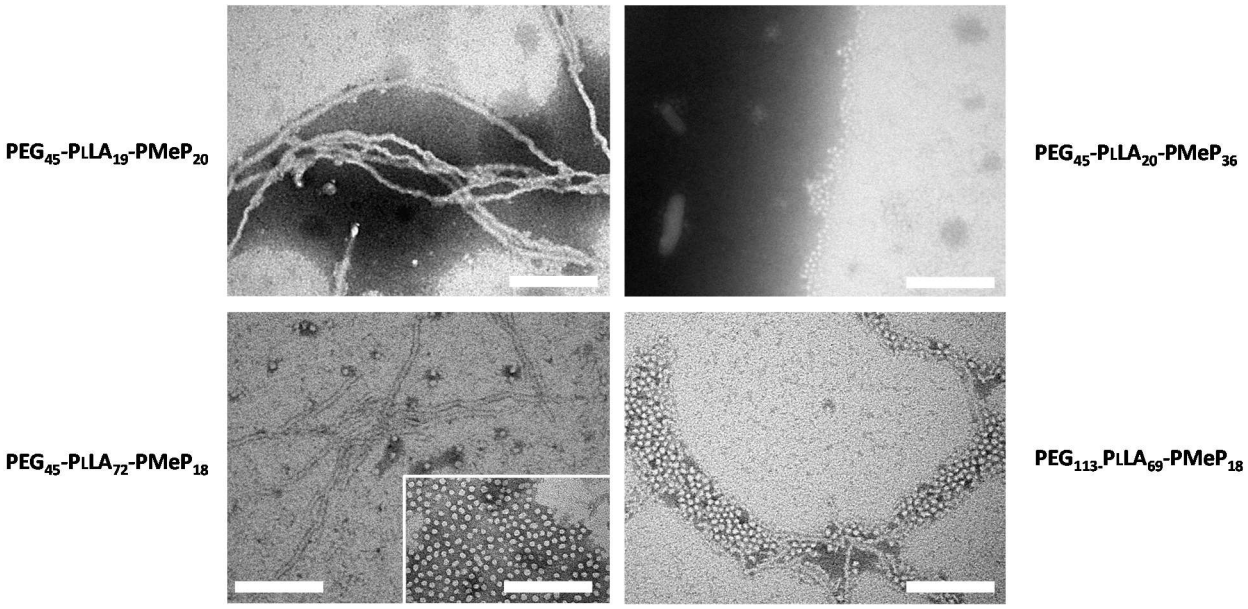

Figure 61: *TEM images (negative staining) of aggregates resulting from PEG-PLLA-PMeP copolymers; scale bar = 200 nm.*

In contrast to all the PMeP-based copolymers presented in Table 9, $P^{i}PrP_{36}$-$PDLA_{20}$ was produced via ROP of lactide in the second step, where transesterification is less relevant due to a low concentration of the catalyst. Consequently, the block copolymer sequence is controlled and the self-assembly is comparable to the experiments presented in chapters 5 and 6. Therefore it is less surprising that this block copolymer shows similar self-assembly behavior to the PEG-PLA block copolymers presented before. As indicated by DLS with a measured $R_h \sim 90$ nm, the pure $P^{i}PrP_{36}$-$PDLA_{20}$ block copolymers self-assemble into long worm-like structures with core diameters of 12 nm, as seen in Figure 62. By mixing $P^{i}PrP_{36}$-$PDLA_{20}$ with the opposite PEG-PLA enantiomer as PEG_{45}-$PLLA_{18}$, PEG_{113}-$PDLA_{18}$, and $PLLA_{20}$-PEG_{113}, the observed structures present clustered spherical morphologies or pearl-neckless structures again that occur through stereocomplexation. Therefore, the polymer sequence of the added block copolymers or the PEG chain length seems to be irrelevant in the presented cases.

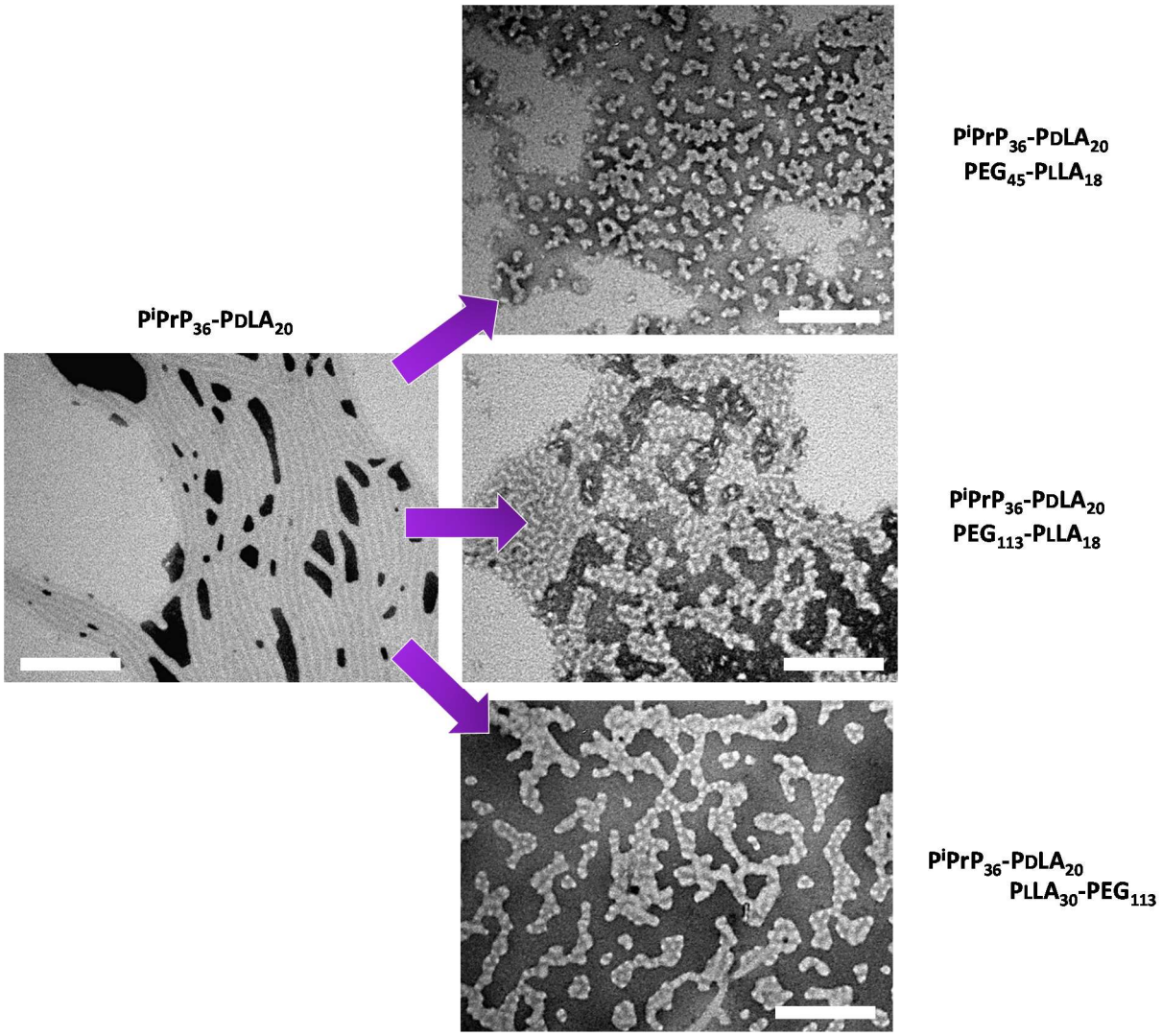

***Figure 62**: TEM images (negative staining) of aggregates resulting from PiPr36-PDLA and it stereocomplexed mixtures with PEG_{45}-$PLLA_{18}$, PEG_{113}-$PLLA_{18}$ and $PLLA_{28}$-PEG_{113}; scale bar = 200 nm.*

7.3 Conclusion

Under the already described conditions, self-assembly experiments for the PLA-PMeP–based copolymers were performed and characterized by DLS and TEM. In general, compared to the PEG-PLA block copolymers similar spherical and worm-like morphologies were obtained, albeit with smaller diameters for the spherical structures. The mixtures of P^iPrP_{36}-$PDLA_{20}$ with the corresponding PEG-PLA block copolymers (PEG_{45}-$PLLA_{18}$, PEG_{113}-$PLLA_{18}$, and $PLLA_{30}$-PEG_{113}) resulting once again in clustered spheres and pearl-neckless like aggregates and therefore does not differentiate to the results presented in Chapter 4. Therefore, the influence of the hydrophilic segments and sequence of the block copolymers seems to be irrelevant to the macrostructure when stereocomplexation is involved.

8 Summary and Outlook

Synthesis of PEG-PLA Block Copolymers

In this doctoral work, poly(ethylene glycol)-poly(lactide) block copolymers with different polymer-sequences (PEG-PLA and PLA-PEG) were produced, where the PLA block is synthesized by ring-opening polymerization (ROP). For the PEG-PLA block copolymers, PEG-OH with different molar masses (i.e., $M_n \approx 2$kDa and $M_n \approx 5$kDa) were used as the initiating species, resulting in block copolymers where the hydrophilic PEG block is bonded at the carbonyl-end of PLA. In order to reduce unwanted transesterifications during the DBU mediated ROP, an alternative catalyst was investigated for the PLA-based block copolymer synthesis. However, the acid/base-conjugate[64] DBU/BA was unable to produce well-defined block copolymers under the chosen conditions. In addition to planned ROP initiated by PEG-OH, a competitive PLA homopolymerization was detected. It is proposed, that in contrast to the reported mechanism of this catalyst, the unprotonated DBU is the reactive species, which, however, has a reduced reactivity due to the acid/base equilibrium. Consequently, on the one hand, the polymerization of lactide is very slow; on the other hand, DBU can also act as a nucleophile and produce a DBU inserted homo-PLA, as reported in literature.[70] Therefore the DBU/BA catalyst was impractical for the PLA-based block copolymer synthesis. Since the side reactions induced by DBU could be regulated by adjusted polymerization conditions, DBU was finally used to produce all PEG-PLA block copolymers with controlled chain lengths and narrow molar mass distributions.

For the PLA-PEG-block copolymers, a homo-PLA was produced first, modified with succinic anhydride, and finally linked to the PEG via Steglich-esterification. As a result, the hydrophilic PEG is attached at the alcohol end of the PLA, and therefore the sequence of the corresponding block copolymers is opposite to the PEG-PLA block copolymers. The purification of the PLA-PEG block copolymers was challenging, and the separation of the unreacted precursor was incomplete. As shown in SEC, the resulting products contained 3 to 6 wt% of unreacted PLA. Nevertheless, nine PEG-PLLA and nine PEG-PDLA block copolymers were obtained and used for self-assembly experiments in aqueous solutions.

In this study, the organo-catalyzed polymerization of PLA-based block copolymers with different polymer-sequence was investigated. In order to achieve a better understanding of side-reactions induced by DBU and its derivate, future work should involve the synthesis of PLA-based block copolymers. On the first look, it may seem to be unconventional to create block copolymers, which are usually more complex systems than homopolymers are; however, the advantage of using long precursors could also end in an advantage in the workup and evaluation of the products. When a competitive homopolymerization occurs, the generated species could be dramatically different when

a long precursor is used, especially at low monomer conversion. With the ability to fractionate these species and investigate them, the obtained data could give a more accurate picture of the DBU-mediated ROP.

Self-assembly

The self-assembly of the PEG-PLLA block copolymers in aqueous solutions resulted in spherical and worm-like species, dependent on the PLA block length. More precisely, while the diameters and the amount of the spherical micelles increase with increasing PLA chain lengths, the diameters of the worm-like morphologies stay relatively constant but the amount of which decreases with an increasing PLA block length. Supported by DSC experiments that presented increasing melting enthalpies of the PLLA blocks with time, it is proposed that the formation of the worm-like species is induced by crystallization of PLLA. Interestingly, the formation of the worm-like morphologies relies on different mechanisms dependent on the PLA-block lengths. On the one hand, PEG-PLLA block copolymers with small PLLA block length (e.g., PEG_{45}-$PLLA_{18}$) are soluble in water and have high chain mobility in solution. Conclusively, the core of the micelles primarily contains amorphous PLLA, and a unimer exchange occurs up to a point when the PLLA crystallize. On the other hand, for block copolymers with increasing PLLA block length (e.g., PEG_{45}-$PLLA_{72}$), an additional common solvent is needed to self-assemble the polymers in solution. Since all experiments were carried out at room temperature, the chain mobility of the block copolymers with larger PLLA block can be seen as reduced, and the primarily formed spheres are supposed to be “frozen” micelles. Due to incipient crystallization, the micelles become “unstable” and epitaxial growth between the micelles occurs. However, the formation of worm-like morphologies is influenced by the length of the PEG block. Due to a higher steric effect, longer PEG blocks seem to suppress the formation of worm-like structures. It has to be noted that with increasing PLA block length the polymer chains are packed more densely, which indicates a higher amount of crystallization in the micelles before becoming unstable.

Self-assembled polymer mixtures of PEG-PLLA and PEG-PDLA result in stereocomplexed species that are less defined than their parent polymers in solution and are unaffected by the polymer sequence of the mixing partners. Pearl-neckless or lozenge-like structures were observed, whereby with an increasing weight fraction of PLLA/PDLA, the morphologies were more complex, which indicated slower chain mobility. The PLLA- and PDLA block copolymers show a great affinity to each other. Despite the individual formation of the parent block copolymers in solution for 24 hours before the partners were mixed, no homopolymer crystals were obtained in DSC experiments. This phenomenon additionally supports the unimer exchange mechanism also occurring at room temperature for block copolymers with small PLA blocks, because, otherwise, no stereocomplex would be formed or homo-crystals would be obtained in the mixture.

To specify the self-assembly behavior of PLA-based block copolymers, the mechanism needs to be examined more in detail in the future. Since different morphologies can also be formed from block copolymer samples with broad molar mass distribution, fractionation of the self-assembled morphologies could help to identify the individual chain length. In the process of this thesis, there have been indications that the self-assembled structures can be influenced by small molecular additives such as dyes (i.e., pyrene), even if the sample preparation was similar to the presented method described in this work. It is also noteworthy that the transesterification can influence the self-assembled morphologies in aqueous solutions. In the Appendix (Chapter 11.6) a small study of a self-assembled PEG-PLLA copolymer is presented that showed a transformation of obtained morphologies, depending on the amount of transesterifications. However, this effect needs to be examined more in detail in the future. The stereocomplexation could also give new insights into the obtained morphologies. In cases of self-assembled block copolymers with a small PLA block, it is conceivable that an equimolar polymer mixture could influence the length of worm-like structures by preventing the homo-crystallization. Similar to the small molecular additives for single block copolymers, a mixture of a PLLA-based block copolymer and a homo PDLA-homopolmer could end in interesting results, which, however, are difficult to predict. Finally, temperature-dependent self-assembly experiments could give insight about the chain mobility of the copolymers in dependence of the PLA block lengths.

Poly(phosphonate) and Poly(lactide)-based Copolymers

During this work poly(alkyl phosphonate)- and PLA-based copolymers were synthesized by ROP of the corresponding lactide and alkyl phosphonate monomers. Due to a different reactivity generated by the isopropyl group, the more active catalyst TBD was used to polymerize 2-isopropyl-1,3,2-dioxaphospholane (^{i}PrP), whereby for 2-methyl-1,3,2-dioxaphospholane (MeP) DBU was used. The catalyst was chosen in an equimolar ratio to the initiator, and in all cases polymeric products were obtained. However, ^{1}H-NMR spectroscopy revealed a high field shifted split of the proton in the methine group in the corresponding lactyl repeating unit when a PLA-based precursor was used to initiate the phosphonate monomer. The split intensity is dependent on the used catalyst, whereby TBD affect this phenomenon more intensely than DBU. Additionally, the protons obtain a cross-relaxation with the phosphorus in the backbone, which, however, is not induced by self-assembly in the corresponding solvent as presented by temperature-dependent NMR spectroscopy. It is supposed that the described phenomena are caused by transesterifications between the PLA and poly(alkyl phosphonate) block.

The self-assembly of a $P^{i}PrP$-PLA-based block copolymer and its mixtures with PEG-PLA block copolymers result in similar morphologies to those observed in Chapter 5 and 6, whereby the $P^{i}PrP$-PLA-based block copolymer solution formed worm-like species in aqueous with a diameter of approximately $\sim$ 12 nm and a length of several micrometers. The block copolymer mixtures, regardless of the polymer sequence, resulted in clustered spheres.

Future work should focus on the actual reaction kinetics and their parameter sensitivity in order to investigate the peak split in ^{1}H-NMR spectroscopy that is caused by transesterification. It is worth studying the influence of the catalyst in more detail in order to minimize unwanted side reactions. Due to the different hydrophilic properties of the phosphonate, the final multi-block products can give new insight into PLA-based block copolymer self-assembly, whereby the development of different shape morphologies can further benefit from this polymer class.

9 Experimental Section

9.1 Reagents

Unless otherwise stated, all reagents were purchased from commercial sources and used as received. Triethylamine (TEA) (99.9% pure), 1,4-dioxane (99.98%, HPLC grade), chloroform-d_1 ($CDCl_3$) (99.8 atom D), ethylenediamine (99%), and 1,8-naphthalic anhydride (99.9%) were purchased from Acros Organics. L-Lactide (L-LA) and D-lactide (D-LA) were purchased from PURAC Biochem BV, and freeze-dried from 1,4-dioxane before use. Poly(ethylene glycol) methyl ether (PEG-OH, $M_n \approx 2$ kDa and 5 kDa), tetrahydrofuran (THF) (99%), pyridine (99%), succinic anhydride (96%), benzyl alcohol (99.8%), dimethyl phosphate (97%), tetraphenylphosphonium bromide (97%), and 1,5,7-Triazabicyclo[4.4.0]dec-5-ene (TBD) (98%) were purchased from Sigma Aldrich. Dichloromethane (DCM) (99.99%, HPLC grade), ethanol (pure; 99.94%), and Diethyl ether (99.5%) was purchased from VWR. Benzoic acid (analytical grade) was received from Fischer. 1,8-Diazabiccyclo(5.4.0)undec-7-ene (DBU) (99%), and 1,2-dibromoethane (98%) were received from Fluka. N-(3-dimethylaminopropyl)-N´-ethylcarbodiimide hydrochloride (EDC·HCl) (98%) was received from Alfa Aesar.

9.2 Analytical Instrumentation and Methods

9.2.1 Nuclear magnetic resonance (NMR) spectroscopy

NMR spectra were recorded on Bruker Avance 300 MHz, 500 MHz, or Bruker Avance III 600 MHz spectrometers. Samples were prepared in $CDCl_3$ or DMSO-d_6. Signals were referenced to the respective solvent peaks; $CDCl_3$ δ (^{1}H) 7.26 ppm, δ (^{13}C) 77.16 ppm; DMSO-d_6 δ (^{1}H) 2.50 ppm, δ (^{13}C) 39.52 ppm.

9.2.2 Size exclusion chromatography (SEC)

SEC with simultaneous UV and RI (differential refractive index) detection was performed with two different eluents and stationary phases: (*i*) THF, 0.5 mL·min^{-1}, rt, 300 x 8 mm2 PSS SDV linear M column (3 µm particle size, molar mass range 102-106 Da) and (*ii*) NMP + 0.5 wt% LiBr, 0.5 mL·min^{-1}, room temperature, 300 x 8 mm2 PSS-GRAM analytical linear column (particle size 7 µm, separation range 102-106 Da). Solutions containing ~0.15 wt% polymer were filtered through 0.45 µm filters; the injected volume was 100 µL. Polystyrene standards (PSS, Mainz, Germany) were used for calibration.

9.2.3 Dynamic and Static Light Scattering (DLS, SLS)

Dynamic light scattering (DLS) measurements were performed using ALV-7004 multiple tau digital correlator equipped with CGS-3 Compact Goniometer system (fixed at an angle of 90°), 22 mW He-Ne laser (wavelength λ = 632.8 nm) and pair of avalanche photodiodes operated in a pseudo-cross-correlation mode. The measured intensity correlation functions $g^2(t)$ were analyzed using the algorithm REPES performing the inverse Laplace transformation according to

$$g^2(t)=1+\beta\left[\int A(t)\exp(-t/\tau)d\tau\right]^2=1+\beta\left[\sum_{i=1}^{n}A_i\exp(-t/\tau_i)\right]^2$$

(where t is the delay time of the correlation function and β an instrumental parameter) and yielding distribution A(τ) of relaxation times τ. The relaxation time τ is related to the diffusion coefficient D and relaxation (decay) rate Γ by the relation: $\Gamma = 1/\tau = Dq^2$, where q is the scattering vector defined as $q = (4\pi n/\lambda)\sin(\vartheta/2)$ where n is the refractive index of the solvent and ϑ is the scattering angle. The hydrodynamic radius R_h of the particles was calculated from the diffusion coefficient using the Stokes-Einstein equation: $D = k_B T/6\pi\eta R_h$, where T is absolute temperature, η the viscosity of the solvent, and k_B the Boltzmann constant.

9.2.4 Thermogravimetric Analysis (TGA)

TGA was done on a Mettler Toledo TGA/SDTA851 from 25-900 °C at a heating rate of 10 K min^{-1} under a nitrogen flow of 20 mL min^{-1}.

9.2.5 Differential Scanning Calorimetry (DSC)

DSC was carried out on a Mettler Toledo DSC822e or Netzsch DSC 214 Polyma at 0-220 °C under a nitrogen flow. The glass transition temperature was determined at a heating rate of 10 K min^{-1}.

9.2.6 Wide-Angle X-Ray Diffraction (WAXD)

WAXD was conducted using a Bruker-Nonius AXS D8 Advance Diffractometer (Cu-Kα radiation 1.54 Å, 10 keV) with a scanning speed of 1.5 or 2 s, an increment of 0.05 or 0.01, in a 2θ range from 2 – 40°, at room temperature. Silicon substrates have been used to reduce background scattering.

9.2.7 Electron Microscopy (TEM, cryo-TEM; cryo-SEM)

TEM measurements were performed on a JEM-1011 (JEOL, Japan) at an acceleration voltage of 80 kV. Aqueous polymer samples were dropped on a carbon-coated TEM grid, negatively stained with phosphotungstic acid, and dried in air. In addition to TEM, a Hitachi S-4800 scanning electron microscope (SEM) was used. Therefore, the sample was shock frozen by plunging into nitrogen slush at atmospheric pressure and afterward freeze fractured at −180 °C, etched for 45 s at −98 °C, and sputtered with platinum in the GATAN Alto 2500-S cryo-preparation chamber to expose the inner structure of the vesicles.

9.2.8 Fourier Transformation Infrared Spectroscopy (FT-IR)

FT-IR was performed on a Bruker Vertex 70 fitted with a PLATINUM ATR. Liquid samples were placed directly on the ATR diamond under an argon flow. The spectra were acquired and processed with the OPUS 7.0 software. The number of scans was 32, the built-in atmospheric correction function was turned on, and the background was automatically subtracted; in the case of liquid samples, the background was generated using the very same solvent as the one used for the sample.

9.2.9 Matrix-assisted laser desorption/ionization-time-of-flight mass spectrometry (MALDI-TOF MS)

The MALDI-TOF MS experiments were performed with an Autoflex III mass spectrometer (Bruker Daltonik GmbH, Bremen) equipped with a Smartbeam laser (200 Hz, 355nm). All measurements were recorded in the linear positive ion mode. The samples (2 mg mL-1) and matrix (10 mg mL^{-1}, trans-2-[3-(4-tert-butylphenyl)-2-methyl-2-propenylidene]malononitrile – DCTB) were dissolved in chloroform, and premixed in a ratio of 2:5 (v:v). 2 µL of a solution of potassium trifluoroacetate (TFA) in tetrahydrofuran (THF) was added to promote the exclusive formation of potassium adduct ions. These premixed sample solutions were spotted on the target plate. 2000 single spectra were accumulated for one spectrum.

9.3 Synthetic Procedures

9.3.1 Monomer Synthesis of Alkyl Phosphonate

As a hydrophilic alternative to poly(ethylene glycol), poly(methyl phosphonate) and poly(isopropyl phosphonate) were chosen. However, the monomer 2-isopropyl-2-oxo-1,3,2-dioxaphospholane (^{i}PrP) was provided by the group of Dr. Wurm from the MPI in Mainz. 2-methoxy-2-oxo-1,3,2-dioxaphospholane (MeP) was synthesized based on the diploma thesis of Ilka Zerbe.[138] All relevant NMR spectra are available in the Appendix.

9.3.1.1 2-methoxy-2-oxo-1, 3, 2-dioxaphospholane

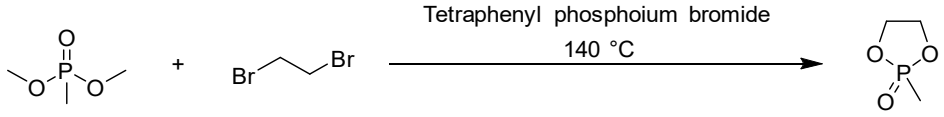

37.2 g of dimethyl methylphosphonate (1 equiv), 56.3 g of 1,2-dibromoethane (1Äq) and 5.86 g of Tetraphenylphosphonium bromide (0.05 equiv) was placed in a flame-dried and nitrogen-purged, three-neck round bottom flask with a reflux condenser. The mixture was stirred at 140°C for three days and become yellow and viscous. After cooling down, the mixture was solved in 100 mL dry dichloromethane (DCM) and filtered over neutral aluminum oxide (Al_2O_3). Subsequently, the solvent was removed again at the rotary evaporator. Finally, the yellow sticky mixture was purified through fractionated distillation under high vacuum.

Yield = 53%

Boiling point = 98°C ($1*10^{-2}$ mbar)

^{1}H-NMR (300MHz, $CDCl_3$): δ (ppm) 4.60-4.01 (m, 4H), 1.56 (d, J = 17.5 Hz, 3H).

^{13}C-NMR (75MHz, $CDCl_3$): δ (ppm) 65.79 (s) 10.74 (d. J = 135.5 Hz).

^{31}P-NMR (121 MHz, $CDCl_3$): δ (ppm) 49.92 (s).

9.3.2 Polymer Synthesis

9.3.2.1 Poly(lactide) Homopolymers

With the aim to produce PLA-PEG block copolymers, PLA homopolymers were synthesized that were further used as precursors or modified with succinic anhydride to attach the hydrophilic block (PEG-OH) via Steglich esterification.

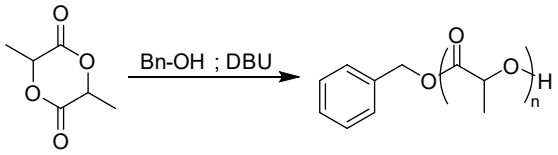

Typically, the amount of L or D-lactide (20-70 equiv) was placed in a round bottom flask, dissolved in dioxane and freeze-dried overnight. The next day, the monomer was dissolved in dry DCM (0.5 – 1 mol L^{-1} lactide). The corresponding amount benzyl alcohol (1 equiv) was added via stock solution, and everything stirred subsequently for 30 min at room temperature. Within this time the catalyst stock solution was prepared. The polymerization was started through injection of the catalyst stock solution and quenched after 15 to 60 min by an excess of benzoic acid added to the solution. The mixture was precipitated in diethyl ether, centrifuged and subsequently dissolved in THF to dialyze the obtained polymer. Finally, the product was freeze-dried to obtain a solid white powder that was stored at -20°C and were stable for months.

Yield > 90%

PLLA$_{24}$: *$[M]_0$ = 0.5 M; t = 15 min. ^{1}H-NMR (300 MHz, $CDCl_3$): δ (ppm) 7.37 (m, 5H), 5.35 – 4..91 (m, 25H), 4.37 (q, J = 6.9 Hz, 1H), 1.81 – 1.27 (m, 75H). FTIR: ṽ (cm^{-1}) = 2997 (CH), 2947 (CH), 1756 (C=O), 1457 (CH), 1360 (CH), 1184 (C-O), 1091 (C-O). SEC (NMP, PS calibration) M_n^{app} = 2.000 g mol^{-1}, $Đ^{app}$ = 1.40.). SEC (THF, PS calibration) M_n^{app} = 3.000 g mol^{-1}, $Đ^{app}$ = 1.12.*

PDLA$_{23}$: *$[M]_0$ = 0.5 M; t = 15 min ^{1}H-NMR (600 MHz, $CDCl_3$): δ (ppm) 7.39 – 7.28 (m, 5H), 5.27 – 5.09 (m, 24H), 4.37 (q, J = 6.9 Hz, 1H), 1.64 – 1.55 (m, 60H) 1.53 – 1.46 (m, 12H). FTIR: ṽ (cm^{-1}) = 2997 (CH), 2947 (CH) 1756 (C=O) 1457 (CH) 1360 (CH) 1184 (C-O) 1091 (C-O). SEC (NMP, PS calibration) M_n^{app} = 1.900 g mol^{-1}, $Đ^{app}$ = 1.40.). SEC (THF, PS calibration) M_n^{app} = 3000 g mol^{-1}, $Đ^{app}$ = 1.11.*

PLLA$_{68}$: *$[M]_0$ = 1.0 M; t = 1 h ^{1}H-NMR (500 MHz, $CDCl_3$): δ (ppm) 7.39- 7.29 (m, 5H), 5.37 – 5.09 (m, 69H), 4.44 – 4.29 (m, 1H), 1.73 – 1.38 (m, 218H). SEC (NMP, PS calibration) M_n^{app} = 6.700 g mol^{-1}, $Đ^{app}$ = 1.35.). SEC (THF, PS calibration) M_n^{app} = 8.300 g mol^{-1}, $Đ^{app}$ = 1.13.*

9.3.2.2 Modification of Poly(lactide) Homopolymers

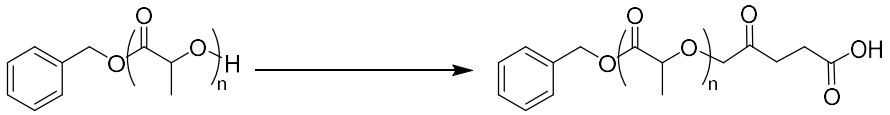

Typically, 1 equiv of the corresponding homo PLLA or PDLA, and 10 equiv of succinic anhydride was placed in a schlenk-tube with a magnetic stirrer. The addition of the corresponding amount of DCM (dry) (0.1 M PLA solution) created a suspension, which further was completely dissolved by the addition of 4 equiv of triethylamine (TEA). The solution was stirred at room temperature for 24 hours and turned yellowish with time. Subsequently, the solution was concentrated by evaporation of the solvent and the polymer purified by precipitation in methanol twice. The white obtained polymer was subsequently dissolved in dioxane and freeze-dried. The product was stored at -20°C and was stable for months.

Yield ≈90%

PLLA$_{28}$-COOH: *^{1}H-NMR (600 MHz, $CDCl_3$): δ (ppm) 7.43-7.27 (m, 5H), 5.23 – 5.09 (m, 30H), 2.75 – 2.61 (m, 4H), 1.63 – 1.44 (m, 85H). SEC (THF, PS calibration) M_n^{app}= 3.600 g mol^{-1}, $Đ^{app}$= 1.06.*

PDLA$_{26}$-COOH: *^{1}H-NMR (600 MHz, $CDCl_3$): δ (ppm) 7.41-7.28 (m, 5H), 5.24 – 5.07 (m, 27H), 2.76 – 2.61 (m, 4H), 1.66 – 1.36 (m, 79H). SEC (THF, PS calibration) M_n^{app}= 3.400 g mol^{-1}, $Đ^{app}$= 1.06.*

9.3.2.3 Poly(isopropyl phosphonate) Homopolymer

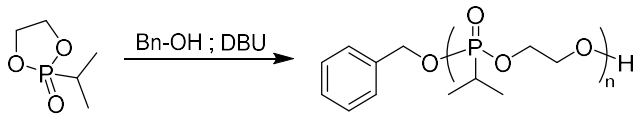

470 mg (3.13 mmol, 33 equiv) of the monomer was placed into a flame-dried schlenk-tube, dissolved in 1 mL benzene, and dried by lyophilization. Further, the monomer was dissolved in 0.8 mL dichloromethane (4 mol L^{-1}) and placed in a flame dried schlenk-tube equipped with a magnetic stirrer. Subsequently, 0.47 mL of a stock solution of benzyl alcohol in dichloromethane (0.2 mol L^{-1}; 0.1 mmol; 1 equiv) was added to the monomer solution that was cooled to 0°C. The polymerization was started with the addition of 0.47 mL of a stock solution of TBD dissolved in dichloromethane (0.2 mol L^{-1}; 0.1 mmol; 1 equiv). Polymerization was terminated by the rapid addition of an excess of benzoic acid dissolved in dichloromethane (50 mg; 0.4 mmol, 4 equiv) after 60 min. The viscous polymer was purified by precipitation in cold diethyl ether and additionally dialyzed in Millipore water for 24 hours.

Finally, the polymer solution was freeze-dried and the obtained viscous product stored at -20°C under inter gas.

Yield: 72%

$P^{i}PrP_{40}$: ^{1}H-NMR (300 MHz, $CDCl_3$): δ (ppm) 7.43 – 7.33 (m, 5H), 5.10 (d, J 0 8.3 Hz, 2H), 5.11 – 3.86 (m, 160H), 2.19 – 1.80 (m, 40H) 1.69 – 0.72 (m,244H).

9.3.3 General Synthesis of PEG-PLA Block Copolymers

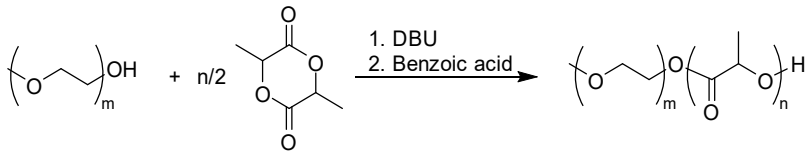

Typically, 1 equiv PEG and the corresponding amount of L or D-lactide (10-70 equiv) were placed in a round bottom flask, dissolved in dioxane and freeze-dried overnight. The next day, the mixture was dissolved in dry DCM (0.5 – 3 mol L^{-1} lactide) and stirred for 30 min at room temperature. Within this time the catalyst stock solution was prepared. The polymerization was started through injection of the catalyst stock solution and quenched after 1.5 to 120 min by an excess of benzoic acid to the solution. The mixture was precipitated in diethyl ether or isopropanol, centrifuged and subsequently dissolved in a THF/water mixture to dialyze against water. Finally, all samples were freeze-dried to obtain a solid white powder (By dialyzing against THF, the solvent was afterward removed at the rotary evaporator, solved in 1,4-dioxane and freeze-dried as well.).

Yield > 90%

PEG_{45}-$PLLA_{18}$: *$[M]_0$ = 0.5 M; t = 1 h. ^{1}H-NMR (600 MHz, $CDCl_3$): δ (ppm) 5.31-5.08 (m, 17H), 4.42 – 4.17 (m, 3H), 3.80-3.44 (m, 177H), 3.37 (s, 3H), 1.65 – 1.55 (m, 49H), 1.50 (dd, J = 18.0, 7.0 Hz, 6H). FTIR: ṽ (cm^{-1}) = 2883 (CH), 1756 (C=O), 1342 (CH), 1107 (C-O), 1091 (C-O) 961 (C-O) 843 (C-O). SEC (NMP, PS calibration) M_n^{app}= 4.400 g mol^{-1}, $Đ^{app}$= 1.28. SEC (THF, PS calibration) M_n^{app}= 5.400 g mol^{-1}, $Đ^{app}$= 1.10.*

PEG_{45}-$PLLA_{49}$: *$[M]_0$ = 1.0 M; t = 2 h.^{1}H-NMR (500 MHz, $CDCl_3$): δ (ppm) 5.18 (m, 48H), 4.45 – 4.18 (m, 3H), 3.85-3.48 (m, 176H), 3.38 (s, 3H), 1.65 – 1.31 (m, 150H). FTIR: ṽ (cm^{-1}) = 2876 (CH), 1748 (C=O), 1451 (CH), 1179 (C-O), 1081 (C-O). SEC (THF, PS calibration) M_n^{app}= 8.200 g mol^{-1}, $Đ^{app}$= 1.10.*

PEG_{45}-$PLLA_{72}$: *$[M]_0$ = 1.0 M; t = 2 h. ^{1}H-NMR (600 MHz, $CDCl_3$): δ (ppm) 5.38-5.08 (m, 71H), 4.42 – 4.17 (m, 3H), 3.80-3.44 (m, 177H), 3.37 (s, 3H), 1.64 – 1.29 (m, 49H). FTIR: ṽ (cm^{-1}) = 2876 (CH), 1748 (C=O),*

1451 (CH), 1179 (C-O), 1081 (C-O). SEC (NMP, PS calibration) M_n^{app} *= 8.900 g mol^{-1},* $Đ^{app}$ *= 1.44. SEC (THF, PS calibration)* M_n^{app} *= 10.900 g mol^{-1},* $Đ^{app}$ *= 1.21.*

PEG$_{45}$-PLLA$_{145}$: *[M]$_0$ = 1.0 M; t = 15 min. ^{1}H-NMR (500 MHz, CDCl$_3$): δ (ppm) 5.42-5.07 (m, 144H), 4.45 – 4.14 (m, 3H), 3.85-3.41 (m, 182H), 3.38i (s, 3H), 1.78 – 1.38 (m, 470H). SEC (THF, PS calibration)* M_n^{app} *= 13.400 g mol^{-1},* $Đ^{app}$ *= 1.10.*

PEG$_{113}$-PLLA$_{18}$: *[M]$_0$ = 0.5 M; t = 1 h. ^{1}H-NMR (500 MHz, CDCl$_3$): δ (ppm), 5.49 – 5.00 (m, 17H), 4.41 – 4.19 (m, 3H,) 3.77 (dd, J = 5.6, 4.2 Hz, 2H), 3.72 – 3.44 (m, 453H), 3.37 (s, 3H), 1.62 – 1.53 (m, 50H), 1.39 (dd, J = 15.2, 7.0, 6H). FTIR: ṽ (cm^{-1}) = 2883 (CH), 1756 (C=O), 1342 (CH), 1107 (C-O), 1091 (C-O) 961 (C-O) 843 (C-O). SEC (NMP, PS calibration)* M_n^{app} *= 9.300 g mol^{-1},* $Đ^{app}$ *= 1.16. SEC (THF, PS calibration)* M_n^{app} *= 10.800 g mol^{-1},* $Đ^{app}$ *= 1.04.*

PEG$_{113}$-PLLA$_{39}$: *[M]$_0$ = 1.0 M; t = 2 h. ^{1}H-NMR (500 MHz, CDCl$_3$): δ (ppm), 5.34 – 5.09 (m, 38H), 4.47 – 4.17 (m, 3H,) 3.80 – 3.45 (m, 477H), 3.37 (s, 3H), 1.68 – 1.37 (m, 120H). FTIR: ṽ (cm^{-1}) = 2876 (CH), 1748 (C=O), 1451 (CH), 1179 (C-O), 1081 (C-O). SEC (THF, PS calibration)* M_n^{app} *= 11.800 g mol^{-1},* $Đ^{app}$ *= 1.07.*

PEG$_{113}$-PLLA$_{69}$: *[M]$_0$ = 1.0 M; t = 2 h. ^{1}H-NMR (600 MHz, CDCl$_3$): δ (ppm), 5.35 – 5.07 (m, 68H), 4.47 – 4.13 (m, 3H), 3.79 – 3.46 (m, 477H), 3.37 (s, 3H), 1.64 – 1.36 (m, 213H). FTIR: ṽ (cm^{-1}) = 2876 (CH), 1748 (C=O), 1451 (CH), 1179 (C-O), 1081 (C-O). SEC (NMP, PS calibration)* M_n^{app} *= 13.400 g mol^{-1},* $Đ^{app}$ *= 1.27. SEC (THF, PS calibration)* M_n^{app} *= 15.400 g mol^{-1},* $Đ^{app}$ *= 1.11.*

PEG$_{113}$-PLLA$_{124}$: *[M]$_0$ = 3.0 M; t = 1.5 min. ^{1}H-NMR (500 MHz, CDCl$_3$): δ (ppm), 5.38 – 5.03 (m, 123H), 4.43 – 4.16 (m, 3H,) 3.85 – 3.41 (m, 461H), 3.38 (s, 3H), 1.65 – 1.35 (m, 384H). SEC (THF, PS calibration)* M_n^{app} *= 17.100 g mol^{-1},* $Đ^{app}$ *= 1.07.*

PEG$_{45}$-PDLA$_{19}$: *[M]$_0$ = 0.5 M; t = 1 h. ^{1}H-NMR (600 MHz, CDCl$_3$): δ (ppm) 5.31-5.07 (m, 18H), 4.42 – 4.20 (m, 3H), 3.80-3.44 (m, 177H), 3.37 (s, 3H), 1.65 – 1.55 (m, 49H), 1.50 (dd, J = 18.0, 7.0 Hz, 6H). FTIR: ṽ (cm^{-1}) = 2883 (CH), 1756 (C=O), 1342 (CH), 1107 (C-O), 1091 (C-O) 961 (C-O) 843 (C-O). SEC (NMP, PS calibration)* M_n^{app} *= 4.400 g mol^{-1},* $Đ^{app}$ *= 1.28. SEC (THF, PS calibration)* M_n^{app} *= 5.400 g mol^{-1},* $Đ^{app}$ *= 1.10.*

PEG$_{45}$-PDLA$_{45}$: *[M]$_0$ = 1.0 M; t = 2 h.^{1}H-NMR (500 MHz, CDCl$_3$): δ (ppm) 5.18 (m, 44H), 4.44 – 4.18 (m, 3H), 3.83-3.41 (m, 178H), 3.37 (s, 3H), 1.65 – 1.31 (m, 139H). FTIR: ṽ (cm^{-1}) = 2876 (CH), 1748 (C=O), 1451 (CH), 1179 (C-O), 1081 (C-O). SEC (THF, PS calibration)* M_n^{app} *= 7.800 g mol^{-1},* $Đ^{app}$ *= 1.07.*

PEG$_{45}$-PLLA$_{74}$: *[M]$_0$ = 1.0 M; t = 2 h. ^{1}H-NMR (600 MHz, CDCl$_3$): δ (ppm) 5.32-5.05 (m, 73H), 4.47 – 4.21 (m, 3H), 3.86-3.46 (m, 178H), 3.37 (s, 3H), 1.67 – 1.39 (m, 230H). FTIR: ṽ (cm^{-1}) = 2876 (CH), 1748 (C=O),*

1451 (CH), 1179 (C-O), 1081 (C-O). SEC (NMP, PS calibration) M_n^{app} *= 9.500 g mol*$^{-1}$*,* $Đ^{app}$ *= 1.41. SEC (THF, PS calibration)* M_n^{app} *= 10.300 g mol*$^{-1}$*,* $Đ^{app}$ *= 1.21.*

PEG*$_{45}$*-PLLA*$_{131}$ *: *[M]*$_0$ *= 1.0 M; t = 15 min.* ^{1}*H-NMR (500 MHz, CDCl*$_3$*): δ (ppm) 5.43-5.07 (m, 130H), 4.39 – 4.20 (m, 3H), 3.91-3.41 (m, 178H), 3.38 (s, 3H), 1.64 – 1.35 (m, 409H). SEC (THF, PS calibration)* M_n^{app} *= 13.300 g mol*$^{-1}$*,* $Đ^{app}$ *= 1.10.*

PEG*$_{113}$*-PDLA*$_{18}$*: *[M]*$_0$ *= 0.5 M; t = 1 h.* ^{1}*H-NMR (500 MHz, CDCl*$_3$*): δ (ppm), 5.27 – 5.08 (m, 17H), 4.43 – 4.18 (m, 3H,), 3.72 – 3.44 (m, 466H), 3.37 (s, 3H), 1.64 – 1.32 (m, 50H). FTIR: ṽ (cm*$^{-1}$*) = 2876 (CH), 1748 (C=O), 1451 (CH), 1179 (C-O), 1081 (C-O). SEC (NMP, PS calibration)* M_n^{app} *= 9.100 g mol*$^{-1}$*,* $Đ^{app}$ *= 1.17. SEC (THF, PS calibration)* M_n^{app} *= 9.100 g mol*$^{-1}$*,* $Đ^{app}$ *= 1.17.*

PEG*$_{113}$*-PDLA*$_{38}$*: *[M]*$_0$ *= 1.0 M; t = 2 h.* ^{1}*H-NMR (500 MHz, CDCl*$_3$*): δ (ppm), 5.34 – 5.09 (m, 37H), 4.44 – 4.15 (m, 3H,) 3.80 – 3.45 (m, 455H), 3.37 (s, 3H), 1.67 – 1.33 (m, 116H). FTIR: ṽ (cm*$^{-1}$*) = 2876 (CH), 1748 (C=O), 1451 (CH), 1179 (C-O), 1081 (C-O). SEC (THF, PS calibration)* M_n^{app} *= 11.900 g mol*$^{-1}$*,* $Đ^{app}$ *= 1.07.*

PEG*$_{113}$*-PDLA*$_{68}$*: *[M]*$_0$ *= 1.0 M; t = 2 h.* ^{1}*H-NMR (600 MHz, CDCl*$_3$*): δ (ppm), 5.35 – 4.95 (m, 68H), 4.47 – 4.15 (m, 3H), 3.79 – 3.46 (m, 479H), 3.37 (s, 3H), 1.63 – 1.36 (m, 208H). FTIR: ṽ (cm*$^{-1}$*) = 2876 (CH), 1748 (C=O), 1451 (CH), 1179 (C-O), 1081 (C-O). SEC (NMP, PS calibration)* M_n^{app} *= 12.700 g mol*$^{-1}$*,* $Đ^{app}$ *= 1.25. SEC (THF, PS calibration)* M_n^{app} *= 15.100 g mol*$^{-1}$*,* $Đ^{app}$ *= 1.08.*

PEG*$_{113}$*-PDLA*$_{127}$*: *[M]*$_0$ *= 3.0 M; t = 1.5 min.* ^{1}*H-NMR (500 MHz, CDCl*$_3$*): δ (ppm), 5.40 – 5.07 (m, 126H), 4.44 – 4.19 (m, 3H,) 3.85 – 3.41 (m, 488H), 3.37 (s, 3H), 1.64 – 1.39 (m, 394H). SEC (THF, PS calibration)* M_n^{app} *= 15.600 g mol*$^{-1}$*,* $Đ^{app}$ *= 1.08.*

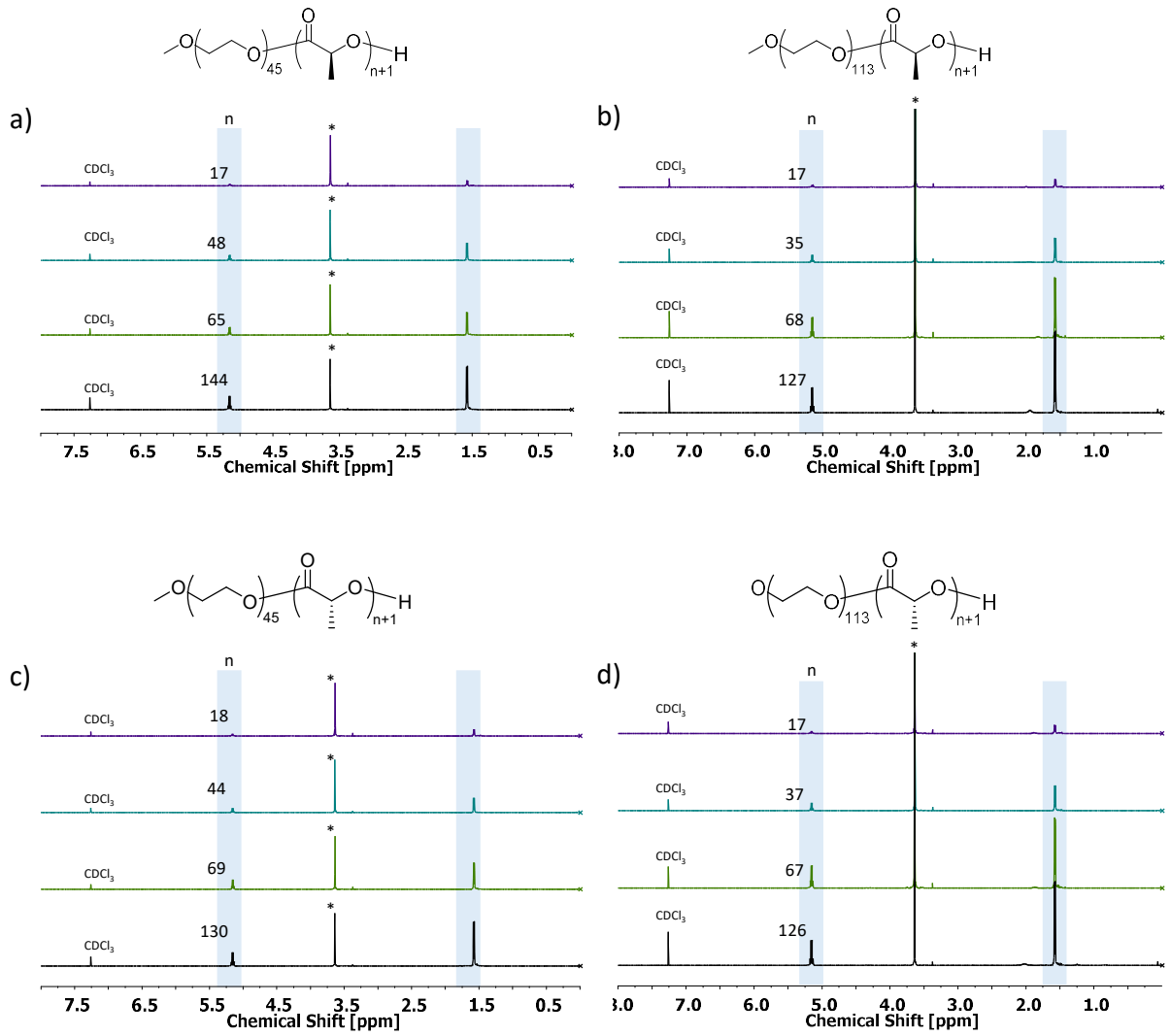

***Figure 63**: ^{1}H NMR spectra (500 MHz) of synthesized PEG-PLA block copolymers in $CDCl_3$; normalized to signal intensity of -CH_2O- (*) peak of PEG_{45} or PEG_{113}, respectively.*

9.3.4 General Synthesis of PLA-PEG Block Copolymers

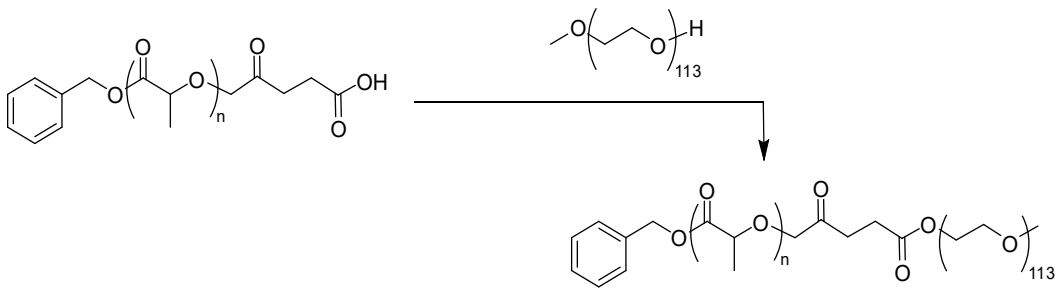

Typically, 1 equiv PEG (M_n = 5000 g mol^{-1}), 1 equiv of the corresponding PLA-COOH ($M_n \approx$ 2000 g mol^{-1}) and 1 equiv of DMAP were dissolved in dry dichloromethane at a concentration of 0.05 mol L^{-1}, and The solution was cooled to 0°C. A stock solution of EDC·HCl in dry dichloromethane at a concentration

of 0.2 mol L^{-1} was prepared, and the calculated amount (4 equiv) added to the precursor solution via syringe. The solvent was removed at the rotation evaporator, dissolved in dioxane. The precipitate was filtered off, and the obtained clear solution freeze-dried. The white product was dissolved in water, centrifuged, and finally dialyzed against water (MWCO 50 kDa). The solution was freeze-dried and the product stored at -20°C, and was stable over months.

Yield ≈ 70-80%

PLLA$_{28}$-PEG$_{113}$: *^{1}H-NMR (600 MHz, $CDCl_3$): δ (ppm) 7.41- 7.29 (m, 5H), 5.24 – 5.06 (m, 30H), 4.29-4.15 (m, 2H), 3.80 - 3.50 (m, 458H), 3.37 (s, 3H) 2.86 – 2.49 (m, 4H) 1.65 – 1.31 (m, 87H). FTIR: ṽ (cm^{-1}) = 2879 (CH), 1754 (C=O), 1467 (CH), 1342 (CH), 1185 (C-O), 1099 (C-O), 981 (C-O), 841 (C-O). SEC (THF, PS calibration) M_n^{app} = 11.900 g mol^{-1}, $Đ^{app}$ = 1.03.*

PDLA$_{30}$-PEG$_{113}$: *^{1}H-NMR (600 MHz, $CDCl_3$): δ (ppm) 7.42- 7.30 (m, 6H), 5.33 – 5.08 (m, 32H), 4.29-4.20 (m, 2H), 3.80 - 3.50 (m, 458H), 3.37 (s, 3H) 2.85 – 2.57 (m, 5H) 1.64 – 1.41 (m, 89H). FTIR: ṽ (cm^{-1}) = 2879 (CH), 1754 (C=O), 1467 (CH), 1342 (CH), 1185 (C-O), 1099 (C-O), 981 (C-O), 841 (C-O) SEC (THF, PS calibration) M_n^{app} = 11.500 g mol^{-1}, $Đ^{app}$ = 1.03.*

9.3.5 General Synthesis of PEG-PLA-PMeP Copolymers

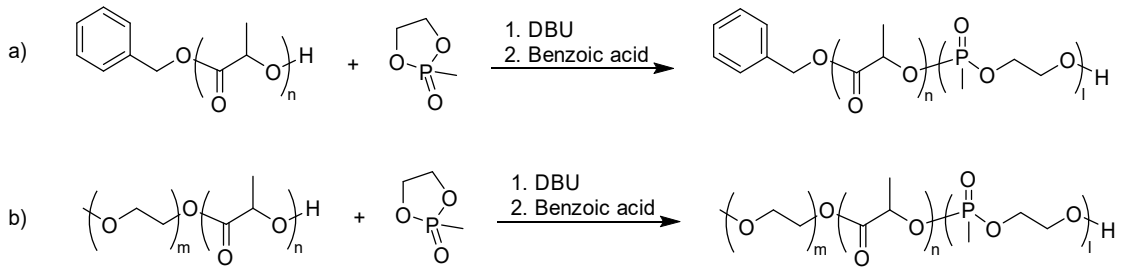

Typically, 41 equiv of the monomer MeP was placed into a flame-dried schlenk-tube, dissolved in 1 mL benzene, and subsequently dried by lyophilization. Further, the monomer was dissolved in dichloromethane at a concentration of 4 mol L^{-1} and placed in a flame dried schlenk-tube equipped with a magnetic stirrer. Subsequently, a stock solution of the respective PLA-based precursor in dichloromethane (0.2 mol L^{-1}; 0.1 mmol; 1 equiv) was added to the monomer at room temperature. A stock solution of DBU in dry dichloromethane was prepared (0.2 mol L^{-1}). The polymerization was initiated with the addition of 0.47 mL of a catalyst solution containing 1.0 equiv of DBU with respect to the initiator. Polymerization was terminated by the rapid addition of an excess of benzoic acid dissolved in dichloromethane (4 equiv) after 60 min or 120 min. The colorless, amorphous to viscous polymer was purified by precipitation in cold diethyl ether and additionally dialyzed in Millipore water

for 24 hours. Finally, the polymer solution was freeze-dried and the obtained viscous product stored at -20°C under inert gas.

Yield ≈ 70%

PLLA$_{33}$-PMeP$_{50}$: *t = 2 h. ^{1}H-NMR (500 MHz, $CDCl_3$): δ (ppm) 7.38 – 7.28 (m, 5H), 5.25 – 4.90 (m, 33H), 4.50 – 3.93 (m, 184H), 1.84 – 1.34 (m, 239H). SEC (NMP, PS calibration) M_n^{app} = 8.600 g mol^{-1}, $Đ^{app}$ = 1.70.*

PLLA$_{88}$-PMeP$_{49}$: *t = 2 h. ^{1}H-NMR (300 MHz, $CDCl_3$): δ (ppm) 7.38 – 7.28 (m, 5H), 5.50 – 4.75 (m, 88H), 4.49 – 3.96 (m, 190H), 1.72 – 1.12 (m, 418H). SEC (NMP, PS calibration) M_n^{app} = 12.400 g mol^{-1}, $Đ^{app}$ = 2.00.*

PEG$_{45}$-PLLA$_{19}$-PMeP$_{20}$: *t = 2 h. ^{1}H-NMR (500 MHz, $CDCl_3$): δ (ppm) 5.29 – 4.92 (m, 17H), 4.64– 3.96 (m, 81H), 3.92 – 3.43 (m, 180H), 3.39 (s, 3H), 1.84 – 1.37 (m, 120H). SEC (NMP, PS calibration) M_n^{app} = 5.800 g mol^{-1}, $Đ^{app}$ = 1.35.*

PEG$_{45}$-PLLA$_{20}$-PMeP$_{36}$: *t = 2 h. ^{1}H-NMR (500 MHz, $CDCl_3$): δ (ppm) 5.26 – 4.90 (m, 20H), 4.63– 3.91 (m, 147H), 3.91 – 3.44 (m, 178H), 3.36 (s, 3H), 1.81 – 1.30 (m, 172H). SEC (NMP, PS calibration) M_n^{app} = 5.800 g mol^{-1}, $Đ^{app}$ = 1.35.*

PEG$_{45}$-PLLA$_{72}$-PMeP$_{18}$: *t = 2 h. ^{1}H-NMR (500 MHz, $CDCl_3$): δ (ppm) 5.26 – 4.90 (m, 20H), 4.63– 3.91 (m, 147H), 3.91 – 3.44 (m, 178H), 3.36 (s, 3H), 1.81 – 1.30 (m, 172H). SEC (NMP, PS calibration) M_n^{app} = 5.800 g mol^{-1}, $Đ^{app}$ = 1.35.*

PEG$_{113}$-PDLA$_{82}$-PMeP$_{33}$: *t = 2 h. ^{1}H-NMR (600 MHz, $CDCl_3$): δ (ppm) 5.27 – 4.98 (m, 82H), 4.51– 4.03 (m, 130H), 3.88 – 3.42 (m, 183H), 3.37 (s, 3H), 1.70 – 1.34 (m, 283H). SEC (NMP, PS calibration) M_n^{app} = 12.000 g mol^{-1}, $Đ^{app}$ = 1.59.*

PEG$_{113}$-PLLA$_{18}$-PMeP$_{20}$: *t = 2 h. ^{1}H-NMR (500 MHz, $CDCl_3$): δ (ppm) 5.25 – 4.96 (m, 73H), 4.42– 4.08 (m, 70H), 3.81 – 3.52 (m, 178H), 3.40 (s, 3H), 1.76 – 1.46 (m, 352H). SEC (NMP, PS calibration) M_n^{app} = 8.700 g mol^{-1}, $Đ^{app}$ = 1.53.*

PEG$_{113}$-PDLA$_{18}$-PMeP$_{25}$: *t = 2 h. ^{1}H-NMR (500 MHz, $CDCl_3$): δ (ppm) 5.27 – 4.92 (m, 17H), 4.55– 3.97 (m, 100H), 3.81 – 3.52 (m, 469H), 3.37 (s, 3H), 1.72 – 1.36 (m, 129H). SEC (NMP, PS calibration) M_n^{app} = 9.400 g mol^{-1}, $Đ^{app}$ = 1.37.*

PEG$_{113}$-PLLA$_{69}$-PMeP$_{24}$: *t = 2 h. ^{1}H-NMR (600 MHz, $CDCl_3$): δ (ppm) 5.27 – 4.93 (m, 68H), 4.43– 3.95 (m, 70H), 3.81 – 3.52 (m, 478H), 3.37 (s, 3H), 1.70 – 1.40 (m, 283H). SEC (NMP, PS calibration) M_n^{app} = 12.900 g mol^{-1}, $Đ^{app}$ = 1.29.*

PEG$_{113}$-PDLA$_{64}$-PMeP$_{29}$: *t = 2 h. ^{1}H-NMR (600 MHz, $CDCl_3$): δ (ppm) 5.30 – 4.98 (m, 64H), 4.48– 4.08 (m, 114H), 3.81 – 3.52 (m, 465H), 3.37 (s, 3H), 1.74 – 1.35 (m, 287H). SEC (NMP, PS calibration) M_n^{app}= 13.100 g mol^{-1}, $Đ^{app}$= 1.31.*

9.3.6 General Synthesis of PEG-PLA-P^{i}PrP Copolymers

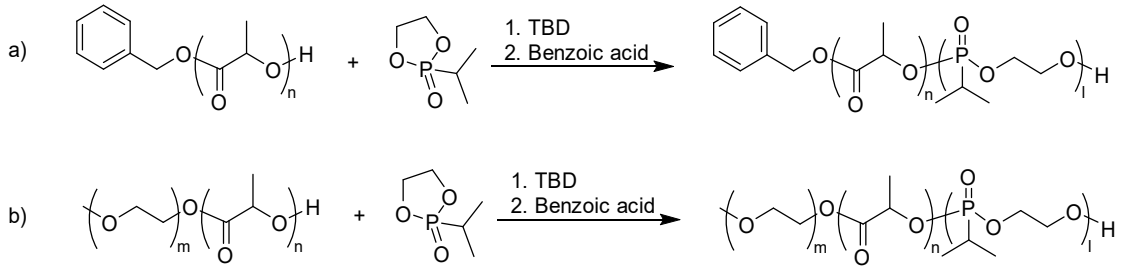

Typically, 33 equiv of the monomer ^{i}PrP was placed into a flame-dried schlenk-tube, dissolved in 1 mL benzene, and subsequently dried by lyophilization. Further, the monomer was dissolved in dichloromethane at a concentration of 4 mol L^{-1} and placed in a flame dried schlenk-tube equipped with a magnetic stirrer. A stock solution of the respective PLA-based precursor in dichloromethane (0.2 mol L^{-1}; 0.1 mmol; 1 equiv) was added to the monomer at room temperature. A stock solution of TBD in dry dichloromethane was prepared (0.2 mol L^{-1}). The polymerization was initiated with the addition of the calculated volume of the catalyst solution containing 1.0 equiv of DBU with respect to the initiator. Polymerization was terminated by the rapid addition of an excess of benzoic acid dissolved in dichloromethane (4 equiv) after 60 min. The colorless, amorphous to viscous polymer was purified by precipitation in cold diethyl ether. Finally, the polymer was freeze-dried from dioxane and stored at -20°C under inter gas.

PLLA$_{22}$-PMeP$_{27}$: *t = 1 h. ^{1}H-NMR (300 MHz, $CDCl_3$): δ (ppm) 7.46 – 7.29 (m, 5H), 5.37 – 4.77 (m, 21H), 4.67 – 3.84 (m, 112H), 2.39 – 1.68 (m, 30H), 1.68 – 1.35 (m, 64H), 1.33 – 0.75 (m, 167H). SEC (NMP, PS calibration) M_n^{app}= 6.100 g mol^{-1}, $Đ^{app}$= 1.80.*

PLLA$_{22}$-PMeP$_{26}$: *t = 1 h. ^{1}H-NMR (300 MHz, $CDCl_3$): δ (ppm) 7.52 – 7.31 (m, 5H), 5.37 – 4.77 (m, 21H), 4.67 – 3.84 (m, 101H), 2.39 – 1.68 (m, 27H), 1.68 – 1.35 (m, 62H), 1.33 – 0.92 (m, 153H). SEC (NMP, PS calibration) M_n^{app}= 5.500 g mol^{-1}, $Đ^{app}$= 1.88.*

PEG$_{113}$-PLLA$_{11}$-P^{i}PrP$_{18}$: *t = 1 h. ^{1}H-NMR (300 MHz, $CDCl_3$): δ (ppm) 5.43 – 4.78 (m, 10H), 4.65– 4.01 (m, 63H), 3.81 – 3.25(m, 450H), 1.71 – 1.35 (m, 15H), 1.71 – 1.35 (m, 62H), 1.33 – 0.53 (m, 153H). SEC (NMP, PS calibration) M_n^{app}= 8.500 g mol^{-1}, $Đ^{app}$= 1.28.*

10 References

(1) Navia, M. A.; Peattie, D. A. *Immunol. Today* **1993**, *14* (6), 296–302.

(2) Allen, T. M.; Cullis, P. R. *Adv. Drug Deliv. Rev.* **2013**, *65* (1), 36–48.

(3) Champion, J. A.; Katare, Y. K.; Mitragotri, S. *J. Control. Release* **2007**, *121* (1–2), 3–9.

(4) Kanti Sen, T.; Khilar, K. C. *Adv. Colloid Interface Sci.* **2006**, *119* (2–3), 71–96.

(5) Chayen, J. *Cell Biochem. Funct.* **1996**, *14* (1), 75–75.

(6) Kumar, A.; Abbott, N. L.; Biebuyck, H. A.; Kim, E.; Whitesides, G. M. *Acc. Chem. Res.* **1995**, *28* (5), 219–226.

(7) Grantcharova, V.; Alm, E. J.; Baker, D.; Horwich, A. L. *Curr. Opin. Struct. Biol.* **2001**, *11* (1), 70–82.

(8) Lehn, J. M. *Reports Prog. Phys.* **2004**, *67* (3), 249–265.

(9) McManus, J. J.; Charbonneau, P.; Zaccarelli, E.; Asherie, N. *Curr. Opin. Colloid Interface Sci.* **2016**, *22*, 73–79.

(10) Murphy, M. P.; LeVine, H. *J. Alzheimer's Dis.* **2010**, *19* (1), 311–323.

(11) Discher, D. E.; Ahmed, F. *Annu. Rev. Biomed. Eng.* **2006**, *8* (1), 323–341.

(12) Mai, Y.; Eisenberg, A. *Chem. Soc. Rev.* **2012**, *41* (18), 5969.

(13) Yu, W.; Inam, M.; Jones, J. R.; Dove, A. P.; O'Reilly, R. K. *Polym. Chem.* **2017**, *8* (36), 5504–5512.

(14) Discher, D. E. *Science* **2002**, *297* (5583), 967–973.

(15) Frangville, C.; Li, Y.; Billotey, C.; Talham, D. R.; Taleb, J.; Roux, P.; Marty, J.-D.; Mingotaud, C. *Nano Lett.* **2016**, *16* (7), 4069–4073.

(16) Cölfen, H. *Macromol. Rapid Commun.* **2001**, *22* (4), 219–252.

(17) Willersinn, J.; Schmidt, B. V. K. J. *J. Polym. Sci. Part A Polym. Chem.* **2017**, *55* (22), 3757–3766.

(18) Karayianni, M.; Pispas, S. *Fluorescence Studies of Polymer Containing Systems*; Procházka, K., Ed.; Springer Series on Fluorescence; Springer International Publishing: Cham, 2016; Vol. 16.

(19) McKenzie, B. E.; De Visser, J. F.; Friedrich, H.; Wirix, M. J. M.; Bomans, P. H. H.; De With, G.; Holder, S. J.; Sommerdijk, N. A. J. M. *Macromolecules* **2013**, *46* (24), 9845–9848.

(20) Riess, G. *Prog. Polym. Sci.* **2003**, *28* (7), 1107–1170.

(21) Hadjichristidis, N. *J. Polym. Sci. Part A Polym. Chem.* **1999**, *37* (7), 857–871.

(22) Hayashi, M.; Kojima, K.; Hirao, A. *Macromolecules* **1999**, *32* (8), 2425–2433.

(23) Matsuo, A.; Watanabe, T.; Hirao, A. *Macromolecules* **2004**, *37* (17), 6283–6290.

(24) Williams, R. J.; Dove, A. P.; O'Reilly, R. K. *Polym. Chem.* **2015**, *6* (16), 2998–3008.

(25) Bertin, A. *Macromol. Chem. Phys.* **2012**, *213* (22), 2329–2352.

(26) Slager, J.; Domb, A. J. *Adv. Drug Deliv. Rev.* **2003**, *55* (4), 549–583.

(27) Brizzolara, D.; Cantow, H. J.; Mülhaupt, R.; Domb, A. J. *J. Comput. Mater. Des.* **1996**, *3* (1–3), 341–350.

(28) Ikada, Y.; Jamshidi, K.; Tsuji, H.; Hyon, S. H. *Macromolecules* **1987**, *20* (4), 904–906.

(29) Tsuji, H.; Horii, F.; Hyon, S. H.; Ikada, Y. *Macromolecules* **1991**, *24* (10), 2719–2724.

(30) Tsuji, H.; Hyon, S. H.; Ikada, Y. *Macromolecules* **1991**, *24* (20), 5651–5656.

(31) Tsuji, H.; Hyon, S. H.; Ikada, Y. *Macromolecules* **1991**, *24* (20), 5657–5662.

(32) Tsuji, H.; Hyon, S. H.; Ikada, Y. *Macromolecules* **1992**, *25* (11), 2940–2946.

(33) Tsuji, H.; Ikada, Y.; Teujit, H. **2002**, *25* (May), 5719–5723.

(34) Tsuji, H.; Ikada, Y. *J. Appl. Polym. Sci.* **1994**, *53* (8), 1061–1071.

(35) Tsuji, H.; Ikada, Y.; Hyon, S. -H; Kimura, Y.; Kitao, T. *J. Appl. Polym. Sci.* **1994**, *51* (2), 337–344.

(36) Tsuji, H.; Ikada, Y. *Polymer* **1995**, *36* (14), 2709–2716.

(37) Brochu, S.; Prud'homme, R. E.; Barakat, I.; Jérôme, R. *Macromolecules* **1995**, *28* (15), 5230–5239.

(38) Brizzolara, D.; Cantow, H. J.; Diederichs, K.; Keller, E.; Domb, A. J. *Macromolecules* **1996**, *29* (1), 191–197.

(39) Bates, F. S.; Fredrickson, G. H. *Phys. Today* **1999**, *52* (2), 32–38.

(40) Katsaras, J.; Gutberlet, T. *Lipid Bilayers*, 1st ed.; Springer Berlin Heidelberg: Berlin, Heidelberg, 2001.

(41) Flory, P. J. *J. Chem. Phys.* **1942**, *10* (1), 51–61.

(42) Huggins, M. L. *J. Am. Chem. Soc.* **1942**, *64* (7), 1712–1719.

(43) Leibler, L. *Macromolecules* **1980**, *13* (6), 1602–1617.

(44) Matsen, M. W.; Schick, M. *Phys. Rev. Lett.* **1994**, *72* (16), 2660–2663.

(45) Khandpur, A. K.; Foerster, S.; Bates, F. S.; Hamley, I. W.; Ryan, A. J.; Bras, W.; Almdal, K.; Mortensen, K. *Macromolecules* **1995**, *28* (26), 8796–8806.

(46) Zheng, W.; Wang, Z.-G. *Macromolecules* **1995**, *28* (21), 7215–7223.

(47) Zhang, L.; Eisenberg, A. *Macromolecules* **1999**, *32* (7), 2239–2249.

(48) Gohy, J.-F. In *Block Copolymers II*; Springer-Verlag: Berlin/Heidelberg; pp 65–136.

(49) Storks, K. H. *J. Am. Chem. Soc.* **1938**, *60* (8), 1753–1761.

(50) Frank, F. C.; Tosi, M. *Proc. R. Soc. A Math. Phys. Eng. Sci.* **1961**, *263* (1314), 323–339.

(51) Point, J. J. *Macromolecules* **1979**, *12* (4), 770–775.

(52) Point, J.-J. *Faraday Discuss. Chem. Soc.* **1979**, *68*, 167.

(53) M. H. Hartmann. *Biopolymers from Renewable Resources*; Kaplan, D. L., Ed.; Springer Berlin Heidelberg: Berlin, Heidelberg, 1998.

(54) H. Benninga. *A History of Lactic Acid Making*, 1st ed.; Springer Netherlands, 1990.

(55) Kirk-Othmer (Editor). *Kirk-Othmer Encyclopedia of Chemical Technology,* Volume 13,.; John Wiley and Sons: New York, 2005.

(56) Datta, R.; Tsai, S.-P.; Bonsignore, P.; Moon, S.-H.; Frank, J. R. *FEMS Microbiol. Rev.* **1995**, *16*, 221–231.

(57) Sinclair, R. G. *J. Macromol. Sci. Part A* **1996**, *33* (5), 585–597.

(58) Carothers, W. H.; Dorough, G. L.; Natta, F. J. van. *J. Am. Chem. Soc.* **1932**, *54* (2), 761–772.

(59) Lohmeijer, B. G. G.; Pratt, R. C.; Leibfarth, F.; Logan, J. W.; Long, D. A.; Dove, A. P.; Nederberg, F.; Choi, J.; Wade, C.; Waymouth, R. M.; Hedrick, J. L. *Macromolecules* **2006**, *39* (25), 8574–8583.

(60) Zhang, L.; Nederberg, F.; Messman, J. M.; Pratt, R. C.; Hedrick, J. L.; Wade, C. G. *J. Am. Chem. Soc.* **2007**, *129* (42), 12610–12611.

(61) Bouyahyi, M.; Grunova, E.; Marquet, N.; Kirillov, E.; Thomas, C. M.; Roisnel, T.; Carpentier, J.-F.

Organometallics **2008**, *27* (22), 5815–5825.

(62) Blakey, I.; Yu, A.; Howdle, S. M.; Whittaker, A. K.; Thurecht, K. J. *Green Chem.* **2011**, *13* (8), 2032.

(63) Coady, D. J.; Fukushima, K.; Horn, H. W.; Rice, J. E.; Hedrick, J. L. *Chem. Commun. (Camb).* **2011**, *47* (11), 3105–3107.

(64) Miao, Y.; Stanley, N.; Favrelle, A.; Bousquet, T.; Bria, M.; Mortreux, A.; Zinck, P. *J. Polym. Sci. Part A Polym. Chem.* **2015**, *53* (5), 659–664.

(65) Qian, H.; Wohl, A. R.; Crow, J. T.; MacOsko, C. W.; Hoye, T. R. *Macromolecules* **2011**, *44* (18), 7132–7140.

(66) Kricheldorf, H. R. *Chemosphere* **2001**, *43* (1), 49–54.

(67) Kricheldorf, H. R.; Sumbél, M. *Eur. Polym. J.* **1989**, *25* (6), 585–591.

(68) Kricheldorf, H. R.; Kreiser-Saunders, I.; Stricker, A. *Macromolecules* **2000**, *33* (3), 702–709.

(69) Garlotta, D. *J. Polym. Environ.* **2001**, *9* (2), 63–84.

(70) Sherck, N. J.; Kim, H. C.; Won, Y.-Y. *Macromolecules* **2016**, *49* (13), 4699–4713.

(71) Brown, H. A.; De Crisci, A. G.; Hedrick, J. L.; Waymouth, R. M. *ACS Macro Lett.* **2012**, *1* (9), 1113–1115.

(72) Baran, J.; Klosinski, P.; Penczek, S. *Die Makromol. Chemie* **1989**, *190* (8), 1903–1917.

(73) Penczek, S.; Duda, A.; Kaluzynski, K.; Lapienis, G.; Nyk, A.; Szymanski, R. *Makromol. Chemie. Macromol. Symp.* **1993**, *73* (1), 91–101.

(74) Chen, D.-P.; Wang, J. *Macromolecules* **2006**, *39* (2), 473–475.

(75) Xiao, C.-S.; Wang, Y.-C.; Du, J.-Z.; Chen, X.-S.; Wang, J. *Macromolecules* **2006**, *39* (20), 6825–6831.

(76) Steinbach, T.; Wurm, F. R. *Angew. Chemie Int. Ed.* **2015**, *54* (21), 6098–6108.

(77) Marsico, F.; Wagner, M.; Landfester, K.; Wurm, F. R. *Macromolecules* **2012**, *45* (21), 8511–8518.

(78) Ranganathan, T.; Zilberman, J.; Farris, R. J.; Coughlin, E. B.; Emrick, T. *Macromolecules* **2006**, *39* (18), 5974–5975.

(79) Fulmer, G. R.; Miller, A. J. M.; Sherden, N. H.; Gottlieb, H. E.; Nudelman, A.; Stoltz, B. M.; Bercaw, J. E.; Goldberg, K. I. *Organometallics* **2010**, *29* (9), 2176–2179.

(80) Kim, K.-S. *J. Appl. Polym. Sci.* **1983**, *28* (3), 1119–1123.

(81) Millich, F.; Carraher, C. E. *J. Polym. Sci. Part A-1 Polym. Chem.* **1970**, *8* (1), 163–169.

(82) Wang, S. *Biomaterials* **2001**, *22* (10), 1157–1169.

(83) Lapienis, G.; Penczek, S. *Macromolecules* **1977**, *10* (6), 1301–1306.

(84) Libiszowski, J.; Kałużynski, K.; Penczek, S. *J. Polym. Sci. Polym. Chem. Ed.* **1978**, *16* (6), 1275–1283.

(85) Lapienis, G.; Penczek, S.; Pretula, J. *Macromolecules* **1983**, *16* (2), 153–158.

(86) Clément, B.; Grignard, B.; Koole, L.; Jérôme, C.; Lecomte, P. *Macromolecules* **2012**, *45* (11), 4476–4486.

(87) Liquori, A. M.; Anzuino, G.; Coiro, V. M.; D'Alagni, M.; De Santis, P.; Savino, M. *Nature* **1965**, *206* (4982), 358–362.

(88) Schomaker, E.; Challa, G. *Macromolecules* **1989**, *22* (8), 3337–3341.

(89) Kumaki, J.; Kawauchi, T.; Okoshi, K.; Kusanagi, H.; Yashima, E. *Angew. Chemie - Int. Ed.* **2007**, *46* (28), 5348–5351.

(90) Spinu, M.; Jackson, C.; Keating, M. Y.; Gardner, K. H. *J. Macromol. Sci. - Pure Appl. Chem.* **1996**, *33* (10), 1497–1530.

(91) Han, L.; Pan, P.; Shan, G.; Bao, Y. *Polymer* **2015**, *63*, 144–153.

(92) Urayama, H.; Kanamori, T.; Fukushima, K.; Kimura, Y. *Polymer* **2003**, *44* (19), 5635–5641.

(93) Okihara, T.; Tsuji, M.; Kawaguchi, A.; Katayama, I.; Tsuji, H.; Hyon, S.; Ikada, Y. *J. Macromol. Sci. Part B Phys.* **1991**, *30:1-2* (June 2012), 119–140.

(94) Slager, J.; Domb, A. J. *Eur. J. Pharm. Biopharm.* **2004**, *58* (3), 461–469.

(95) Saravanan, M.; Domb, A. J. *Eur. J. Nanomedicine* **2013**, *5* (2), 81–96.

(96) Slager, J.; Cohen, Y.; Khalfin, R.; Talmon, Y.; Domb, A. J. *Macromolecules* **2003**, *36* (9), 2999–3000.

(97) Tsuji, H.; Noda, S.; Kimura, T.; Sobue, T.; Arakawa, Y. *Sci. Rep.* **2017**, *7* (March), 1–12.

(98) Emil A Vitalis. Polyglycol-polyacid ester treatment of textiles. US2917410A, 1955.

(99) Hagan, S. A.; Coombes, A. G. A.; Garnett, M. C.; Dunn, S. E.; Davies, M. C.; Illum, L.; Davis, S. S.;

Harding, S. E.; Purkiss, S.; Gellert, P. R. *Langmuir* **1996**, *12* (9), 2153–2161.

(100) Riley, T.; Stolnik, S.; Heald, C. R.; Xiong, C. D.; Garnett, M. C.; Illum, L.; Davis, S. S.; Purkiss, S. C.; Barlow, R. J.; Gellert, P. R. *Langmuir* **2001**, *17* (11), 3168–3174.

(101) Zhang, J.; Jiang, W.; Zhao, X.; Wang, Y. *Tsinghua Sci. Technol.* **2007**, *12* (4), 493–496.

(102) Fujiwara, T.; Miyamoto, M.; Kimura, Y. *Macromolecules* **2000**, *33* (8), 2782–2785.

(103) Petzetakis, N.; Walker, D.; Dove, A. P.; O'Reilly, R. K. *Soft Matter* **2012**, *8* (28), 7408.

(104) Petzetakis, N.; Dove, A. P.; O'Reilly, R. K. *Chem. Sci.* **2011**, *2* (5), 955–960.

(105) Sun, L.; Pitto-Barry, A.; Kirby, N.; Schiller, T. L.; Sanchez, A. M.; Dyson, M. A.; Sloan, J.; Wilson, N. R.; O'Reilly, R. K.; Dove, A. P. *Nat. Commun.* **2014**, *5* (1), 5746.

(106) Wang, Z.; Cao, Y.; Song, J.; Xie, Z.; Wang, Y. *Langmuir* **2016**, *32* (37), 9633–9639.

(107) Hiemstra, C.; Zhong, Z.; Li, L.; Dijkstra, P. J.; Feijen, J. *Biomacromolecules* **2006**, *7* (10), 2790–2795.

(108) Hiemstra, C.; Zhong, Z.; Dijkstra, P. J.; Feijen, J. *Macromol. Symp.* **2005**, *224* (1), 119–132.

(109) Calucci, L.; Forte, C.; Buwalda, S. J.; Dijkstra, P. J.; Feijen, J. *Langmuir* **2010**, *26* (15), 12890–12896.

(110) Buwalda, S. J.; Dijkstra, P. J.; Calucci, L.; Forte, C.; Feijen, J. *Biomacromolecules* **2010**, *11* (1), 224–232.

(111) Zhou, D.; Shao, J.; Sun, J.; Bian, X.; Xiang, S.; Li, G.; Chen, X. *Polymer* **2017**, *123*, 49–54.

(112) Ruan, G.; Feng, S.-S. *Biomaterials* **2003**, *24* (27), 5037–5044.

(113) Venkatraman, S. S.; Jie, P.; Min, F.; Freddy, B. Y. C.; Leong-Huat, G. *Int. J. Pharm.* **2005**, *298* (1), 219–232.

(114) Lim, D. W.; Park, T. G. *J. Appl. Polym. Sci.* **2000**, *75* (13), 1615–1623.

(115) Cui, H.; Shao, J.; Wang, Y.; Zhang, P.; Chen, X.; Wei, Y. *Biomacromolecules* **2013**, *14* (6), 1904–1912.

(116) Kang, N.; Perron, M.-È.; Prud'homme, R. E.; Zhang, Y.; Gaucher, G.; Leroux, J.-C. *Nano Lett.* **2005**, *5* (2), 315–319.

(117) Yang, L.; Qi, X.; Liu, P.; El Ghzaoui, A.; Li, S. *Int. J. Pharm.* **2010**, *394* (1–2), 43–49.

(118) Chen, L.; Xie, Z.; Hu, J.; Chen, X.; Jing, X. *J. Nanoparticle Res.* **2007**, *9* (5), 777–785.

(119) Wolfgang Schärtl. *Light Scattering from Polymer Solutions and Nanoparticle Dispersions*; Springer Laboratory; Springer Berlin Heidelberg: Berlin, Heidelberg, 2007.

(120) Williams, D. B.; Carter, C. B. In *Transmission Electron Microscopy*; Springer US: Boston, MA, 2009; pp 23–38.

(121) Goldstein, J. I.; Newbury, D. E.; Michael, J. R.; Ritchie, N. W. M.; Scott, J. H. J.; Joy, D. C. *Scanning Electron Microscopy and X-Ray Microanalysis*; Springer New York: New York, NY, 2018.

(122) JEOL. Scanning Electron Microscope A To Z http://www.jeolusa.com/RESOURCES/Electron-Optics/DocumentsDownloads/EntryId/598 (accessed Aug 28, 2018).

(123) Lohmeijer, B. G. G.; Pratt, R. C.; Leibfarth, F.; Logan, J. W.; Long, D. A.; Dove, A. P.; Nederberg, F.; Choi, J.; Wade, C.; Waymouth, R. M.; Hedrick, J. L. *Macromolecules* **2006**, *39* (25), 8574–8583.

(124) Dove, A. P.; Pratt, R. C.; Lohmeijer, B. G. G.; Waymouth, R. M.; Hedrick, J. L. *J. Am. Chem. Soc.* **2005**, *127* (40), 13798–13799.

(125) Chuma, A.; Horn, H. W.; Swope, W. C.; Pratt, R. C.; Zhang, L.; Lohmeijer, B. G. G.; Wade, C. G.; Waymouth, R. M.; Hedrick, J. L.; Rice, J. E. *J. Am. Chem. Soc.* **2008**, *130* (21), 6749–6754.

(126) Carafa, M.; Mesto, E.; Quaranta, E. *European J. Org. Chem.* **2011**, *2011* (13), 2458–2465.

(127) Coady, D. J.; Fukushima, K.; Horn, H. W.; Rice, J. E.; Hedrick, J. L. *Chem. Commun.* **2011**, *47* (11), 3105.

(128) Jamshidi, K.; Hyon, S.-H.; Ikada, Y. *Polymer* **1988**, *29* (12), 2229–2234.

(129) Faucher, J. A.; Koleske, J. V.; Santee, E. R.; Stratta, J. J.; Wilson, C. W. *J. Appl. Phys.* **1966**, *37* (11), 3962–3964.

(130) Tsuji, H. *Macromol. Biosci.* **2005**, *5* (7), 569–597.

(131) Jain, S.; Bates, F. S. *Science* **2003**, *300* (5618), 460–464.

(132) Antonietti, M.; Förster, S. *Adv. Mater.* **2003**, *15* (16), 1323–1333.

(133) Schlaad, H.; Krasia, T.; Antonietti, M. *J. Am. Chem. Soc.* **2004**, *126* (36), 11307–11310.

(134) Förster, S.; Zisenis, M.; Wenz, E.; Antonietti, M. *J. Chem. Phys.* **1996**, *104* (24), 9956–9970.

(135) Sawai, D.; Tsugane, Y.; Tamada, M.; Kanamoto, T.; Sungil, M.; Hyon, S.-H. *J. Polym. Sci. Part B*

Polym. Phys. **2007**, *45* (18), 2632–2639.

(136) Lucke, A.; Teßmar, J.; Schnell, E.; Schmeer, G.; Göpferich, A. *Biomaterials* **2000**, *21* (23), 2361–2370.

(137) Slager, J.; Brizzolara, D.; Cantow, H. J.; Domb, A. J. *Polym. Adv. Technol.* **2005**, *16* (9), 667–674.

(138) Ilka Zerbe. Neue Zwitterionische Polymere, Fachhochschule Fresenius Wiesbaden, 1990.

(139) Steinbach, T.; Ritz, S.; Wurm, F. R. *ACS Macro Lett.* **2014**, *3* (3), 244–248.

(140) Wolf, T.; Hunold, J.; Simon, J.; Rosenauer, C.; Hinderberger, D.; Wurm, F. R. *Polym. Chem.* **2018**, *9* (4), 490–498.

(141) Wolf, T.; Steinbach, T.; Wurm, F. R. *Macromolecules* **2015**, *48* (12), 3853–3863.

(142) Hsiao, M.-S.; Yusoff, S. F. M.; Winnik, M. A.; Manners, I. *Macromolecules* **2014**, *47* (7), 2361–2372.

11 Appendix A

Analytical Section

11.1 NMR Spectra PLA-based Block Copolymers

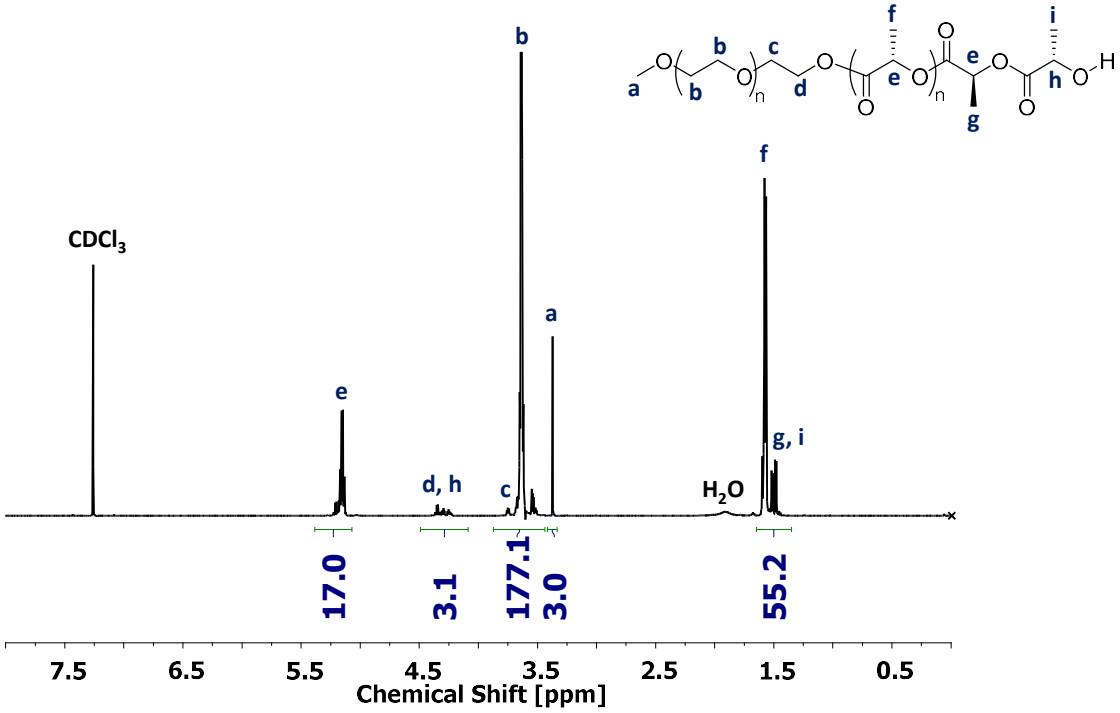

Figure A. 1: *^{1}H-NMR spectrum ($CDCl_3$, 500 MHz) of synthesized PEG_{45}-$PLLA_{18}$*

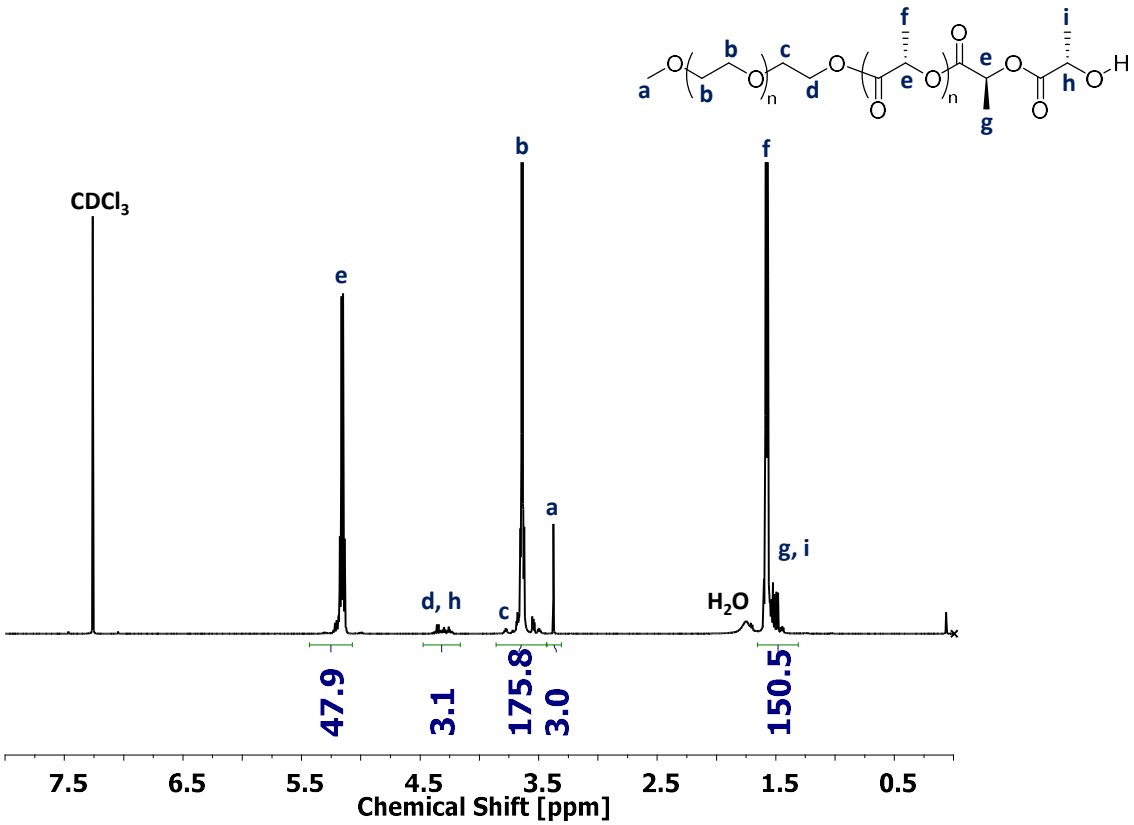

***Figure A. 2**: [1]H-NMR spectrum ($CDCl_3$, 500 MHz) of synthesized PEG_{45}-$PLLA_{49}$*

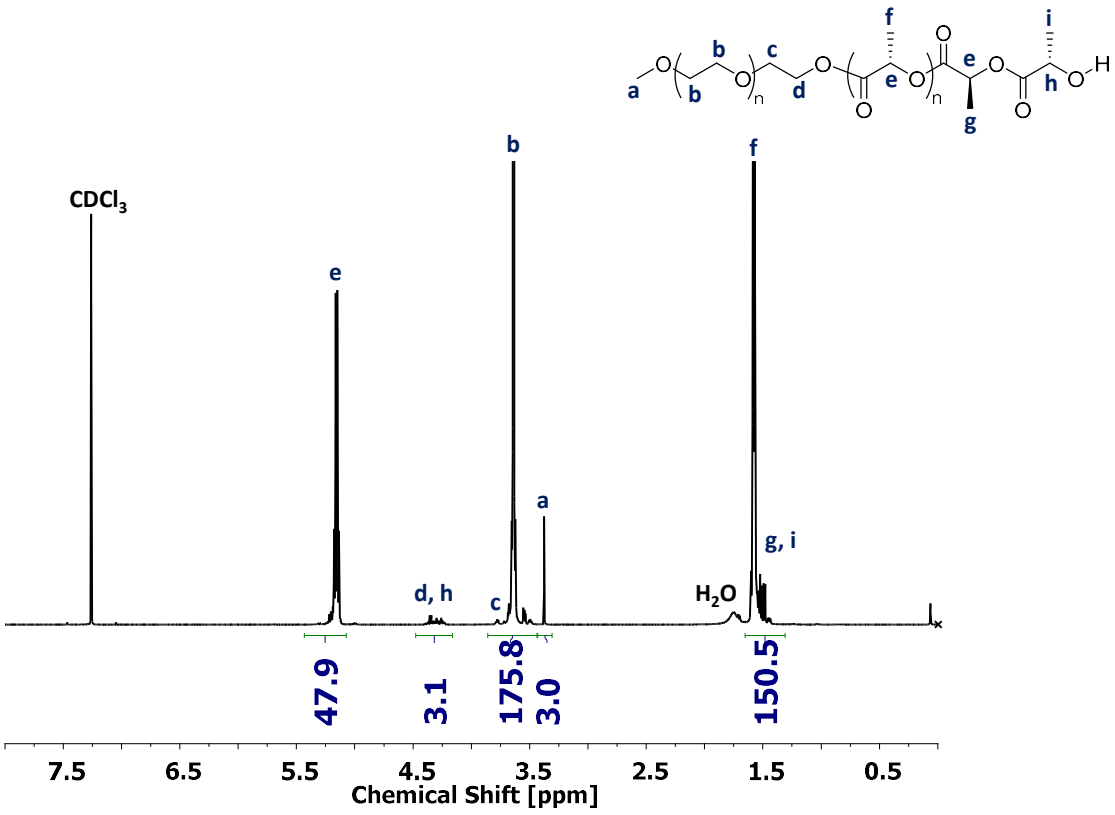

***Figure A. 3:** [1]H-NMR spectrum ($CDCl_3$, 500 MHz) of synthesized PEG_{45}-$PLLA_{72}$*

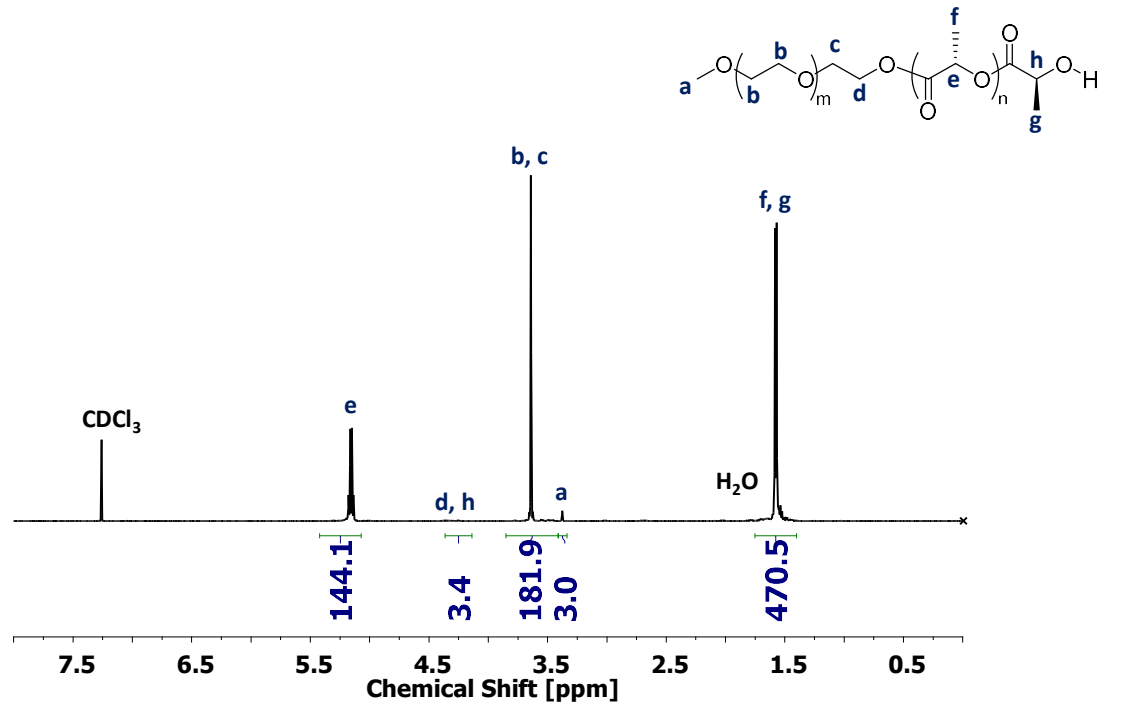

Figure A. 4: *^{1}H-NMR spectrum ($CDCl_3$, 500 MHz) of synthesized PEG_{45}-P$_L$LA_{145}*

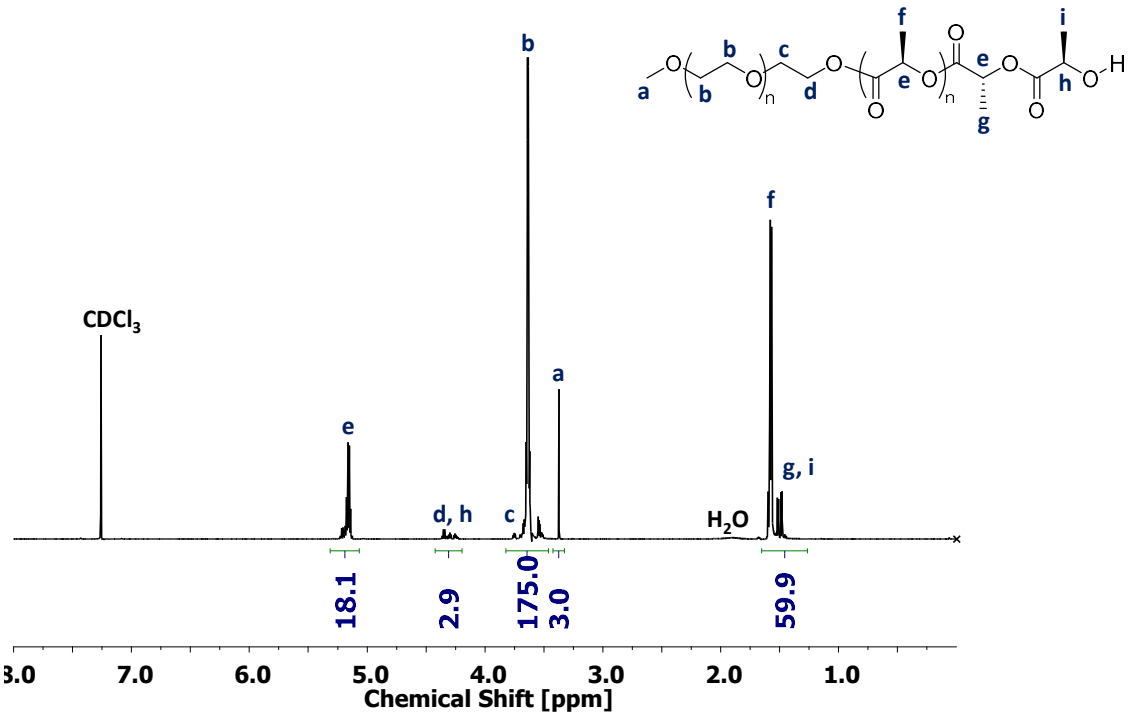

Figure A. 5: *^{1}H-NMR spectrum ($CDCl_3$, 500 MHz) of synthesized PEG_{45}-P$_D$LA_{19}*

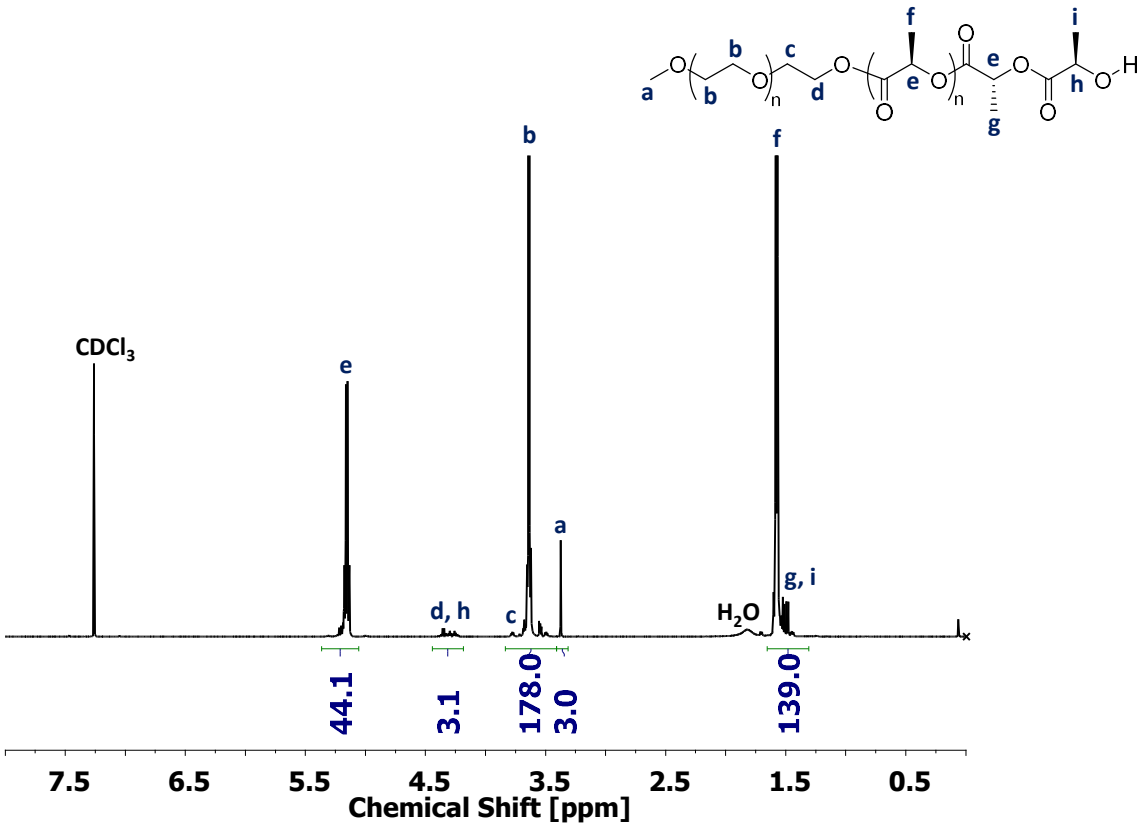

Figure A. 6: *^{1}H-NMR spectrum ($CDCl_3$, 500 MHz) of synthesized PEG_{45}-PDLA_{45}*

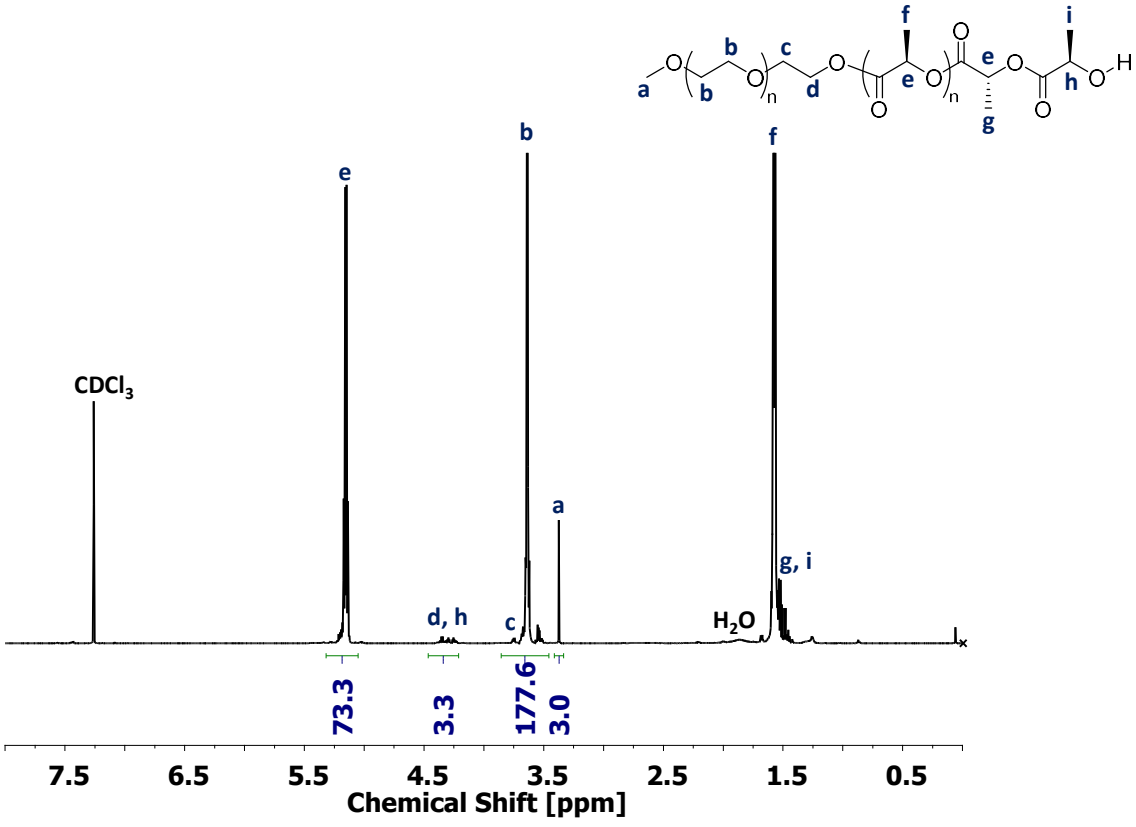

Figure A. 7: *^{1}H-NMR spectrum ($CDCl_3$, 500 MHz) of synthesized PEG_{45}-PDLA_{74}*

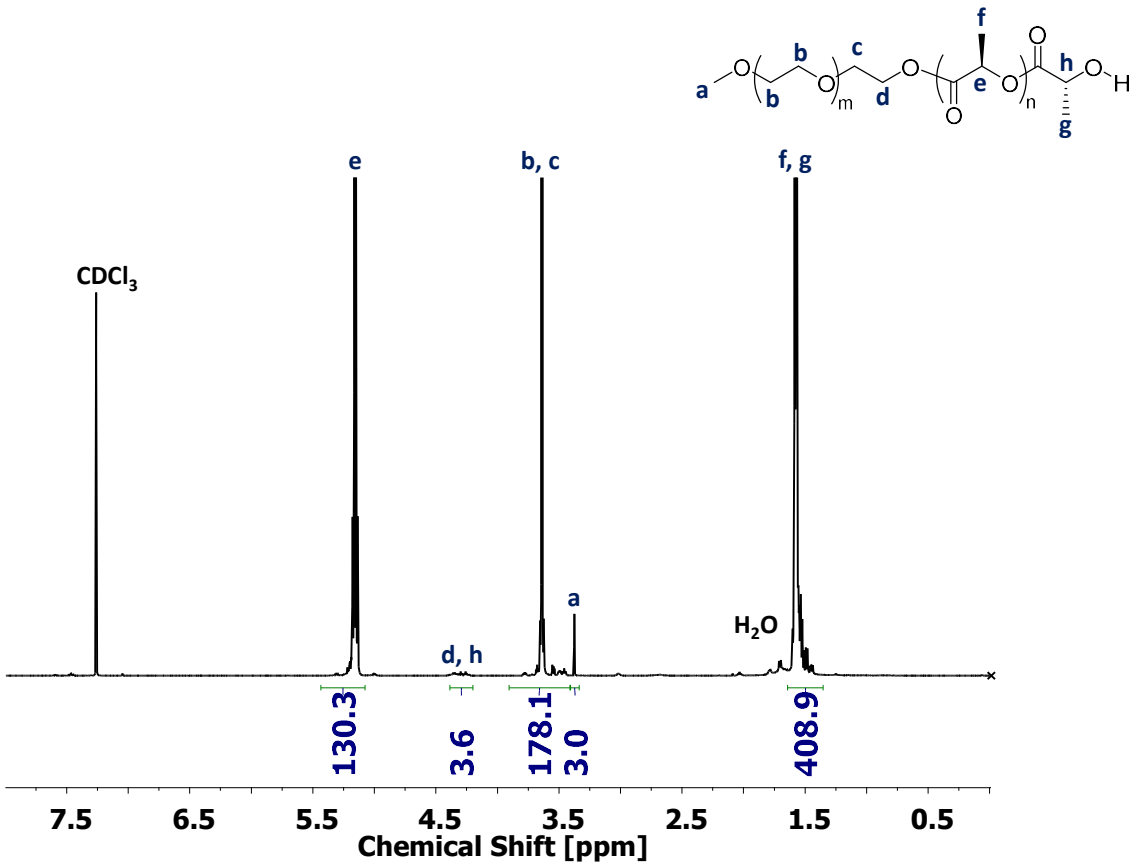

Figure A. 8: *^{1}H-NMR spectrum ($CDCl_3$, 500 MHz) of synthesized PEG_{45}-PDLA_{131}*

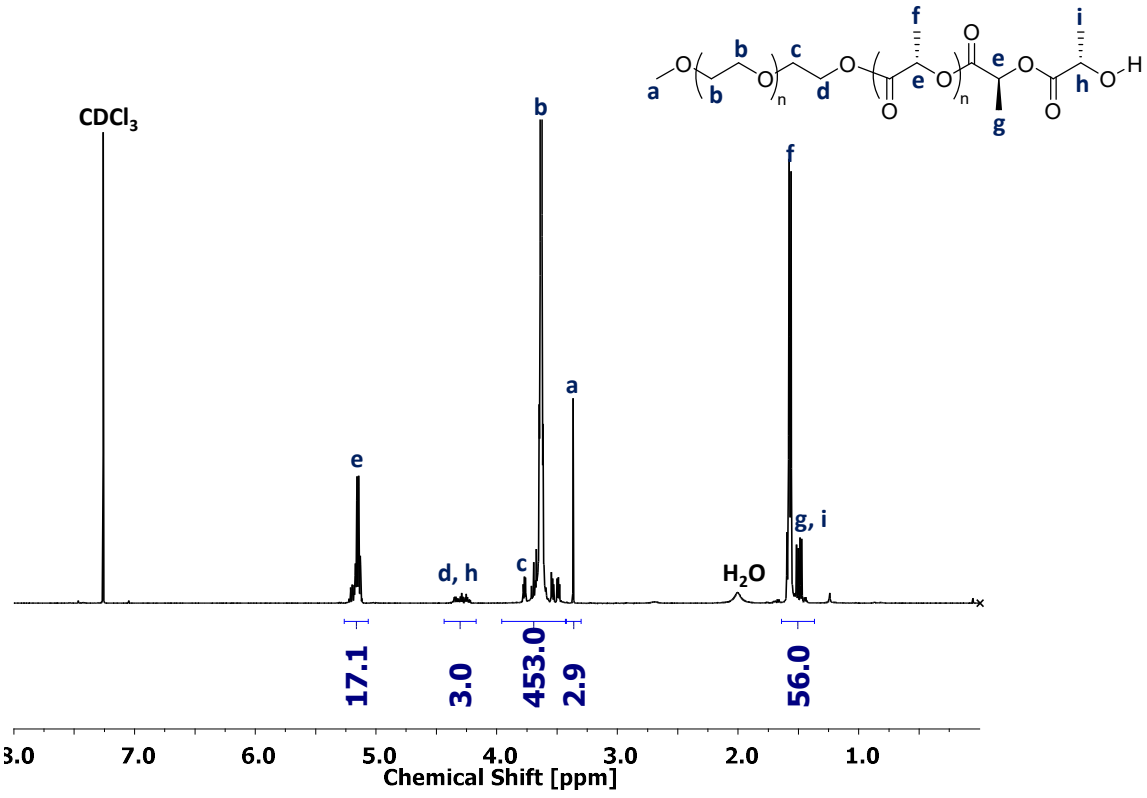

Figure A. 9: *^{1}H-NMR spectrum ($CDCl_3$, 500 MHz) of synthesized PEG_{113}-PLLA_{18}*

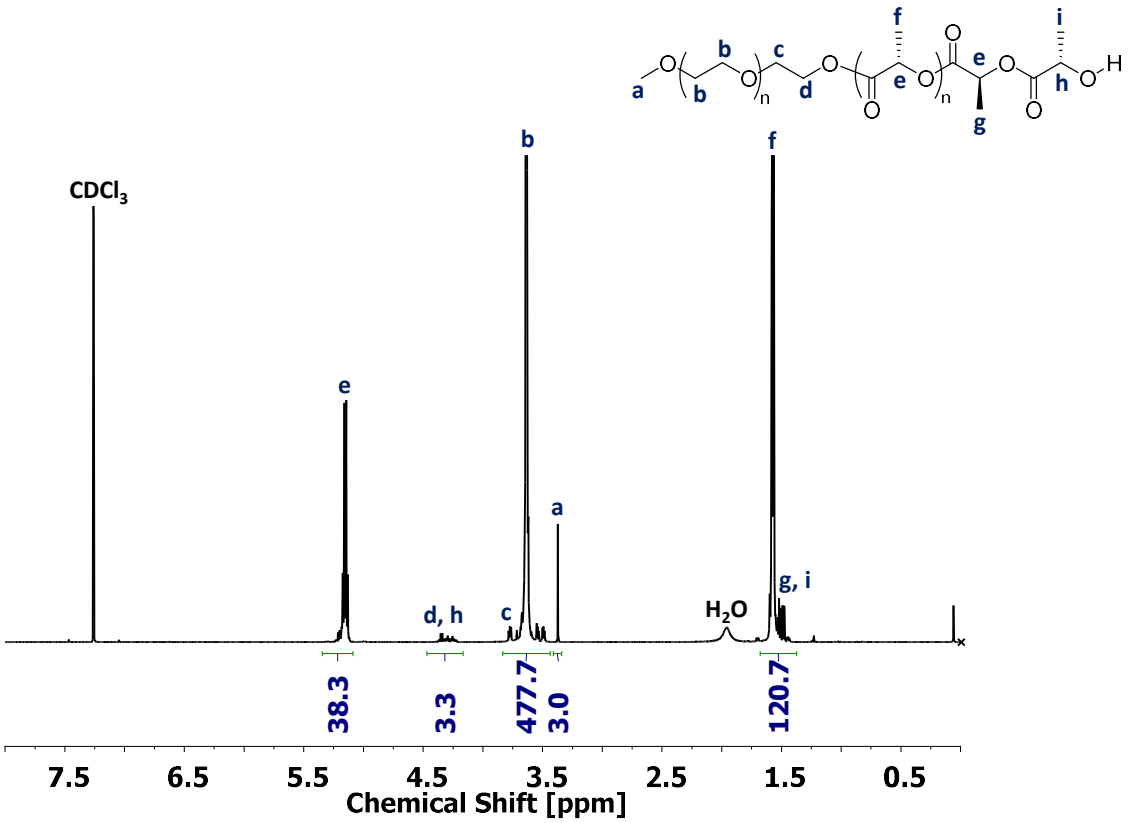

Figure A. 10: *^{1}H-NMR spectrum ($CDCl_3$, 500 MHz) of synthesized PEG_{113}-PLA_{39}*

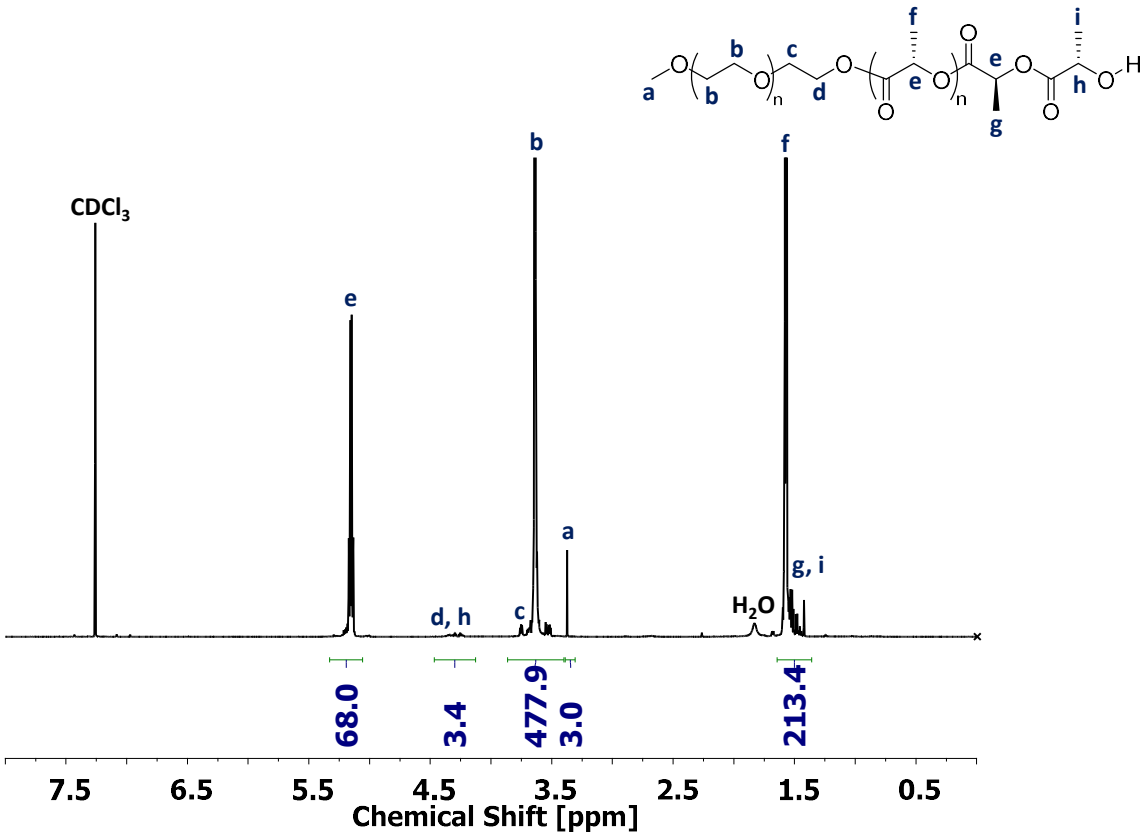

Figure A. 11: *^{1}H-NMR spectrum ($CDCl_3$, 500 MHz) of synthesized PEG_{113}-PLA_{69}*

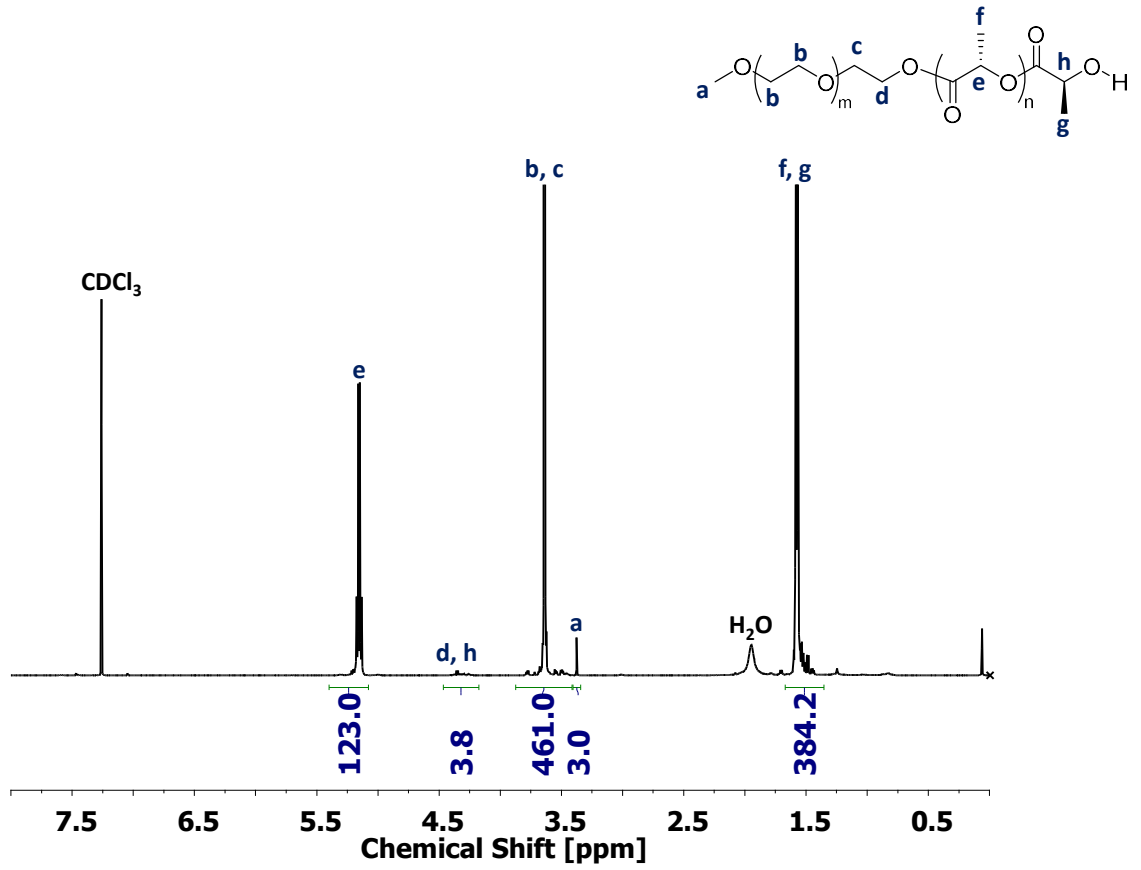

Figure A. 12: *^{1}H-NMR spectrum ($CDCl_3$, 500 MHz) of synthesized PEG_{113}-P$_L$LA_{124}*

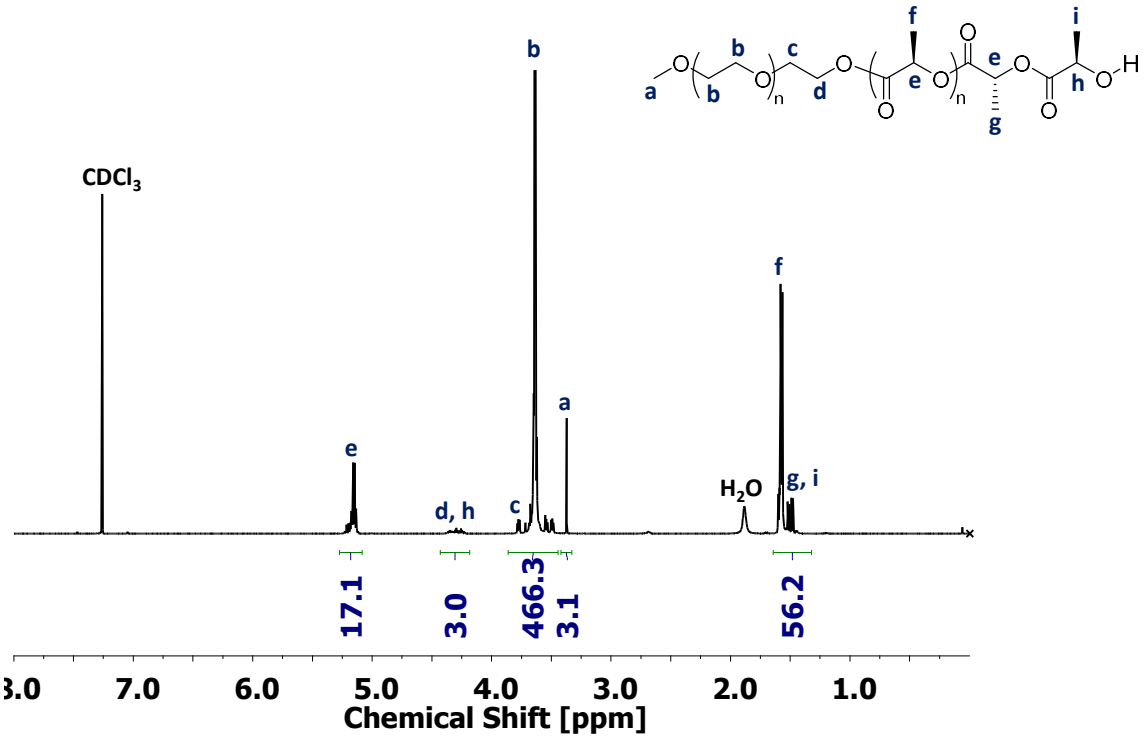

Figure A. 13: *^{1}H-NMR spectrum ($CDCl_3$, 500 MHz) of synthesized PEG_{113}-P$_D$LA_{18}*

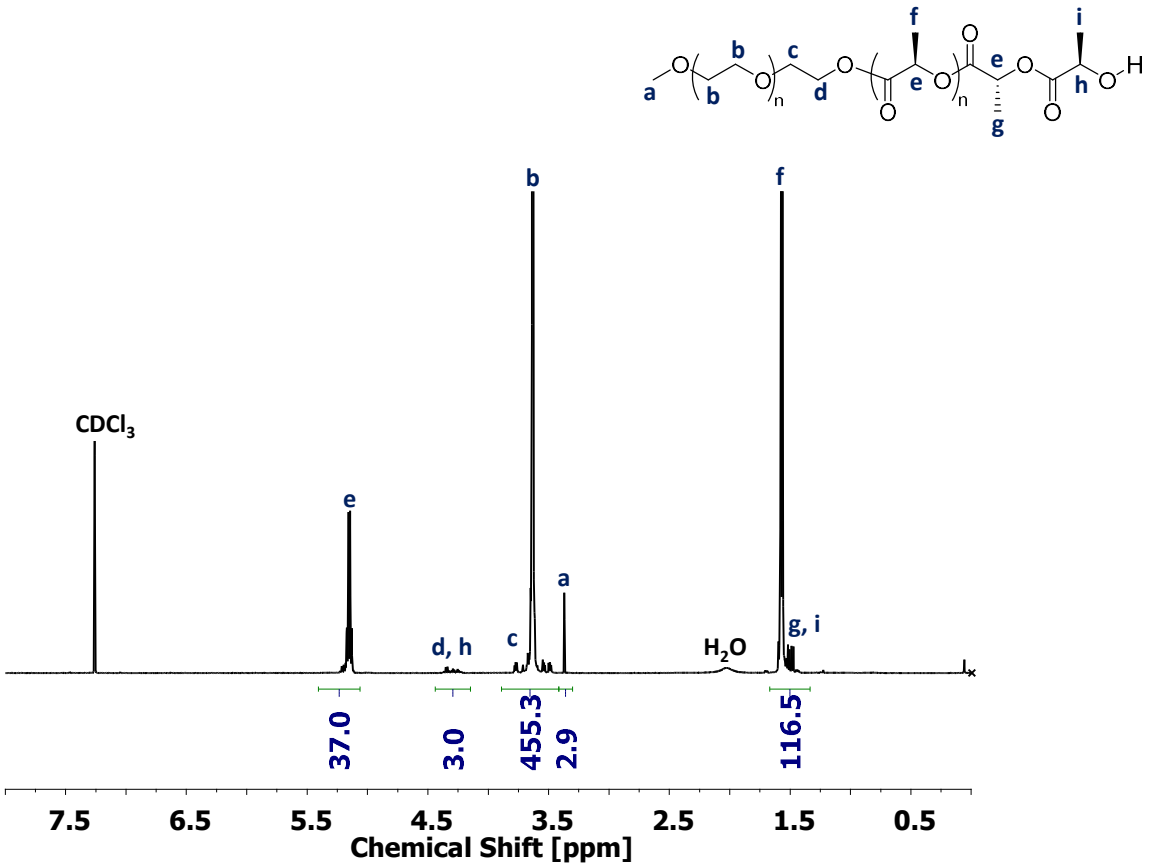

Figure A. 14: *^{1}H-NMR spectrum ($CDCl_3$, 500 MHz) of synthesized PEG_{113}-PDLA_{38}*

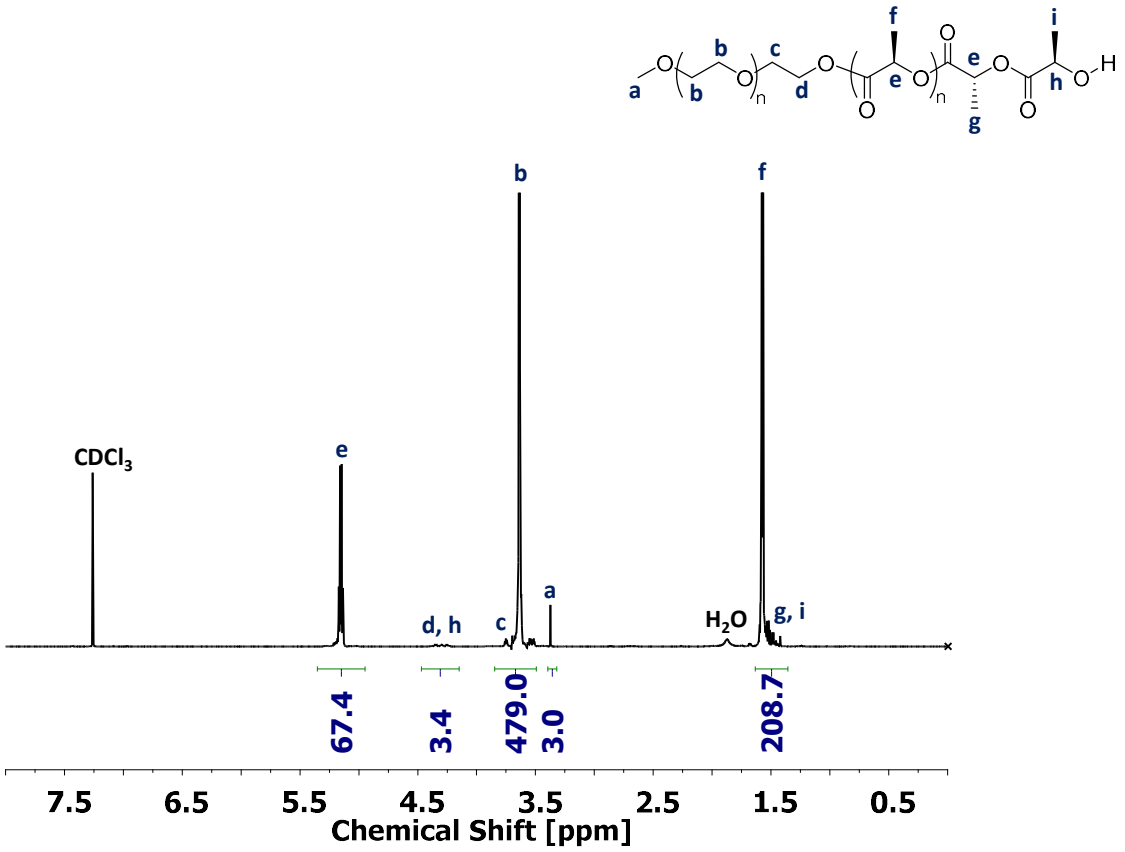

Figure A. 15: *^{1}H-NMR spectrum ($CDCl_3$, 500 MHz) of synthesized PEG_{113}-PDLA_{68}*

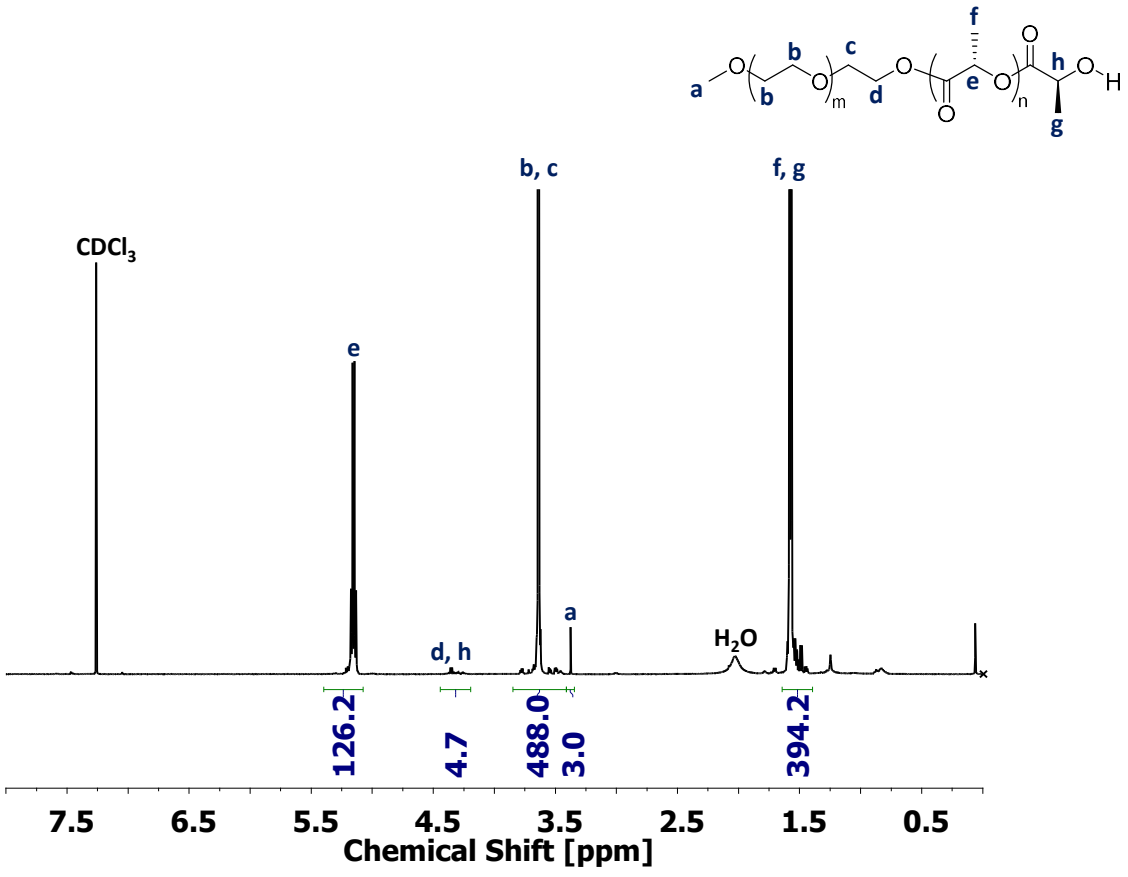

Figure A. 16: *^{1}H-NMR spectrum ($CDCl_3$, 500 MHz) of synthesized PEG_{113}-PDLA_{127}*

11.2 NMR Spectra of Precursors

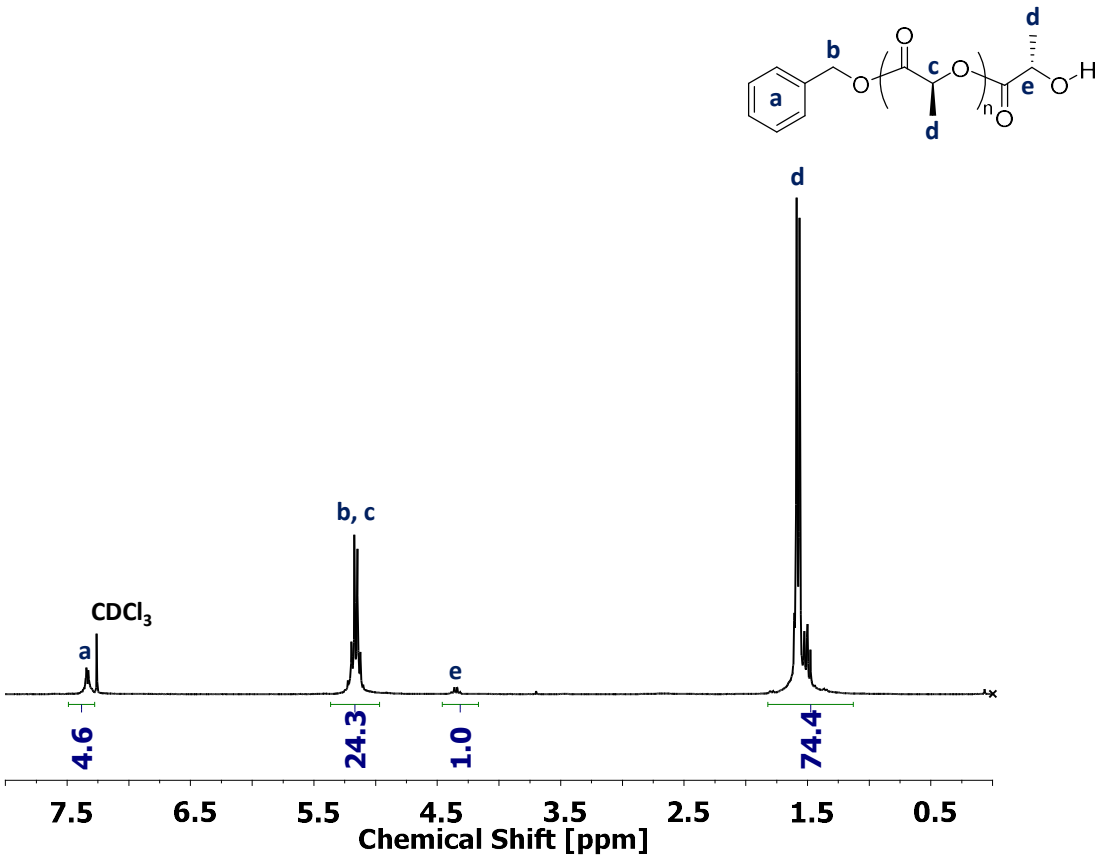

***Figure A. 17**: [1]H-NMR spectrum ($CDCl_3$, 300 MHz) of synthesized P_LLA_{25}*

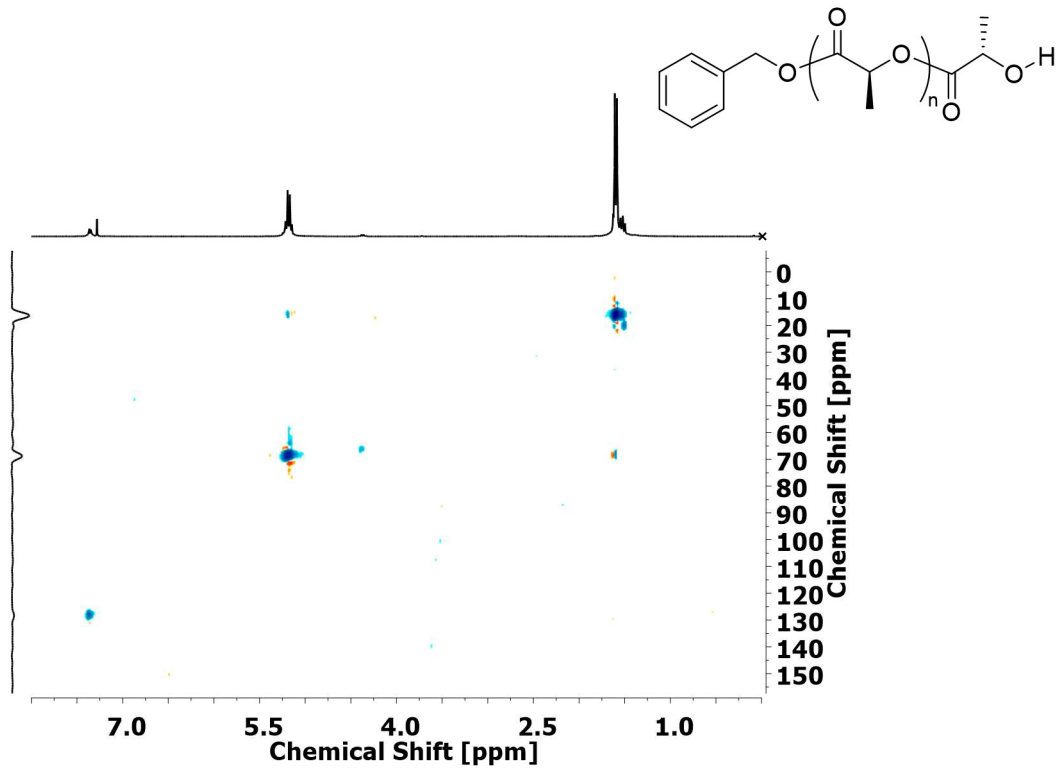

***Figure A. 18:** HSQC-NMR spectrum ($CDCl_3$, 300 MHz) of synthesized P_LLA_{25}*

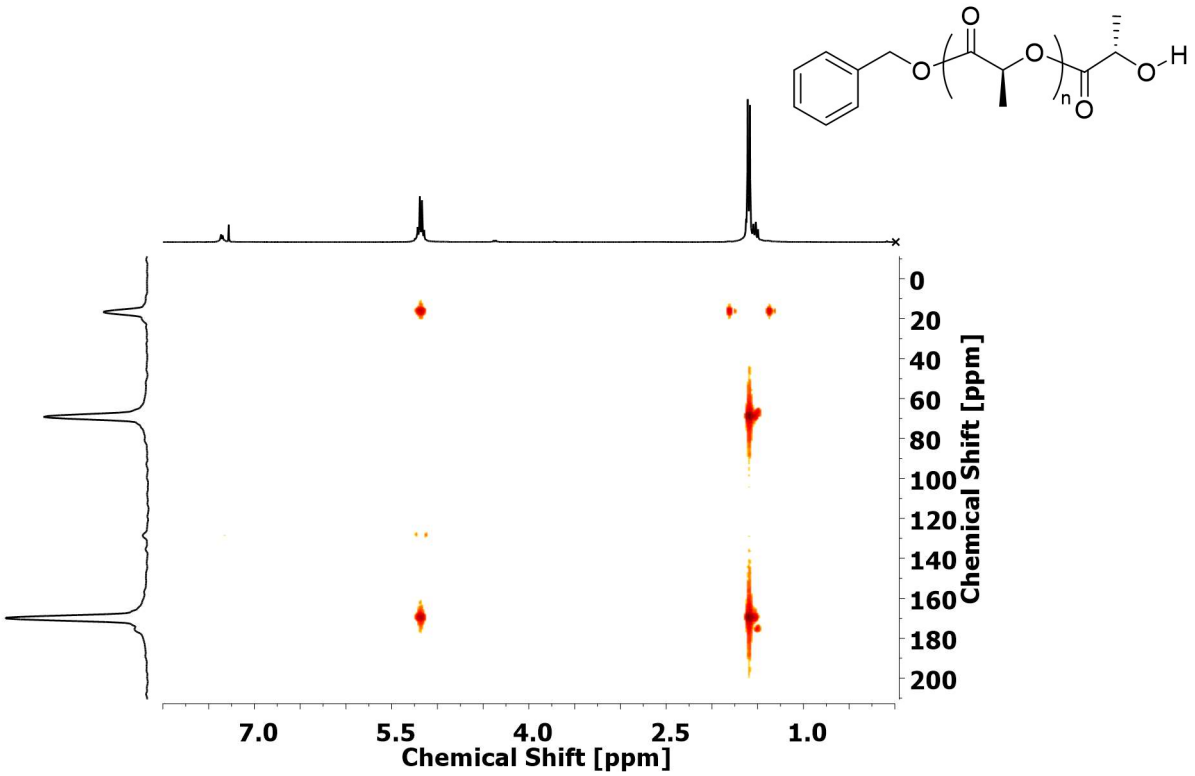

***Figure A. 19**: ^{1}H, ^{13}C-NMR spectrum ($CDCl_3$, 300 MHz) of synthesized $PLLA_{25}$*

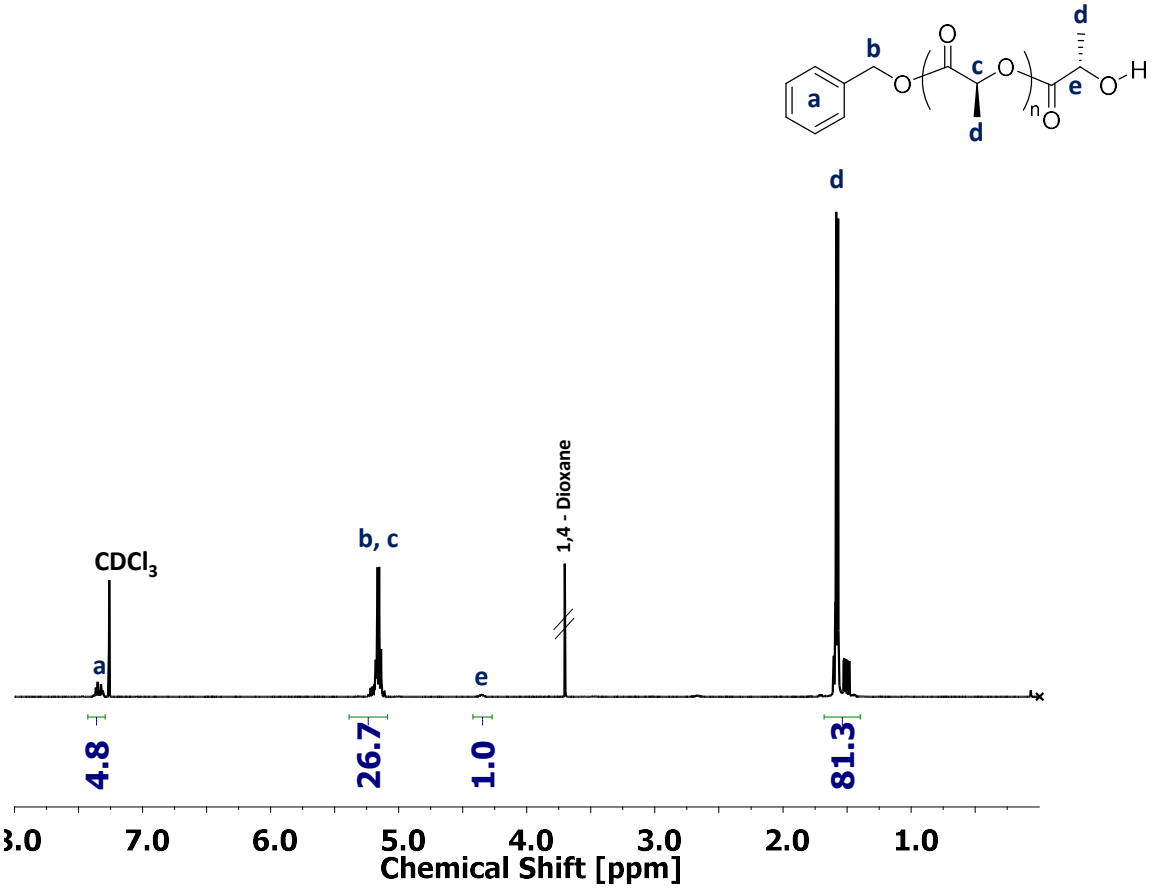

***Figure A. 20:** ^{1}H-NMR spectrum ($CDCl_3$, 300 MHz) of synthesized $PLLA_{26}$*

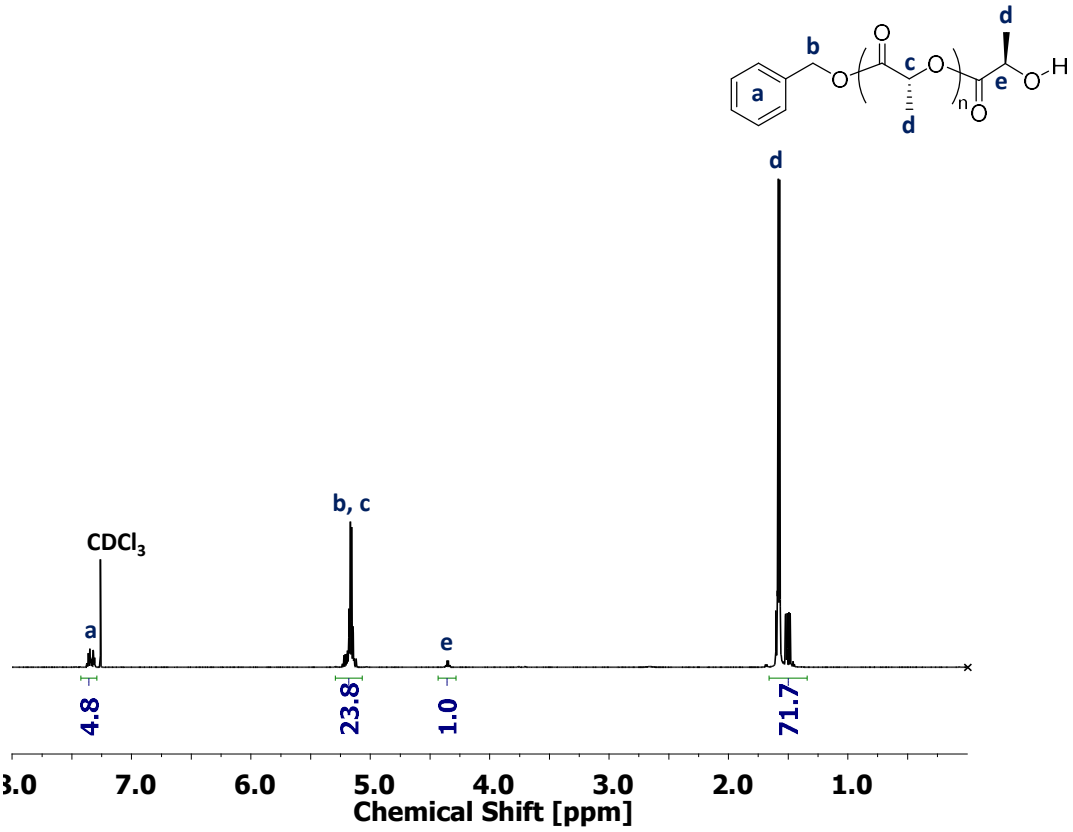

Figure A. 21: *^{1}H-NMR spectrum ($CDCl_3$, 500 MHz) of synthesized PLA_{23}*

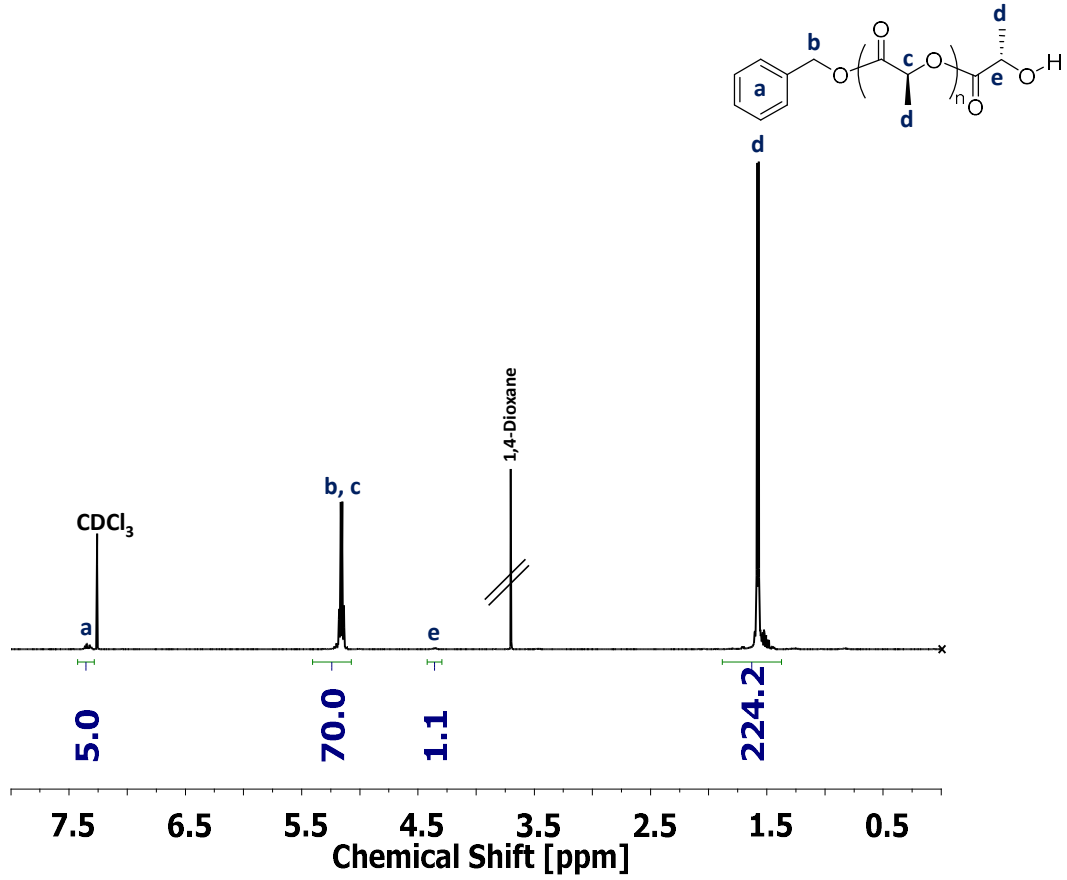

Figure A. 22: *^{1}H-NMR spectrum ($CDCl_3$, 500 MHz) of synthesized PLA_{69}*

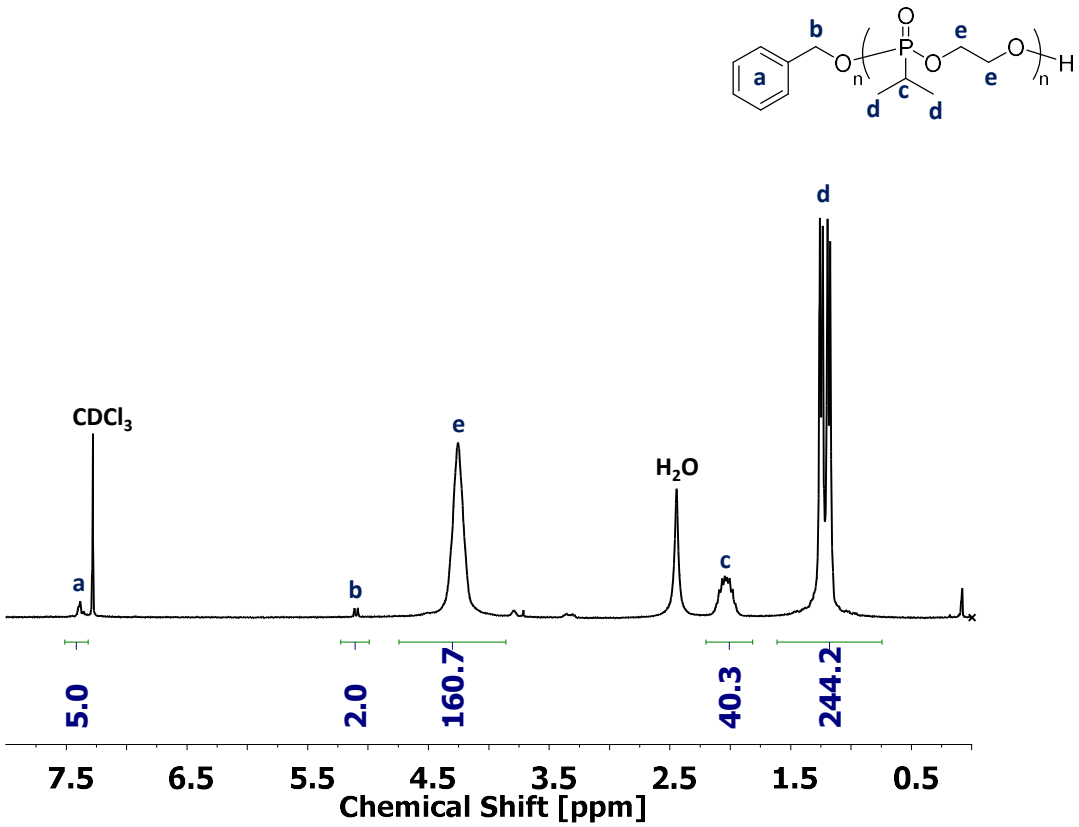

Figure A. 23: *^{1}H-NMR spectrum ($CDCl_3$, 300 MHz) of synthesized $P^{i}PrP_{40}$*

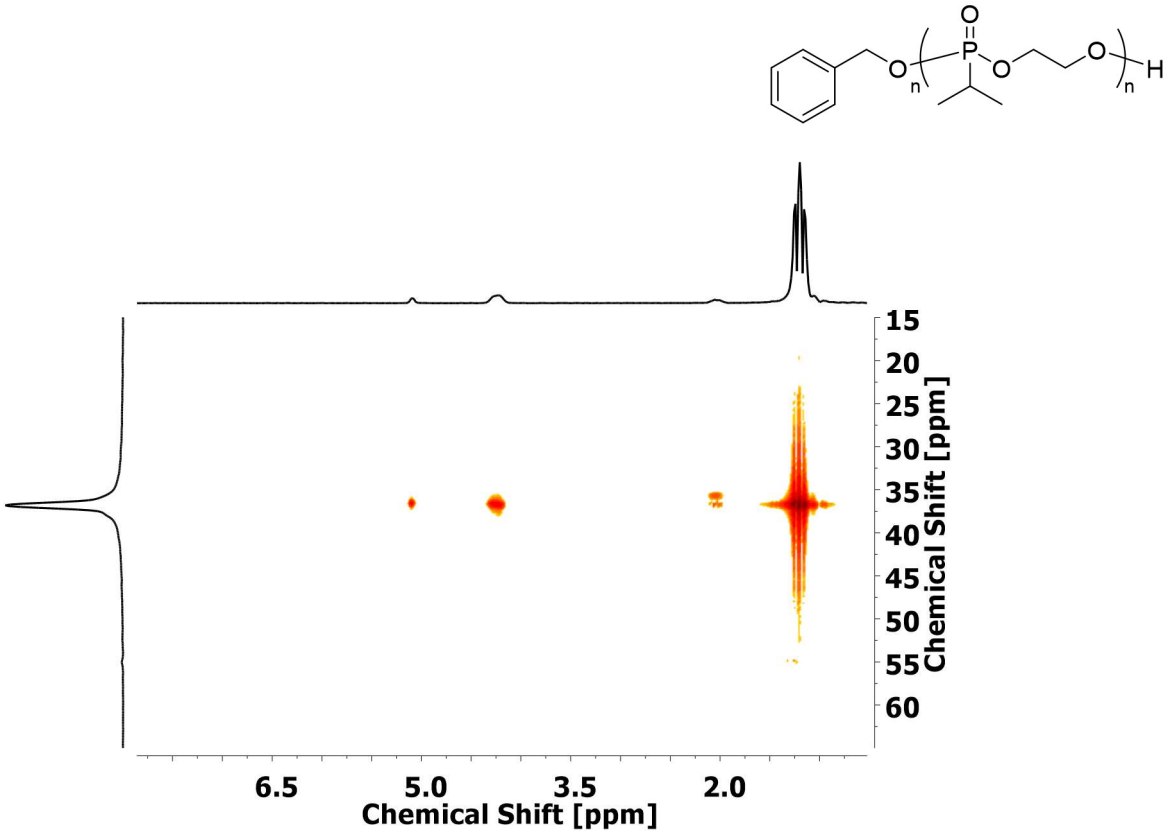

Figure A. 24: *^{1}H, ^{31}P-NMR spectrum ($CDCl_3$, 300 MHz) of synthesized $P^{i}PrP_{40}$*

11.3 NMR Spectra of Poly(alkyl Phosphonate)s and Poly(lactide)-based Copolymers

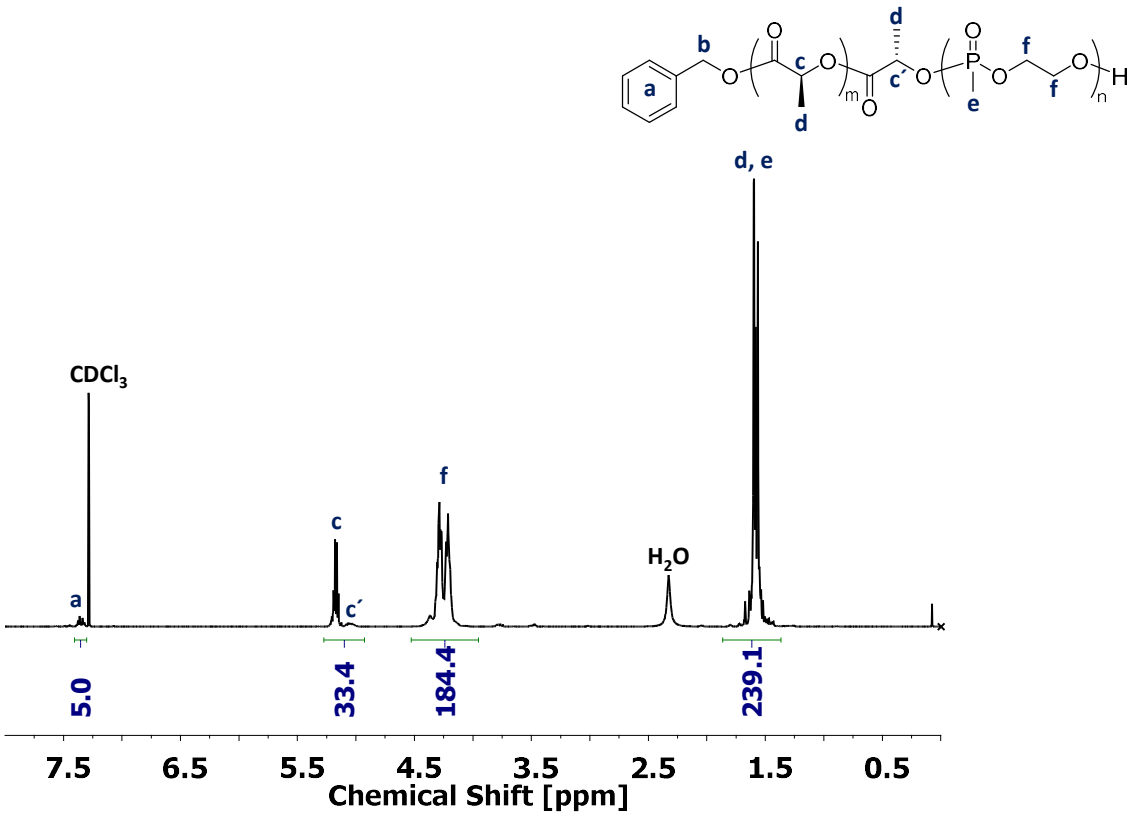

Figure A. 25: *^{1}H-NMR spectrum ($CDCl_3$, 500 MHz) of synthesized $PLLA_{33}$-$PMeP_{46}$*

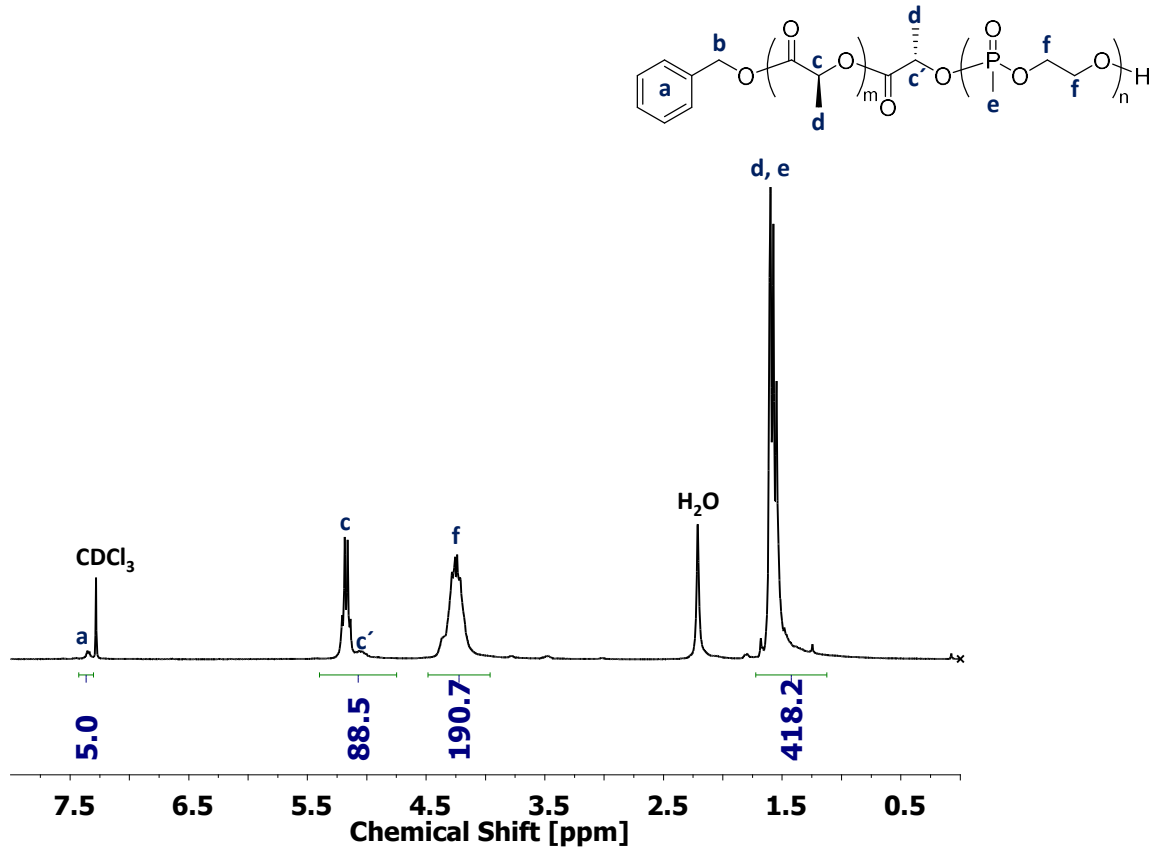

Figure A. 26: *^{1}H-NMR spectrum ($CDCl_3$, 300 MHz) of synthesized P_LLA_{33}-$PMeP_{48}$*

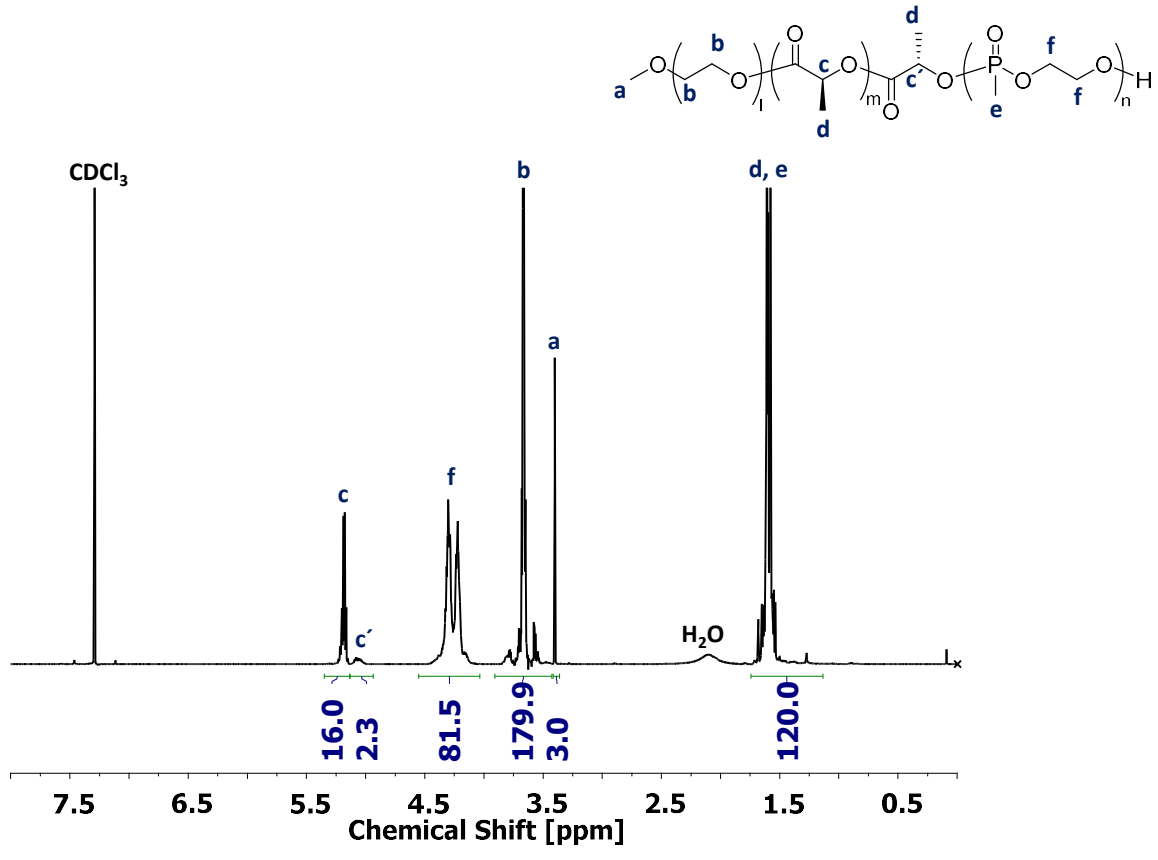

Figure A. 27: *^{1}H-NMR spectrum ($CDCl_3$, 500 MHz) of synthesized PEG_{45}-P_LLA_{19}-$PMeP_{20}$*

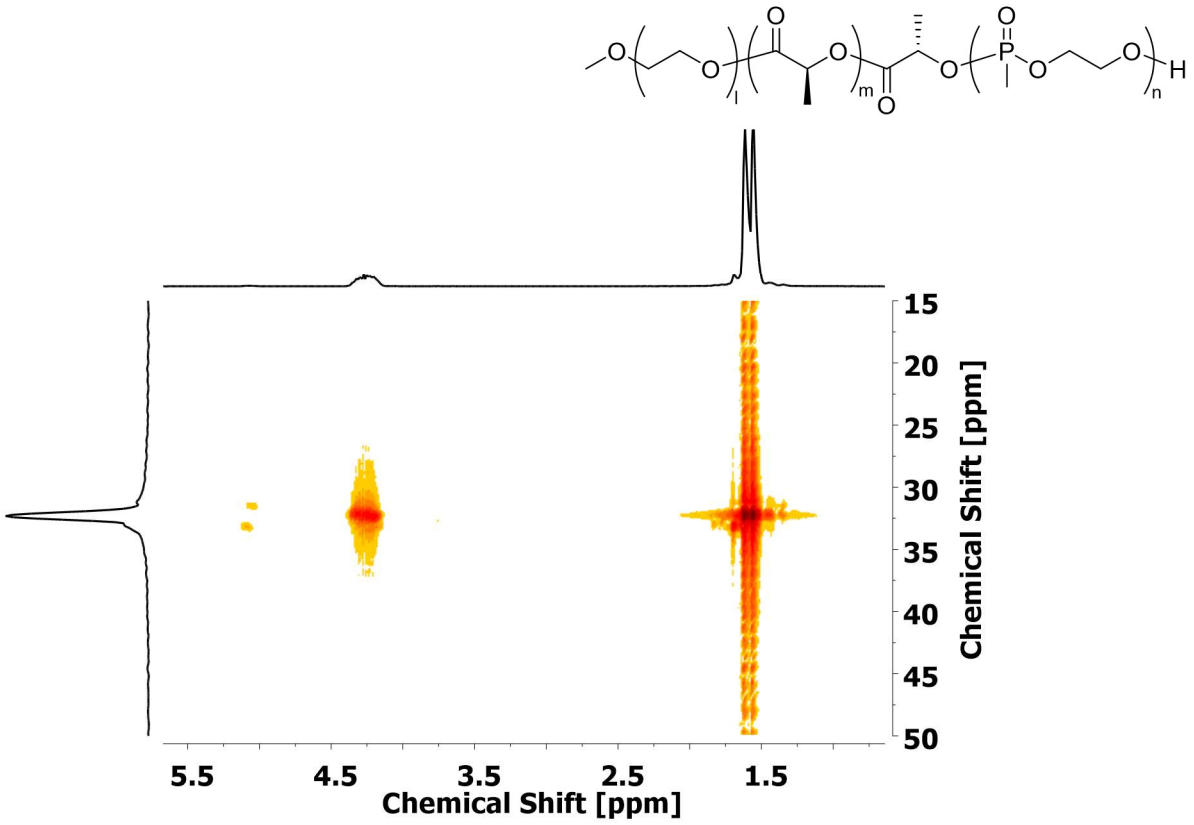

Figure A. 28: *^{1}H, ^{31}P-NMR spectrum ($CDCl_3$, 300 MHz) of synthesized PEG_{45}-PLLA_{19}-$PMeP_{20}$*

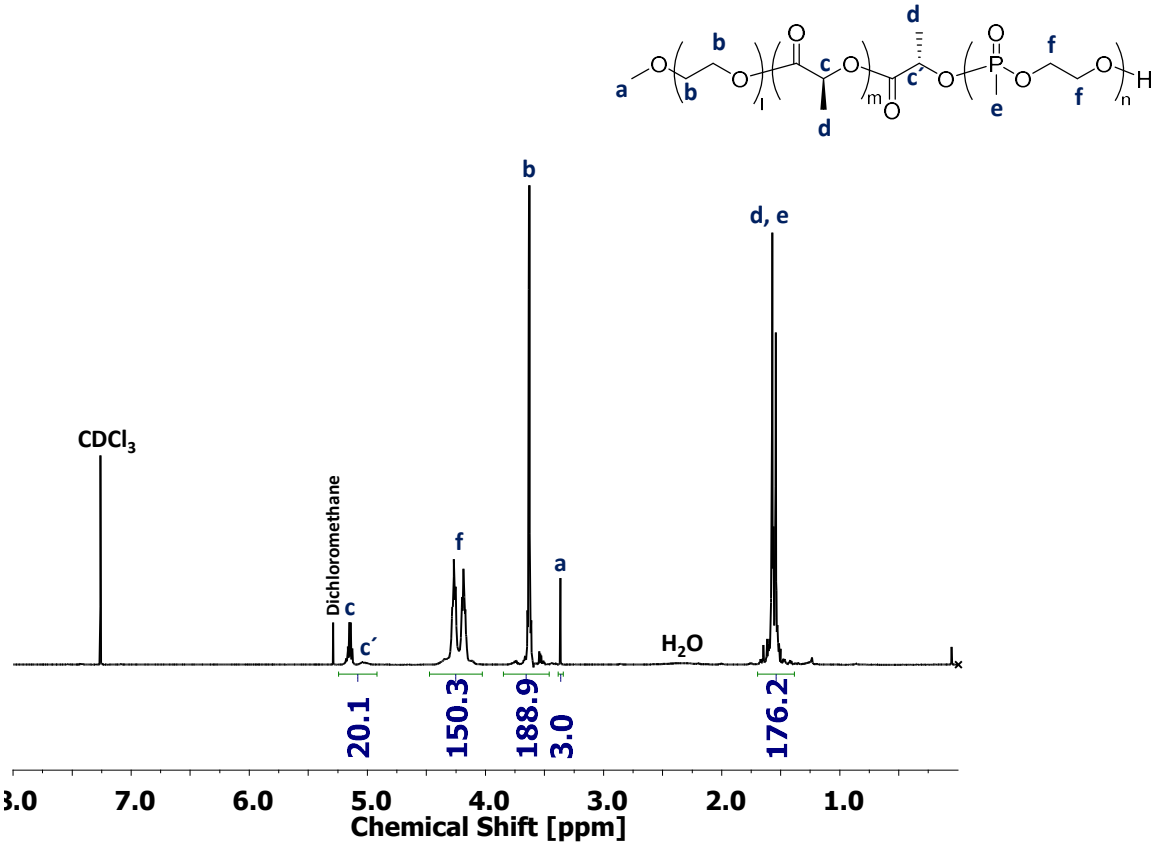

Figure A. 29: *^{1}H-NMR spectrum ($CDCl_3$, 500 MHz) of synthesized PEG_{45}-PLLA_{20}-$PMeP_{37}$*

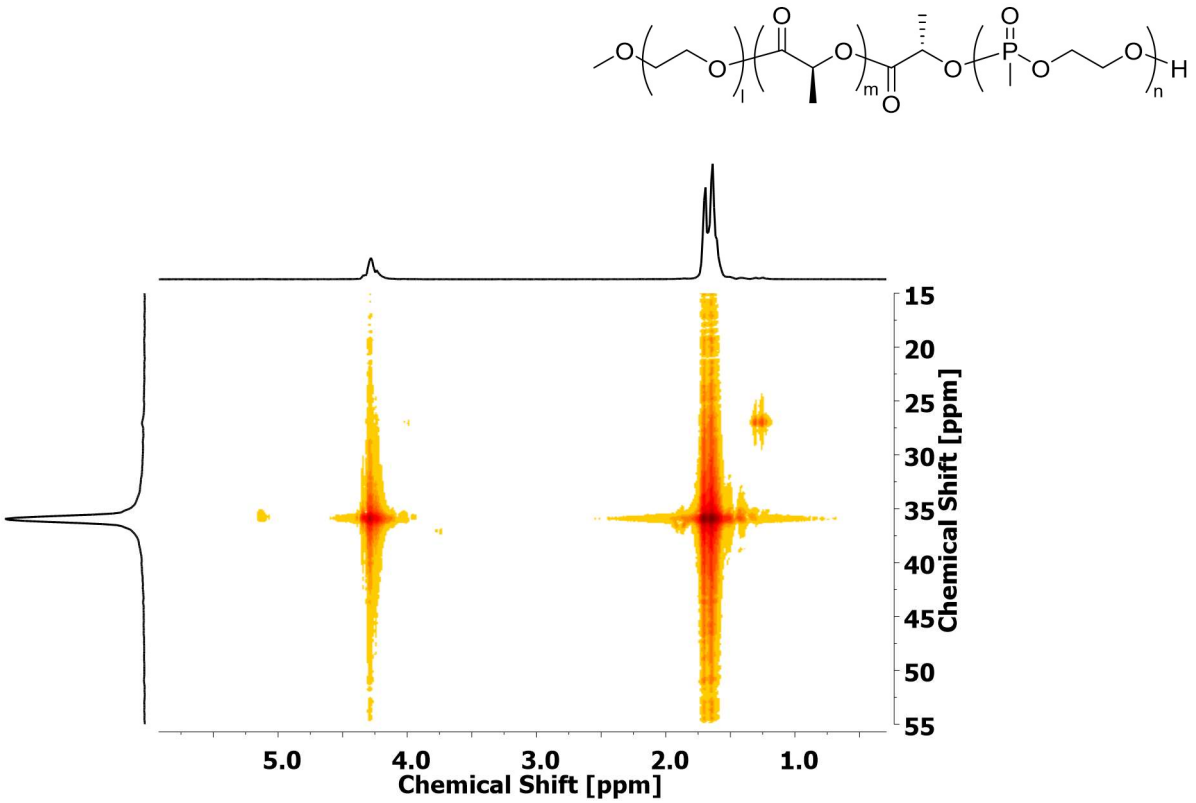

Figure A. 30: *^{1}H, ^{31}P-NMR spectrum ($CDCl_3$, 300 MHz) of synthesized PEG_{45}-$PLLA_{20}$-$PMeP_{37}$*

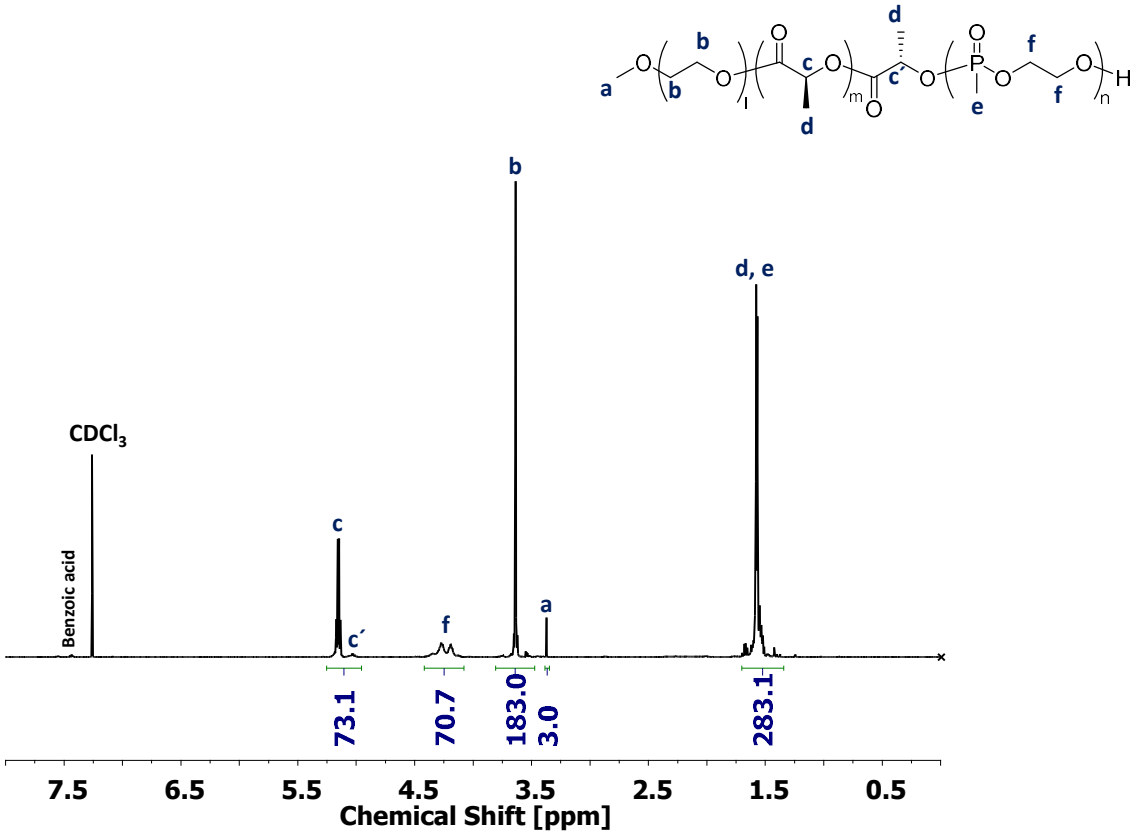

Figure A. 31: *^{1}H-NMR spectrum ($CDCl_3$, 500 MHz) of synthesized PEG_{45}-$PLLA_{73}$-$PMeP_{18}$*

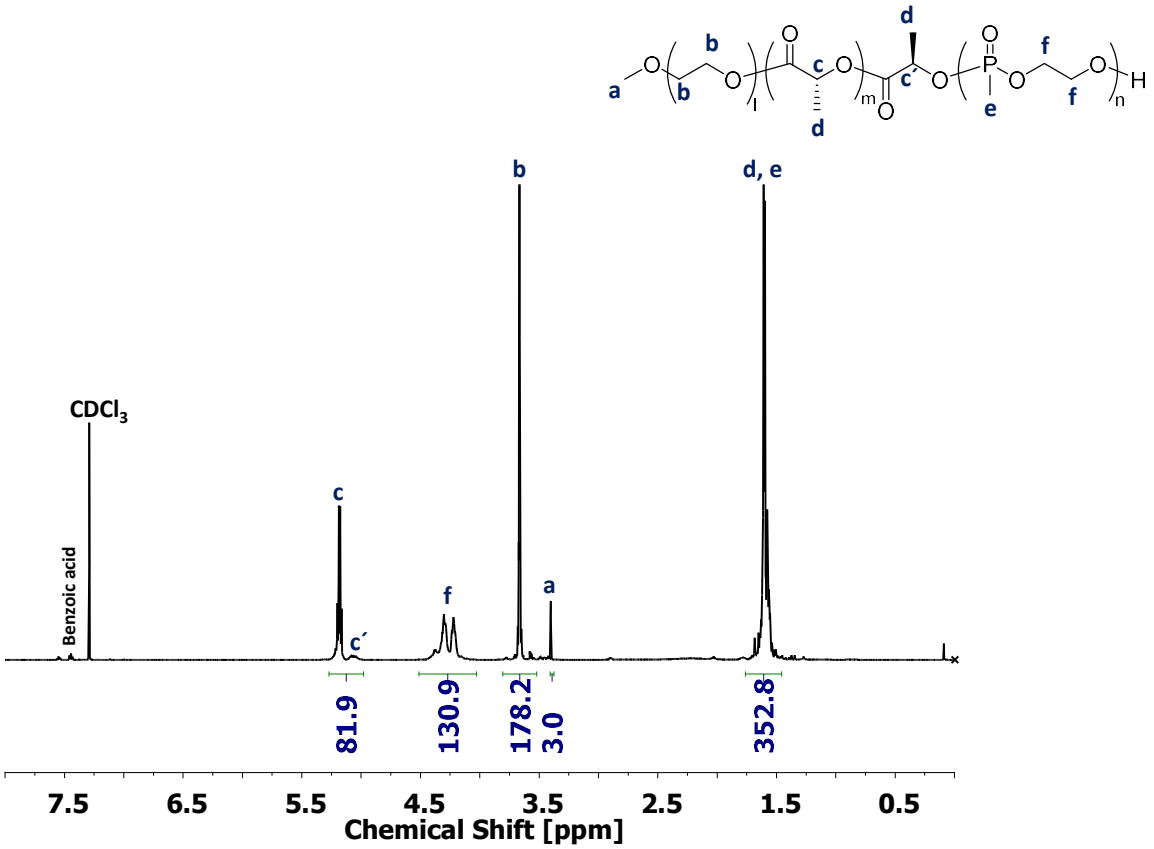

Figure A. 32: *^{1}H-NMR spectrum ($CDCl_3$, 500 MHz) of synthesized PEG_{45}-P$_D$LA_{82}-PMeP_{33}*

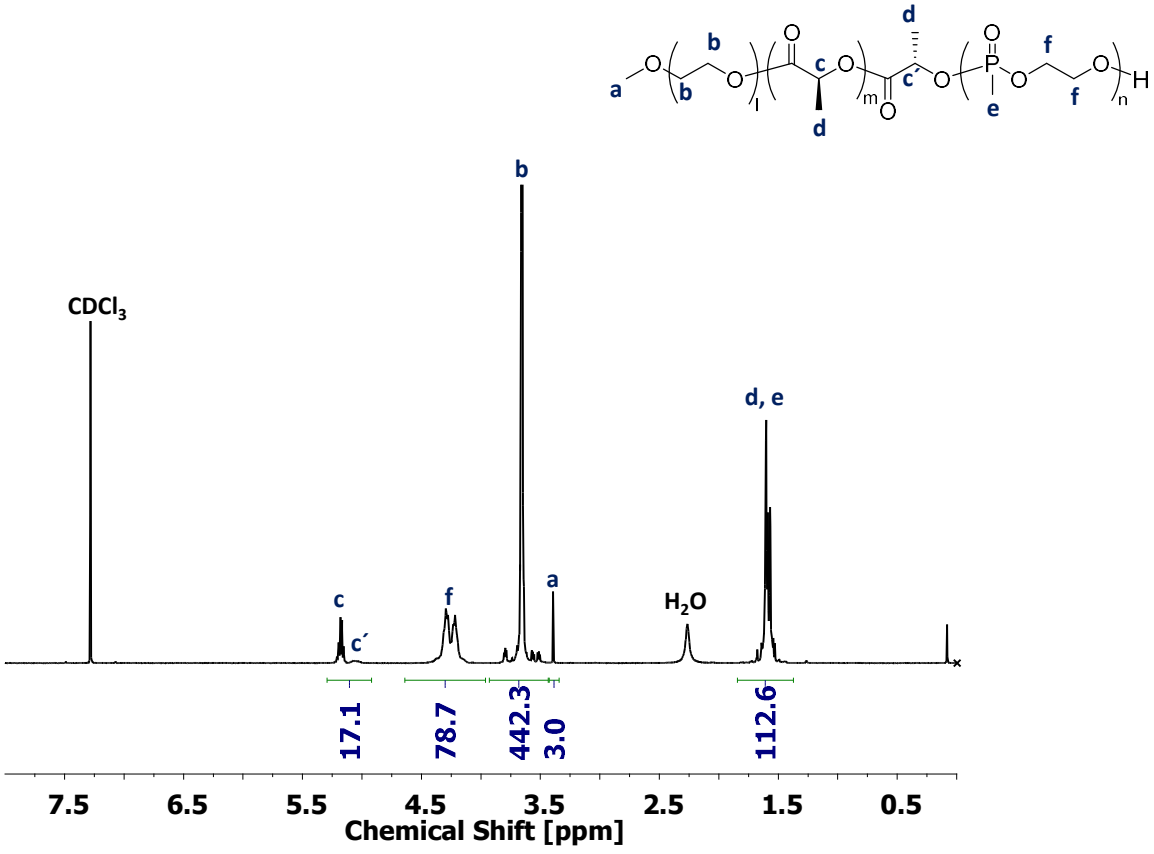

Figure A. 33: *^{1}H-NMR spectrum ($CDCl_3$, 500 MHz) of synthesized PEG_{113}-P$_L$LA_{18}-PMeP_{20}*

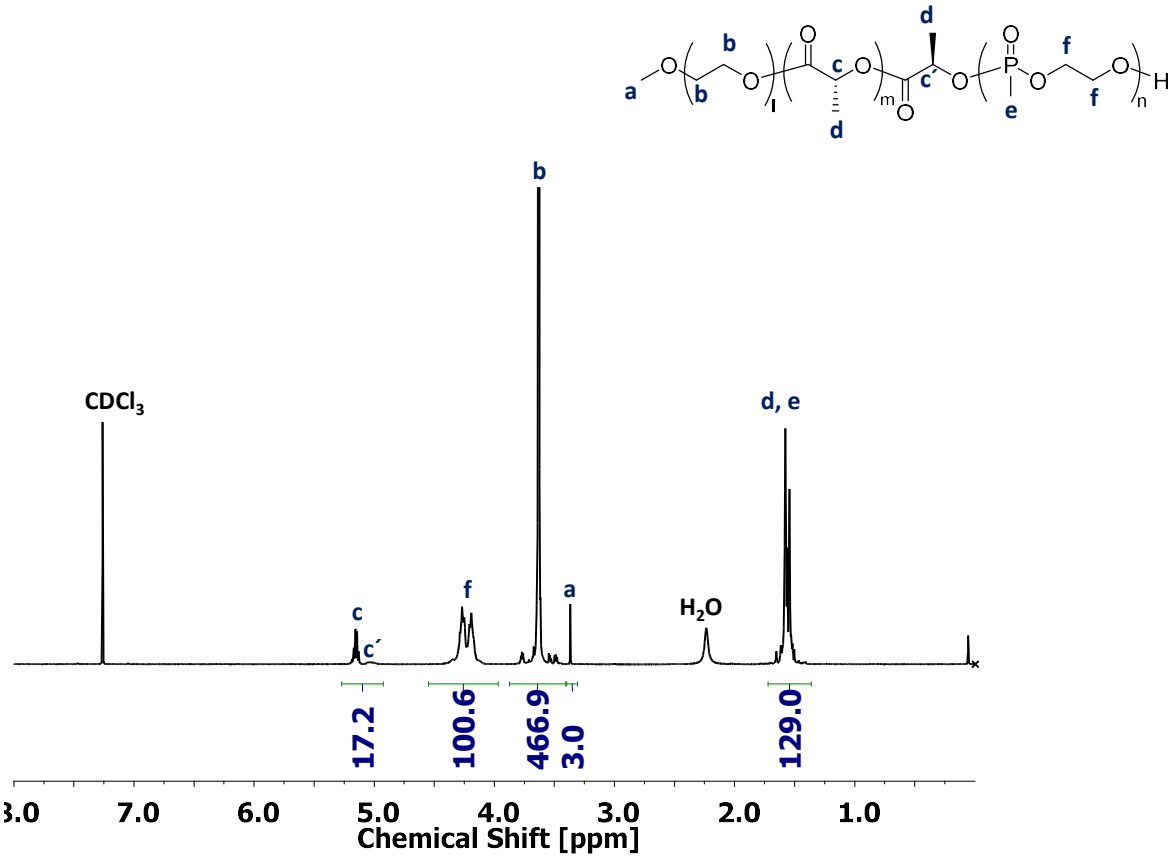

Figure A. 34: *^{1}H-NMR spectrum ($CDCl_3$, 500 MHz) of synthesized PEG_{113}-PDLA_{18}-$PMeP_{25}$*

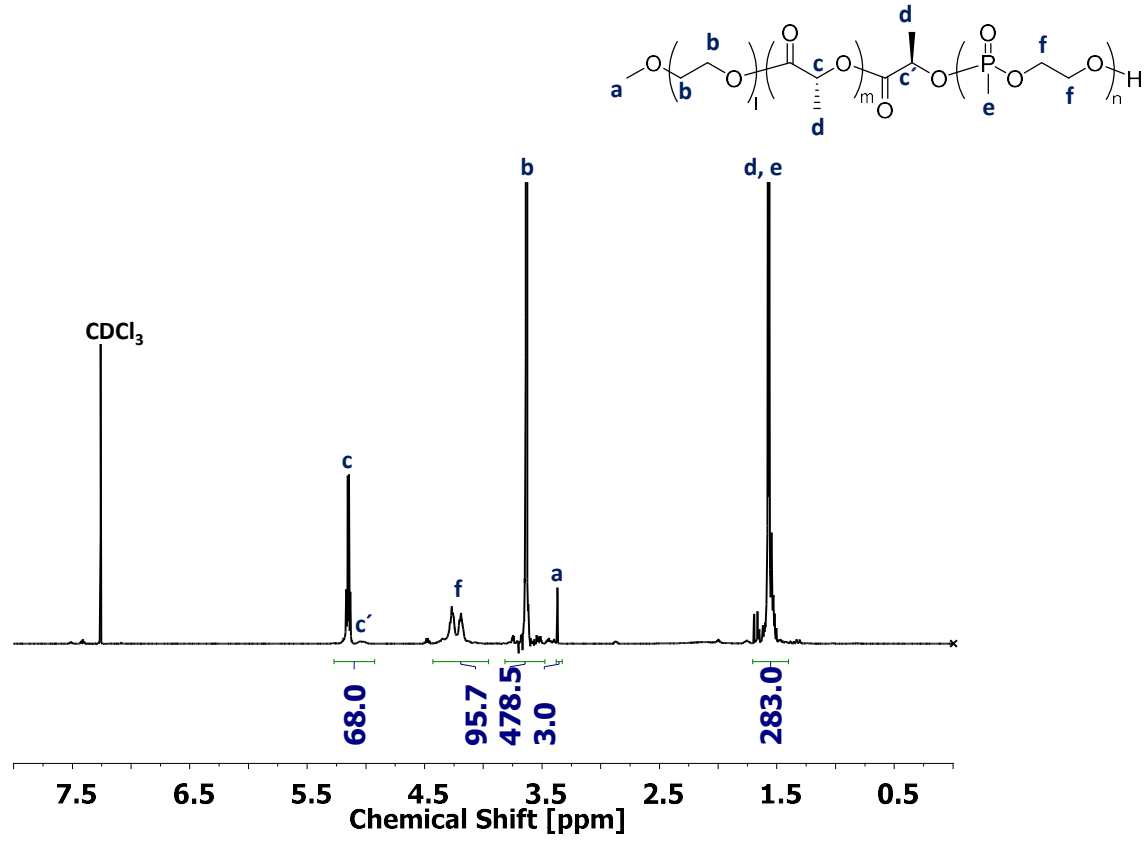

Figure A. 35: *^{1}H-NMR spectrum ($CDCl_3$, 500 MHz) of synthesized PEG_{113}-PDLA_{69}-$PMeP_{24}$*

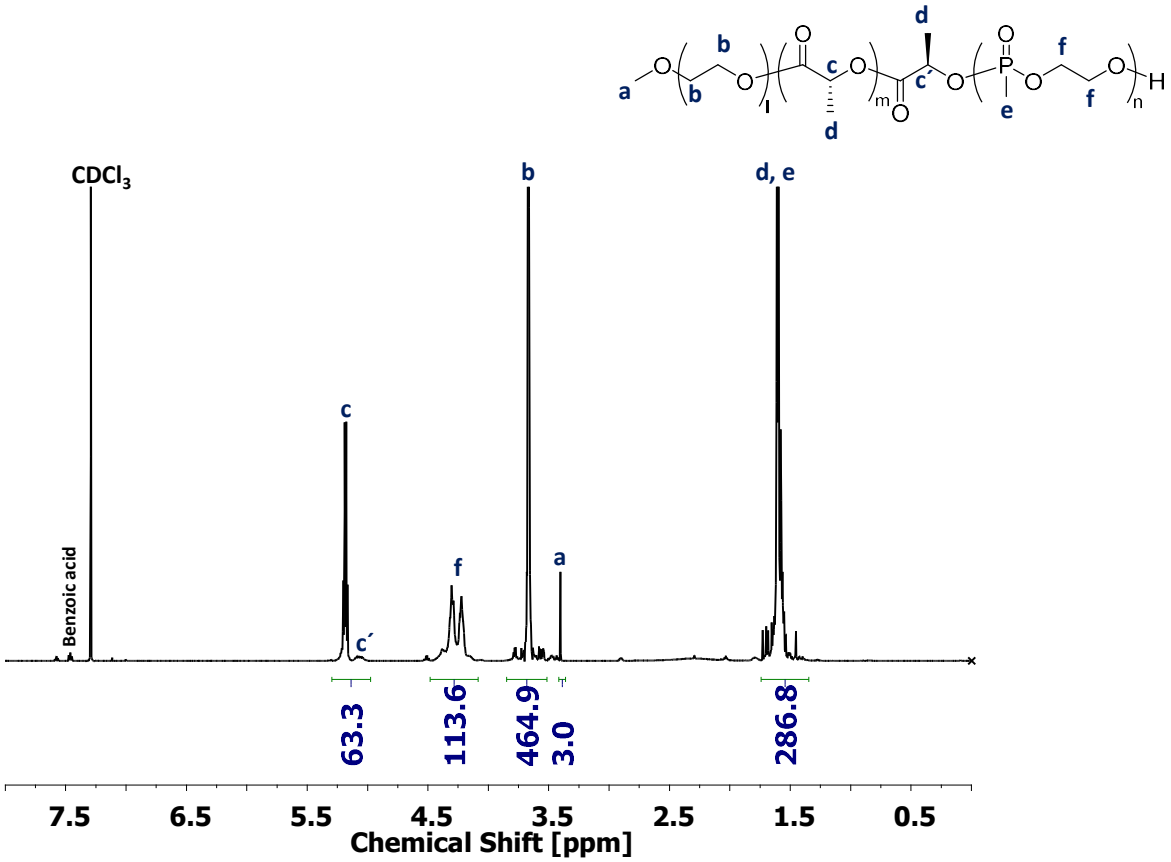

Figure A. 36: *^{1}H-NMR spectrum ($CDCl_3$, 500 MHz) of synthesized PEG_{113}-PDLA_{64}-PMeP_{29}*

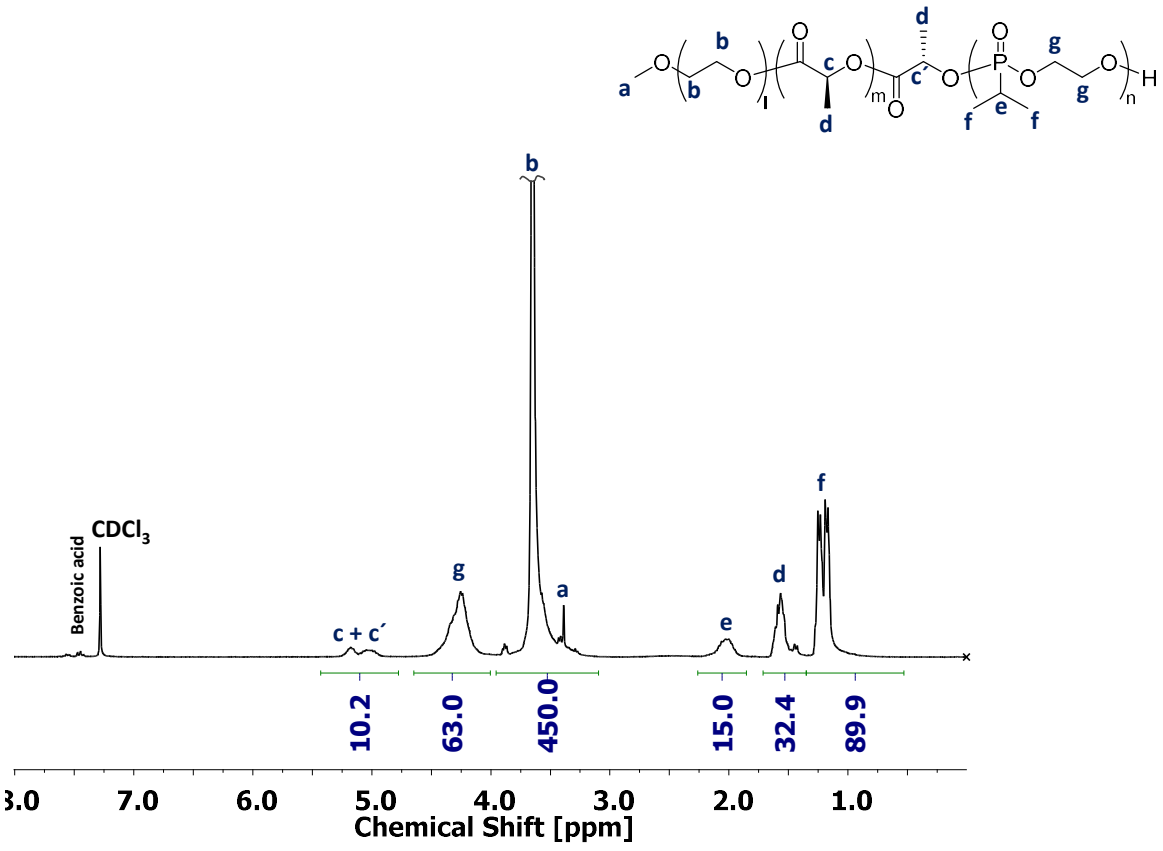

Figure A. 37*: ^{1}H-NMR spectrum ($CDCl_3$, 300 MHz) of synthesized PEG_{113}-PLLA_{10}-P^{i}PrP_{18}*

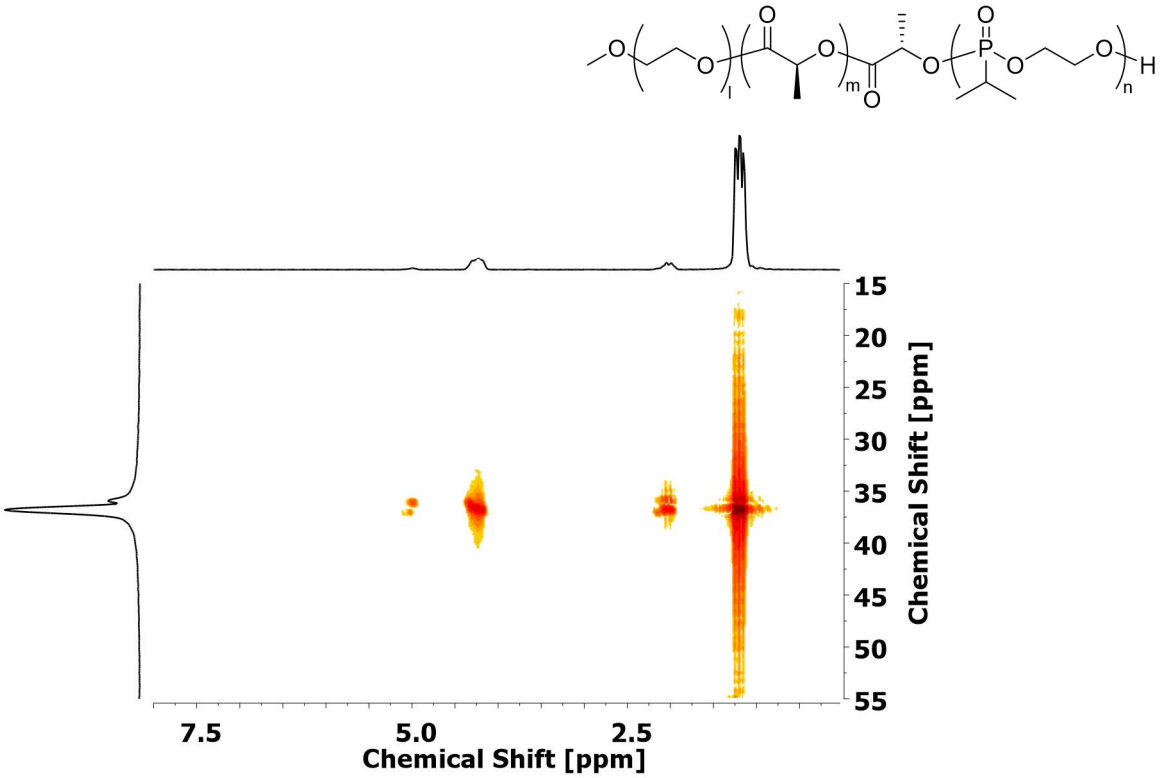

Figure A. 38: *^{1}H, ^{31}P-NMR spectrum ($CDCl_3$, 300 MHz) of synthesized PEG_{113}-$PLLA_{10}$-$P^{i}PrP_{18}$*

11.4 Synthesis and Analytics of Initiator Dye-NH_2

Within this thesis, different initiators were chosen with the try to polymerize DBU mediated $P^{i}PrP$. Even though the polymerization failed, the synthesis and analytics of 2-(2-aminoethyl)-1H-benzo[de]isoquinoline-1,3(2H)-dione (Dye-NH_2)shall be presented in the following.

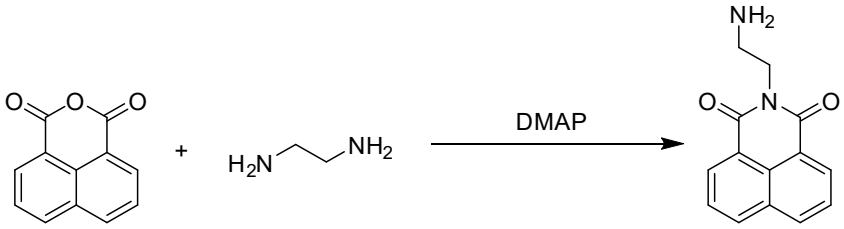

1 mL of 1,2-diaminoethane (15.15 mmol; 3 equiv) was added to a suspension of 1g 1,8-Naphthalic anhydride (5.05 mmol; 1 equiv) and a catalytic amount of 4-dimethylamino pyridine (DMAP) in 40 mL ethanol (dry) that were subsequently refluxed for 16 hours. The resulting yellow solid was removed by filtering the yellow solution at 60°C. Subsequently, the solvent was evaporated off and recrystallized in 1 mL of ethanol (dry). The obtained combined solid further purified by column chromatography over silica (gradient $CHCl_3$: MeOH = 10:1) to receive the yellowish product (R_f = 0.16; 495 mg; 11% yield).

^{1}H-NMR (300 MHz, $CDCl_3$) δ 8.55 (dd, J = 7.3, 0.9 Hz, 2H), 8.25 – 8.12 (dd, 7.3, 0.8 Hz, 2H), 7.71 (t, J = 7.8 Hz, 2H), 4.25 (t, J 0 6.6 Hz, 2H), 3.05 (t, J = 6.6 Hz, 2H), 1.28 (s, 2H). ^{13}C-NMR (75 MHz, $CDCl_3$) δ 164.52, 134.05, 131.65, 131.37, 128.26, 127.00, 122.65, 43.25, 40.65.

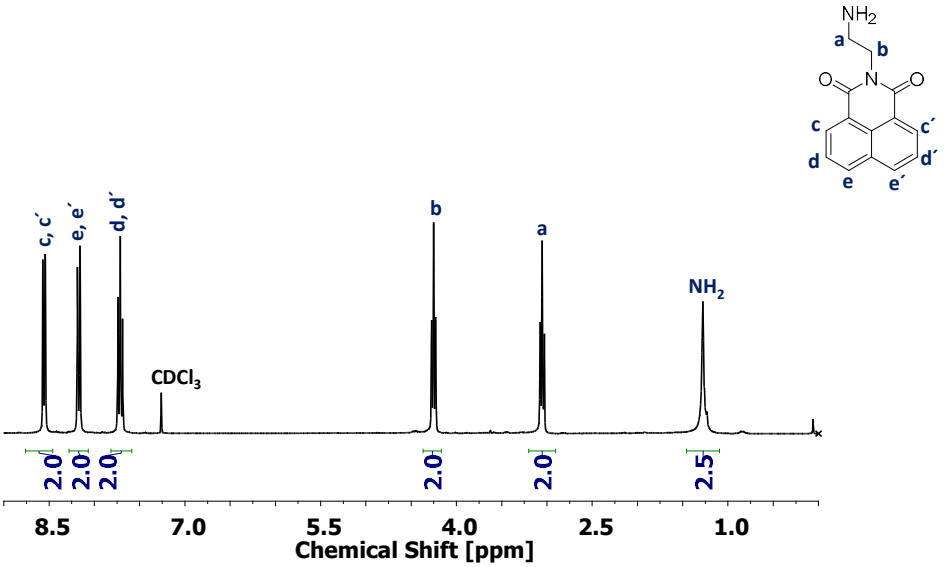

Figure A. 39: *^{1}H-NMR spectrum ($CDCl_3$, 300 MHz) of synthesized Dye-NH_2*

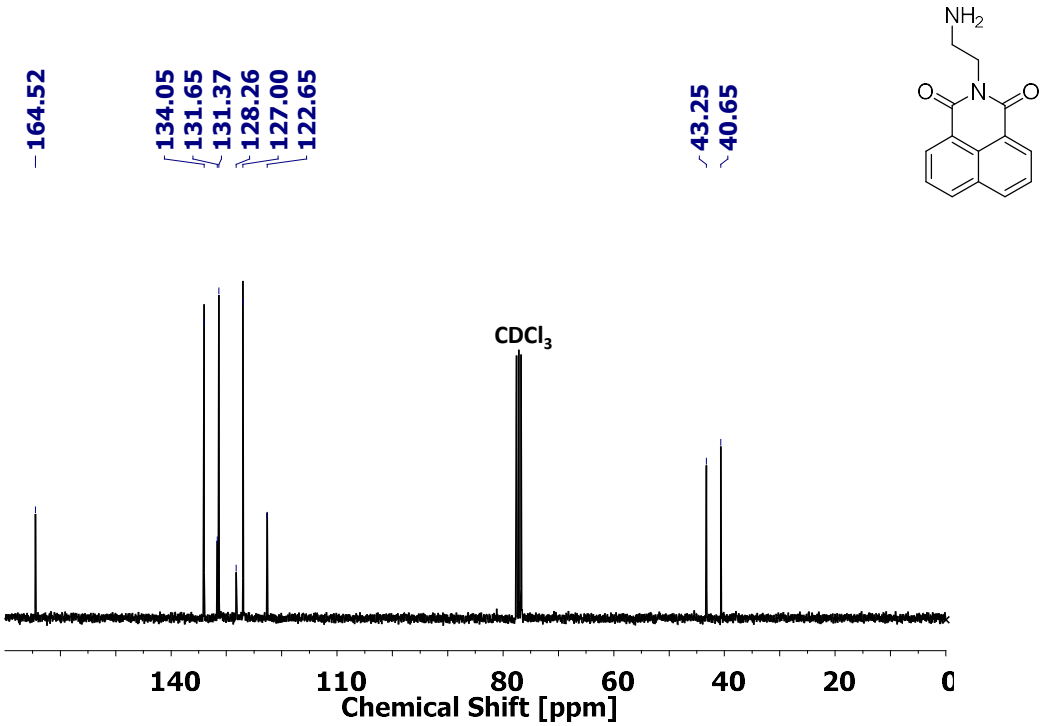

Figure A. 40: *^{13}C-NMR spectrum ($CDCl_3$, 75 MHz) of synthesized Dye-NH_2*

11.5 Time-Dependent Dialysis of Poly(lactide) and Poly(methyl phosphonate)-based Copolymers

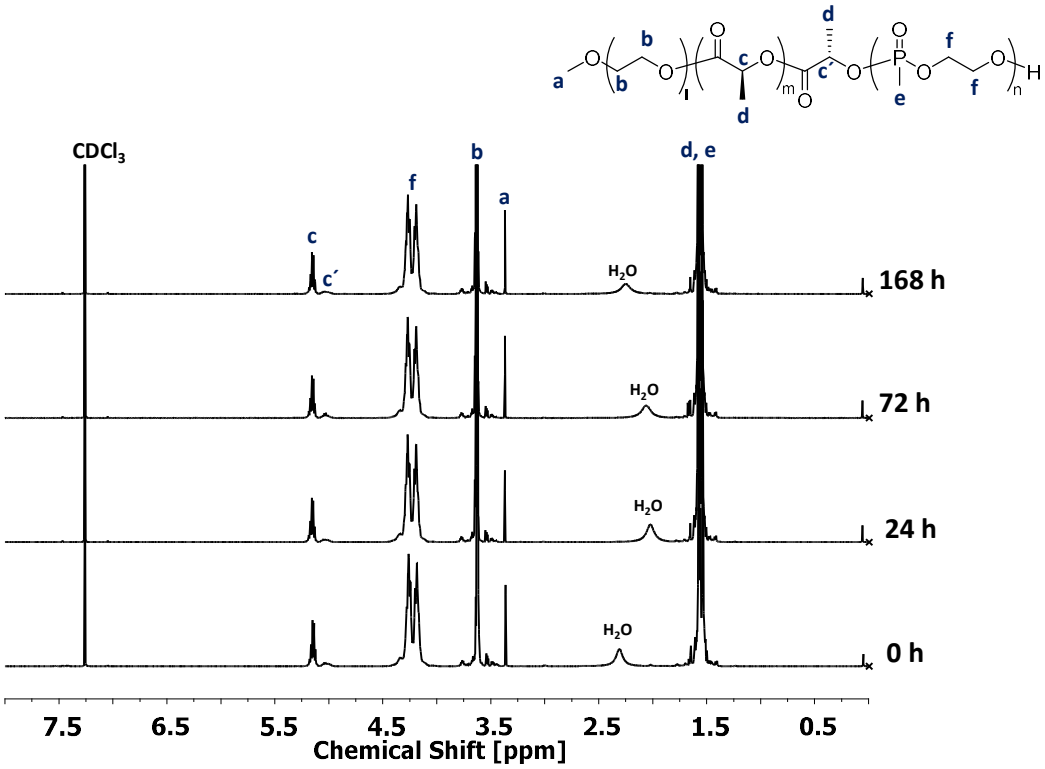

Figure A. 41: *Stacked ^{1}H-NMR spectra ($CDCl_3$, 500 MHz) of synthesized of time-dependent dialysis experiments of PEG_{45}-P_LLA_{20}-$PMeP_{36}$ to exclude polymer degradation in aqueous solutions within the period of self-assembly.*

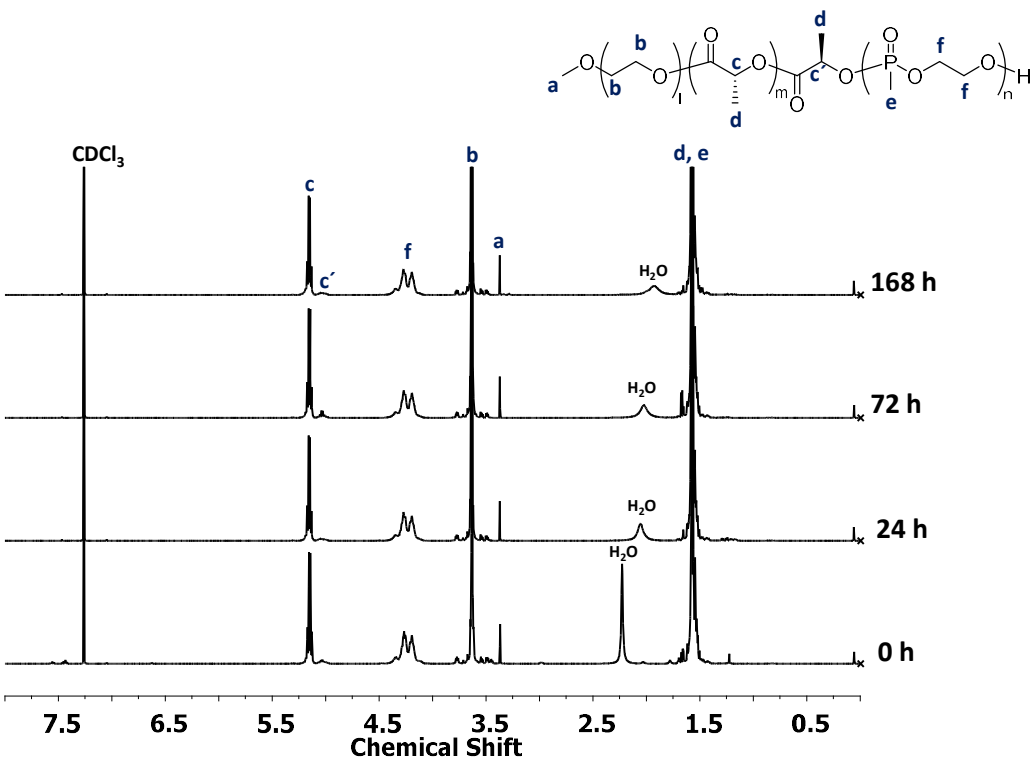

Figure A. 42: *Stacked ^{1}H-NMR spectra ($CDCl_3$, 500 MHz) of synthesized of time-dependent dialysis experiments of PEG_{113}-P_DLA_{64}-$PMeP_{29}$ to exclude polymer degradation in aqueous solutions within the period of self-assembly.*

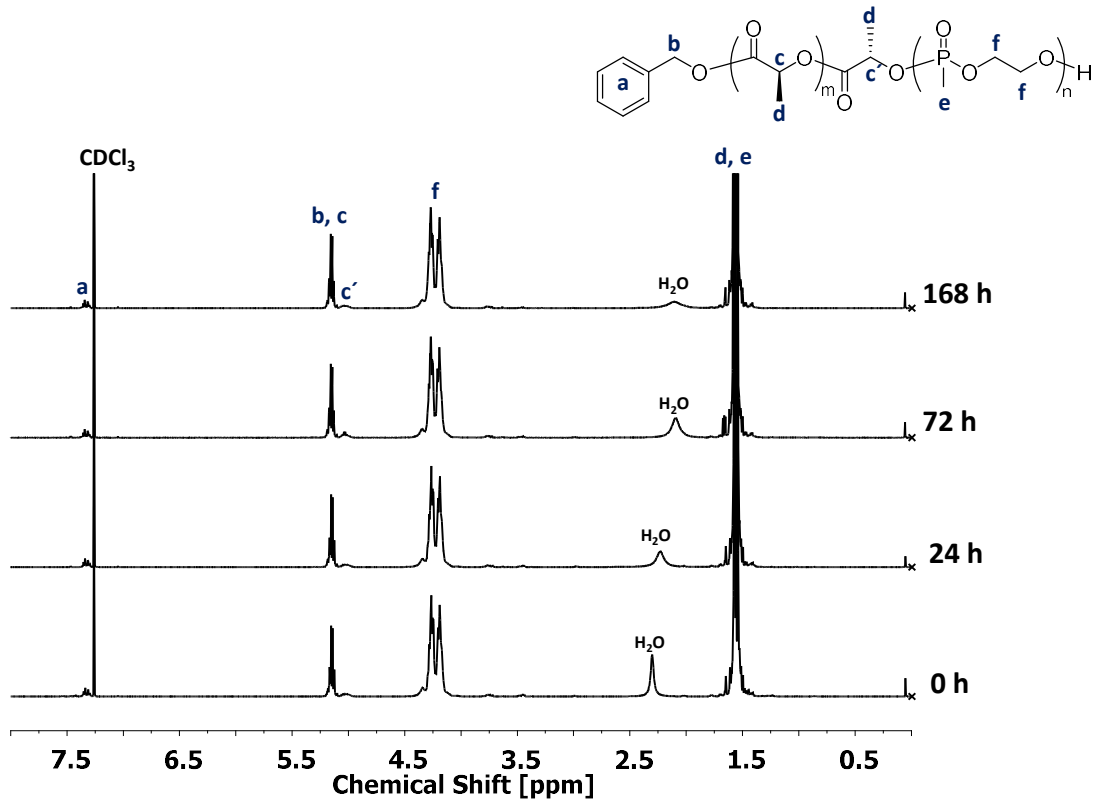

Figure A. 43: *Stacked ^{1}H-NMR spectra ($CDCl_3$, 500 MHz) of synthesized of time-dependent dialysis experiments of $PLLA_{33}$-$PMeP_{50}$ to exclude polymer degradation in aqueous solutions within the period of self-assembly.*

11.6 Transesterification Influenced Self-Assembly of PEG-PLLA Copolymers

As described in Chapter 4.1.1, due to the ability of transesterification within the DBU mediated lactide polymerization, the self-assembly of PLA-based block copolymers can be affected. The transesterification can be recognized by broad molar mass distributions or multimodal elugrams detected by SEC experiments. Depending on the PLA chain length the influence, the effect can be quite large as the following data will present. With the aim to observe the development of the molar mass distribution of PEG-PLLA copolymer with an aimed chain length of 280 lactyl units, a time-controlled polymerization was performed. Within certain periods, the polymerization was quenched with an excess of benzoic acid, subsequently precipitated in diethyl ether, dried in high vacuum, and finally investigated by SEC (eluent: THF) and ^{1}H-NMR spectroscopy. As seen in Figure A. 44, the monomer conversion and therefore the chain growth of PLA is fast. Nevertheless, transesterification cannot be observed by ^{1}H-NMR spectroscopy since the chain length does not change dramatically after 30 minutes.

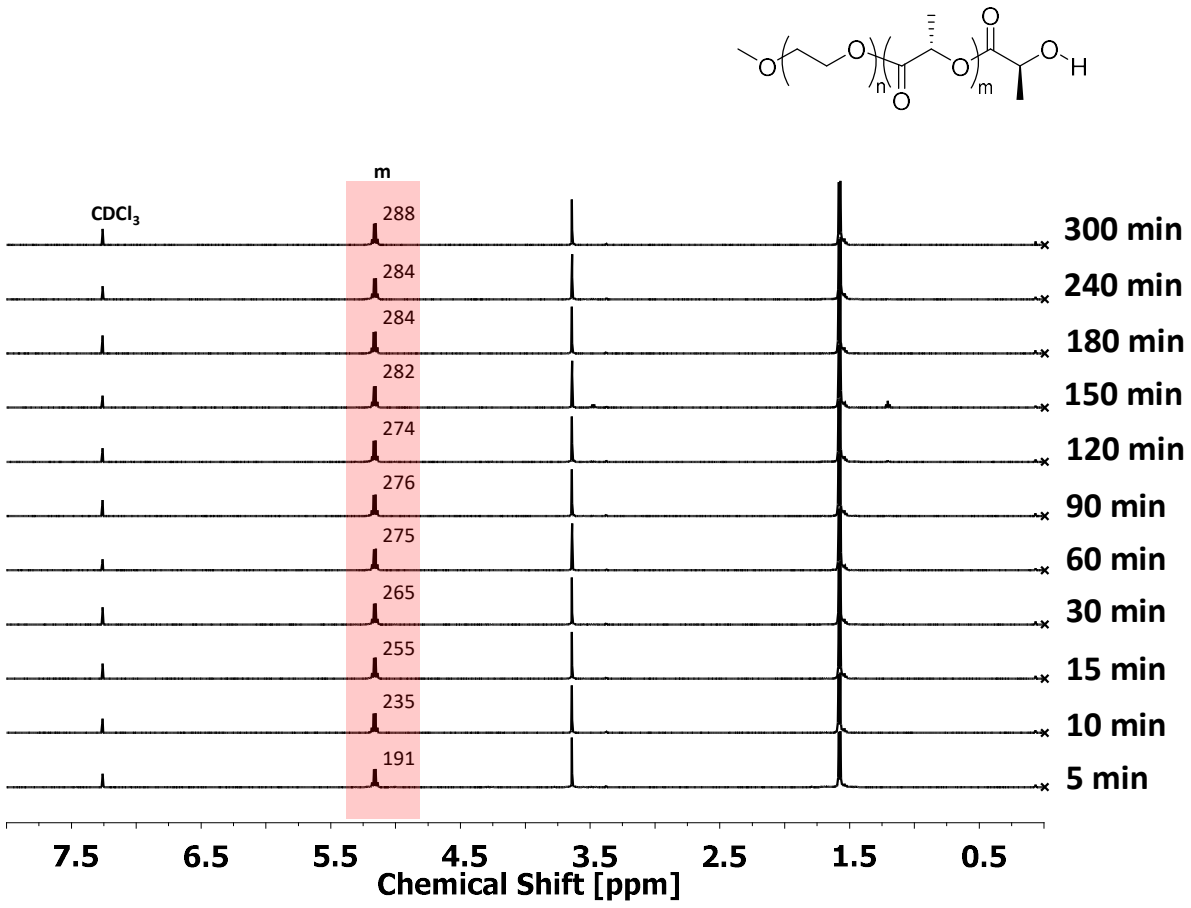

Figure A. 44: *Stacked ^{1}H-NMR spectra ($CDCl_3$, 500 MHz) of time-dependent synthesis of PEG_{113}-$PLLA_{288}$. The red block corresponds to the PLA chain length calculated by end group analysis, normalized to the methoxy group of the PEG.*

However, SEC traces in THF present an essential change with time. After 30 min of polymerization, an increasing shoulder is appearing, which further grows with time. Since the effect cannot be explained completely, but transesterification seems to be the most likely cause for this effect, four resulting polymers were investigated in their self-assembly behavior.

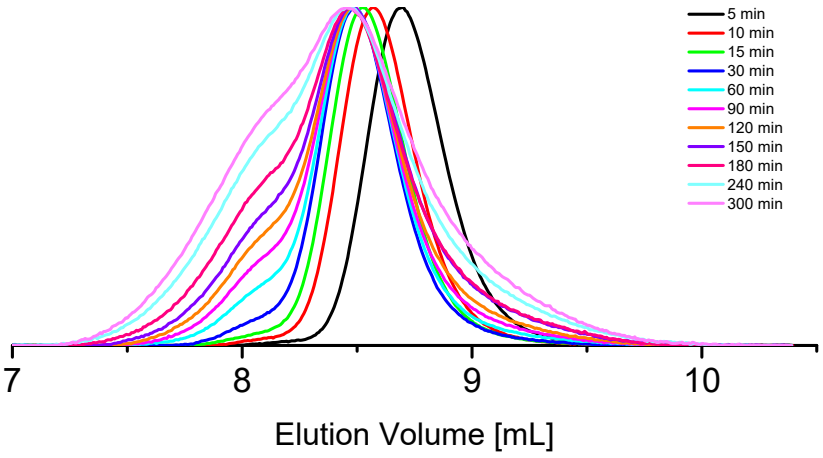

Figure A. 45: *SEC Traces (eluent: THF) of time-dependent PEG-PLLA copolymer synthesis*

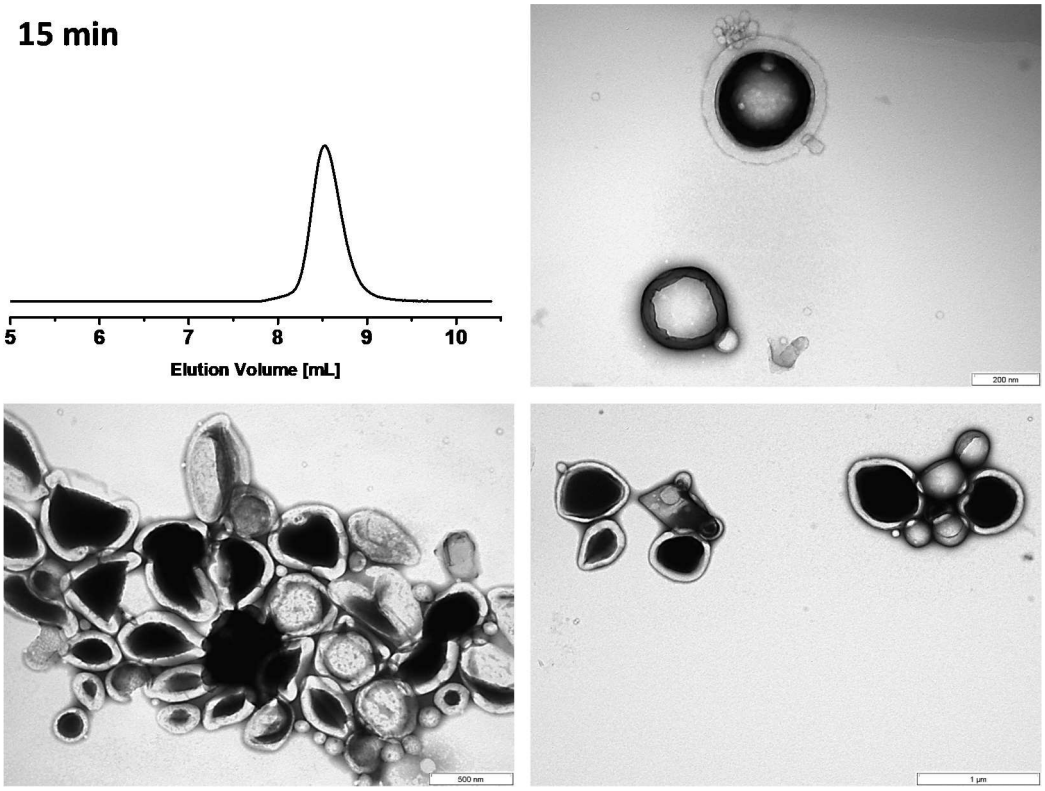

Figure A. 46: *TEM images (negative staining) of aggregates resulting from PEG-PLLA copolymer that was quenched within 15 min of polymerization*

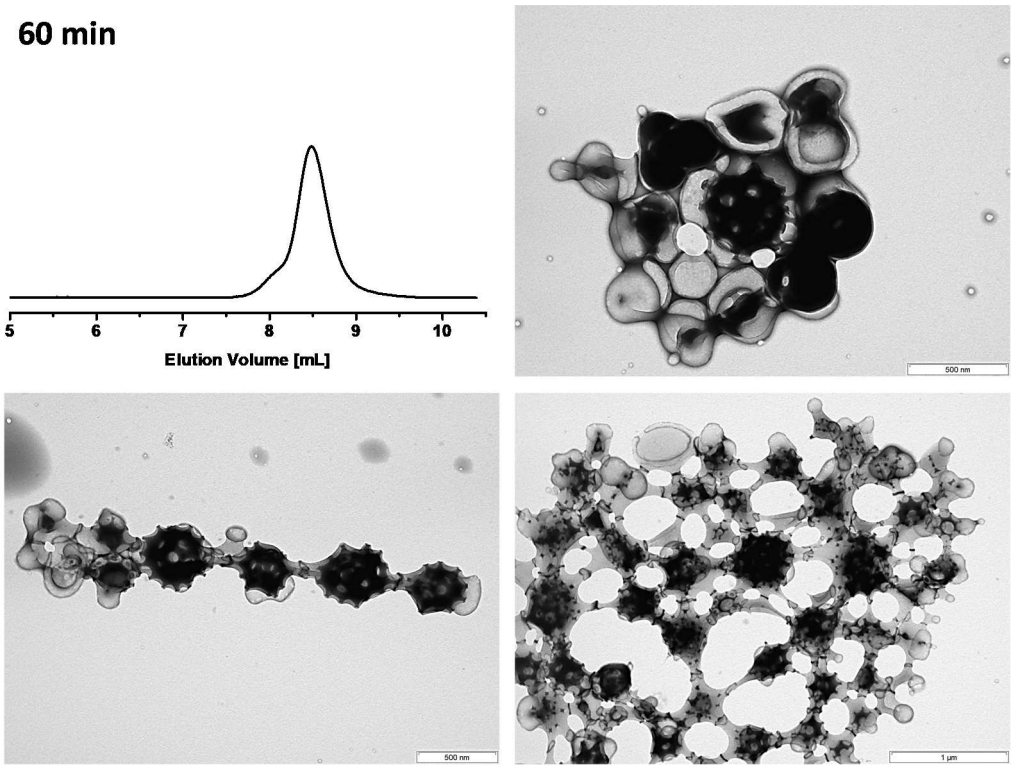

Figure A. 47: *TEM images (negative staining) of aggregates resulting from PEG-PLLA copolymer that was quenched within 60 min of polymerization*

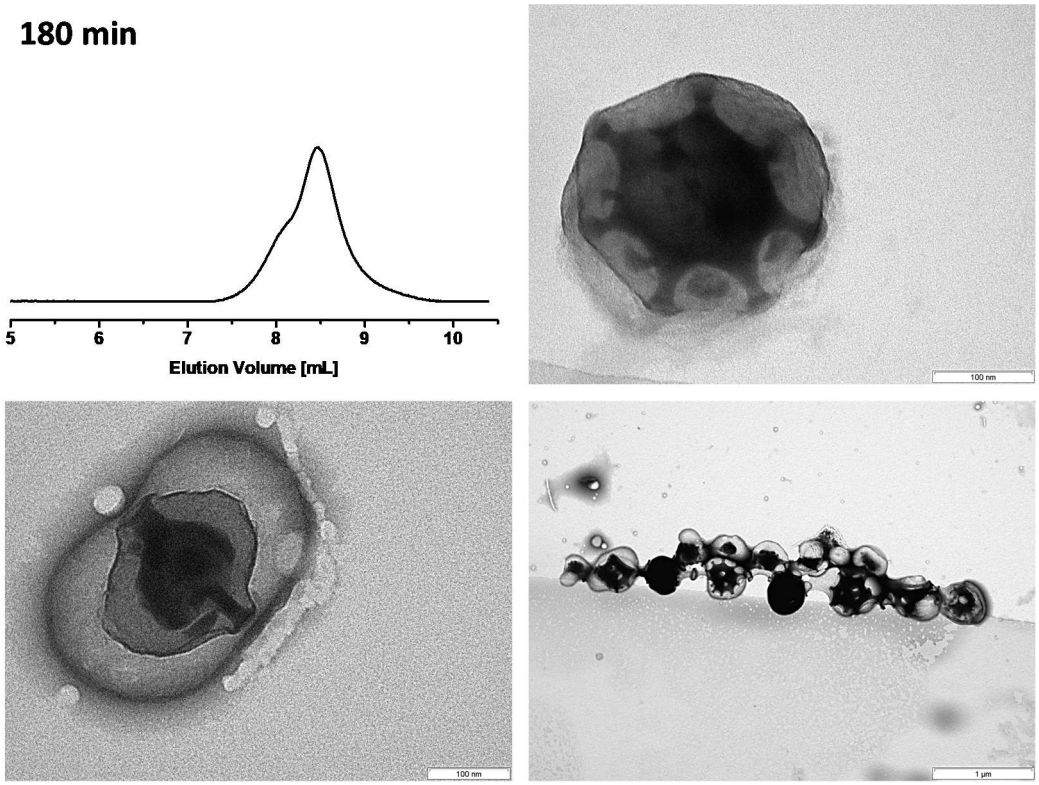

Figure A. 48: *TEM images (negative staining) of aggregates resulting from PEG-PLLA copolymer that was quenched within 180 min of polymerization*

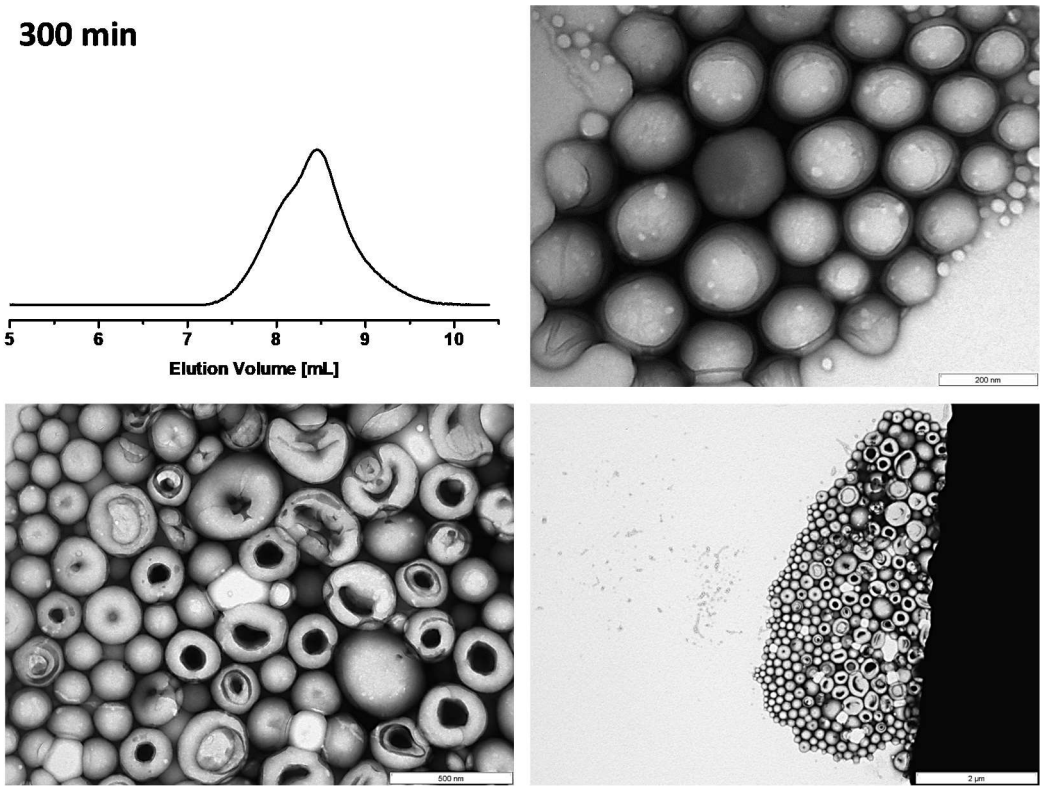

***Figure A. 49**: TEM images (negative staining) of aggregates resulting from PEG-PLLA copolymer that was quenched within 300 min of polymerization*

In the presented TEM images (Figure A. 46, Figure A. 47, Figure A. 48, Figure A. 49) diverse morphologies were observed depending on the polymerization quenching time, including rings, gyroids, and huge spheres that are supposed to be vesicles range in sizes between 200-500 nm. However, since the observed rings never exist in perfect shape, and the negative staining could create artifacts, it is most likely that the observed rings are collapsed vesicles. Nevertheless, the created gyroids are also an interesting morphology; however, due to the previously mentioned side reactions, these morphologies will not be discussed further and need to be more examined in the future.

11.7 Temperature-Dependent Self-Assembly of PEG-PLA

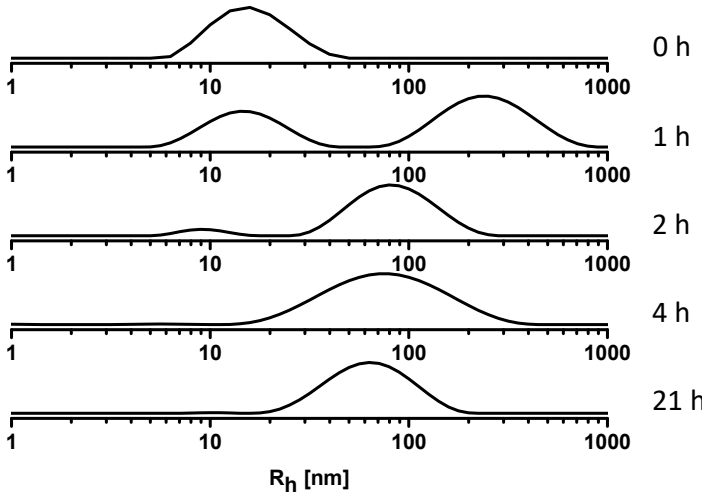

Figure A. 50: *Temperature-and Time-DependentR_h of PEG_{113}-P_LLA_{18} at 60°C*

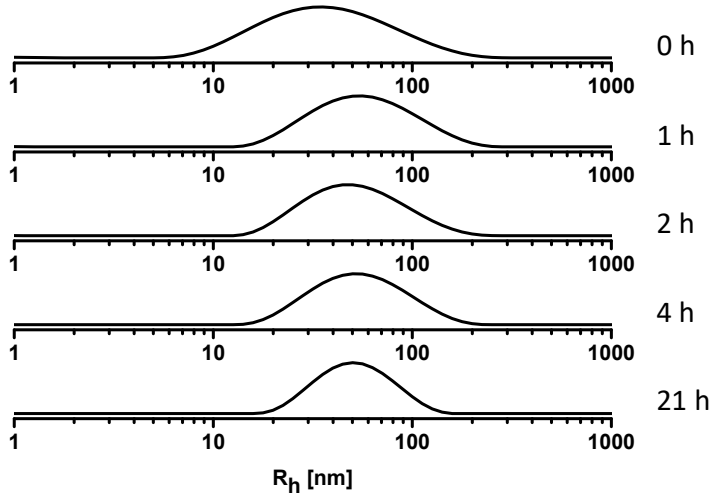

Figure A. 51: *Temperature-and Time-DependentR_h of PEG_{45}-P_LLA_{18} at 60°C*

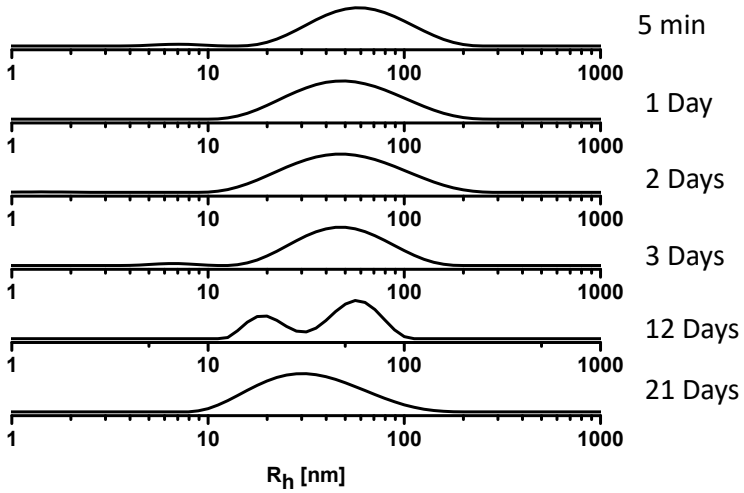

Figure A. 52: *Time-dependent R_h of PEG$_{113}$-PLLA$_{18}$ + PEG$_{113}$-PDLA$_{18}$ at room temperature. The individual polymer solutions of the parent polymers were annealed at 60°C for 21 h before mixing in an equimolar ratio.*

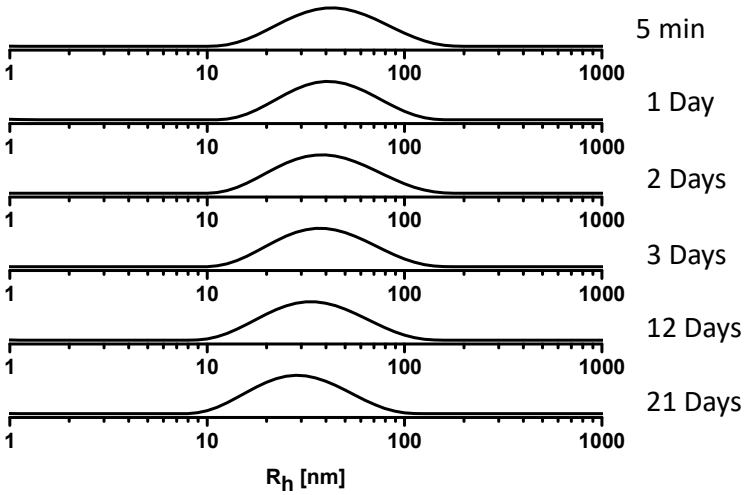

Figure A. 53*: Time-dependent R_h of PEG$_{45}$-PLLA$_{18}$ + PEG$_{45}$-PDLA$_{19}$ at room temperature. The individual polymer solutions of the parent polymers were annealed at 60°C for 21 h before mixing in an equimolar ratio.*

11.8 Time-Dependent Self-Assembly of Block Copolymer Mixtures (SLS Data)

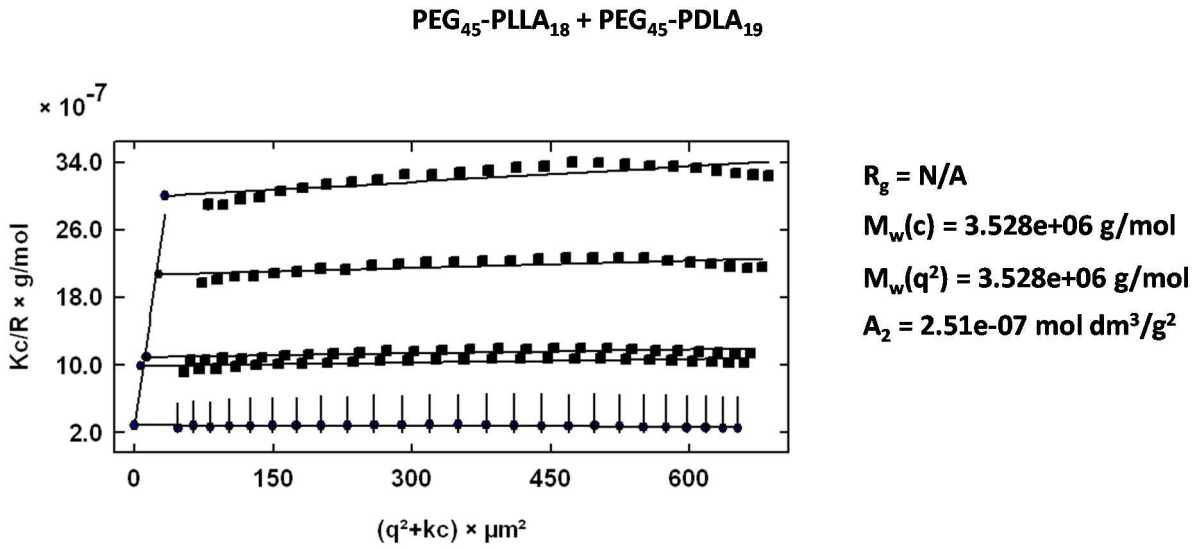

Figure A. 54: *Zimm-Plot from PEG_{45}-PLLA$_{18}$ + PEG_{45}-PDLA$_{19}$ obtained from concentration-dependent SLS measurements*

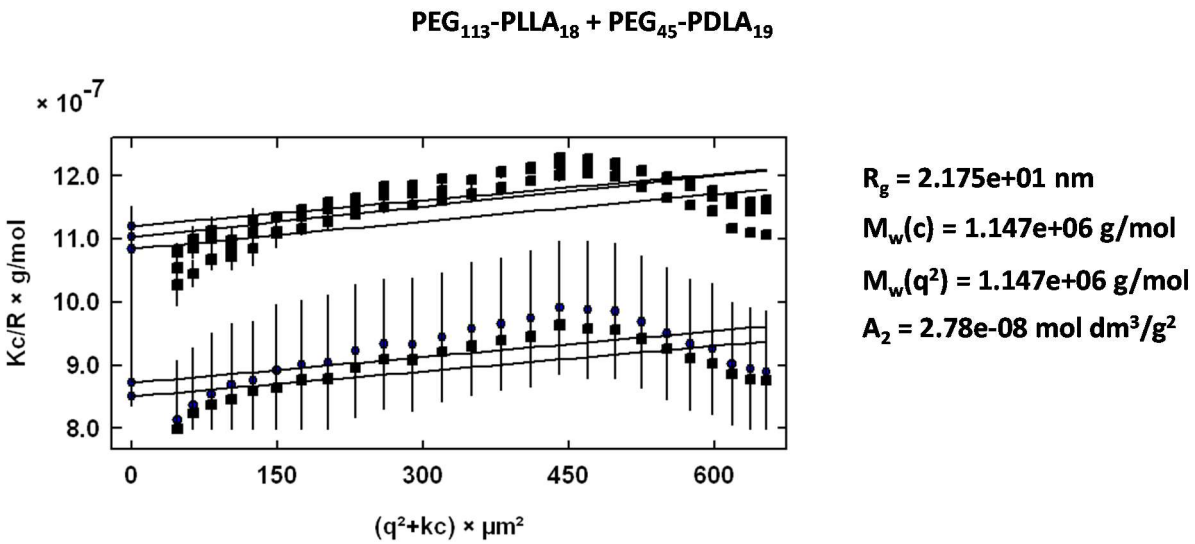

Figure A. 55: *Zimm-Plot from PEG_{113}-PLLA$_{18}$ + PEG_{45}-PDLA$_{19}$ obtained from concentration-dependent SLS measurements*

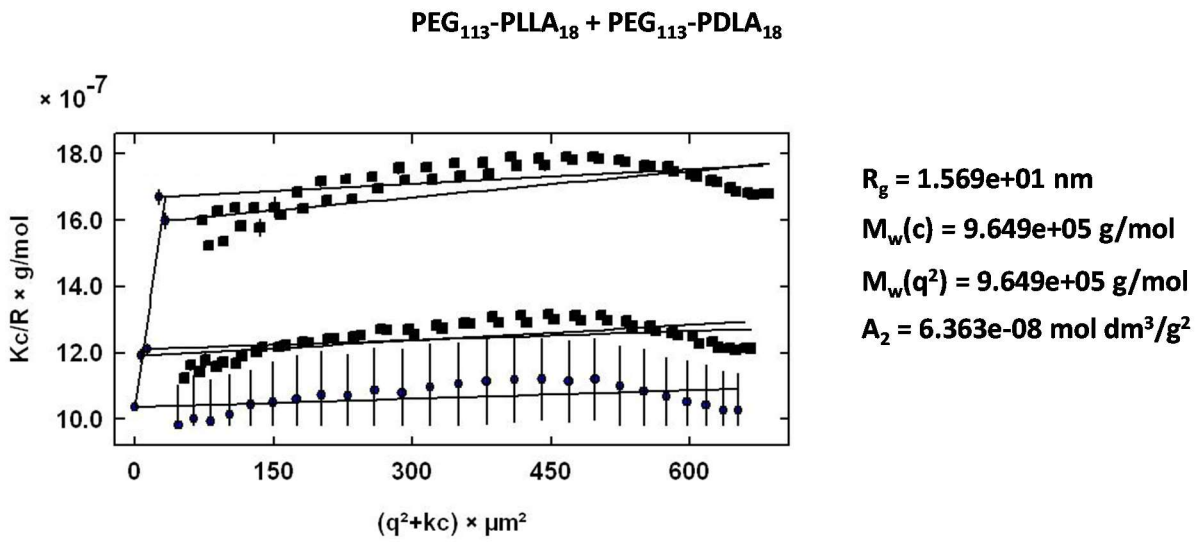

Figure A. 56: *Zimm-Plot from PEG_{113}-$PLLA_{18}$ + PEG_{113}-$PDLA_{18}$ obtained from concentration-dependent SLS measurements*

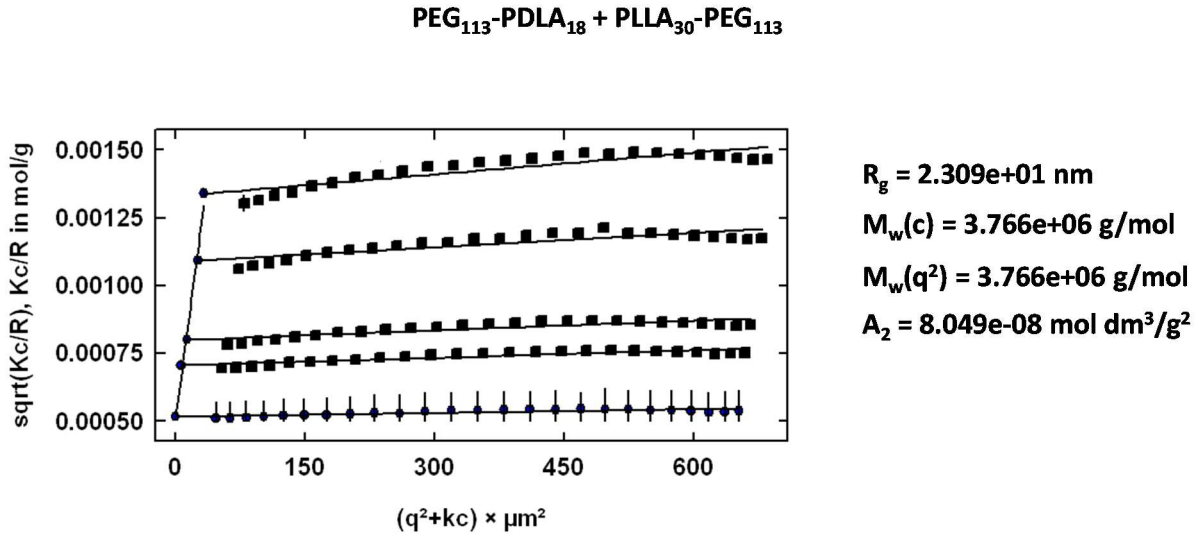

Figure A. 57: *Zimm-Plot from PEG_{113}-$PDLA_{18}$ + $PDLA_{30}$-PEG_{113} obtained from concentration-dependent SLS measurements*

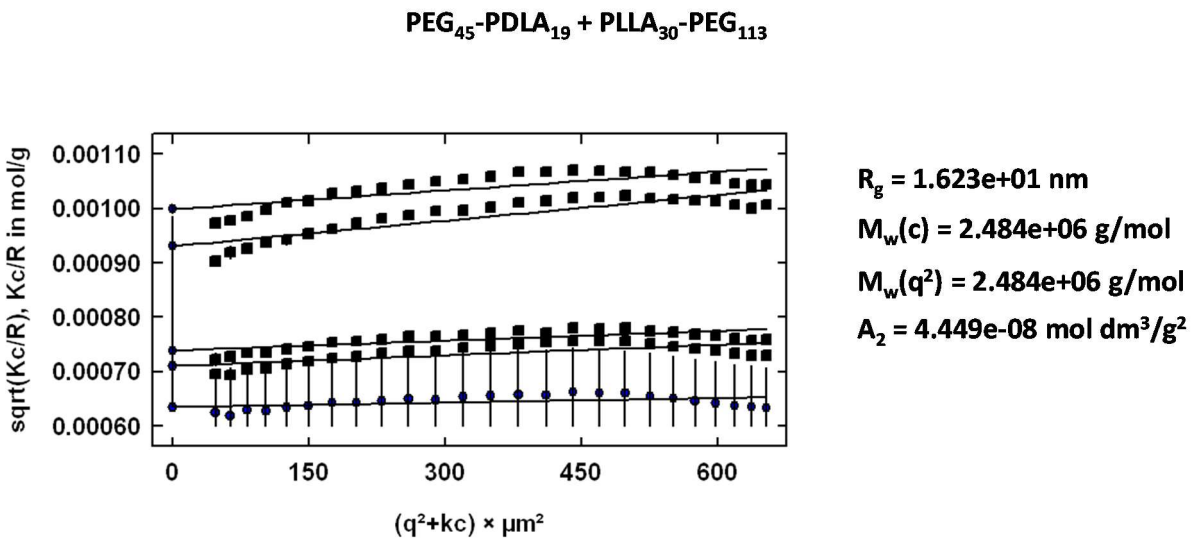

Figure A. 58: *Zimm-Plot from PEG_{45}-$PDLA_{19}$ + $PDLA_{30}$-PEG_{113} obtained from concentration-dependent SLS measurements*

11.9 DBU initiated Poly(lactide) Polymerization

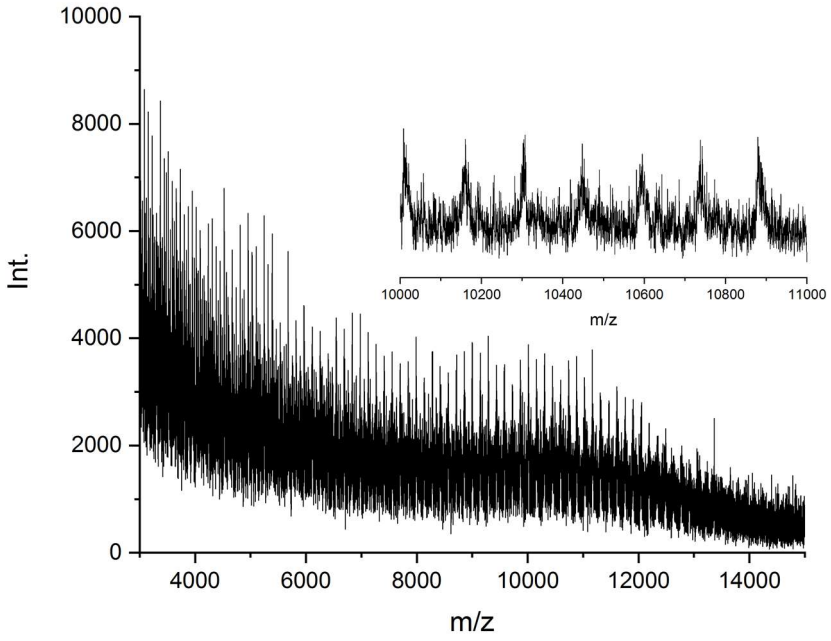

Figure A. 59*: MALDI-TOF MS spectrum of DBU initiated PLLA (reaction time 120 min)*

12 Appendix B

List of Publications and Conference Contributions

12.1 Journal Publications

Polylactide-Based Amphiphilic Block Copolymers: Crystallization-Induced Self-Assembly and Stereocomplexation

S. Noack, D. Schanzenbach, J. Koetz, H. Schlaad, *Macrolmol. Rapid Commun.*, 2019, 40 (1), 1800639.

Poly L-Lactic acid (PLLA), by Near-Ambient Pressure XPS (NAP-XPS)

D. I. Patel, S. Noack, C. D. Vacogne, H. Schlaad, S. Bahr, P. Dietrich, M. Meyer, A. Thißen, M. R. Linford, *Surf. Sci. Spectra,* **2018**, *Submitted.*

Poly-Benzyl L-Glutamate (PBLG), by Near-Ambient Pressure XPS (NAP-XPS)

V. Jain, C. D. Vacogne, S. Noack, H. Schlaad, S. Bahr, P. Dietrich, M. Meyer, A. Thißen, M. R. Linford, *Surf. Sci. Spectra,* **2018**, *Submitted.*

Controlling nucleation in quasi-two-dimensional Langmuir poly(L-lactide) films through variation of the rate of compression

A. Das, A. S. El-Tawargy, E. Khechine, S. Noack, H. Schlaad, G. Reiter, R. Reiter *Langmuir,* 2019, *Submitted.*

12.2 Conference Contributions

Tag der Chemie (TDC), Berlin, 2017 (Poster and Presentation)

S.Noack, A. Bogomolova, H. Schlaad, Aggregation behavior of self-assembling amphiphilic block copolymers based on poly(lactide) with opposite orientations.